Holocene climate variability in tropical South America : case history from a high-mountain wet zone in NW Colombia based on palynology and X-ray microfluorescence

Munoz Uribe, Paula Andrea

UNIVERSITE DE GENEVE
Département des Sciences de la Terre

FACULTÉ DES SCIENCES
Professeur G.E. Gorin

UNIVERSIDAD NACIONAL DE COLOMBIA,
SEDE MEDELLIN

FACULTAD DE CIENCIAS
Professeur C.A. Velásquez Ruíz

HOLOCENE CLIMATE VARIABILITY IN TROPICAL SOUTH AMERICA : CASE HISTORY FROM A HIGH-MOUNTAIN WET ZONE IN NW COLOMBIA BASED ON PALYNOLOGY AND X-RAY MICROFLUORESCENCE

THÈSE

Présentée à la Faculté des Sciences de l'Université de Genève pour obtenir le grade de Docteur ès sciences, mention Sciences de la Terre

Par

Paula Andrea MUÑOZ URIBE

de Medellin (Colombie)

Thèse No 4466

GENEVE
Atelier de reprographie ReproMail
2013

La Faculté des sciences, sur le préavis de G. GORIN, professeur honoraire et directeur de thèse (Département de géologie et paléontologie), C. A. VELÁSQUEZ RUÍZ, professeur et codirecteur de thèse (Facultad de Ciencias, Universidad Nacional de Colombia, sede Medellin, Colombia), D. ARIZTEGUI, professeur associé (Département de géologie et paléontologie), L. N. PARRA SANCHÉZ, professeur (Facultad de Ciencias, Universidad Nacional de Colombia, sede Medellin, Colombia) et H. HOOGHIEMSTRA, professeur (Institute for Biodiversity and Ecosystem Dynamics, Faculty of science, University of Amsterdam, The Netherlands), autorise l'impression de la présente thèse, sans exprimer d'opinion sur les propositions qui y sont énoncées.

Genève, le 26 septembre 2012

Thèse - 4466 -

Le Doyen, Jean-Marc TRISCONE

Abstract

Key words: subandean forest, Andean forest, aquatics, Holocene, ENSO; ITCZ, Páramo, rainfall, temperature, Ti, Fe, Younger Dryas.

The Llano Grande wet zone studied here is situated at 3,460 m amsl in the Páramo de Frontino at the northwestern termination of the Western Cordillera in the Colombian Andes. It is ideally located to have registered the climatic influence of both Atlantic and Pacific oceans in an anthropogenically-undisturbed environment. It contains a continuous, over 14 m thick, sedimentary sequence spanning the Late Glacial and the Holocene (17,000 - 0 cal yr BP).
This sequence has been fully cored using a device that does not compact the sediments. It has been accurately dated through 30 AMS C^{14} analyses that show the absence of hiatuses. It can be lithologically subdivided into three units: 1) a lower unit made of light-coloured mineral mud with dark laminae of glacial origin dated as pre-16,700 cal yr BP; 2) an intermediate unit made of dark brown organo-mineral mud locally rich in diatoms spanning a time interval of ca. 16,700 to 11,400 cal yr BP; 3) an upper unit made of dark brown peat/organic mud rich in vegetal filaments/fragments and in diatoms at its base, spanning the whole Holocene (11,400 – 0 cal yr BP). It is this last unit that has been the object of the present research.
For the first time, this investigation presents an interpretation of climatic variations in the Holocene of north-western South America with a decadal to yearly time resolution using palynological and geochemical proxies. The palynological investigation presented here covers the time interval of ca. 11,500 until 4,300 cal yr BP (i.e., early and middle Holocene) with a time resolution of ca. 35 years. In order to get a full coverage of the vegetation evolution through the Holocene, our palynological data can be merged with those of Velásquez (2005), who studied the interval 4,300 until 0 cal yr BP with a ca. 20 years time resolution. This palynological record can then be compared with the X-ray microfluorescence (µXRF) data obtained over the whole Holocene. Using the existing concepts of vegetation belts (páramo, Andean/upper montane forest, subandean/lower montane forest) and upper forest line (UFL, derived from the relative proportion of arboreal pollen), the interpreted altitudinal variation of the latter can be used as a proxy to estimate changes in mean average temperatures (MAT). In parallel, the relative variations in the local aquatic vegetation have been used as a proxy to estimate the water depth in the mire/lake, i.e., an indicator for precipitations in the drainage basin of Llano Grande wet zone. µXRF provides a direct signature of the water runoff in the basin with a sub-yearly time resolution, i.e., it is a proxy for rainfall. In this study, we have concentrated on the elements Ti and Fe, whose record has been analyzed for time series.
After a cold and wet Younger Dryas equivalent (El Abral stadial in Colombia), the base of the Holocene becomes very warm and dry before returning to colder and dry conditions at around 10,000 cal yr BP. Between 9,500 and 7,000 cal yr BP an overall warm and dry interval can be interpreted as “Holocene thermal maximum”, although it might be interrupted by colder breaks (e.g., at around 8,000 cal yr BP with a peak in dryness). During this warm interval, average temperatures were slightly below, but close to, the present-day MAT. Most of the rest of the Middle Holocene until ca. 4,000 cal yr BP is much colder with estimated average temperatures some 2°C lower than today. From ca. 6,000 cal yr BP, conditions become much wetter, with a peak in rainfall between 5,000 and 4,000 cal yr BP. Between

4,500 and 3,500 cal yr BP, the amount of rainfall decreases considerably and becomes much lower than in the early and middle Holocene for the rest of the Late Holocene. The lower part of the Late Holocene shows estimated temperatures some 3°C higher than today associated with very dry conditions. From ca. 2,500 cal yr BP, the forest line drops again considerably and, until ca. 130 cal yr BP, the late Holocene has estimated average temperatures at least 2°C lower than today with a minimum between ca. 1,400 and 750 cal yr BP where temperature might have been 4°C lower than today, like in the final part of the Younger Dryas equivalent. During the last 200 years the temperature is estimated to have risen by some 2°C.

Therefore, both geochemical and palynological proxies demonstrate that the Holocene record in the Páramo de Frontino is marked by rapid and very significant changes in temperature and precipitations. Temperatures may have varied (up or down) of a few degrees centigrade over less than a century. Although the lack of other studies with a similar time resolution is a limiting factor, these results have been compared with existing regional information in north-western South America/Central America, in an attempt to interpret the climate driving mechanisms in the Holocene of the Páramo de Frontino.

The temperature model obtained from palynology fits the overall picture known in this zone. A cold YD equivalent is comparable with data in the Eastern Cordillera of Colombia, in Costa Rica, Guatemala and in the Venezuelan Andes. An abrupt increase in temperature marks the base of the early Holocene. The observed « Holocene thermal maximum » is also interpreted in most of the sites used for comparison. The upper part of the middle Holocene in Frontino is considerably colder, which seems to match a colder interval observed from sea surface temperature (SST) in the Atlantic basin of Cariaco (Venezuela). Colder conditions are also observed in high-altitude sites of Peru. In the first part of the late Holocene, the temperature maximum observed in Llano Grande cannot be correlated with other records, except in the SST curve of the Cariaco Basin which also shows a high. In the upper part of the late Holocene, conditions are much colder in Llano Grande, except for the last two hundred years. Cold conditions also prevailed in the Colombian Eastern Cordillera and in high-altitude sites of Ecuador and Peru.

Because of its high-resolution XRF data, the Cariaco Basin (in the Caribbean Sea) is to date the only accurate comparison point as rainfall proxy in northern South America. This comparison leads to the following conclusions: a) during the late Younger Dryas (YD) and early Holocene, Cariaco (and Central American sites) show a gradual transition from a dry YD to wet conditions demonstrating the northward migration of the ITCZ following the glacial period. This contrasts with the sharp transition in Frontino from a wet YD to a dry early Holocene. The latter suggests that Frontino climate might have been more under the influence of the Pacific Ocean or local conditions and less affected by the ITCZ at that time; b) during the middle and late Holocene, the rainfall pattern is similar in both regions with a rapid decrease in rainfall between ca. 4,500 and 3,500 cal yr BP, a period during which the ENSO variability was very high (as supported by time series analysis of Ti and Fe signals); the general shift to dry conditions in the late Holocene is associated to the southward migration of the ITCZ; therefore, during this period our study provides a new record illustrating the potential teleconnections existing between tropical Pacific and Caribbean (Atlantic) Sea climatic conditions.

Résumé

Mots-clé: ENSO, Fe, forêt andine, forêt subandine, Holocene, ITCZ, páramo, plantes aquatiques, pluviosité, température, Ti, Fe, Younger Dryas.

La zone humide de Llano Grande étudiée ici est située à 3460 m dans le Páramo de Frontino, à la terminaison nord-ouest de la Cordillère Occidentale des Andes colombiennes. Elle est idéalement située pour avoir enregistré l'influence climatique à la fois de l'Océan Pacifique et Atlantique, dans un environnement non affecté par l'homme. Cette zone humide contient un enregistrement sédimentaire continu de plus de 14 m d'épaisseur couvrant le Tardiglaciaire et l'Holocène (17,000 – 0 cal yr BP).

Cette séquence a été entièrement carottée en utilisant un appareil qui ne compacte pas les sédiments. Elle a été précisément datée par 30 analyses AMS de C^{14} qui démontrent l'absence de hiatus. La séquence peut être divisée lithologiquement en trois unités : 1) une unité inférieure d'argiles claires avec des lamines sombres, d'origine glaciaire, et datée pré-16,700 cal yr BP ; 2) une unité intermédiaire faite d'argiles organiques sombres localement riches en diatomées s'étendant environ de 16,700 à 11,400 cal yr BP ; 3) une unité supérieure faite de boue organique/tourbe, riches en filaments et fragments végétaux et à sa base en diatomées, couvrant tout l'Holocène (11,400 – 0 cal yr BP). C'est cette dernière unité qui fait l'objet de la recherche présentée ici.

Cette investigation présente pour la première fois une interprétation des variations climatiques dans l'Holocène de l'Amérique du Sud nord-occidentale avec une résolution temporelle décadale à annuelle en utilisant des proxys palynologiques et géochimiques. La recherche palynologique présentée ici couvre un intervalle de temps allant d'environ 11'500 à 4'300 cal yr BP (c'est-à-dire l'Holocène inférieur et moyen) avec une résolution temporelle d'environ 35 ans. Afin d'analyser l'évolution de la végétation pour tout l'Holocène, nos données palynologiques ont été rajoutées à celles de Velasquez (2005), qui a étudié l'intervalle allant de 4'300 cal yr BP à l'actuel avec une résolution d'environ 20 ans. Cet enregistrement palynologique peut ensuite être comparé avec les données de microfluorescence-X (µXRF) obtenues sur tout l'Holocène. Utilisant les concepts existants de ceintures de végétation (páramo, forêt andine, forêt sub-andine) et de limite supérieure de la forêt (dérivée du pourcentage de pollen d'arbres), les variations d'altitude de cette dernière peuvent être utilisées comme proxy pour estimer les changements de la température moyenne annuelle. En parallèle, les variations relatives de la végétation aquatique locale ont été utilisées pour estimer les variations de la profondeur d'eau de la lagune, c'est-à-dire comme un indicateur de précipitations dans le bassin versant de la lagune. La µXRF donne un enregistrement direct de la quantité des eaux de ruissellement dans le bassin versant avec une précision sub-annuelle, c'est donc un proxy pour les précipitations.

Après un équivalent du Youger Dryas (YD, appelé interstadiaire El Abral en Colombie) froid et humide, la base de l'Holocène devient très chaude et sèche avant de redevenir à des conditions froides et sèches vers 10'000 cal yr BP. Entre 9'500 et 7'000, un intervalle dans l'ensemble chaud et sec peut être interprété comme le « maximum thermique Holocène », bien qu'il puisse être interrompu par des intervalles plus froids (par exemple vers 8'000 cal yr BP avec un pic de sécheresse). Pendant cette période chaude, les températures étaient légèrement inférieures, mais proches, de la température annuelle moyenne actuelle. L'essentiel du reste de l'Holocène moyen jusqu'à environ 4'000 cal yr BP est beaucoup plus

froid avec des températures annuelles moyennes estimées d'environ 2°C plus basses qu'à présent. A partir d'environ 6'000 cal yr BP, les conditions deviennent beaucoup plus humides avec un pic de précipitations entre 5'000 et 4'000 cal yr BP. Entre 4'500 et 3'500 cal yr BP, les précipitations diminuent considérablement et deviennent inférieures à celles estimées pour l'Holocène inférieur et moyen. La partie inférieure de l'Holocène supérieur est charactérisée par des températures estimées d'environ 3°C plus hautes que maintenant, associées à des conditions très sèches. Depuis environ 2'500 cal yr BP, la limite supérieure de la forêt redescend considérablement et, jusqu'à environ 130 cal yr BP, l'Holocène supérieur a des températures moyennes estimées d'au moins 2°C plus basses que maintenant, avec un minimum entre environ 1'400 et 750 cal yr BP où la température pourrait être descendue jusqu'à 4°C plus bas que maintenant (comme dans le Younger Dryas). Durant les 200 dernières années, les températures sont remontées d'environ 2°C.

Par conséquent, les proxys géochimiques et palynologiques montrent que l'enregistrement de l'Holocène dans le Páramo de Frontino est marqué par des changements rapides et significatifs de température et précipitations. Les températures moyennes annuelles pourraient avoir varié (vers le haut ou le bas) de quelques degrés centigrades en moins d'un siècle. Bien que le manque d'autres études avec une résolution temporelle similaire soit un obstacle considérable, ces résultats ont été comparés avec l'information régionale existant en Amérique du Sud nord-occidentale et en Amérique centrale, afin d'essayer d'interpréter les mécanismes ayant influencé le climat du Páramo de Frontino.

Le modèle de température obtenu à partir des données palynologiques correspond en gros à ce qui est connu à l'échelle régionale. Un équivalent du YD froid est comparable aux données de la Coridillère Orientale en Colombie, du Costa Rica, du Guatémala et des Andes vénézuéliennes. Une augmentation brusque de la température marque la base de l'Holocène inférieur. Le « maximum thermique holocène » est aussi observé dans la plupart des sites utilisés pour comparaison. La partie supérieur de l'Holocène moyen est considérablement plus froide, ce qui semble se corréler avec un intervalle plus frais observé dans le bassin atlantique de Cariaco (Vénézuéla) à l'aide des températures de surface de la mer (SST). Des conditions plus froides sont aussi observées dans des sites de haute altitude au Pérou. A la base de l'Holocène supérieur, le maximum de température observé à Llano Grande ne peut pas être corrélé avec d'autres enregistrements, à l'exception de la courbe de SST dans le bassin de Cariaco qui montre aussi une augmentation. Dans la partie supérieure de l'Holocène supérieur, les conditions sont beaucoup plus froides à Llano Grande, à l'exception des 200 dernières années. Des conditions froides sont aussi observées dans la Cordillère Orientale de Colombie et dans les sites de haute altitude en Equateur et Pérou.

A cause de ses données XRF de haute résolution, le basin de Cariaco (Océan Atlantique) est à ce jour l'unique point de comparaison précis comme proxy de précipitations en Amérique du Sud septentrionale. Cette comparaison permet les conclusions suivantes : (a) pendant la partie supérieure du YD et l'Holocène inférieur, Cariaco (et d'autres sites en Amérique centrale) montrent une transition graduelle de conditions sèches vers des conditions humides, ce qui démontre la migration vers le nord de l'ICTZ à la fin de la période glaciaire. Cela contraste fortement avec le Páramo de Frontino où l'on observe une transition brusque entre un YD humide une base de l'Holocène sèche. Cela suggère que Frontino à cette époque pourrait avoir été plus sous l'influence du Pacifique ou de conditions locales et moins affecté par l'ITCZ ; (b) pendant l'Holocène moyen et supérieur, la signature des précipitations est semblable dans les deux régions, avec une diminution rapide entre environ

4'500 et 3'500 cal yr BP, une période pendant laquelle la variabilité de ENSO était très haute (ce qui est confirmé par l'analyse de série temporelle du Ti et Fe) ; la transition générale vers des conditions sèches à l'Holocène supérieur est associée à la migration vers le sud de l'ITCZ ; c'est pourquoi, pendant cette période, notre étude représente une nouvelle évidence des téléconnections potentielles existant entre les conditions climatiques de l'Océan Pacifique tropical et celles de la Mer des Caraïbes (Océan Atlantique).

Resumen

Palabras claves: bosque subandino, bosque andino, vegetación acuática, Holoceno, ENSO, ZCIT, páramo, precipitación, temperatura, Ti, Fe, Dryas Reciente.

La zona húmeda de Llano Grande estudiada en éste trabajo se encuentra situada a 3.460 msnm en el Páramo de Frontino, en la terminación noroeste de la Cordillera Occidental de los Andes colombianos. Su ubicación geográfica es ideal para registrar la influencia climática tanto del Océano Pacífico como Atlántico en un ambiente sin perturbación antrópica. Esta zona húmeda contiene un registro sedimentario contínuo de más de 14 m de longitud cubriendo el lapso temporal desde el Tardiglaciar al Holoceno (17.000 - 0 a cal AP).

La secuencia fue extraída con una sonda que no compacta los sedimentos y posteriormente datada con 30 muestras de ^{14}C (AMS) que confirman la ausencia de hiatos. La secuencia litológica comprende tres unidades: 1) una unidad inferior de arcillas claras con laminaciones oscuras de origen glaciar y datada alrededor de 16.700 a cal AP; 2) una unidad intermedia compuesta por arcillas orgánicas oscuras, localmente ricas en diatomeas extendiéndose aproximadamente desde 16.700 hasta 11.400 a cal AP; 3) una unidad superior compuesta de un barro/turba orgánica, rica en filamentos y fragmentos vegetales con una base de diatomeas que cubre todo el Holoceno entre 11.400 a cal AP hasta el presente. Esta última unidad es el objeto de éste estudio.

Esta investigación presenta por primera vez una interpretación de las variaciones climáticas en el Holoceno de América del Sur, con una resolución temporal decadal a anual empleando proxies palinológicos y geoquímicos. La investigación palinológica cubre un intervalo de tiempo que va desde 11.500 a cal AP hasta 4.300 a cal AP (es decir el Holoceno inferior a medio) con una resolución temporal cercana a los 35 años. Con el fin de analizar la evolución de la vegetación para todo el Holoceno, nuestros datos palinológicos se adicionaron a los de Velásquez (2005), quien estudió el intervalo comprendido entre 4.300 a cal AP hasta el presente con una resolución temporal de aproximadamente 20 años. Posteriormente, estos registros palinológicos fueron comparados con resultados de la microfluorescencia de rayos X (µXRF) para el mismo testigo durante todo el Holoceno. Utilizando el concepto de cinturones de vegetación (bosque subandino, andino y páramo) y de límite superior del bosque (derivado del porcentage de pollen arbóreo), las variaciones de altitud de éste última pueden ser empleados como un proxy para estimar las variaciones de la temperatura media anual. Paralelamente, las variaciones relativas de la vegetación acuática local se utilizaron para estimar las variaciones de la profundidad de la laguna (lámina de agua), es decir como un indicador de precipitación en la cuenca hidrográfica de la laguna. Los datos de µ-XRF proporcionan una estimación directa de la cantidad de agua de escorrentía en la cuenca hidrográfica con una precisión subanual, por lo tanto pueden ser utilizados como un indicador de erosión que puede ser usado para inferir regimenes de precipitación.

Después de un período frío y húmedo equivalente al Dryas Reciente (DR, identificado en Colombia como Estadío El Abra), el clima dominante a la base del Holoceno es más cálido y seco antes de volver a condiciones frías y secas cerca de los 10.000 a cal AP. Entre 9.500 y 7.000 a cal AP, un intervalo en general caliente y seco puede ser interpretado como el « máximo térmico del Holoceno », el cual presenta igualmente intervalos fríos (por ejemplo a 8.000 a cal AP acompañado con un pico seco). Durante éste periodo cálido, las temperaturas eran ligeramente inferiores, cercanas a la temperatura media anual actual. La

mayor parte del resto del Holoceno medio hasta cerca de los 4.000 a cal AP se caracteriza por ser un periodo mucho más frío con temperaturas medias anuales estimadas alrededor de -2 ºC respecto a la temperatura media anual actual. A partir de alrededor de los 6.000 a cal AP, las condiciones se tornan un poco más húmedas con un pico en los regimenes de precipitación entre 5.000 a 4.000 a cal AP. Entre 4.500 y 3.500 a cal AP, las precipitaciones disminuyen considerablemente y se tornan inferiores a las estimadas para el Holoceno inferior y medio. La parte inferior del Holoceno superior se caracteriza por temperaturas estimadas alrededor de 3ºC por encima de las actuales, asociadas a condiciones muy secas. Posteriormente, alrededor de 2.500 a cal AP, el límite superior de la línea de bosque desciende significativamente y hasta 130 a cal AP, el Holoceno superior presenta temperaturas medias estimadas al menos 2°C por debajo de la temperatura actual, con un mínimo entre 1.400 y 750 a cal AP donde la temperatura pudo haber descendido hasta 4°C por debajo de la temperatura actual (condiciones similares a las exhibidas durante la parte final del DR). Durante los 200 últimos años las temperaturas estimadas muestran un constante aumento de alrededor de los 2°C.

Los proxies geoquímicos y palinológicos muestran que en el Páramo de Frontino el Holoceno estuvo marcado por rápidos y significativos cambios de temperatura y precipitaciones. Las temperaturas medias anuales pudieron haber aumentado o disminuido de algunos grados centígrados en un periodo inferior a un siglo. Aunque la falta de otros estudios con similar escala temporal es un obstáculo considerable, nuestros resultados fueron comparados con información regional existente para la parte noroccidental de Sur América y Centro América durante el mismo periodo de tiempo, con el fin de interpretar los mecanismos que han influenciado el clima en el Páramo de Frontino.

El modelo de temperatura obtenido a partir de los datos palinológicos presenta un ajuste (similitud) significativo a los conocidos en la escala regional. Un equivalente al DR frío es comparable a los datos de la Cordillera Oriental en Colombia, Costa Rica, Guatemala y en los Andes venezolanos. Un aumento abrupto de la temperatura marca la base del Holoceno inferior. El « máximo térmico del Holoceno », es igualmente observado en la mayoría de sitios empleados en la comparación. La parte superior del Holoceno medio es considerablemente más fría, el cual puede ser correlacionado con un intervalo más frío observado en la cuenca de Cariaco (Venezuela) empleando como proxy la temperatura superficial del mar (TSM). Condiciones más frías han sido igualmente identificadas en sitios de alta altitud en Perú. Para la base del Holoceno superior, la temperatura máxima observada en Llano Grande no puede ser correlacionada con otros registros, excepto con la curva de TSM en la cuenca de Cariaco la cual muestra igualmente un incremento. En la parte superior del Holoceno superior las condiciones son mucho más frías en Llano Grande, con un incremento en los últimos 200 años. Condiciones frías han sido igualmente identificadas en la Cordillera Oriental de Colombia y en sitios de alta altitud en Ecuador y Perú.

Dado que la cuenca de Cariaco (Mar Caribe) cuenta con datos de fluorescencia de rayos X de alta resolución, éste es el único punto de comparación como proxy de precipitación en América del Sur Septentrional. Esta comparación permite inferir las siguientes conclusiones: (a) durante la parte superior del DR y el Holoceno inferior, Cariaco (y otros sitios en América Central) muestran una transición gradual de condiciones secas a húmedas que refleja la migración hacia el sur de la Zona de Convergencia Intertropical (ZCIT) al final del periodo glacial. Esto contrasta con las resultados en el Páramo de Frontino, donde se observa una

transición abrupta entre un DR húmedo a un Holoceno temprano seco. Esto último sugiere que durante éste periodo Frontino pudo tener más influencia de las fuerzas climáticas ejercidas por el Océano Pacífico o a condiciones locales y el ZCIT tuvo un efecto menor; (b) durante el Holoceno medio y tardío, las señales de precipitación son similares en ambas sitios, presentando una rápida disminución aproximadamente entre 4.500 y 3.500 a cal AP, un periodo durante el cual la variabilidad del ENSO fue muy alta (lo cual queda confirmado por el análisis de las series temporales del Ti y Fe); la transición general hacía condiciones secas en el Holoceno tardío está asociada a la migración hacia el sur del ZCIT; por lo tanto durante éste periodo, nuestro estudio representa una nueva evidencia de las potenciales teleconexiones existentes entre las condiciones climáticas del Océano Pacífico tropical y el Mar Caribe (Océano Atlántico).

Remerciements

Tout d'abord au Professeur Georges Gorin (Université de Genève), directeur de cette thèse pour avoir accepté m'accompagner dans ce chemin, pour sa disponibilité, son enthousiasme et son énorme patience.

Au Professeur Daniel Ariztegui (Université de Genève) pour ses conseils scientifiques et son aide dont j'ai toujours eu besoin.

Au Professeur César Velásquez et au Laboratoire de Paléoécologie (Université Nationale de Colombie, Medellin): merci d'avoir mis à ma disposition tout le matériel palynologique et d'accepter de co-diriger ce travail.

Au Profeseur Norberto Parra (Université Nationale de Colombie, Medellin): no hay palabras. Gracias por tu disponibilidad, tu confianza y los aportes que has hecho en mi camino de vida.

Au Professeur Henry Hooghiemstra (Université d'Amsterdam, Pays-Bas): pour avoir accepté d'évaluer ce travail (c'est un honneur), pour vos recommandations, votre générosité et disponibilité.

A Carlos Monsalve et à toute l'équipe de travail sur le terrain, mil gracias.

A Marcela Jojoa pour me fournir ses informations palynologiques qui ont aidé à compléter ce travail.

A Diego Lemus Polania pour m'avoir appris le monde fantastique de la statistique.

Au Drs Dorothy Peteet et Michael Kaplan de Lamont Observatory (Columbia University, N.Y.) pour m'avoir donné la merveilleuse opportunité d'être dans leur laboratoire.

A toutes les personnes de Lamont (Columbia University, N.Y.): Sandra Tiwari, Daniel Ruíz, Luisa, Gilma Mantilla, Hugo Oliveros, Laura, Paula et Dr Walter Baethgen.

Un grand merci au Fond National Suisse de la Recherche Scientifique (FNSNF) pour son aide financière et à la Conférence Universitaire de Suisse Occidentale (CUSO) pour sa contribution financière à l'organisation de multiples cours sur le terrain.

A Jaquelline FELLMANN pour son aide chaque fois que j'allais lui demander tout ce qui me passait par la tête.

Aux Professeurs Rossana MARTINI et Walter WILDI, et aux Drs. Elias SAMANKASSOU et Mario SARTORI pour être toujours souriants et amicaux avec moi.

A Sandra LEVAI pour sa patience et son aide de toujours pour m'y retrouver dans la bibliothèque.

Ma profonde gratitude à mes collègues de travaux pratiques pour leur aide : Dr. Guy SIMPSON, Aurèle VUILLEMIN et Camille THOMAS.

A mes collègues de 3ème étage : Cristina R, Aurèle, Matar, Muriel, Camille T., Mélanie G, Katrina, Lina, Agathe, Chloé, Mortaza, Jennifer, Jérôme, Sylvain, Camille P. et Antonio, entre autres.

A tout le personnel technique de la Section des Science de la Terre: Fréderic Arlaud, Olivier Kaufmann, François Gischig.

J’adresse mes plus sincères remerciements aux nombreuses personnes qui de près ou de loin m’ont soutenue pendant toutes ces années.

MERCI à tous et toutes mes ami(e)s pour leur compagnie et la confiance qu’ils m’ont toujours témoignée:

Mirna Donoso pour son amitié inconditionnelle et permanente.

Eleonora, Mireille-Yves-Lucas, Cristina, Maria José, Carlitos-Léo, Famille De Haller, Graziella et Giovanni, Mónica-Rosana, Muriel P., Gabriel Sánchez, Aurora-Massimo Barbieri, Aldo et Chloé A.

Stephen Wood pour m’accompagner avec son amour et sa patience.

Claude Cornaz et Alfredo Camello pour leurs conseils et encouragements.

Aux géomaticiens: Elme, Victor, Gabriel, Véro, Jessica et Julia

Aux personnes qui partagent avec moi ma passion pour le sport: les bikers, Aurélie, Mirka, Philippe,Sylvie, Nuria, Marie, Danielle, Stefy, Luis-Fabiola, Chloé.

La présence de ma mère pour m’avoir aidée à franchir les barrières physiques et temporelles; tu es toujours là.

Un grand merci à toute ma famille pour me respecter et m’encourager tout le temps.

Table of contents

List of figures

List of tables

Appendices

CHAPTER 1

INTRODUCTION

1. INTRODUCTION

1.1. General framework

Records of climate change in the Central/South American tropics are particularly important, because at these latitudes major thermal energy interchanges take place between oceans and atmosphere. Climatic events like the migration of the Intertropical Convergence Zone (ITCZ, e.g., Haug et al., 2001; Haug et al., 2003, Peterson and Haug, 2006; Yancheva et al., 2007; Wanner et al., 2008) and the El Niño-Southern Oscillation (ENSO, e.g., Thompson, 2000; Moy et al, 2002; Riedinger et al., 2002;) are typically associated with the tropics, but influence the global climate. In this respect, the high-altitude site studied here, the Páramo de Frontino, (PF) is strategically located at the northern termination of the Colombian Western Cordillera (Fig. 1), because it is exposed to the climatic influence of both the Atlantic and Pacific oceans.

Fig. 1.1. Location of study area (Páramo de Frontino).

In the last 50 years, Colombia has been one of the best studied tropical countries with respect to climate changes in the Quaternary and associated variations in the distribution of vegetation. Palynology has been the main tool for these investigations (Van der Hammen and Gonzalez, 1960a and 1960b; González et al., 1965; Van der Hammen et al., 1973 and 1980; Van Geel and Van der Hammen, 1973; Hooghiemstra, 1984; Kuhry, 1988; Thouret et al., 1996; Mommersteeg, 1998; Wille et al., 2001; Van der Hammen and Hooghiemstra,

2003; Groot et al., 2011, among others). The period since the last glacial maximum is the best covered by pollen-based records from a variety of biomes (páramo, montane forest, savana, rainforest, dry forest), which were used to unravel the dynamic history of these ecosystems (e.g., Marchant et al., 2001; 2002 and 2006). In mountain areas, the Eastern Cordillera of Colombia is best studied palaeoecologically, whereas the history of ecosystems in the Western Cordillera (where the Páramo de Frontino is located) is poorly known. Nevertheless, information about montane forests and tropical alpine grasslands (= páramos), including those of the Western Cordillera, can be found in Rangel (1995-2010) and Van der Hammen et al. (2005).

Good-quality, high-resolution palynological studies over the last 15,000 years, which can provide good proxies for climate variations, are rare in the South American tropics. Outside of Colombia, pollen records of the Holocene have been well studied in Venezuela (Bradbury et al., 1981; Rull et al., 2005; Stansell et al., 2010), Ecuador (Bakker et al., 2008; Moscol-Olivera et al., 2009; Niemann et al., 2009; Brunschön and Behling, 2010; Weng et al., 2002), Peru (Weng et al., 2006) or Central America (e.g., Leyden, 2002 and Carrillo-Bastos et al., 2010 in Yucatan; Islebe et al., 1995 in Costa Rica; Piperno and Jones, 2003 in Panama). Although Colombia probably presents the largest number of palynological publications in all tropical countries, high-resolution studies (i.e., those with a time resolution of less than 100 years) are noticeably lacking: in Colombian lowlands, Behling and Hooghiemstra (2000) studied the last 8,700 years at Loma Linda (altitude 370 m) with a time resolution of ca. 130 years and Wille et al. (2003) the last 11,000 years at Lake Las Margarita (altitude 290 m) with a time resolution of 50 years.

At high altitude, Velásquez (2005) analyzed the last 3,000 years in the Laguna de Llano Grande in the Páramo de Frontino (altitude 3460 m amsl) with a time resolution of 20 years, making it the first palynological study of Late Holocene in Colombia at decadal timescale. Other high-altitude sites have been tested by palynology in the subtropical Andes, spanning the Lateglacial and Holocene, e.g., in Venezuela (Rull et al., 2005; Stansell et al., 2010), in Ecuador (Hansen et al., 2003; Brunschön and Behling, 2010), or Peru (Weng et al., 2006). Nevertheless they lack the high-resolution aspect. Another problem in Holocene continental records is the stratigraphical continuity of the investigated intervals, which are often affected by significant hiatuses (Van't Veer and Hooghiemstra, 2000). A continuous stratigraphical sequence with proper age dating is a must for high resolution. Finally, palynological data should be supported by other proxies, such as geochemistry, sedimentary data or other organisms (diatoms, chironomids, etc.), e.g., Vélez et al. (2001).

1.2. Aims of project

The choice of the ecosystem is important. The research presented here is centered on the tropical alpine grassland (= páramo) of the Páramo de Frontino, in the Laguna Llano Grande situated at 3460 m amsl (Fig. 1). This zone is exposed to the influence of both Pacific and Atlantic oceans. It is characterized by steep environmental gradients and short spatial distances over which communities change, which makes this zone particularly sensitive to climate change. Moreover, because of its high altitude and isolation, the Páramo de Frontino

has not been affected by anthropogenic influences. For this reason, it has been studied for the past twenty years (Jaramillo and Parra, 1993; Lozano et al., 1999; Parra and Jaramillo, 1999; Velásquez, 1999b and 1999c; Velásquez, 2005; Parra et al., 2010a; 2010b and 2010c among others) The first core in LLG was taken in 1998 (LLG-1) (Velásquez and Hooghiemstra, 2010. submitted to PALBOT) on the flank of the Llano Grande depression and subsequently a second core (LLG-2) was recovered in 1999 close to the centre of the basin. The latter showed that the sampled sediments presented a continuous Holocene sequence (Parra et al., 2010b). It is in this core that Velásquez (2005) investigated the pollen record of the Late Holocene at decadal timescale.

In the framework of a research project supported by the Swiss National Science Foundation, other cores were taken in Llano Grande close to the centre of the depression. They provided further material for sedimentological, geochemical and palynological studies. The research presented here concentrates on the Early and Middle Holocene interval (ca. 11,500 - 4,000 cal yr BP), using palynology and geochemistry (microfluorescence-X or µXRF) as proxies for temperature and precipitations to decipher climatic variations at decadal timescales. In a second phase, palynological data of Velásquez (2005) over the Late Holocene are integrated and compared with the newly acquired geochemical information. This provides a full palynological and geochemical cover at decadal timescale over the last 11,500 years (i.e., the Holocene) in this strategic location of northwestern Colombia. By correlating this data at regional scale, it is hoped to better understand the mechanisms that have driven the observed climatic variations.

The palynological and geochemical data of the Late Glacial interval (11,500 - 17,000 cal yr BP) in the Llano Grande core are investigated in the framework of the same project by another Ph.D student, Carlos Monsalve, based in Medellin but also registered at the University of Geneva.

CHAPTHER 2

GEOGRAPHICAL AND CLIMATIC SETTINGS

2. GEOGRAPHICAL AND CLIMATIC SETTINGS

2.1 LOCATION

The Colombian territory is located in the northwestern part of the South American continent, near the equator. It consists of two major topographic regions: a flat zone east of the Andes, formed by the Llanos Orientales and the Amazon basin and the Andean cordilleras, which occupy the center and the west (Fig. 1.1). The Colombian Andes consist of three subparallel cordilleras crossing the country in a north-south direction: the essentially sedimentary Eastern Cordillera, the volcanic Central Cordillera and the Western Cordillera of oceanic origin (Muñoz, 2007) .

The high-mountain zone of the **Páramo de Frontino** is strategically situated in the Western Cordillera close to the Pacific and Atlantic oceans (Fig. 1.1). It is located at 6° 29' N - 76° 06' W and is part of the municipalities of Urrao, Caicedo, Abriaquí and Frontino. It covers an area of approximately 25 km^2 and stands at altitudes above 3000 meters.

The study area is surrounded by culminations exceeding 3000 meters amsl in northwestern Colombia, such as the Farallones del Citará and the Macizo de Tatamá in the south and the Cerro Paramillo in the north, all located in the Western Cordillera (Fig. 2.1). To the east, only the Páramos de Belmira and de Sonsón reach this altitude in the Central Cordillera (Velásquez, 2005).

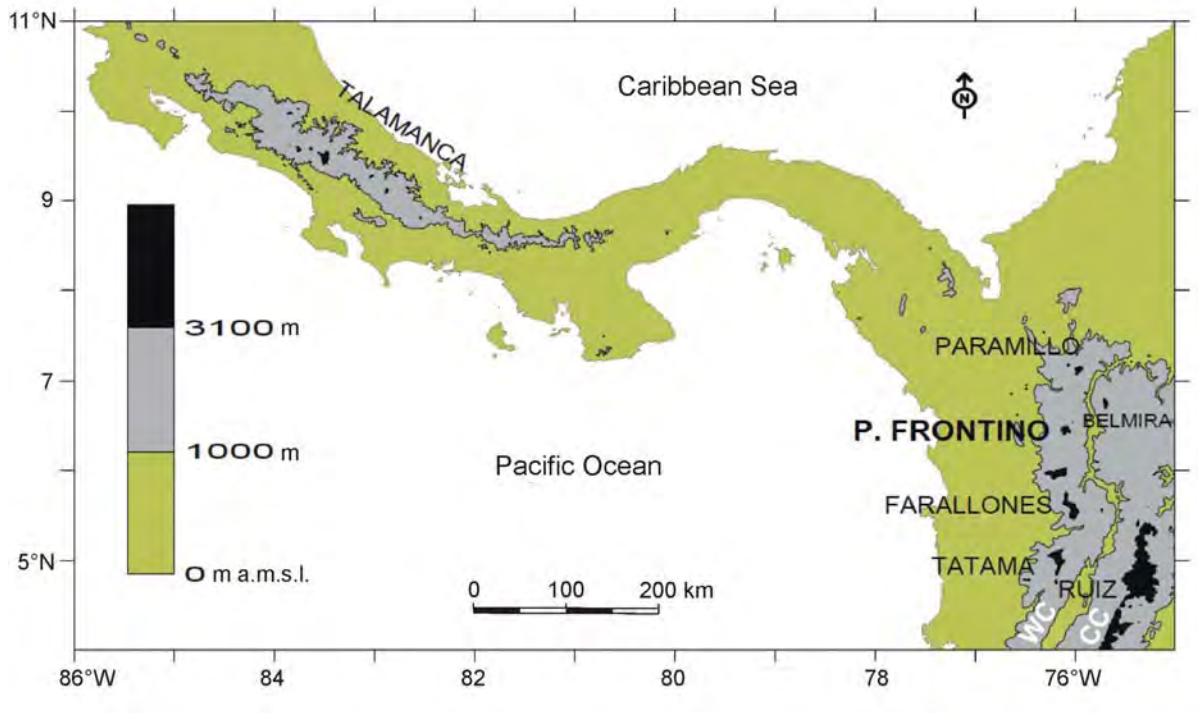

Fig. 2.1. Location of Páramo de Frontino with respect to other páramos in NW Colombia and Central America (modified after Parra, 2005). WC = Western Cordillera, CC = Central Cordillera

This study is concentrated on the **Llano Grande wet zone**, located at the extreme northeast of the Páramo de Frontino at a height of 3460 m amsl (Figs. 2.2 and 2.3). From a geomorphological point of view, the Llano Grande wet zone is situated just at the contact between the floor and the west flank of an ancient glacial valley. The latter consists of low hills separated by depressions with evidence of erosion by ice. The wet zone studied is in a deep depression carved by ice in the volcanic rocks. It is the lowest point of a local watershed where sediments supplied by the drainage basin accumulate (Parra et al., 2010a).

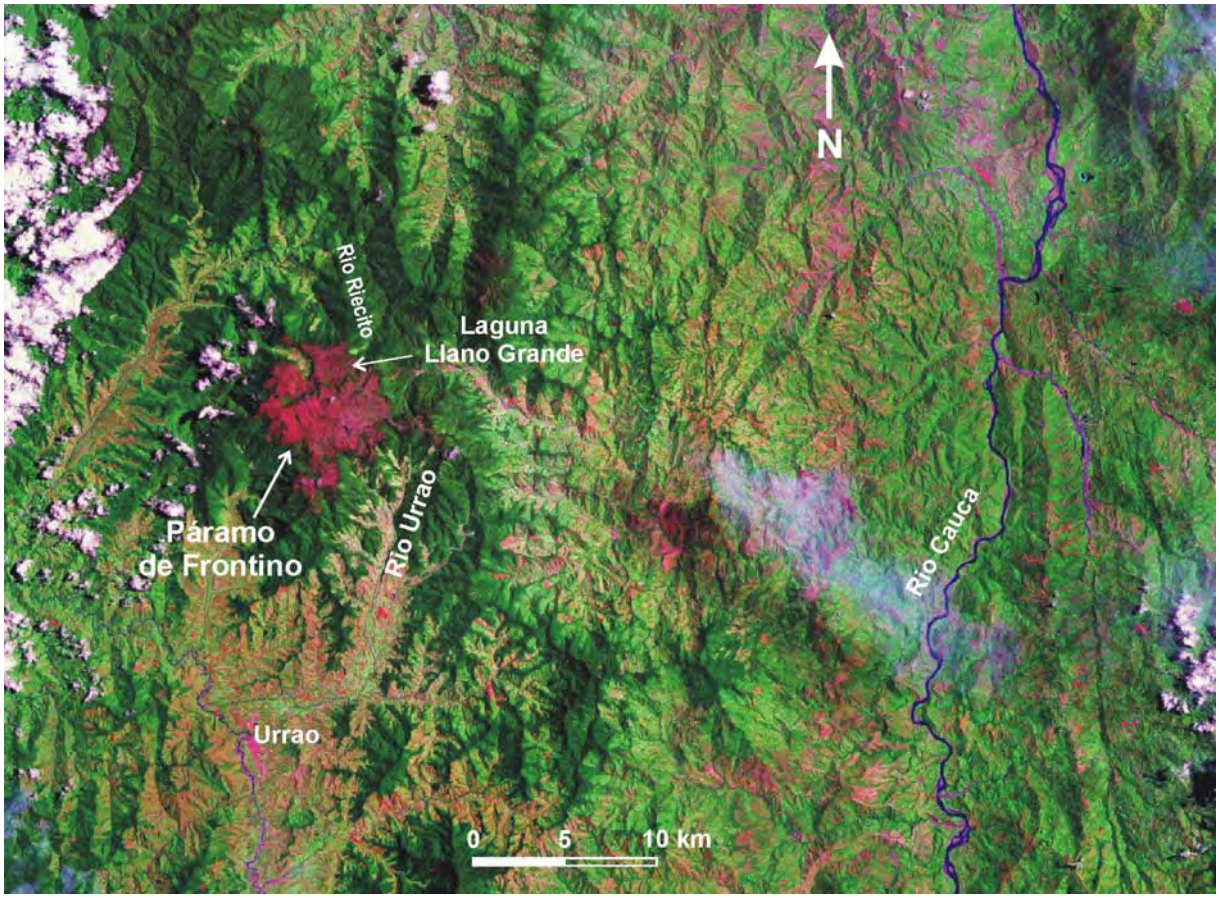

Fig. 2.2. Location of the Páramo de Frontino (red patch) with respect to the Rio Cauca and the city of Urrao (Landsat photo).

The Llano Grande wet zone is occupied by hydrophyte plants which have adapted themselfes to aquatic environments. It is surrounded by open Páramo vegetation (Fig. 2.5). The adjacent regional vegetation at lower altitudes is represented by continuous high Andean forest. High-Andean forest patches are penetrating into the páramo forming linear corridors that connect the two types of vegetation (Figs. 2.3 and 2.4).

2.2 GEOMORPHOLOGY

2.2.1. INTRODUCTION

The upper part of the Páramo de Frontino is made of a polygenic complex of volcanic rocks with ages spanning the Pliocene to Pleistocene, which was formed by the collapse of a dioritic Miocene pluton. Diorites outcrop on the slopes of the mountain in association with metamorphics developed on Cretaceous marine sediments (Parra et al., 2010a). Glacier activity have been active in recent geological history and left numerous tracks above an altitude of 2800 m amsl.

The Páramo de Frontino is considered as a cone-shaped mountain with a base at 2500 m amsl and a flattened upper zone. Within the latter, Scheibe (1933) identified major landforms such as: "llanos" or plains surrounded by ridges, isolated hills and valleys such as Puente Largo, Patio Bonito y El Pulpito. The most representative ridge is that of Campanas-Frontino elongated in an E-W direction and culminating above 3900 m amsl (Fig. 2.4). The most remarkable culmination is called La Mosca.

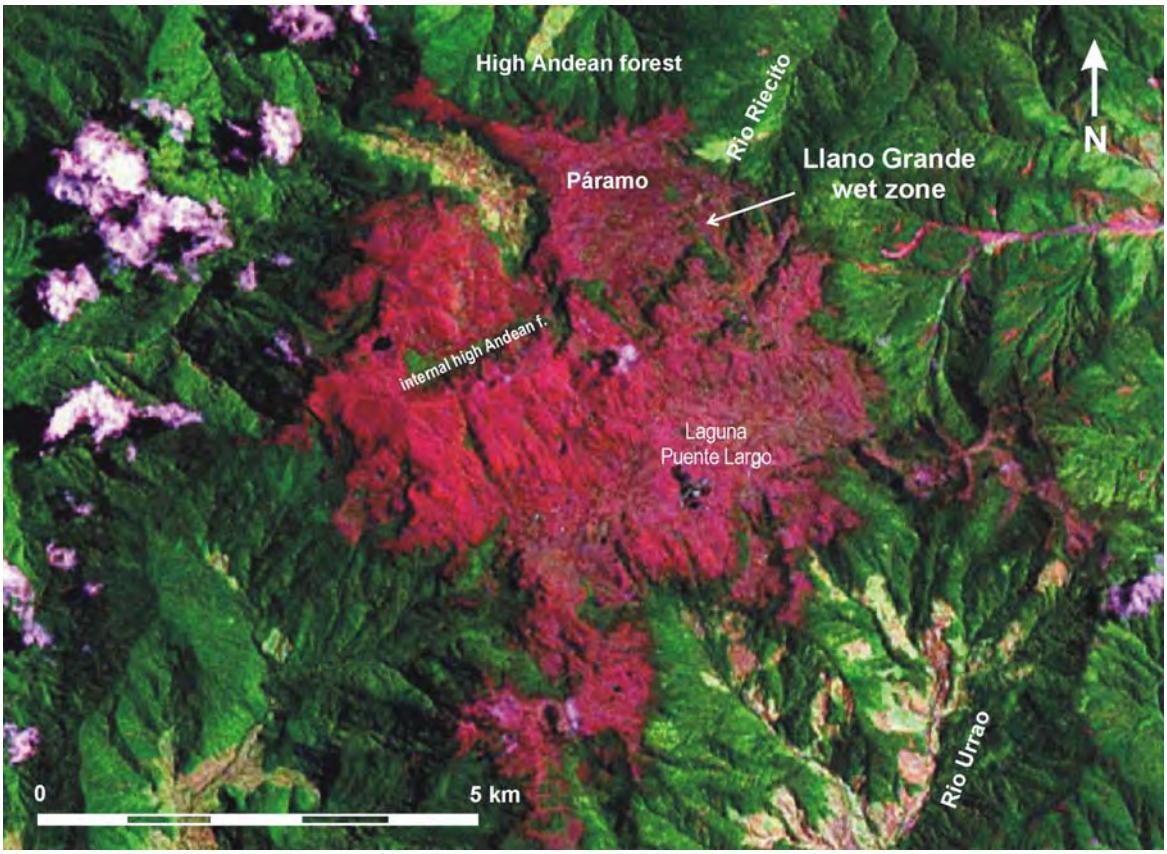

Fig. 2.3. Páramo de Frontino (enlargment of Landsat photo in figure 2.2). The studied Llano Grande wet zone is located to the NE of the Páramo. Red colour corresponds to páramo vegetation, dark-green to high Andean forest. Note the corridors of "internal" high Andean forest within the páramo (compare with figure 2.4).

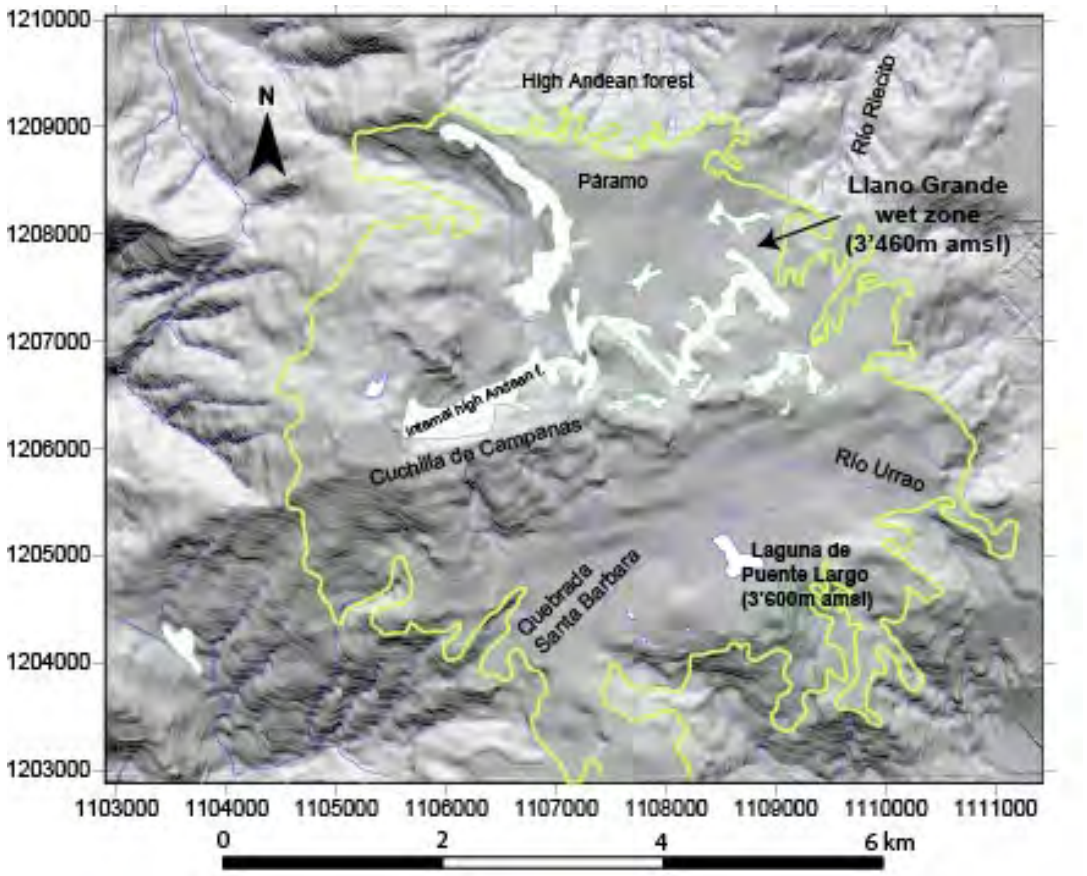

Fig. 2.4. Location of the Llano Grande wet zone in the Páramo de Frontino. The light-green line marks the limit between high Andean forest and páramo vegetation. White patches bounded by dark-green lines correspond to "internal" zones of high Andean forest (compare with figure 2.3). Planar coordinates with origin in Bogotá

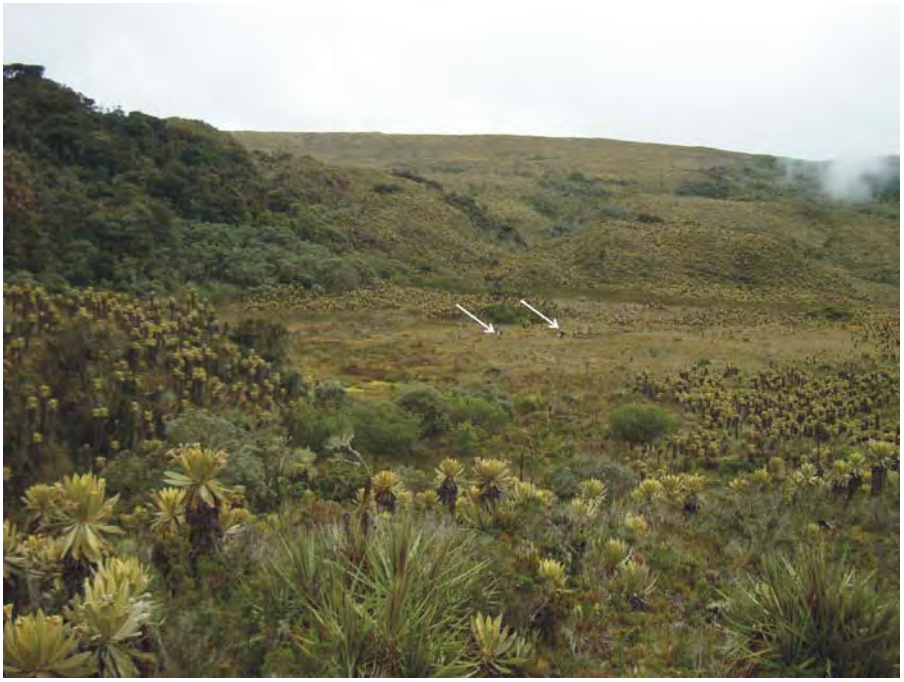

Fig. 2.5. View of the Llano Grande wet zone. Scale given by persons shown with arrows (Photo C. Monsalve).

2.2.2 GLACIAL SUBSYSTEM OF PÁRAMO DE FRONTINO

Glaciers erode landscapes and generate characteristic glacial signatures. They deposit the erosional products as distinctive landforms. In Colombia, The Páramo de Frontino is one of the best examples of evidence of glacier processes at medium scale. In the tropics, the glacial, periglacial and fluvioglacial subsystems are arranged in a vertical gradient reflected by the relative position of landforms and deposits of glaciogenic rocks (Parra et al., 2010a). The study of glacial deposits and landforms led Zuluaga and Mattsson (1981) to propose the possible existence of two glaciations.

The most detailed study of glacial processes and erosive landforms in the Páramo de Frontino was described by Parra (1991). It can be summarized as follows:

Ice-smoothed rock drumlins
In Frontino they can exist as isolated landforms of various sizes or small groups. They are found mainly in the plains and on the floor of glacial valleys. In general, these landforms are good indicators of the direction of ice advance.

Glacial valleys
The following types can be distinguished:

- *Flat-floor glacial valleys with steep flanks:* their longitudinal profile is marked by depressions filled with wet zones and rocky cross bars. The altitude of these valleys does not exceed 3200 m amsl.
- *U-shaped parabolic glacial valleys:* They are valleys that descend down to lower altitudes. They are present in the valleys of Santa Barbara, El Burro and the Río Urrao.
- *Alpine glacial valleys:* They are located above 3400 m amsl and present a cirque that continues with a short glacial valley where small lakes can be present. Some of these alpine glacial valleys can be suspended and cut across the parabolic glacial valleys.
- *Combined glacial valleys:* They are characterized by a superposition of the landforms described above.

Drumlin fields
They are plains formed by the action of a slow-moving ice cap. Locally referred to as savannah, they present a rugged surface occupied by open vegetation of páramo grasslands. They consist of a combination of hills carved directly in the bedrock and depressions adjacent to one another, which do not automatically correspond to the glacial valley floor. In these plains, traces of moraines and erratic blocks are common. The most extensive savannahs are Puente Largo, San Juan de Rodas, Patio Bonito and El Pulpito. The depressions are occupied by swamps, shallow lakes or flat areas. The **Llano Grande wet zone** studied here is one of them (Fig. 2.5).

Glacial and fluvioglacial deposits
In the plains and glacial valleys of the Páramo de Frontino, it is possible to identify remains of glacial deposits (Zuluaga and Mattsson, 1981). In the low plains surrounding the massif there are multiple levels of fluvioglacial deposits produced directly by melt water from glaciers and other sediments reworked by actual current river action. In areas above 3000 m amsl,

sediments have been deposited directly by glaciers. In particular, depressions like the **Llano Grande wet zone** are likely to have been partially filled by glacial deposits.

2.3. CLIMATE

2.3.1. REGIONAL CLIMATE

2.3.1.1. Introduction

The northern Andes are characterized by a very moist climate, low thermal seasonality, and marked diurnal temperature variations. Temperature variation is driven by altitude gradients and air humidity, both determined by local conditions (Buytaert et al., 2006). The near-surface environmental lapse rates (i.e., the decrease in air temperature with elevation) produce strong ecological zonation with respect to altitude. These lapse rates may show differences between eastern and western slopes of the Andes and between different flanks of inter-Andean valleys (Chaves and Jaramillo, 1998; Ruíz et al., 2009). Frost and snow occur regularly at elevations above 4000 m amsl. Precipitation patterns are influenced by the tropical Atlantic Ocean, the Pacific Ocean and the Amazon basin (Martínez et al., 2011). Although rainfall is highly variable, pluviometric optimum maxima are observed at elevations of around 1800-2400 m (Oster, 1979; Vélez et al., 2000), an interval that harbours dense cloud forests.

The Andean region of Colombia is considered as a rain shadow or ‘‘dry island’’ surrounded by precipitation induced by the orographic uplift of Atlantic and Pacific winds (López and Howell, 1967). Precipitation in western Colombia is strongly influenced by the strength of the southeast trade winds which, north of the equator, are deflected eastwards towards the continent, i.e., the Choco Jet which enters the continent at ~5°N carrying large amounts of moisture (Martínez et al., 2003).

The climate of the Colombian Andes can be classified as tropical diurnal showing in average small differences of less than 3 $^{\circ}$C over the year, but daily fluctuations of the order of 20 $^{\circ}$C. The heaviest orographic rainfalls are present in the Chocó region (> 7000 mm/year) due to its proximity to the Pacific Ocean and the rapid topographic elevation of the Western Cordillera. In the Eastern Cordillera the highest rainfalls occur over the eastern flank facing the eastern plains. The concave shape of the Eastern Cordillera acts as a natural receptor of moisture that comes from the Atlantic Ocean with the trade winds. The weakest rainfalls are generated in low-altitude areas of the Magdalena Valley and inter-Andean plains (Kuhry et al., 1983). In the Andean region, the air temperature regime is characterized by the presence of thermal layers, marked by the decline in average temperature with respect to altitude. The average decrease with altitude is of about 0.6 $^{\circ}$C per 100 m (IDEAM, 2001)

Colombia's climate is influenced by multiple factors which interact with each other such as microclimatic phenomena determined by the topographic characteristics of every region and macroclimatic phenomena including the ITCZ, ENSO, Mesoscale Convective Systems (MCSs), jet stream of Choco (CHOCO), eastern Pacific, Quasi-biennial Oscillation, Maden –

Julian Oscillation and North Atlantic Oscillation (NAO) (Mesa et al., 1997). At decadal or interdecadal timescales the climate is mostly influenced by the Pacific Decadal Oscillation (PDO) (Martínez et al., 2011). Among all these macroclimatic events, we describe in the text only ITCZ and ENSO, which will be used extensively in the discussion. A more detailed presentation of all the macroclimatic phenomena at regional scale can be found in Appendix A1 (Regional climate).

2.3.1.2. Macroclimatic phenomenas (ITCZ, ENSO)

SEASONAL VARIABILITY: ITCZ

The ITCZ is a circum-global atmospheric belt of intense moist convection and rainfall, marking the confluence of the northern and southern trade winds and the rising branch of the Hadley cell (Koutavas and Lynch-Stieglitz, 2005). The displacement of the ITCZ and the action of physical-geographical regional factors, such as orography, determine the rainfall in Colombia.

The Atlantic ITCZ marks the dynamic boundary between the southeast and northeast Atlantic trade winds and is associated with a well organized zonal band of low pressure and high precipitation that occurs predominantly over the ocean basin and extends from South America to the west coast of Africa. Convection associated with the seasonal migration of the ITCZ plays a major role in controlling the patterns of rainfall over the adjacent continents (Hastenrath and Heller, 1977; Poveda and Mesa, 1997).

The hydrological annual cycle in tropical South America is largely controlled by the meridional oscillation of the ITCZ, though spatial variability is introduced by the presence of the Andes and the Amazon River basin, by the surrounding tropical Pacific and Atlantic oceans, and by land-atmosphere feedbacks (Poveda et al., 2001).

Due to the strong linkage between variations in atmospheric and oceanic conditions, the position of the ITCZ follows a seasonal cycle, with an abrupt shift from its northernmost position during boreal summer to its southernmost position during austral summer (Fig. 1.1). These variations of the ITCZ affect the rainfall distribution in equatorial and tropical regions, resulting in alternating wet and dry seasons (Hessler et al., 2010). Far from the equator the dry season (winter) is severe and the rainy season (summer) short. Near the equator, two short dry seasons occur (Ruddiman, 2001).

The annual migration of the ITCZ is influenced by the distribution of land and ocean (Srinivasan and Smith, 1996; Hessler et al., 2010). Over the ocean the ITCZ is well defined by the combination of convergence of trade winds and subsequent convection and heavy rainfall. Over land, the southern oscillation of the ITCZ across the equator responds to the seasonal insolation cycle and the near-surface convergence and convection become widely separated during the season of maximum excursion (northern or southernmost ITCZ position (Hessler et al., 2010).

In Colombia and neighbouring areas of the eastern Pacific Ocean, the ITCZ reaches its extreme meridional position between the months of January and February at about 2°N. Between March and May, the Pacific segment of the ITCZ moves to the north and is positioned between 2–7°N. The continental band joins the segment of the Atlantic Ocean between March and April to form a single system that is located between 5° S and 1°N in the east of the country. These two segments are joined by poorly organized convective zones on the Andean region. Initially, between June and August, the Pacific segment is located near 8°N and ends at 10° N, entering the Caribbean region. The continental segment has a SW-NE orientation over the Colombian territory, and moves towards the north through Ecuador up to 8°N. Between September and November, the Pacific segment begins its movement south to reach between 7-11°N. The continental band also begins moving towards the south from 8°N towards the Ecuador over the Orinoco and Amazon, slowly losing its inclination to coincide with the parallels. In this case, the two segments of the ITCZ are joined by convective zones (IDEAM, 2001).

Forcing during the northern hemisphere summer, when the ITCZ is in its northern position results in La Niña-like conditions and, conversely, forcing during winter, when the ITCZ is in its southern position, results in El Niño conditions (Clement, 1999).

INTERANNUAL VARIABILITY: ENSO

Using the established definitions, El Niño is the warm ocean current frequently (every 3–4 years) observed in the eastern equatorial Pacific off the coast of Ecuador, and the Southern Oscillation (SO) refers to the varying bi-polar nature of atmospheric pressures in the western Pacific (low pressures) and the South Pacific sub-tropical anticyclone (Waylen and Poveda, 2002). It has a time scale of 2-7 years.

The general suite of environmental conditions associated with the two mean states has become known as El Niño (deepened thermocline in the eastern Pacific) and La Niña, anti-El Niño or El Viejo (shallower thermocline in eastern Pacific). Because the exact state of each unstable mean condition varies, no universally accepted definition of El Niño and La Niña can exist in terms of the dominant factors of sea-surface temperatures (SST) and atmospheric pressures (Waylen and Poveda, 2002).

ENSO is the main forcing mechanism of Colombia's hydro-climatology at interannual timescales (Waylen and Poveda, 2002). Overall, during El Niño events, Colombia experiences droughts (reduced rainfall, soil moisture and river discharges) and higher evaporation, along with an increase in air temperature. The reverse is generally valid for La Niña. The impact of ENSO occurs earlier and is stronger in western and central Colombia than in the east (Poveda et al., 2001).

2.3.2 LOCAL CLIMATE

The topography of Colombia is an important factor which influences the behavior of the climate. The altitudinal differences between the three cordilleras allow the ascent of air masses that affect temperature, moisture and other elements. It causes an asymmetry in the climatic zones between the western and eastern slopes in every cordillera (Thouret and Pérez, 1983). Local circulations caused by differential transformation of solar radiation affect local climate variability. They cause the rise of air masses from the valleys to the slopes during the day, resulting in precipitations at a given height (condensation belts). At night, the movement is opposite (Oster, 1979).

In general, Colombia's páramo climate is cold and wet with sudden weather changes. Often there is the presence of fog, rain and strong winds with diurnal cyclicity. According to Vareschi (1970), the determinant weather factors in the high Andes mountains are the following:

- *Atmospheric pressure*: At higher levels the pressure is low; the air has less water vapor and is more permeable to radiation.
- *Radiation:* It increases with the altitude; it is controlled by the intensity of the fog and is converted into heat by the plants and soil.
- *Cloudiness:* Its maximum values are present in zones of condensation located at the boundary between the high Andean forest and páramo.
- *Winds:* their frequency and intensity increase with altitude.

According to Rivera (2001), the equatorial zone of the Andes presents an altitudinal zonation characterized by a decrease in average temperature of about 0.6 °C per 100 m, with a slight difference from 0.52 º C on the western side to 0.66 º C on the eastern side. At 4800 m amsl it shows a nearly constant 0 ° C isotherm.

Detailed climatic conditions in the Páramo de Frontino are still little studied. There are no weather stations on the Páramo and data comes either from spot observations or from weather stations surrounding the Páramo (Fig. 2.6).

The Páramo de Frontino is located at the northwestern end of the Western Cordillera and is equidistant from the Pacific and Atlantic oceans. It is exposed to currents of humid air from the Caribbean Sea to the north, the Pacific and the Atrato from the West (Ospina, 1973) . Because of the topographic barrier of the Western Cordillera, the latter produce a high source of precipitation (García and Londoño, 1984). Therefore, the western slopes are characterized by wetter conditions with precipitations values close to 7000 mm/ year while the eastern slopes have a drier climate with values between 1000-2000 mm / year (Arellano and Rangel, 2008).

There are some reports in the literature about temperature and precipitations in the Páramo de Frontino:

- For Espinal (1992) the Páramo de Frontino comprises the following life zones: premontane wet forest, lower montane wet forest, lower montane rain forest and montane rainforest. It

is characterized by a mean annual bio-temperature of between 6-12 °C and a higher annual average rainfall of 2000 mm.
- For Rangel and Aguilar (1995) the mean annual temperature is 4.6°C, the mean annual maximum 10.5 °C and the mean annual minimum – 1.9 °C.
- The IGAC (Instituto Geográfico Agustín Codazzi) assigned to this zone a mean annual temperature range between 4 and 12 °C and two different values of mean annual precipitations: from 3000 to 4000 mm on the western slope and of about 3000 mm for the eastern slope (Jaramillo and Parra, 1993).
- Velásquez (2005) estimates for the Páramo de Frontino at 3460 m amsl (location of studied cores) and 3600 m amsl that annual rainfall could average between 3000 and 4000 mm/year. The same author has evaluated the mean soil surface temperatures in the páramo between 3100 and 3600 m amsl. At 3400 m amsl, close to the level of the studied Llano Grande location (at 3460 m amsl) a value of 8.3°C has been evaluated,
- The average relative humidity is about 85% and monthly evaporation of 81.8 mm (Rangel et al., 1999).

In the framework of this project, meteorological data from reference stations around the Páramo have been obtained from the IDEAM (Colombian Institute of hydrology, meteorology and environmental studies) and studied in detail by Monsalve (2011). The main data are presented below (Fig. 2.6).

a) Temperatures

Using the average monthly temperature observed in the reference stations, estimates for the lower (IL) and upper limit (UL) of the Páramo de Frontino (Table 2.1**)** can be calculated using the Chaves and Jaramillo's equation (1998). Variations in average monthly temperature are therefore minimal, although the differences between day and night temperatures are considerable (Monsalve, 2011).

b) Precipitations

The annual amounts of precipitation can be estimated for the different vegetation belts:
- The high Andean forest receives 1703 mm/year with a multi-year monthly average of 142 mm and the rainfall distribution regime most often repeated is of the bimodal-four-seasonal type.
- In the subpáramo, the annual amount is of 1716 mm/year with a monthly average of 143 mm and a multi-year distribution regime of biseasonal unimodal type.
- In the páramo the records are of about 1644mm/year with a multi-year monthly average of 137 mm and a distribution regime of biseasonal unimodal type.

The annual amount of precipitation for eight reference stations near to Páramo de Frontino recorded on the western and eastern slopes of the Western Cordillera are presented in table 2.2 (Arellano and Rangel, 2008; Monsalve, 2011).

At annual scale, the months of January and February (in some cases until March) are the driest of the year (ITCZ to the south). The second dry period lasts from June to July, with August to September a little rainy (ITCZ to the north). The highest rainfall months are usually

April, May and October, coinciding with the northward/southward progression of the ITCZ. However it is not clear which one of the two periods is the most rainy one of the annual cycle. On the eastern slopes of the Western Cordillera, rainfall decreases. There, the change between wet and dry periods is tenuous, and does not show abrupt changes at monthly scale. To the north, the mean values of precipitation are higher, and dry periods (December to March, June-August) are more rainy. To the south of the páramo, the wet and dry periods show a similar behavior with a single rainy season from April to November, with a substantial rainfall during the "Indian Summer" in July (Monsalve, 2011).

Station	Altitude (amsl)	Jan	Feb	Mars	April	May	June	July	August	Sep	Oct	Nov	Dec	Annual average
Abriaquí	1920	16,2	16,3	16,5	16,5	16,7	16,5	16,4	16,3	16,2	16,2	16,3	16,2	16,4
Caicedo	1725	17,3	17,4	17,6	17,6	17,8	17,6	17,5	17,4	17,3	17,2	17,4	17,3	17,5
Guasabra	2128	15,1	15,1	15,3	15,4	15,5	15,3	15,2	15,2	15,0	15,0	15,1	15,1	15,2
La Clarita	2150	17,3	17,4	17,6	17,6	17,8	17,6	17,5	17,4	17,3	17,2	17,4	17,3	17,5
La Honda	1850	16,6	16,7	16,9	16,9	17,1	16,9	16,8	16,7	16,6	16,5	16,7	16,6	16,8
Giraldo	1973	15,9	16,0	16,2	16,2	16,4	16,2	16,1	16,0	15,9	15,9	16,0	15,9	16,1
Urrao	1850	17,1	17,2	17,5	17,5	17,5	17,5	17,3	17,3	17,1	16,8	16,9	17,0	17,2
Páramo (LL)	3400	7,9	8,0	8,2	8,2	8,4	8,2	8,1	8,0	7,9	7,9	8,0	8,0	8,1
Páramo (UL)	3930	5,0	5,0	5,2	5,3	5,4	5,3	5,1	5,1	4,9	4,9	5,0	5,0	5,1

Table 2.1. Mean monthly temperature (ºC) for different stations and estimations for the Páramo de Frontino using Chaves and Jaramillo's equation (1998). See location of stations in Fig. 2.6

Municipality	Station	Latitude N	Longitude W	Altitude (amsl)	Annual precipitation (mm)	Period
Abriaquí	Abriaquí	6°38'	76°4'	1920	2171,19	(1975-2009)
Frontino	La Clarita	6°32'	76°9'	2150	3276,93	(1978-2009)
Caicedo	Caicedo	6°24'	75°58'	1725	2001,64	(1970-2009)
Santa Fé de Antioquia	Guasabra	6°30'	75°57'	2128	1564,05	(1975-2009)
Urrao	La Honda	6°21'	76°9'	1850	1686,64	(1990-2009)
Urrao	Urrao	6°19'	76°8'	1850	1905,75	(1969-1972)
Giraldo	Giraldo	6° 41'	75° 57'	1973	1809,890148	(1971-2009)
Urrao	Mandé	6° 26'	76° 21'	495	3599	(1978-1998)
Urrao	El Sireno	6° 23'	76° 14'	1210	1896	(1978-1998)
Urrao	Santa Barbara	6° 24'	76° 24'	2595	2044	(1978-1998)
Santa Fé de Antioquia	Cañafisto	6° 25'	76° 49'	500	1049	(1988-2000)
Caicedo	La Noque	6° 25'	75° 59'	1750	1831	(1980-1985), (1989-2002)

Table 2.2. Annual amount of precipitations on the western and eastern slopes of the Cordillera (Arellano and Rangel, 2008; Monsalve, 2011). See location of stations in Fig. 2.

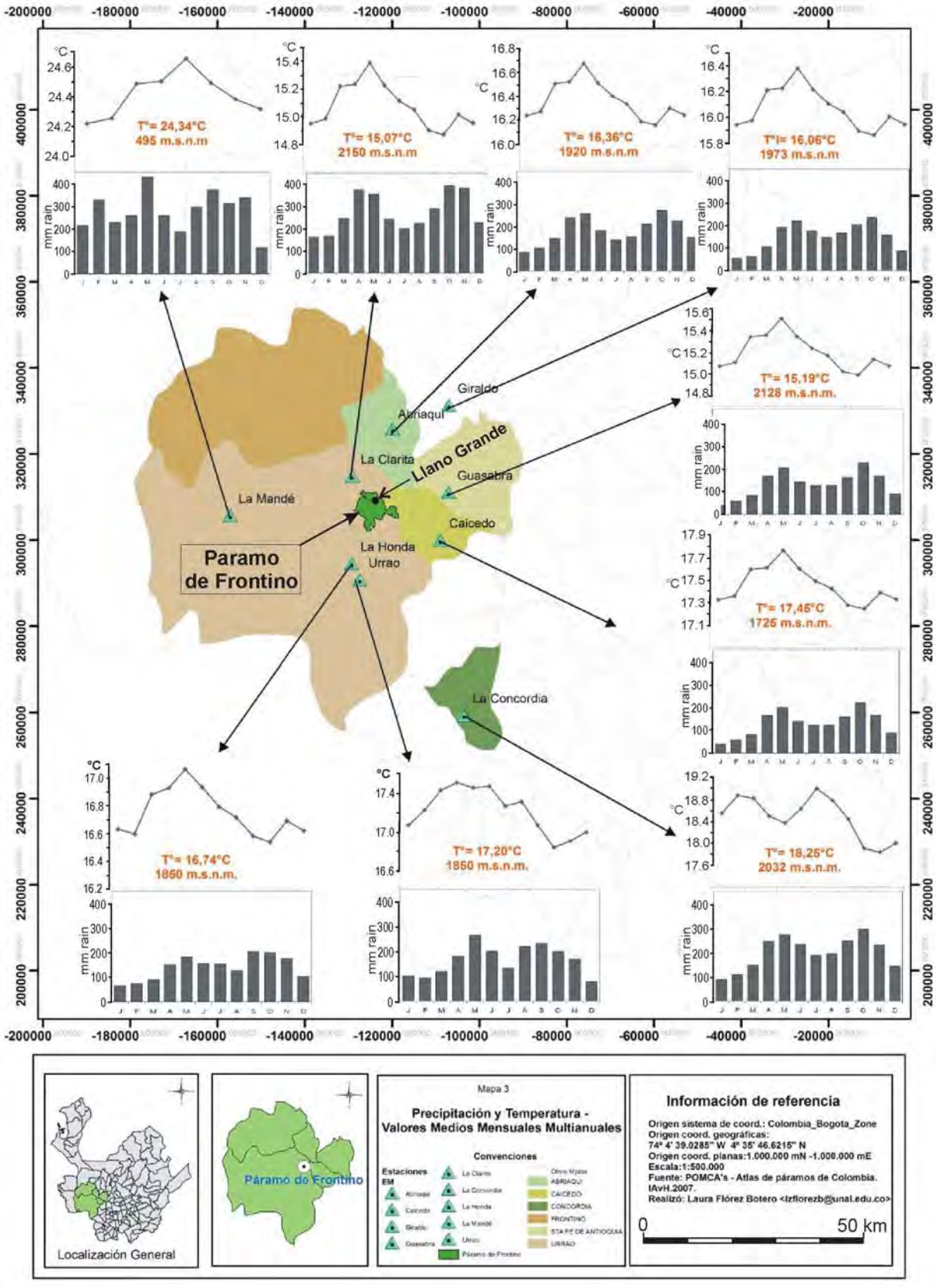

Fig. 2.6. Annual cycle of precipitations and temperature at nine weather stations surrounding the Páramo de Frontino (modified after IDEAM and Monsalve, 2011).

This annual picture is further affected by the Niño and Niña phenomena. During Niño phases, rainfall in northwestern Colombia decreases by 22.5%, whereas it increases by 17.3% during la Niña phases (Mejía et al., 1999) with the western flank of the Cordillera receiving the most.

To summarize, no precise present-day meteorological data are available at the location of the Llano Grande wet zone studied in this research (at 3460 m amsl). Nevertheless, from all the information presented above, the following can be stated: at present-day, the Llano Grande zone studied has a mean annual temperature of ca. 8.3°C, annual precipitations between 2000 and 3000 mm/year and is quite prone to the influence of solar radiations.

2.4 PRESENT-DAY VEGETATION

The present-day vegetation in the Páramo de Frontino shows a clear response to climatological variables that change along the altitudinal gradient. From low to high elevations different vegetations belts can be recognised. These vegetation belts have temperature constraints and, in response to global climate change, have migrated along the altitudinal gradient during the Holocene (Van der Hammen, 1974; Van der Hammen and González, 1960b).

The general altitudinal distribution of vegetation in the northern Andes was characterized by Van der Hammen (1974). The main vegetation belts used in this research have been studied by Cuatrecasas (1958), Van der Hammen and González (1960a; 1960b and 1963), Van der Hammen (1974), Lozano and Schnetter (1976), Sturm (1978), Van der Hammen et al. (1980), Cleef (1981), Rangel et al. (1982), Rangel and Lozano (1986). The altitudinal range of the main vegetation belts may slightly differ between the dry and wet sides of the mountains, between the Eastern and Western cordilleras, and between northern Colombia, central Colombia (Cleef and Hooghiemstra, 1984) and southern Colombia (Wille et al., 2001). The páramo vegetation in the Western Cordillera has been investigated by Rangel et al. (1999) and Cleef et al. (2005). In the Páramo de Frontino it has been studied by Espinal et al. (1983), Sánchez (1998), Rangel et al. (1999) and Sánchez (1999).

Many taxa show similar altitudinal ranges and justify the recognition of general vegetation zones (or vegetation belts), characterized by suites of taxa that co-occur and form identifiable plant associations (Bogotá-Angel et al., 2011). The vertical distribution of vegetation belts in the Páramo de Frontino is summarized in Fig. 2.7 (after Velásquez, 2005). Characteristic taxa found in the pollen record are mentioned in parentheses below:

Sub Andean forest (SF) from ~1000 to 2100 m amsl (*Acalypha, Alchornea, Billia colombiana, Bignoniaceae, Cecropia, Celtis*, Euphorbiaceae, Meliaceae, Mimosaceae, Palmae, *Pilea, Piper,* Sapotaceae, *Trema*, Urticales). This group corresponds to the “Lower montane forest” of Groot et al. (2011)

Andean forest (AF) from 2100 to 3450 m amsl: *Alnus, Bocconia, Clethra,* Cyatheaceae, *Drimys, Escallonia, Eugenia*, *Gaiadendron*, *Hedyosmum, Hesperomeles, Ilex, Juglans*, Melastomataceae, *Miconia, Morella, Monnina*, *Myrsine, Podocarpus, Prunus, Quercus, Weinmannia*, *Vallea*. This group incorporates the Andean and high Andean forest groups of Velásquez (2005). It corresponds to the "Upper montane forest" of Groot et al. (2011).

Subpáramo (SP) from 3450 to 3550 m amsl: Compositae Tub., Ericaceae and *Polylepis.*

Páramo (P) from 3550 to 4100 m amsl: *Aragoa*, Caryophyllaceae, Compositae Lig., *Coprosoma,* Gentianaceae, *Geranium*, *Gunnera, Hypericum, Loricaria, Lupinus, Lycopodium's foveolada spore (Lycopodium foveolata in this work) Paepalanthus, Peperomia,* Poaceae*, Puya, Rubus*, *Rumex*, Scrophulariaceae, *Xyris, Valeriana*.

The transition from SF to AF is mainly determined by the occurrence of night frost (in particular during the dry season), the AF-SP limit reflects the upper forest line (UFL, Fig. 2.7) and its altitudinal position is driven by mean annual temperature (MAT) and at longer timescales also by changing atmospheric *p*CO2 (Groot et al., 2011). The altitudinal position of the transition from shrubby SP to herbaceous P is related to the increase in Poaceae and *Espeletia* populations.

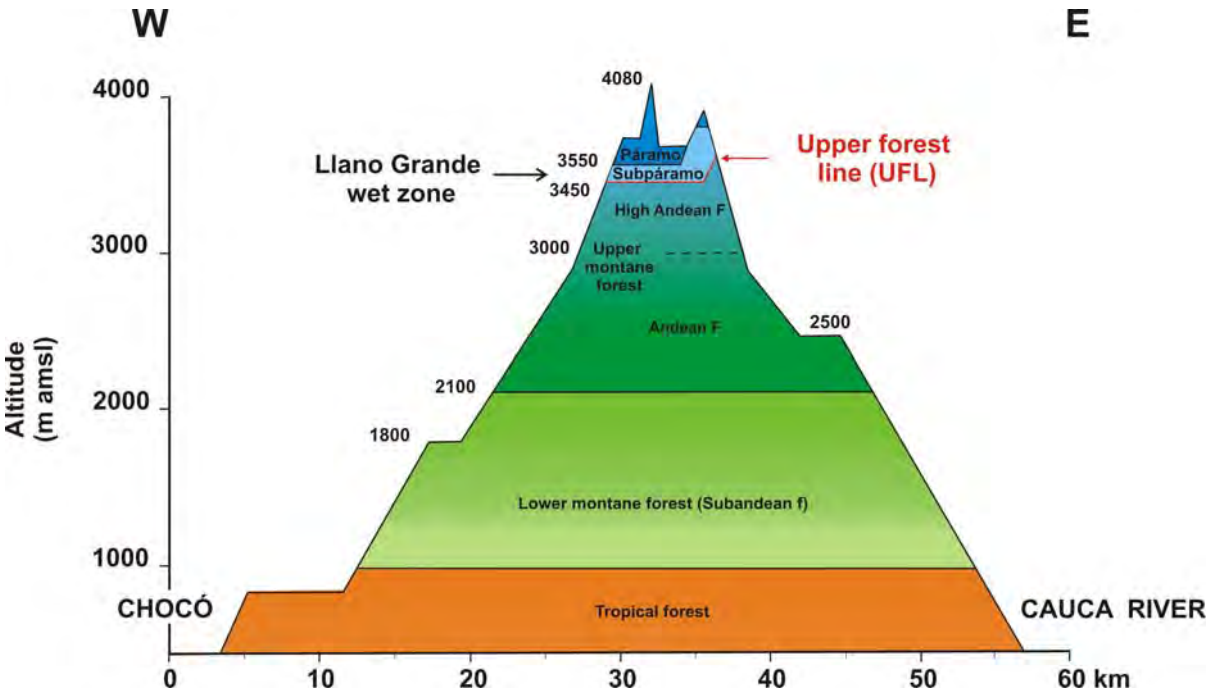

Fig. 2.7. Summarized vertical distribution of present-day vegetation belts in the Páramo de Frontino (modified from Velásquez, 2005). Location of Upper Forest Line.

Climatic change affects every single taxon. However, because ecological envelopes of many taxa are similar (Wille et al., 2001; Bogotá-Angel, 2011), present-day main vegetation belts tend to respond as a whole. But when some taxa do not respond to climate Climatic change affects every single taxon. However, because ecological envelopes of many taxa

are similar (Wille et al., 2001; Bogotá-Angel et al., 2011), present-day main vegetation belts tend to respond as a whole.

But when some taxa do not respond to climate change in the same way as the overwhelming majority of taxa, this causes a change in the the taxonomic composition when the main vegetation belts migrate vertically. Therefore, pollen records reflect frequently plant associations without modern analogs (e.g. Van der Plas et al., 2011). Consequently calibration of past plant associations to modern undisturbed vegetation must be carried out with care.

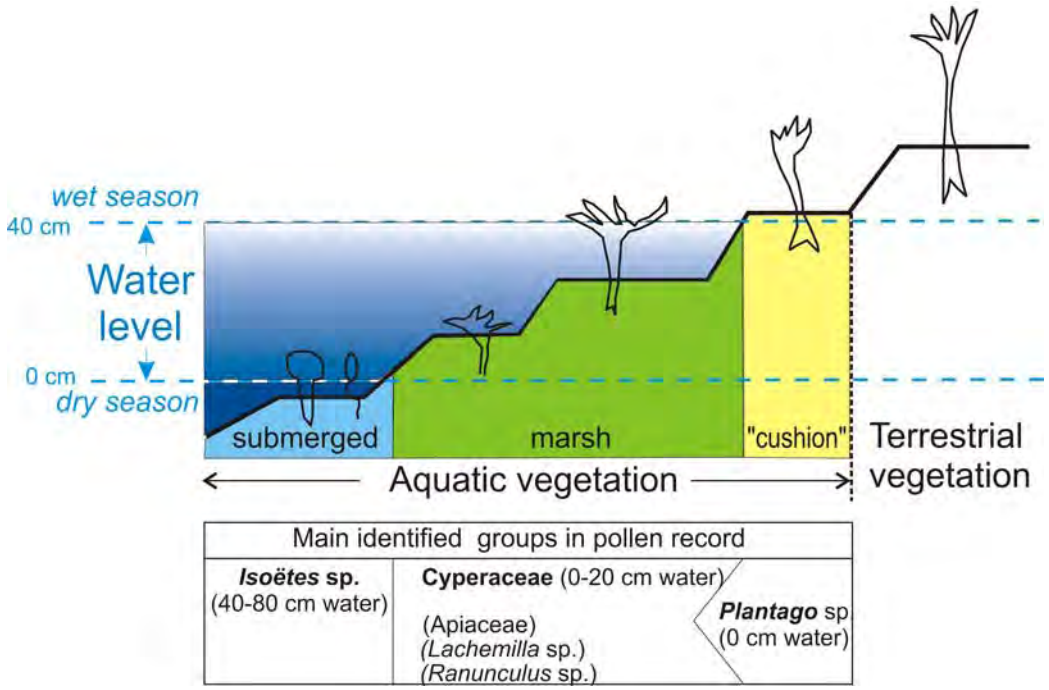

Fig. 2.8. Environmental distribution model of aquatic vegetation in the Llano Grande wet zone (modified from Parra et al., 2010c)

Water level changes in a lake or a peatbog can be reconstructed on the basis of changing proportions of plants belonging to the local hydrophile group (see Espinal et al., 1983; García and Londoño,1985; Sánchez 1998 and 1999; Van 't Veer and Hooghiemstra, 2000; Torres, 2005; Bogotá-Angel, 2011). In the Páramo de Frontino the following ecological groups can be used to establish a spatial zonation from submerged to emergent zones (Parra et al., 2010c): submerged plants (*Isoëtes*), cushion plants in shallow water (*Plantago, Lysipomia*), and plants from marshy shores (Apiaceae (mainly *Hydrocotyle*), *Juncus*, Cyperaceae (*Carex, Eleocharis, Luzula, Rynchospora, Scirpus*), *Ranunculus*, *Lachemilla*. Spores from pteridophyta, bryopyta, and fungi, as well as algal colonies are less specific for establishing such a zonation.

CHAPTER 3

METHODS

3. METHODS

3.1 CORING AND SAMPLING

LLG peatbog fills a subcircular depression of over 100 m in diameter (Figs. 3.1 and 3.2). Because of its high altitude and isolation, the Páramo de Frontino it does not exist clear evidence of anthropogenic influences. For this reason, it has been scientifically studied since more than ten years (Parra, 1991; Jaramillo and Parra, 1993; Flórez and Parra, 1999; Lozano et al., 1999; Parra and Jaramillo, 1999; Rangel et al. 1999; Sánchez, 1998 and 1999; Velásquez, 1999b and 1999c; Parra, 2005, Velásquez, 2005; Parra et al., 2010a; 2010b and 2010c).

The first core LLG-1 was taken in 1998 and showed that the sampled sediments presented a fairly continuous Holocene sequence. A depth survey was later carried out and showed that LLG-1 was drilled on the flank of the basin. Subsequently, core LLG-2 was recovered in 1999 closer to the centre of the basin (Fig. 3.2). This core LLG-2 has been thoroughly studied and provided a facies model for the deposition of sediments in the LLG basin (Parra, 2005; Parra et al., 2010a and 2010b). Its upper 2.2 m (corresponding to ca. the last 4,000 years) have been analyzed through high resolution palynology by Velásquez (2005). Between 2006 and 2010 cores LLG-3 to LLG-9 were further recovered in the central part of the basin (Fig. 2.2). Together with LLG-2 they provided the material used in this study.

Cores were recovered using a “Russian” corer. This sampler has been designed by Russian research workers and described by Jowsey (1966).This device has the great advantage of not compacting or churning the sediments. It is widely used for stratigraphical work in peats because of its clean action and speed operation (Moore et al., 1991).

The Russian corer cuts 50 cm long half cores (Fig. 3.3). The main blade of the sampler passes the material to be sampled as it descends, and the 180° rotation of the movable chamber cuts a semicylinder of peat/sediments and withdraws it intact upon the surface of the fin. When the sampler is withdrawn, the opening of the chamber yields the entire sample in a clean and undisturbed condition (Fig. 3.3). This is ideal for field measurements and description for stratigraphical work. The full exposure of the core provides excellent material for recording sediments features such as colours, banding, lamination, charcoal layers, humification changes, etc. (Moore et al., 1991).

In this research, most of the cores (i.e., cores 2, 5, 7, 8 and 9) reached glacial clays below a thick organic-rich sequence. In order to insure of the continuity of cores at the interface of the 50 cm long core fragments, twin cores were taken at locations 6, 7, 8 and 9 with a vertical offset of 0.25 cm (e.g., core 9A from 0 to 15 m and core 9B from 0.25 to 15.25 m). All cores were photographed in the field. Core 2 was further sampled for detailed palynological investigations. Cores 5 to 9 were packed in plastic half tubes to be carried to the laboratory for further studies/sampling at the National University of Colombia in Medellín.

Fig. 3.1. View of the Llano Grande depression and location of coring zone of cores 2 to 9. (Parra and Monsalve, 2010 unplubl.).

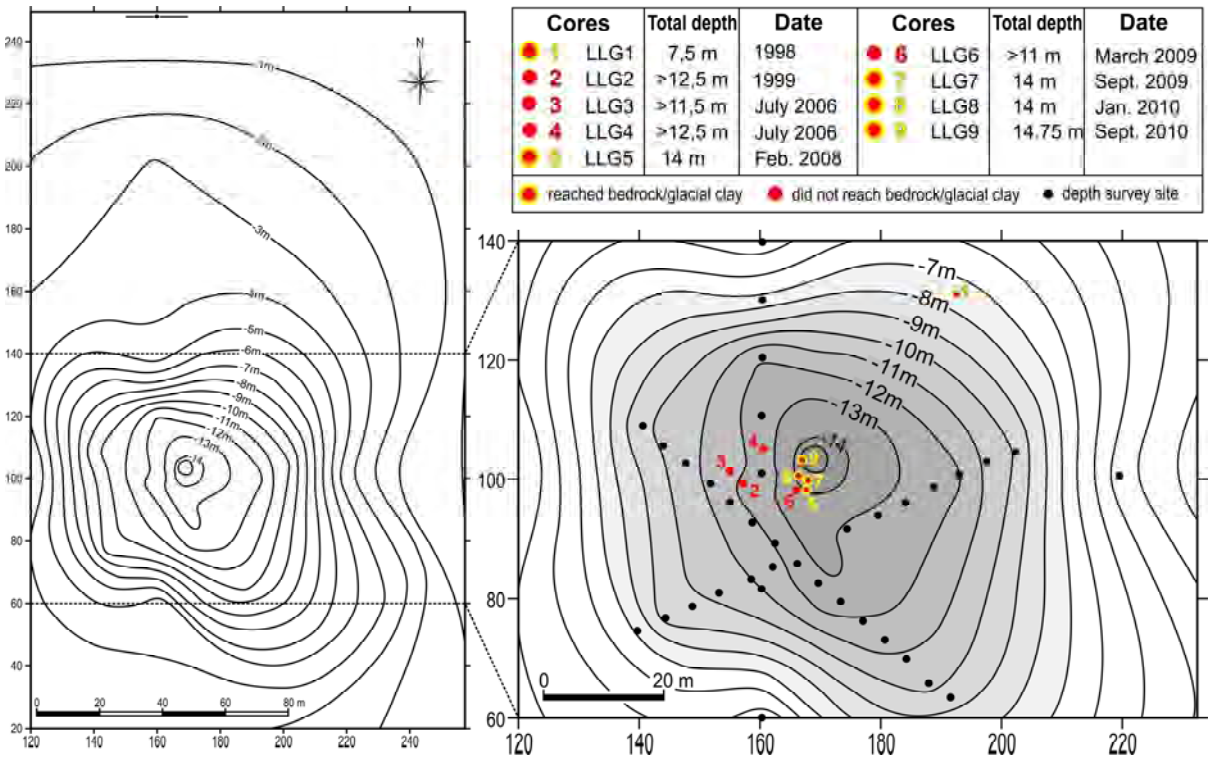

Fig. 3.2. Depth map of the Llano Grande Quaternary depression and location of LLG cores 1 to 9.

Fig. 3.3. A) Russian corer ready for use; B) example of a 50 cm long half core.

3.2. POLLEN ANALYSIS

3.2.1. PALYNOLOGY

Palynology is the study of pollen and spores and their dispersal, and applications thereof (Hyde and Williams, 1944). The term includes both modern and fossil pollen and spores. Although some other microfossils are considered, the widespread use of palynology in the reconstruction of the environment is related to the characteristics of pollen and spores such as their great resistance to degradation, small size (mostly less than 200 microns) that permits their transport and deposition as sedimentary particles, their morphological complexity, and the general high production which facilitates to have a statistically significant assemblage (Tschudy and Scott, 1969c).

Pollen analysis is a useful technique to study past climates and vegetation. Much effort has been spent on the reconstruction of changes occurring in the Holocene, during which the earth has recovered form its latest glaciation and human pressures upon global vegetation have become increasingly intense (Moore et al., 1991). The principle of this method is that the variation of pollen percentages may be followed through the section of a sedimentary deposit and it gives a quantitative expression of changes in the vegetation cover during the period of formation of this deposit.

To identify these paleoecological processes, it is possible to develop mathematical relationships between fossil pollen data (such as percentage of pollen) and climatic variables (such as mean temperature). On the basis of such models, it becomes possible to establish reconstructions of relative past temperatures (Webb, 1980). This approach is based on the

influence of climate on global vegetation patterns. Nevertheless, one must keep in mind different factors, such as local soil influences, the impact of human settlements, the slow response of vegetation (particularly forest) to climate change, stochastic elements, while trying to determine the pattern of plant arrivals at a site (Moore et al., 1991).

Fossil pollen obtained from sediment matrices should be considered in relation to a number of factors that have exerted an influence on them during the time between their dispersion and their recovery from the rock. Pollen and spores are almost never accumulated in their pure state as a fossil deposit. They are accompanied by various amounts of other organic material, and by clay, sand, inorganic clasts or other rock-forming clastic material (Tschudy, 1969b). The application of palynology to geological or stratigraphical problems involves the definition and delineation of the specific strata in the stratigraphical column, because palynomorphs are derived from these rocks (Tschudy, 1969a and 1969b).

3.2.2. PROCESSING

To achieve an appropriate processing of the sedimentary material is vital in palynological research. The different techniques of extraction and maceration could adversely impact the subsequent analyses. Therefore, it is important to carry out a good palynological processing to get the best results. Many methods have been developed depending on the studied material and results desired. The standard sequence may be adapted to the needs for individual palynological studies (Wood et al., 1996). Several publications outline techniques for extracting palynomorphs from rock samples, and comment on modifications for specifics needs (Brown, 1960; Gray, 1965a and 1965b; Barss and Williams, 1973; Doher, 1980; Phipps and Playford, 1984; Traverse, 1988; Bryant and Wrenn, 1998; Jones and Rowe, 1999, among others).

The objective in preparing a peat or sediment sample is to concentrate spore and pollen grains and get them as visible as possible by (1) defloculation, (2) removal of other matter and (3) embedding them in a suitable medium. After each step in the treatment, samples are concentrated by centrifugation (Faegri and Iversen, 1964). The technique employed in this research is that of acetolysis developed by Ertdman (1960), because it is the most effective for removing the cellulose through acid hydrolysis.

The preparation sequence is as follows:

Extraction of the sample from the sediment: This involves the cutting away of the superficial material that may have suffered some contamination, either from adjacent sediments, coring equipment or from the atmosphere.

- For this study, 1 cm^3 samples were extracted from the core with a spatula within 1 cm-thick core slices.

Treatment with KOH (5%): It breaks the organic matter structure, dissolves humic acids and removes unsaturated organic soils colloids:

- Place the 1 cm^3 sample into a tube and add 10 ml of KOH (5%);

- Filter the sample through a 150 ų sieve. It lets all pollen and spores pass through but retains larger particulate material such as sand grains, minerals and plant fragments;
- The filtrate is collected in a centrifuge tube and centrifuged for 5 minutes at 3500 r.p.m.;
- Decant off the liquid.

Acetolysis: This process removes oil lipids, protoplasm and intine remains of pollen and spore which allows a better study of the grain structure and facilitates their identification.

- Resuspend the residue in glacial acetic acid (CH_3COOH) to dehydrate the organic material;
- Centrifuge for 5 minutes at 3500 r.p.m.;
- Decant off the liquid;
- Add 6 ml of acetolysis mixture: acetic anhydride $(CH_3CO)_2O$ mixed with sulphuric acid H_2SO_4 with a ratio of 9:1 by volume;
- Centrifuge as above and decant the liquid phase;
- Resuspend in glacial acetic acid (CH_3COOH), centrifuge and decant as above three times;
- Resuspend the residue in distilled water, centrifuge and decant as above three times.

Use of exotic markers: Usually palynologists studying Pleistocene and Holocene sediments determine pollen concentrations within a sample (per/gram/cm^3) by adding a known quantity of exotic markers (pollen, spores, microspheres) as a standard to calculate the relative quantities of indigenous taxa (Maher, 1972 and 1981; Ogden, 1986) or palynomorph concentration (Velásquez, 2005). The basis of this technique is that a known number of exotic marker pollen or spore grains are added to a known volume of sample at the beginning of processing. All subsequent abundance determinations can then be carried out in relation to counts of the marker grains (Moore et al., 1991).

The technique was first employed by Benninghoff (1962) and has subsequently been modified by Matthews (1969), Pennington and Bonny (1970) and Bonny (1972). Comparative quantification using tablet of “exotic” spores or pollen was introduced by Stockmarr (1971). In this research *Lycopodium* spore tablets were introduced prior to glycerine addition. This tablet contains a specific amount of spores (Stockmarr, 1971 and 1973). Because they are easy to recognize, spores of *Lycopodium clavatum* are the most commonly used, what was done in this study.

Glycerine jelly mounting: It is easy to handle; it melts when placed in a boiling water bath but is solid at room temperature. Moreover it has excellent optical properties (Batten and Morrison, 1983). Because it is solid at room temperature, it means that when slides are stored the grains remain in position (Moore et al., 1991). Mounting in glycerine jelly is carried out as follows:

- Melt glycerine jelly in a beaker suspended in a boiling water bath. Add to the palynological residue a volume of jelly about twice the volume of residue;
- Keep the tube in water warm and stir thoroughly to produce a uniform suspension;
- Heat a microscope slide and coverslip on a slide-drying hotplate and put a glycerine portion onto the slide;
- Add 7 ųml of pollen solution on the slide;
- Seal the slide by surrounding the sample with liquid paraffin and cover it with the coverslip;

- After cooling, the slides should be labelled and stored horizontally in trays.

All the palynological slides studied in this research were prepared from LLG-2 core samples at the Laboratory of Paleoecology of the National University of Colombia in Medellín.

3.2.3. IDENTIFICATION AND COUNTING

Counting provides the qualitative and quantitative database for paleoecological studies. The identification of pollen grains and spores is obtained from the morphological characteristics of the exine using an optical microscope. The pollen count is carried out by visual examination of microscopic slides with a high magnification (up to 100X). To improve the identification we took pictures at a magnification of 40X, 63X and 100X, in order to compare with grains already identified. To locate pollen grains when the slide is transferred from one microscope to another, we used the “England finder”. The latter is a slide with an etched grid that provides coordinates for locating a position that is completely independent of individual mechanical stages on microscope (Rybníčková and Rybníček, 1971; Traverse, 1988).

The two most important considerations when counting are, on one hand, to obtain relatively reliable percentages of the main species present, and, on the other hand, to include a substantial number of species present in the sample population (Velásquez et al., 2004). The number of recorded grains of a given taxon indicates its relative importance in the original ecosystem. Nevertheless, the detection or absence of a taxon in the pollen spectrum can be influenced by its response to some factors such as the differential resistance of the taxon to diagenetic agents, transport vectors, pollen extraction techniques and slide preparation (Velásquez, 2005).

In this study, we counted the total number of pollen and spores in 21 µml of each sample. The grains were observed, and identified using several published references on the morphology of the Colombian pollen, especially Hooghiemstra (1984), Salomons (1986), Roubik and Moreno (1991) and Velásquez (1999a) and by using the reference collections existing at the Laboratory of Paleoecology of the National University of Colombia in Medellín and at the IBED (Institute for Biodiversity and Ecosystem Dynamics) of the University of Amsterdam (Holland).

3.2.4. THE POLLEN SUM

The relative frequency of fossils dealt in pollen analysis can be expressed as percentages of a total. To establish the *pollen sum* is the basis for the calculation of percentages which should comprise all species that are part of the plant communities under investigation (Faegri and Iversen, 1964).

Included in the pollen sum

When data are available, it is possible to express pollen and spore data in terms of numbers accumulating per unit area of sediment per unit of time. This means that a value for any given

taxon is independent of all others in its expression, and one can follow trends in pollen influx of that taxon in time, which is part of the group *"included in the pollen sum"* (Moore et al., 1991). For the Páramo de Frontino the *taxa included in the sum pollen* were set according to the concept of vegetation belts (Table 3.1) and their present-day vertical distribution has been summarized above in Fig. 2.7 (modified from Velásquez 2005). In this study, we will use in fact only three belts (see Groot et al., 2011): 1) the subandean forest (or lower montane forest); 2) the Andean forest (or upper montane forest) regrouping Andean and high Andean forest; 3) the páramo regrouping subpáramo and páramo.

Vegetation belt	Altitude range (m amsl)	Taxa
Subandean forest (lower montane f.)	1000 - 2100	*Acalypha, Alchornea,* Bignonaceae, *Cecropia,* Fabaceae, Mimosaceae, *Pilea, Sapium* and Urticales
Andean forest (upper montane f.)	2100 - 3000	*Alnus, Ardisia, Bocconia, Clethra, Clusia,* Cyatheaceae, *Drimys, Eugenia, Juglans*, Myrtaceae, *Podocarpus, Quercus,* Solanaceae, *Symplocos*, *Thalictrum and Viburnum*
High Andean forest (upper montane f.)	3000 - 3450	Araliaceae*, Gaiadendron*, *Hedyosmum, Hesperomeles, Ilex,* Melastomataceae, *Miconia, Morella, Myrsine, Prunus, Vallea and Weinmannia*
Subpáramo	3450 - 3500	Asteraceae, Ericaceae, and *Polylepis*
Páramo	3500 - 4100	*Aragoa*, *Arcytophyllum*, *Blechnum,* Caryophyllaceae, Gentianaceae, *Geranium*, *Gunnera, Hypericum,* Lamiaceae, Lycopodiaceae*,* Poaceae*, Rumex*, *Sisyrinchum* and *Valeriana*.

Table 3.1. Taxa *"included in the pollen sum"* for the Páramo de Frontino (Antioquia -Colombia). Modified from Velásquez (2005).

Not included in the pollen sum

When the input of given taxa can influence significantly the total sum of pollen, it is necessary to express these taxa as a percentage of the total sum. These are called the taxa *"not included in the pollen sum"*. They represent local pollen and spore taxa with a high or low input in the assemblage and which undergo large fluctuations during the time interval covered by a pollen diagram. One solution to this difficulty is to remove such local species form the pollen sum (Faegri and Iversen, 1964). This requires the recognition of which plants are indeed local and need to be removed (Rybníčková and Rybníček, 1971).

In the case of the Llano Grande wet zone studied, the local vegetation is made of aquatic vegetation (see table 3.2) which shows a strong influence on all other components of the sum. We have separated the aquatic vegetation according to its environmental significance directly related to the water depth of the mire. The environmental model of aquatic vegetation in Llano Grande is derived from Parra et al. (2010c) and has been shown above in Fig. 2.8.

Aquatic vegetation	Depth range cm	Taxa
Submerged	40 - 80	*Isoëtes*
Marsh	0 - 20	Apiaceae, Cyperaceae, *Hydrocotyle, Lachemilla, Ranunculus*
Cushion	0	*Plantago*

Table 3.2. Aquatic vegetation *"Not included in the pollen sum"* for the Páramo de Frontino (Antioquia - Colombia) (see Parra et al. 2010c).

3.2.5. INTERPRETATION OF POLLEN DIAGRAMS:

Once the pollen sum has been decided upon, the results of analyses may be expressed as percentages (Faegri and Iversen, 1964). Pollen data from stratified sediments are generally displayed graphically in the form of a stratigraphical pollen diagram. The first step in the interpretation of pollen diagrams is the reconstruction of the original vegetation. Once this has been achieved, explanations for variations in the diagram and vegetation changes can be searched (Muñoz, 2007).

Reconstructions of vegetation are a difficult process considering the large number of processes involved in the production of fossil assemblages from the original vegetation. To find an analogy with the communities of the past, one has to use pollen samples collected in recent known communities (Williams et al., 1998).

The pollen diagram displays the stratigraphical variations of ecological groups and taxa (Velásquez, 2005). The pollen diagram provides the following information:

Arrangement: The vertical axis represents the depth or age of the samples with respect to the sedimentary core. The horizontal axis corresponds to the abundance of pollen taxa in either proportional or absolute terms.

Stratigraphy: The lithostratigraphical column of sediment types is represented diagrammatically on the left/right handside. It may help for an adequate interpretation of fluctuating pollen curves.

Pollen curves: The proportion of the various pollen types is indicated at each level of sampling either by a bar histogram or by a point on a continuous curve. It is obtained from the sum as a percentage of species or taxa characterizing different vegetation belts. In these diagrams the horizontal scale represents the relative percentage of each taxon from the pollen sum "*included in the sum".* Vertical variations of percentages highlight climatic fluctuations recorded in the sediments, i.e. colder periods (dominance of subpáramo and páramo vegetation) and warmer periods (dominance of the and Andean vegetation).

Individual taxa diagram: It represents the relative frequency of each taxon within the total number of elements of the sum of pollen.

Pollen abundance scales: The horizontal scale should be consistent throughout the diagram or where minor components need emphasis, any variation in horizontal scale should be made clearly apparent.

Pollen diagram zonation: It is convenient to divide the pollen diagram into a series of zones on the basis of their pollen assemblages. They represent periods clearly distinguishable from each other in terms of composition and / or abundance of taxa. To achieve this zonation one seeks to identify the time intervals that have relatively constant pollen assemblages, which can be interpreted through the taxa and / or association "types" (which reflect the environmental conditions) and their proportions (Velásquez, 2005).

The recognition and selection of appropriate pollen zone boundaries can be identified by applying statistical methods (Gordon and Birks, 1972). These zones are established using cluster analysis (CONISS, cluster analysis) incorporated in the program TILIA 2.0.2 (Grimm, 1987). CONISS uses the method of "incremental sum of squares."

In this research the computer programs used were TILIA 2.0.2 and TILIAGRAPH (Grimm, 1987). The latter were developed for the management, manipulation and graphical representation of the stratigraphical pollen data (Jackson, 1999).

In this research, our palynological data will be merged with other palynological data from LLG-2 core obtained by Velásquez (2005) and those of Jojoa (2007). Jojoa (2007) has investigated loosely the same interval studied here (Early and Middle Holocene) and her results are incorporated with ours. Velásquez (2005) has carried out a high-resolution palynological study in the interval directly overlying that of our study (of Late Holocene age). In the discussion, his palynological results will be incorporated to have an overview of the whole Holocene in Frontino. Their pollen and spore assemblages are identical to ours and their relative proportions of taxa can be compared with ours and merged into one single pollen diagram.

3.3 RADIOCARBON DATING

3.3.1. INTRODUCTION TO DATATION TECHNIQUES

Interpreting Earth history is a prime goal of geology, therefore the early approaches to dating the past were closely associated with attempts to establish the age of Earth (Tarbuck and Lutgens, 2008). Geological events have a real meaning only when it is possible to put them into a time perspective. Dating is a key element in Quaternary research because it allows establishing the timing of climate changes and of their effects on the Earth's system.

Dating techniques are fundamental to the understanding of the natural and cultural changes which have taken place during the Holocene (Roberts, 1998). Precise dating is particularly

important for paleoclimatic studies. If there are no reliable estimates of the age of past events, it is not possible to know with certainty whether these events occurred synchronously or if some occurred before or after others, nor is it possible to know the rate at which environmental changes occur. There exists two methods to estimate the ages, i.e., relative and absolute dating. Therefore, it is important to know the limitations of these dating methods with respect to the data collected.

Relative dating: in undisturbed sediments younger layers overlie older ones and vice-versa. This law of superposition indicates which layer was deposited first, but it fails to provide the actual age of either (Roberts, 1998). This method only can tell us about how events are followed/preceded by another, but it can not provide information about how long ago such events took place.

Absolute dating: information about the relative sequence of sedimentary layers is important, but it is necessary to assign to each of them absolute ages in years. For this purpose one needs to use absolute dating techniques, more specifically radiometric methods (Roberts, 1998). Theses techniques are based on the fact that certain naturally-occurring elements are unstable and undergo spontaneous changes in their structure and organization in order to achieve more stable forms. This process is time-dependent , and if the rate of decay for a given element can be determined, the ages of the host rocks and fossils can be established (Walker, 2005). Each radioactive isotope used for dating has been decaying at a fixed rate since the formation of the rocks in which it occurs and the products of decay have been accumulating at a corresponding rate (Tarbuck and Lutgens, 2008). In our case, dating of the Llano Grande sediments has been carried out using the radiocarbon method.

3.3.2. RADIOCARBON DATING

The radiocarbon dating technique has been discovered by Arnold and Libby (1949) and applied since the second half of the twentieth century. It is probably the most widely used of all radiometric techniques, because it is specifically applicable to only a relatively short span of Quaternary times (last 50,000 years or so; Walker, 2005). This method was used for the first time over 50 years ago by an American chemistry professor in Chicago, Willard Libby, who was later awarded with the Nobel Prize in Chemistry in 1960 (Burleigh, 1981; Walker, 2005).

There are three principal isotopes of carbon which occur naturally: two in a stable form, ^{12}C (98.9%) and ^{13}C (1,11%); one in an unstable or radioactive form, ^{14}C (one part in 10^{10}%). The latter decays to a stable form of nitrogen ^{14}N through emission of beta (β) particles. One β particle is released from the nucleus for every atom of ^{14}C that decays. It is this instability or radioactivity, which gives the name of “radiocarbon” (Walker, 2005).

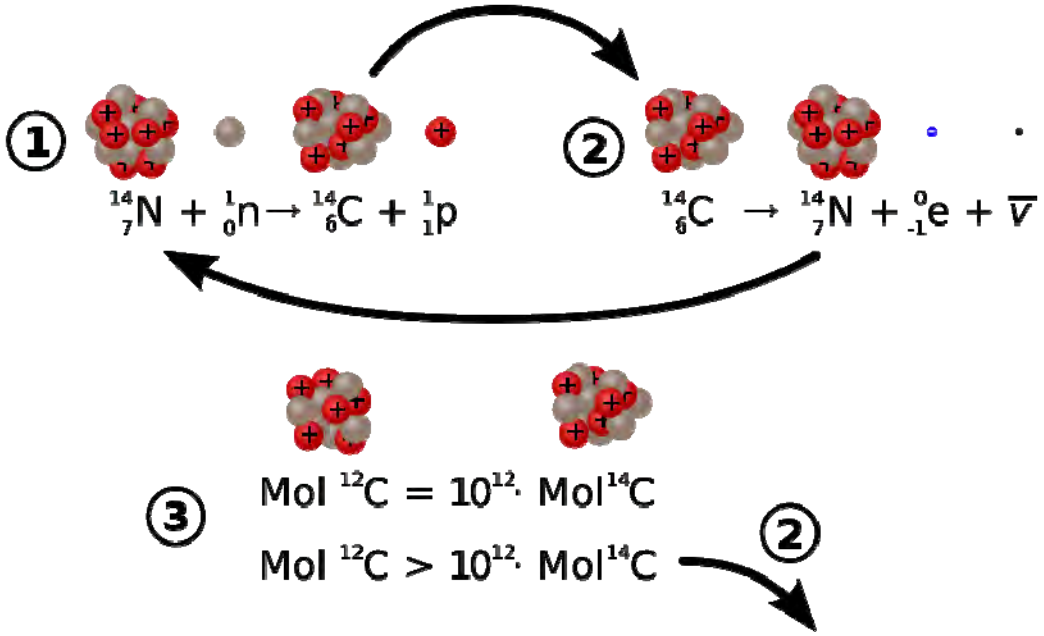

Fig. 3.4. The physics of decay and origin of ^{14}C for radiocarbon dating. (1) Formation of ^{14}C, (2) Decay of ^{14}C and (3) The "equal" equation is for living organisms, and the unequal one is for non-living ones, in which the ^{14}C then decays (hence the 2). *Source:* C14_methode_physikalische_grundlagen.svg.

Atoms of ^{14}C are formed in the upper atmosphere through the interaction between cosmic ray neutrons (Walker, 2005; Tarbuck and Lutgens, 2008). Cosmic rays (high-energy nuclear particles) shatter the nuclei of gas atoms, releasing neutrons. Some of the neutrons are absorbed by nitrogen atoms ^{14}N (atomic number 7, mass number 14), causing each nucleus to emit a proton, as a result, the atomic number decreases by 1 (to 6), and a different element, ^{14}C is created (see fig 3.4). This isotope of carbon is rapidly oxidized to $^{14}CO2$ and enters the earth's plant and animal lifeways through photosynthesis and the food chain.

As long as an organism is alive, the decaying in carbon is continually replaced, and the proportions of ^{14}C and ^{12}C remain constant. However, as soon as an organism dies, ^{14}C decays to ^{14}N (Tarbuck and Lutgens, 2008). By measuring the amount of ^{14}C that remains in the sample of a fossil material and comparing this to modern ^{14}C in standard material, an age can be inferred for the death of the organism, postulating that the content of ^{14}C remained stable during the last 50,000 years. In order to be able to do this, it is necessary to know the rate at which ^{14}C decays (Walker, 2005).

The decay of ^{14}C is not linear but exponential (Walker, 2005; Tarbuck and Lutgens, 2008). The half-time of a ^{14}C atom is 5,730 years (Fig. 3.5), and under normal circumstances, the limit of measurements of ^{14}C activity is eight half-lives, therefore giving an upper age limit of around 45,000 years (Walker, 2005). This technique is useful only for a range of biogenic materials, such as wood, charcoal, peat, organic sediment, plant and animal remains, bones, shell and corals. It is also possible to obtain radiocarbon dates from unconventional material such as cloth, metal work or fossil pigments (Walker, 2005; Tarbuck and Lutgens, 2008) and old sea water, lake and marine sediments and atmospheric CO_2 trapped in glaciers (Bradley, 1999).

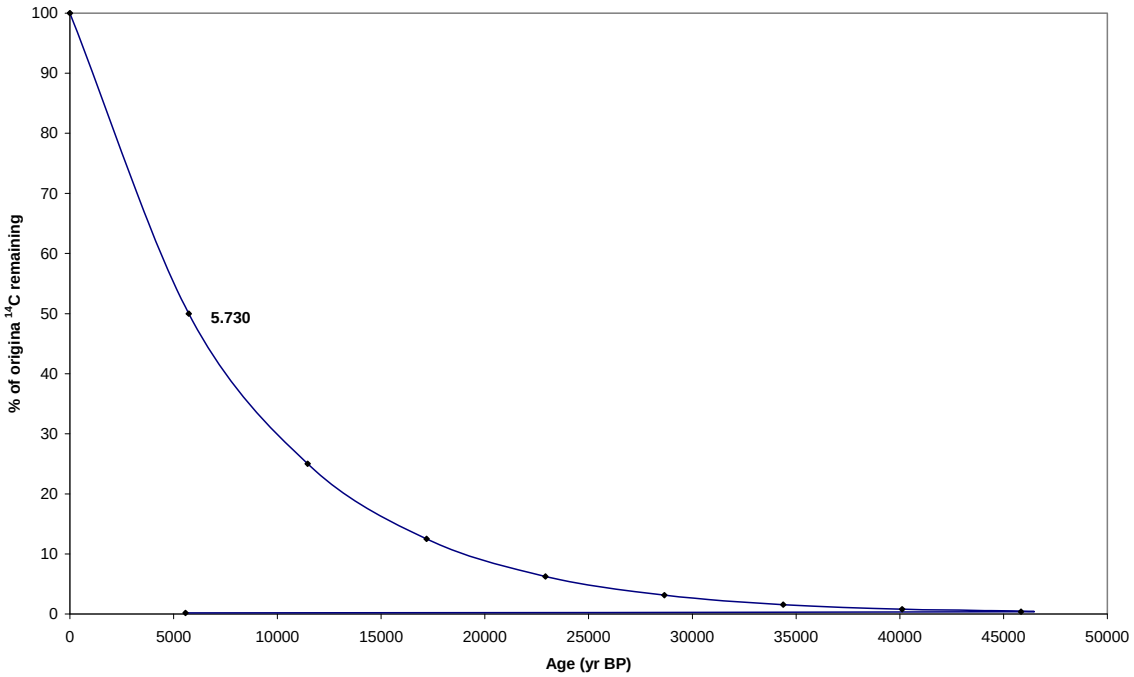

Fig. 3.5. Decay curve of ^{14}C. The decay curve for radiocarbon is exponential. This means that the percentage of decrease in number of atoms in a given unit of time is constant.

The usefulness of radiocarbon dating is limited by several factors: (1) the variations of ^{14}C in the atmospheric CO_2 in the past, (2) the overall accuracy of the radiocarbon analysis (Trumbore, 2000) and (3) the contamination of samples in the field. The ^{14}C method can not be applied to recent samples because the definition of the younger time range limit can be affected by the called *Suees effect,* because the increase in combustion of fossil fuels since the Industrial Revolution has caused an injection of geologically old carbon into the atmosphere that has led to a decrease in ^{14}C contents and made recent samples "older" that they actually are (Walker, 2005; Roberts, 1998; Trumbore, 2000). The main problem in the upper age limit is linked to the contamination of samples with little amounts of modern carbon in the soil or in laboratory processes or because of ^{14}C produced in situ in the sample by cosmic ray bombardment.

3.3.3. SOURCES OF ERROR IN RADIOCARBON DATING

Contamination: Refers to addition of younger or older carbon in the sample material. In field sampling it is easy to introduce younger materials into older horizons and in ponds or lakes, bioturbation caused by microorganisms on the lake bed can lead to disturbance of the sediment sequence and the downward movements of younger sediments (Walker, 2005). Contamination can also occur in the laboratory by fungal growth during the period of sample storage (Wohlfarth et al., 1998) or through modern contamination by dust, skin etc.

In the Llano Grande mire, no bioturbation is present. Nevertheless, in the peaty sediments forming most of the Holocene section, the age of some samples has probably been affected

by younger roots present in the samples, which yields a younger age than normal. For this reason, it is preferred to date the bulk organic residue rather than only vegetal fragments. All samples dated have been stored in refrigerator at 4°C prior to being sent to the dating lab, and special care has been taken to avoid any modern contamination. In our study, some samples picked in what turned out to be oxydized paleosoils have been excluded from the data base.

Isotopic fractionation: Chemical and biological reactions fractionate isotopes according to their mass. The $^{14}C/^{12}C$ ratio in atmospheric CO_2 will differ from organic carbon fixed from the atmosphere by photosynthesis (Trumbore, 2000). In general, the terrestrial plants prefer to take the lighter isotope, hence there is an enrichment in ^{12}C and a decrease in ^{14}C, therefore datations in fossil plants can be different according to their pathway to take up carbon. The contrary occurs in marine organisms, because there is a preferential absorption of heavier isotope ^{14}C in ocean water, and marine organisms will seem younger than they are (Walker, 2005).

Marine reservoirs effects: The age of marine organisms, which take in dissolved carbonate to build their skeletal structures, will have to be corrected, because ^{14}C in intermediate and deep water decays without replenishment from the surface (Walker, 2005).

Long-Term variations in ^{14}C: This is the main problem in radiocarbon dating because it is not possible to sustain the fundamental assumption that ^{14}C levels have not varied significantly over time. Large variations in atmospheric ^{14}C concentrations have been detected beyond 25,000 years (Beck et al., 2001; Hughen et al., 2004). The causes of these variations are not well known. According to Stuiver et al. (1991) and Mazaud et al. (1992) the modulation of cosmic ray flux by changes in the earth's geomagnetic field or by variations in the intensity of solar activity may have an important influence. The other hypotheses are reduction in solar activity (Van Geel et al., 2003), or changes in patterns of oceanic circulation (Goslar et al., 1995).

The sedimentary record in Llano Grande covers only the last 17,000 years and datings should therefore not be affected.

3.3.4. RADIOCARBON MEASUREMENTS

According to Walker (2005), two approaches are employed to measure residual ^{14}C activity in samples relatively to modern standards:

Beta counting (standard method): Involves the detection and counting of ß emission from ^{14}C atoms over a period of time, based on the principle that the rate of emission will reflect the residual level of ^{14}C activity within the sample.

Accelerator Mass Spectrometry (AMS): This technique uses particle accelerators such as mass spectrometers to count the relative number of ^{14}C in a sample, as opposed to the decay products. Mass spectrometers detect atoms of particular elements on basis of differences in atomic weights. Given that the amount of ^{14}C atoms is very small and difficult to measure in

total, it is not an absolute number that is being measured. Therefore, AMS determines the isotope ratio of ^{14}C relatively to that of the stable isotopes of carbon ^{12}C and ^{13}C, and the age is determined by comparing this ratio with that of a standard of known ^{14}C content. This method is much more precise than the standard one.

3.3.5. CALIBRATION OF THE RADIOCARBON TIMESCALE

Because of temporal variations in the radiocarbon content of atmospheric carbon dioxide, it is possible to say that the ^{14}C clock runs at a varying pace, different from real time: ^{14}C time is not equivalent to historical time (Van der Plicht, 2002). Therefore conventional radiocarbon dates need to be *"calibrated".* This conversion of ^{14}C ages to calibrated ages is especially important for improving the validity of time estimates.

The ^{14}C timescale is expressed in BP (Before Present), where “Present” is the standard year 1950AD (date of the first nuclear tests in the world affecting the natural radioactivity level). Radiocarbon measurements are done with respect to a standard (Oxalic Acid with radioactivity of 0.226 Bq/gC) which corresponds to 1950 radioactivity.

Accuracy of the radiocarbon dating depends of the calibration curve used to convert ^{14}C years to calendar years. According to (Trumbore, 2000), the overall accuracy of calibrated ages from radiocarbon dating depends on the time interval during which the sample was formed. Dates may be expressed as either uncalibrated or calibrated years. The conversion of a radiocarbon age given in radiocarbon years B.P. (i.e., radiocarbon years elapsed since the origin of the sample) to a true calendar year makes necessary certain assumptions with respect to: (1) the half-life of ^{14}C, (2) the production rate of ^{14}C by cosmic rays, (3) the size of reservoirs into which ^{14}C is distributed and the exchange rate of this distribution (Stuiver and Suess, 1966) and (4) that the ^{14}C content of the atmosphere has been constant (Stuiver and Polach, 1977).

Dendrochronologically dated wood has proved to be an ideal material and currently all radiocarbon calibrations are based on measurements of ^{14}C activity in wood (Klein et al., 1982). Numerous calibration curves have been constructed based on absolutely dated tree-ring chronologies and other archives (Klein et al., 1982; Stuiver, 1982; Pearson and Stuiver, 1986; Pearson and Stuiver, 1993; Stuiver and Becker, 1993; Stuiver et al., 1998). Cal yr BP ages are relative to the year AD 1950, with 0 cal BP equal to AD 1950. The relationship between cal AD/BC and cal BP ages is cal BP =1950 - cal AD, and cal BP =1949 + cal BC. The switch from 1950 to 1949 when converting BC ages is caused by the absence of the zero year in the AD/BC chronology (Pearson and Stuiver, 1993)

Two main calibration methods are used: the dendrochronological and INTCAL calibrations:

Dendrochronological calibration: The pioneer in developing this technique was the American Andrew Douglas who founded the first tree-ring laboratory at the University of Tucson, Arizona in 1937 (Walker, 2005). The basis of this technique is the use of tree-rings as a measure of the annual growth increments as an approach of chronology. A clear identification of tree rings

and counting of these allows inferring the age of the tree. The accuracy of this method depends on the behavior of atmospheric ^{14}C (Trumbore, 2000). The plant growth depends on several environmental factors such as temperature, moisture and nutrient availability. Therefore, it is possible to take on that the width of a tree-ring can make evident the climatic conditions year by year during the tree life. The characteristic ring-width pattern can be used for (1) to make inferences about climatic conditions and (2) as a basis for cross-dating between wood of overlapping age range (Walker, 2005). One advantage of this method is that it can be used for both living and dead trees. This method has a span of time limited to the Holocene.

The INTCAL Calibration: The radiocarbon calibration curve used in this study is INTCAL04 which was developed by Stuiver et al. (1998) and Reimer et al. (2004). It converts radiocarbon ages into calibrated (cal) ages. This calibration data set is valid for terrestrial samples and extends from 0-26,000 cal yr BP. Dendrochronologically-dated tree-ring samples cover the period from 0 to 12,400 cal yr BP. Beyond the latter limit, data from marine records (corals and foraminifera) are converted to the atmospheric equivalent with a site-specific marine reservoir correction to provide terrestrial calibration from 12,400 to 26,000 cal yr BP (Reimer et al., 2004).

In the framework of the present study, 37 AMS datations were available (see part 4 below). Those carried out at the Poznan Laboratory Lab in Poland (13 samples) were calibrated by us using the program CALIB 5.0 (two-sigma calibration values). This program was updated from CALIB 3.0 (Stuiver and Reimer, 1993) and CALIB 4.0 to use the INTCAL04 dataset. The other 24 AMS datations were carried out at the Beta-Analytic Laboratory in Florida, which provides both conventional radiocarbon and two-sigma calibrated ages. The latter calibration used the INTCAL04 data base (Reimer et al., 2004) and the mathematics of Talma and Vogel (1993).

3.4. X-RAY FLUORESCENCE (XRF)

3.4.1. PRINCIPLES

In sedimentological research the possibility to recognise chemical elements which can provide climate and environmental information is of vital importance. In this respect, Jansen et al. (1998), have developed a non-destructive logging technique applying X-ray fluorescence spectrometry (XRF) for the determination of major-element concentrations in split sediment cores.

X-ray fluorescence spectrometry (XRF) makes use of the process of X-ray emission. Incident X-rays eject an electron from an inner shell of an atom. The resulting vacancy is then filled by an electron from an outer shell. The electron gives up its surplus energy in the form of electromagnetic radiation. The surplus energy, which is equal to the energy difference between the two electron shells, appears as X-rays. So, each couple of shells produces a characteristic radiation and, therefore, every chemical element emits its own characteristic energy and wavelength spectra (Jansen et al., 1998). The response depths of the elements in

the sample material depend on the wavelength of the fluorescent radiation and the chemical composition of the matrix (Jenkins and de Vries, 1970).

XRF is a non-destructive system for the logging of split sediment cores. The scanner produces reliable counts of elements, highly correlated with concentrations measured with atomic absorption spectrometry (AAS). Because of the high resolution of its semi-quantitative records, the XRF is a useful tool for detailed time-series analysis, inter-core correlation, and shipboard analysis (Jansen et al., 1998). The XRF Core-Scanner system performs analysis of elements from Al right through to U, in concentrations from 100% down to ppm levels. This technique is particularly successful analysis of heavy elements such as Ca, Ti, and Fe (Jansen et al., 1998; Röhl and Abrams, 2000; Helmke et al., 2005).

The principal advantages of this technique are: (1) it allows high resolution measurements of a continuous record; (2) measurements can be carried out rapidly; (3) the system is non-destructive; (4) it provides data about the actual composition of the sediment, in contrast to tools such as natural gamma-ray, magnetic susceptibility and colour loggers that produce data depending on a combination of sediment properties.

3.4.2. USE OF XRF IN LLANO GRANDE CORES

In the framework of this research, elemental analysis has been performed on the LLG-5 core (see core location in Fig. 3.2) using the EDAX Eagle III XPL µProbe at the Section of Earth Sciences of the University of Geneva. We shall refer to these data as microfluorescence-X (µXRF) data. Material for µXRF analyses was sampled at the National University of Colombia in Medellín in 50 cm-long U-channels from the cores recovered with the Russian corer (see above). U-channels were carefully packed and transported to the University of Geneva. The 50 cm long U-channels were subsequently cut into 10 cm long sections to be analyzed in the Eagle III spectrometer.

Measurements were made at ultra-high resolution, i.e., some 180 to 200 points for each 10 cm segment of the whole core LLG-5 down to 14 m deep. Parameters used for measurements were set at 40 kV, 450 µA, 50/55 Dtm at atmospheric pressure. Two profiles were acquired in various parts of the core, giving consistent results. Measured values are expressed in counts per second (cps). According to the manufacturer, the lowest level of reliability is at around 7cps.

µXRF provides an easy method to quantitatively evaluate the chemical elements present in the mineral fraction of a sediment. They come essentially from running waters in the drainage basin of the Llano Grande wet zone, where the bedrock is made principally of volcanic rocks (andesites, basalts and tufs). We have obtained a high-resolution record of the following elements: Fe, Ti, Mn, Ca, K, Al and Si.

The most commonly used elements are titanium (Ti) and iron (Fe). Some elements like Ti and K are particularly conservative and can be used as proxies for intensity of precipitations in the drainage basin (e.g., Haug et al., 2001; Peterson and Haug, 2006). Fe, although less

conservative, can also be used if not affected by diagenesis. The same applies to manganese (Mn). Calcium (Ca) is a special element: in very cold lacustrine conditions such as those of the Llano Grande laguna, no fauna with limestone shells is encountered and Ca is entirely derived from plagioclases in the drainage area. In this case, it could also be used as a precipitation proxy.

Some elements can also be used as palaeoenvironmental markers, particularly as ratios: for instance, the ratio Si/K is a good indicator for the presence of biogenic silica, i.e., diatoms (Ohlendorf and Sturm, 2008). The use of this ratio is based on the fact that the proportion of silica derived from erosion is always extremely low, whereas erosion of aluminium-rich minerals (plagioclases) increases with precipitations. Al being scarce in Frontino, the more abundant K has been used instead. Consequently, if no other source of Si is present, an increase in runoff will be marked by a decrease of the Si/K ratio (accompanied by an increase in Ti, and usually Fe). When the Si/K ratio increases significantly without an increase in Ti and Fe, this implies an increase in Si, in this case biogenic Si represented by diatoms (Ohlendorf and Sturm, 2008). This can be easily confirmed by the observation of diatoms in smear slides (see results below).

Accessorily, the ratio Fe/Mn can also be used for palaeoenvironmental purposes, being possibly indicative of a change in the redox potential of a lake (Koinig et al., 2003; Haberzettl et al., 2007). Its variation suggests changes in the mixing regime of the lake, in relation with the water depth or intensity of the wind regime. Consequently, although µXRF in the LLG project has been mainly used as a proxy for precipitations, it can also contribute to a better understanding of the lithology, as shown below in the lithological description of core LLG-5.

3.5. STATISTICS

For the treatment of the X-ray fluorescence wavelet analysis has been carried out to do times series and try to indentify significant periods during the whole Holocene recorded mainly by Fe and Ti signal. This chapter starts with a short introduction about times series, Fourier and wavelet analyses.

3.5.1. TIME SERIES

A time series is an ordered sequence of values of a variable obtained through repeated measurements over time. The time parameter may range over the positive and negative integers or all real numbers or subsets of these. A time series is said to have a *trend* when there is a slowly evolving change. The *period* of a cyclic phenomenon is the amount of time for it to repeat itself and its *frequency* is the reciprocal of the period (Fox and Andersen, 2005).

Time series objectives are twofold:

- Obtain an understanding of the underlying forces and structure that produced the observed data.

- Select a suitable mathematical model for the data and proceed to forecasting, monitoring or even feedback and feedforward control.

The fitting of time series models can be an ambitious undertaking and the selection of the appropriate model is taken according to the needs and aims of the user.

There are three basics methods of model fitting:
- Box-Jenkins ARIMA models
- Averaging models (AM)
- Mixed model : Autoregressive and averaging models (ARIMA)

Problems

According to Lobato and Velasco (2007), the treatment of time series can present some problems:
- Scientific problems such as smoothing, prediction, association, index numbers, feedback and control.
- Statistical problems such as election of a model, estimation of parameters such as hidden frequencies, uncertainty computation, goodness of fit and testing.
- Other difficulties such as missing values, censoring, measurement error, irregular sampling, feedback, outliers, shocks, signal-generated noise, aliasing, data observed in two series at different time points.

3.5.2. TIME SERIES FREQUENCY ANALYSIS

Spectral analysis of the time series is the study of individual frequency components. This tool is very useful (ï) to provide useful descriptive statistics (ïï) to check postulated theoretical models and (ïïï) as a diagnostic tool to indicate which further analyses might be relevant (Lobato and Velasco, 2007). For the analysis of times series there exists a wide number of tools and procedures to find an appropriate transformation. In this study we do a brief description of Fourier and wavelet analysis, the latter being the procedure that was applied to our data.

3.5.2.1. Fourier analysis

The Fourier transform (FT) is probably the most commonly used method to analyze a time signal for its frequency content. The Fourier transform retrieves the global information of the frequency content of a signal and assumes that any record of data in the time domain can be represented alternatively in the frequency domain as the sum of a number of sinusoidal waves of different amplitude. The Fournier integral provides a function of frequency called Fourier transform (FT). Although FT is a tool which permits to extract the frequency content of a time series, it has the following problems:
- The Fourier transform uses sine and cosine base functions that have infinite span and are globally uniform in time (Lau and Weng, 1995).

- It does not contain any time dependence of the signal and therefore can not provide any local information regarding the time evolution of its spectral characteristics (Lau and Weng, 1995). Therefore, when passing the signal to the frequency domain the time information is lost.
- FT assumes that a time series is stationary, which means that the value of its mean, variance and covariance does not vary systematically over time.
- The representation of a localized signal in Fourier transform is very inefficient and requires a large number of Fourier components (Lau and Weng, 1995).

3.5.2.2. Wavelet analysis

Wavelet transforms are functions that satisfy certain mathematical requirements. They are used in representing data or other functions and constitute an analysis tool for extracting local-frequency information. Their main properties are as follows:

- The Wavelet transform (WT) is an analysis tool well suited to study time series that contain non-stationary power at many different frequencies occurring over finite spatial and temporal domains (Weng and Lau, 1994).
- Wavelet analysis is able to determine both the dominant modes of variability and how those modes vary in time by decomposing a time series into time–frequency space (Weng and Lau, 1994; Torrence and Compo, 1998).
- A WT uses generalized local base functions (wavelets) that can be stretched and translated with a flexible resolution in frequency as well as in the time domain. In a WT, a time series is examined under a fixed time-frequency window with constant intervals in the time and frequency domains. The flexible windows are adaptable to the entire time-frequency domain, known as the wavelet domain (WD). The latter narrows while focusing on high-frequency signals and widens while searching the low-frequency background. When a wide range of frequencies is involved, the fixed window on the WT tends to contain a large number of high-frequency cycles and a few low-frequency cycles (Lau and Weng, 1995).
- The wavelet analysis procedure is to adopt a wavelet prototype function, called an "analyzing wavelet" or "mother wavelet". The similarity between the signal and the analyzing wavelet function is computed separately for different time intervals, resulting in a two dimensional representation.
- The temporal analysis is performed with a contracted, high-frequency version of the prototype wavelet, whereas the frequency analysis is performed with a dilated, low-frequency version of the prototype wavelet.
- Wavelet analysis can be performed in several ways: a continuous wavelet transform, a discrete continuous wavelet transform and a true discrete wavelet transform.
- The windowed Fourier transform and the wavelet transform are both derived from Fourier methods. The windowed Fourier transform uses a fixed and arbitrarily defined window width resulting in a fixed time-frequency resolution ratio. By adapting the window width in function of the frequency, time-frequency decomposition of the signal using the wavelet transform offers an optimal compromise for time-frequency resolution (Fig. 3.6).

- The wavelet analysis uses a modular stepwise window which changes along the signal, realizing estimates in each spectrum position. When the process is repeated many times with a slight cut in the window (for each cycle), a collection of time-frequency representations of the signal is obtained, each with a different resolution (time-scale representations).

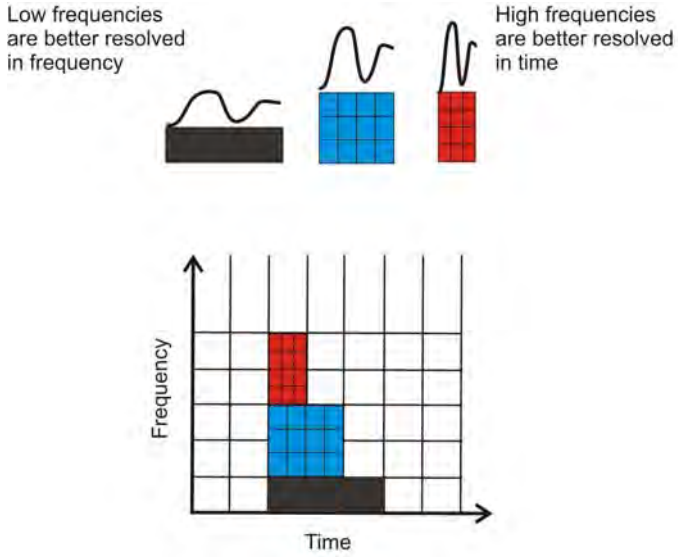

Fig. 3.6. Wavelet analysis. See text for explanation.

There are three distinct classes of wavelet transform: the Continuous Wavelet Transform (CWT), the continuous Wavelet transform with discrete coefficients and the Discrete Wavelet Transform (DWT). The term “Wavelet functions” is used commonly to refer to either orthogonal or unorthogonal wavelets. When an orthogonal basis is applied, this implies the use of the *discrete wavelet transform* (DWT), whereas a unorthogonal wavelet function can be used with either the discrete or the c*ontinuous wavelet transform* (CWT) (Farge, 1992). In this study we used only the **continuous Morlet transform**.

The CWT performs a multi-resolution analysis by contraction and dilatation of the wavelet functions and is used to divide a continuous time function into waves able to build a time-frequency representation and have a good balance between the time domain and frequency domain resolution.

The continuous wavelet transform is calculated in an analogous way to the Fourier transform, i.e., by the convolution between the signal and analysis function. However, the trigonometric analysis functions are replaced by a wavelet function. The continuous wavelet transform retrieves improved information on the time-frequency content (Strang and Nguyen, 1997).

The election of a type of continuous wavelet can influence the time-scale resolution of decomposition. The best known continuous wavelets are the Mexican hat and Morlet (Fig. 3.7). Because the Morlet wavelet has a good localization in time as well as in frequencies, it presents a resolution of high frequency, whereas the Mexican hat wavelet is very inefficient in its frequency localization. Consequently, in this study we shall use the former one.

In our study, wavelet analysis has been used to evaluate the time series of red colour intensity for statistically significant variance. The choice of this method is because of its use on non-stationary signals and by employing the adequate wavelet; it can provide excellent time and frequency localization. Wavelet spectra were calculated on the last 12,000 cal yr BP of the red colour intensity time series using a continuous wavelet transform with significance testing. We have used Morlet wavelet to calculate the wavelet power spectra and to indentify large-scale changes in variance within selected frequency time bands trough time.

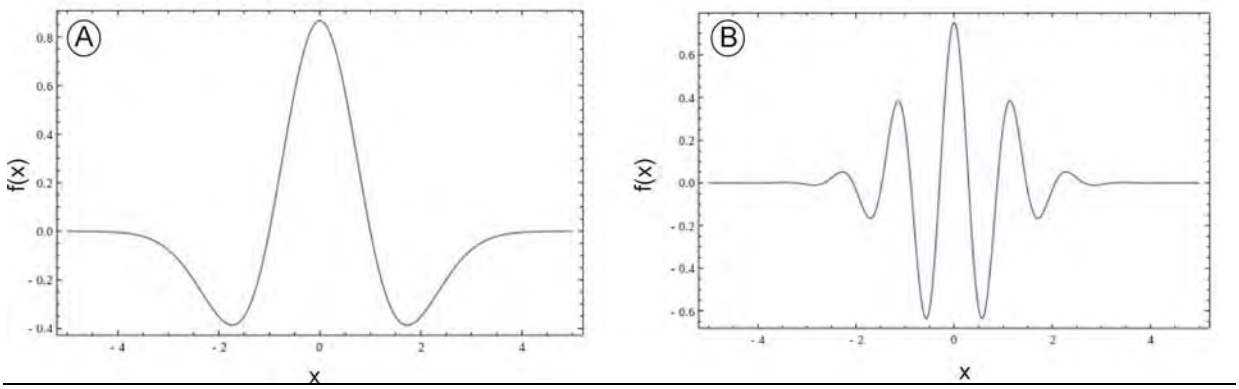

Fig. 3.7. Examples of wavelets: A) Mexican hat wavelet; B) Morlet wavelet. *Source*: Wikipedia.

3.5.2.3. Fourier vs. Wavelet transformation

The most important differences between Fourier and Wavelet transform are:

- Wavelet functions are localized in space, while Fourier sine and cosine functions are not. This localization feature, along with wavelet localization of frequency, makes many functions and operators using wavelets "sparse" when transformed into the wavelet domain. This sparseness, in turn, makes wavelets useful for a number of applications such as data compression, feature detection in images, and noise removal from time series.
- The differences of time-frequency resolution between the two transforms are the ways of looking at the basis function coverage of the time-frequency plane. The Windowed Fourier transform (WFT), where the window is simply a square wave, truncates the sine or cosine function to fit a window of a particular width. Because a single window is used for all frequencies in the WFT, the resolution of the analysis is the same at all locations in the time-frequency plane.
- The variation of windows in WTF is an advantage. In order to isolate signal discontinuities, it is necessary to have some very short basis functions. At the same time, in order to obtain detailed frequency analysis, one would like to have some very long basis functions. A way to achieve this is to have short high-frequency basis functions and long low-frequency ones.
- Wavelet transforms do not have a single set of basis functions like the Fourier transform, which utilizes just the sine and cosine functions. Instead, wavelet transforms have an infinite set of possible basis functions. Thus, wavelet analysis provides immediate access to information that can be obscured by other time-frequency methods such as Fourier analysis (Lobato and Velasco, 2007).
- Wavelet transform is a wave of limited duration whose average value is zero, while sinusoidal waves in Fourier are not limited in time, they extend from $-\infty$ to $+\infty$.

Therefore, taking into account these observations and the characteristics of our signals, which are not stationary neither in average value nor in variance (i.e., their behaviour does not fit with the sinusoidal functions), the wavelet is the most recommendable transformation to apply in this study. On the other hand, the wavelet transform has been used in numerous studies in geophysics, including tropical convection of the ENSO (Gu and Philander, 1995; Wang and Wang, 1996), atmospheric cold fronts (Gamage and Blumen, 1993), central England temperature (Baliunas et al., 1997), the dispersion of ocean waves (Meyers et al., 1993) and coherent structures in turbulent flows.

3.5.3. TIME SERIES ANALYSIS METHOD USED IN THIS STUDY

3.5.3.1. Operative system

Ubuntun 11.10 is a computer operating system based on the Debian Linux distribution and distributed as free and open source software, using its own desktop environment.

3.5.3.2. Statistical software

R version 2.14
R is an open source programming language and software environment for statistical computing and graphics. The R language is widely used among statisticians for developing statistical software and data analysis (Fox and Andersen, 2005).

Paleontological Statistics- PAST
This program is designed as a follow-up to PALSTAT, an extensive package written by Ryan et al. (1995). It includes a number of functions which are commonly used in palaeontology and palaeoecology.

3.5.3.3. Statistical methods used

Description
Descriptive methods are particularly useful for exploratory and summary purposes. They involve graphs and other displays, simple statistics such as means, medians and percentages and the techniques of exploratory data analysis. The most common method of describing a time series is by presenting a graph. Such graphs are basic for communication and assessing a situation. Descriptive values derived from time series data include extremes, turning points, level crossings and the periodogram. Descriptive methods typically involve generating displays using manipulations of time series data via operations such as *differencing, smoothing and narrow band altering.*

Tests

After getting a global idea of the signal, some tests have been made using the following libraries in R in order to identify the main characteristics and the type of signal:

1. Library stats: in this library we have used the following functions:
   - plot: generic function for plotting R objects;
   - density: the S3 function generates a probability density function of data;
   - tsdiag: is a generic function to plot time-series diagnostics to identify residuals, outliers and white noise;
   - arima: fits an ARIMA model to a univariate time series;
   - qqnorm: function to plot the graph QQplot in order to determine if a series has a Gaussian normal distribution.
2. Library urca: it contains the most useful tests to detect unit roots and co-integration of studied time series:
   - Dicky-Fuller test;
   - Increased Dickey-Fuller test;
   - Factional root test (designed by Diego Lemus);
   - Lovato and Velasco test (Lobato and Velasco, 2007);
   - Castaño and Lemus test.
3. Library car and MASS: we have used the following functions:
   - leveneTest: test to detect heteroscedasticity (non constant variance) of a dataset;
   - durbinWatson test to detect correlation in the residual of model;
   - boxCox: to realise the transformation of Box-Cox to lineal models.
4. Library forecast using the functions:
   - forecast.Arima to do prognosis of a time series using ARIMA or ARFIMA models;
   - CV is a function that calculates the cross-validation statistics and makes a hypothesis test of a forecast model.
5. Library fArma uses the function armaRoots to calculate the roots of the characteristic polynomials of an ARMA process (p,q) in order to identify if this latter is stationary and reversible.
6. Library fracdiff: the function fracdiff estimates the maximum-likelihood parameters of a fractional ARIMA model (p.d.q).
7. Library strucchange: this library test monitors and identifies where the structural changes occur in a time series using a linear regression model applying generalized fluctuation tests and F test. In this library we have employed the following functions:
   - breakpoints to identify the age where there exists a significant structural change;
   - sctest.Fstats to test the degree of significance of the structural changes;
   - sctest.efp to do test CUSUM for generalized fluctuation.
8. Library rugarch: this library models and does hypothesis tests to characterize the extreme changes in the variance process through a method known as Volatility characterization, which detects:
   - excess of kurtosis in a time series (Fama, 1963; Mandelbrot, 1963; Fama, 1965);
   - existence of high and low volatility periods denominated Volatility Clustering (Engle, 1982);
   - detection of occasional high volatility periods using the method of Detection of discontinuous price-jump (Figlewski, 1979);
   - detection of long-term high or low volatility periods followed by intermediate volatility

periods (Hsieh, 1995).

9. Library waveslim and wavethresh have been used to perform a level *J* decomposition of the input time series using the pyramid algorithm (Mallat, 1989) and Haar and Daubechies wavelets to infer about seasonal components of signals.
10. We have used the software PAST to generate the Morlet wavelet and the wavelet power spectrum.

CHAPTER 4

RESULTS

4. RESULTS

4.1 INTRODUCTION

In this research, palynological investigations are based entirely on samples from the core LLG-2 (see Fig. 3.2 for location). The investigated interval in LLG-2 spans from 220 cm down to 754 cm and is the direct continuation of the palynological research carried out by Velásquez (2005) over the first 220 cm of the core spanning the Late Holocene.

µXRF investigations were carried out on a more recent core, LLG-5 (see Fig. 3.2 for location). Although the two investigated cores (LLG-2 and -5) are close to each other (ca. 11 m, Fig. 3.2), it is very important to correlate them with precision in order to compare palynological and geochemical data. Moreover, most of the AMS datings below the Late Holocene interval come from the LLG-5 core (see paragraph 4.3). Consequently, a detailed lithological investigation of LLG-5 has been carried out (paragraph 4.2) to allow a proper correlation with LLG-2, the detailed lithology of which was investigated by Parra (2005) and Parra et al. (2010b). At the same time, the correlation has been extended to cover from cores LLG-2 to LLG-9 (paragraph 4.2). Although our research covers only the Holocene, the lithological correlation covers the whole cored interval down to glacial clays, because the interval has to be considered as a whole when establishing an age model (paragraph 4.3).

Paragraph 4.3 presents radiocarbon dating results for the Llano Grande mire and the establishment of an age model. The latter is very important when correlating palynological data of LLG-2 with geochemical data from LLG-5.

Paragraph 4.4 illustrates the high-resolution palynological data for the investigated interval 220-754 cm in LLG-2. For the sake of palynological data continuity until the present day and the comparison with the newly-acquired µXRF data over the whole interval, Velásquez's palynological data covering the Late Holocene will be displayed in the palynological results/discussion. The palynological investigation below 754 cm in LLG-2 corresponds to the ongoing research of Carlos Monsalve.

Finally, paragraph 4.5 presents the results of geochemical investigations through µXRF down to the base of the Holocene. The Late Glacial data are part of the ongoing research of Carlos Monsalve.

4.2 LITHOLOGY OF LLANO GRANDE CORES

4.2.1. LITHOLOGY OF THE LLANO GRANDE CORE 5 (LLG-5)

The lithology of core LLG-5 has been investigated in details using smear slides, in order to better understand the lithological information derived from µXRF analyses performed over the 14 meters of sediments recovered. Figures 4.1a to 4.1d present the results of this study. Although µXRF results are presented as such in paragraph 4.5, some of them are already

incorporated with the lithological description below to improve the results. The LLG-5 core will be described stratigraphically from base to top.
The cored bottom interval (Fig. 4.1a) is dominated by light grey-white mud, with dark laminae. This facies is reminiscent of periglacial sedimentation (varves), as confirmed by the age datings (see paragraph 4.3 below). The lower 30 cm of the core are marked by the abundance of coarse quartz and plagioclase mineral grains within a muddy matrix. This probably indicates proximity of the bedrock.

At 12.4 m a major change in the depositional system occurs (Fig. 4.1a). One goes from periglacial muds into organic-rich mineral muds (referred to as organo-mineral muds). This level represents a major disconformity in the sequence. The organo-mineral facies is encountered up to 8.5 m (Fig. 4.1b). The only important change in this whole interval is the proportion of diatoms. Up to 9.8 m the proportion of diatoms is most of the time over 50%. From 9.8 m up to 8.5 m it is much lower (from a few % to less than 15%), as shown by the Si/K ratio. From 12.4 up to 11.25 m, several intervals of tephra are observed, sometimes obscured through their mixing with dark-brown organic mud (Figs. 4.1a and b).

From visual comparison with the sediment study done in LLG-2 (Parra, 2005; Parra et al., 2010b) some intervals are interpreted as potentially oxidized (see grey bars in Figs. 4.1a and b) and could correspond to paleosoils. This is particularly the case for the interval 12.4 to 11.9 m which exhibits a near black colour. The oxidation is confirmed by the Fe/Mn ratio. The oxidized intervals above are visually less evident, but the use of the Fe/Mn ratio (see above) may contribute to their identification (see interval 9.75-9.5m).

Another major change in the sedimentation regime occurs at 8.5 m. The detrital mineral fraction becomes extremely low and, apart from diatoms, the sedimentation becomes nearly purely organic with dark-brown organic mud rich in vegetal fiber and fragments. From 8.5 m to 6.5 m the organic sedimentation is mixed with abundant diatoms (Figs. 4.1b and c).

The proportion of diatoms is estimated at between 25 and 90%. The diatom-richest intervals (real diatomites) are clearly marked by a high Si/K ratio. The change to the overlying, purely organic sediments is marked by a transitional interval between 6.5 and 6.2 m where the percentage of diatoms, although lower than below 6.5 m, remains significant as also shown by the Si/K ratio.

From 6.2 m up to the surface (Figs. 4.1c and d) sediments consist of dark-brown peat / organic mud very rich in macroscopic vegetal filaments and fragments. The mineral fraction is extremely poor and the content in diatoms very low. The mineral fraction decreases further from ca. 1.8 m upwards and the uppermost interval is dominated by peat (Fig. 4.1d). This transition is shown through the slight decrease in Ti and Fe and increase in Si/K. Two intervals show a slight increase in the mineral fraction. One is located between 4.8 and 5.05 m (Fig. 4.1c). The other one is very thin near 4.1 m and may be interpreted as the equivalent of the “Salamina” tephra (Parra et al., 2010b) clearly visible in other LLG cores (see core correlation below).

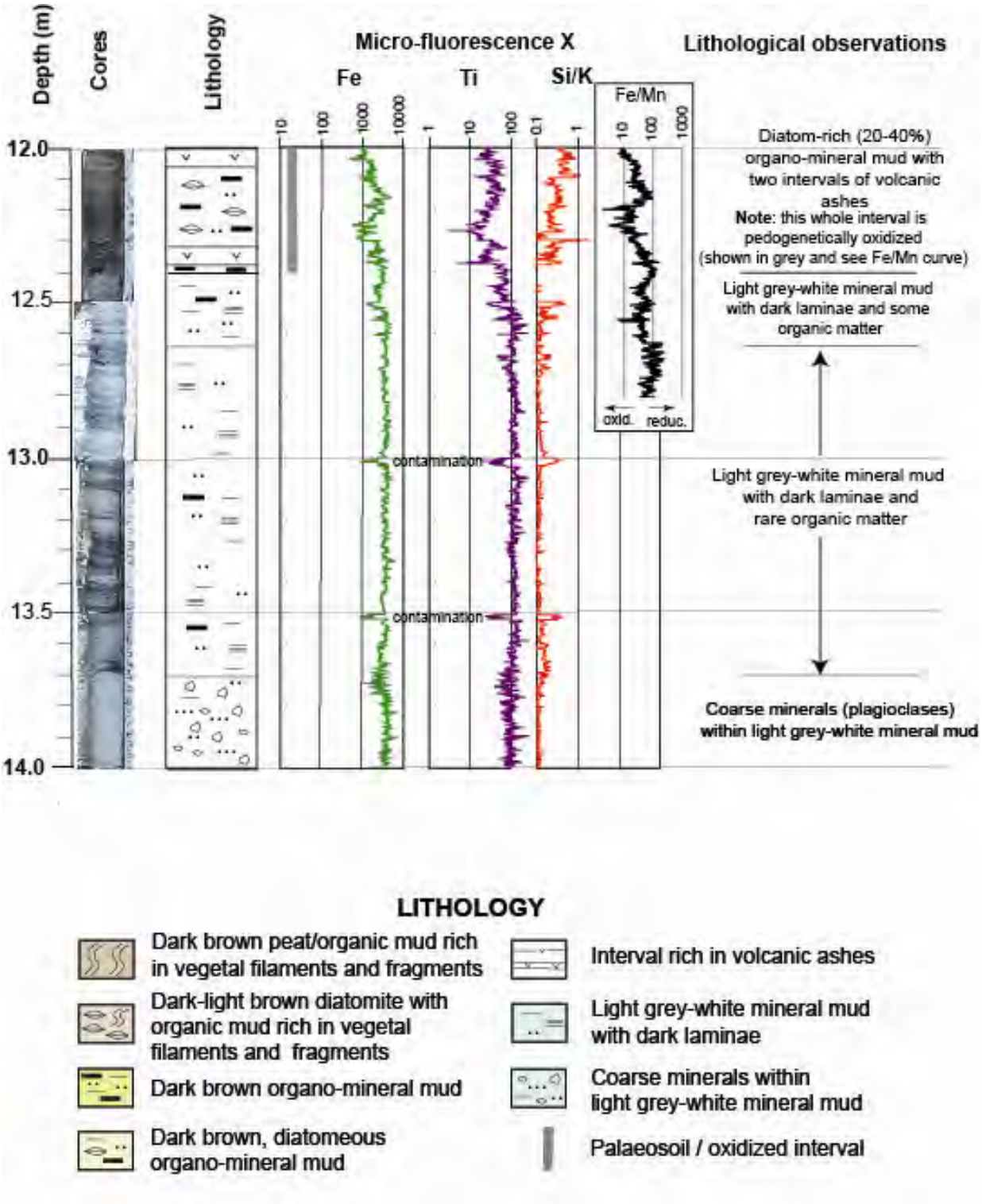

Fig. 4.1a. Lithology of interval 14 - 12 m in core LLG-5.

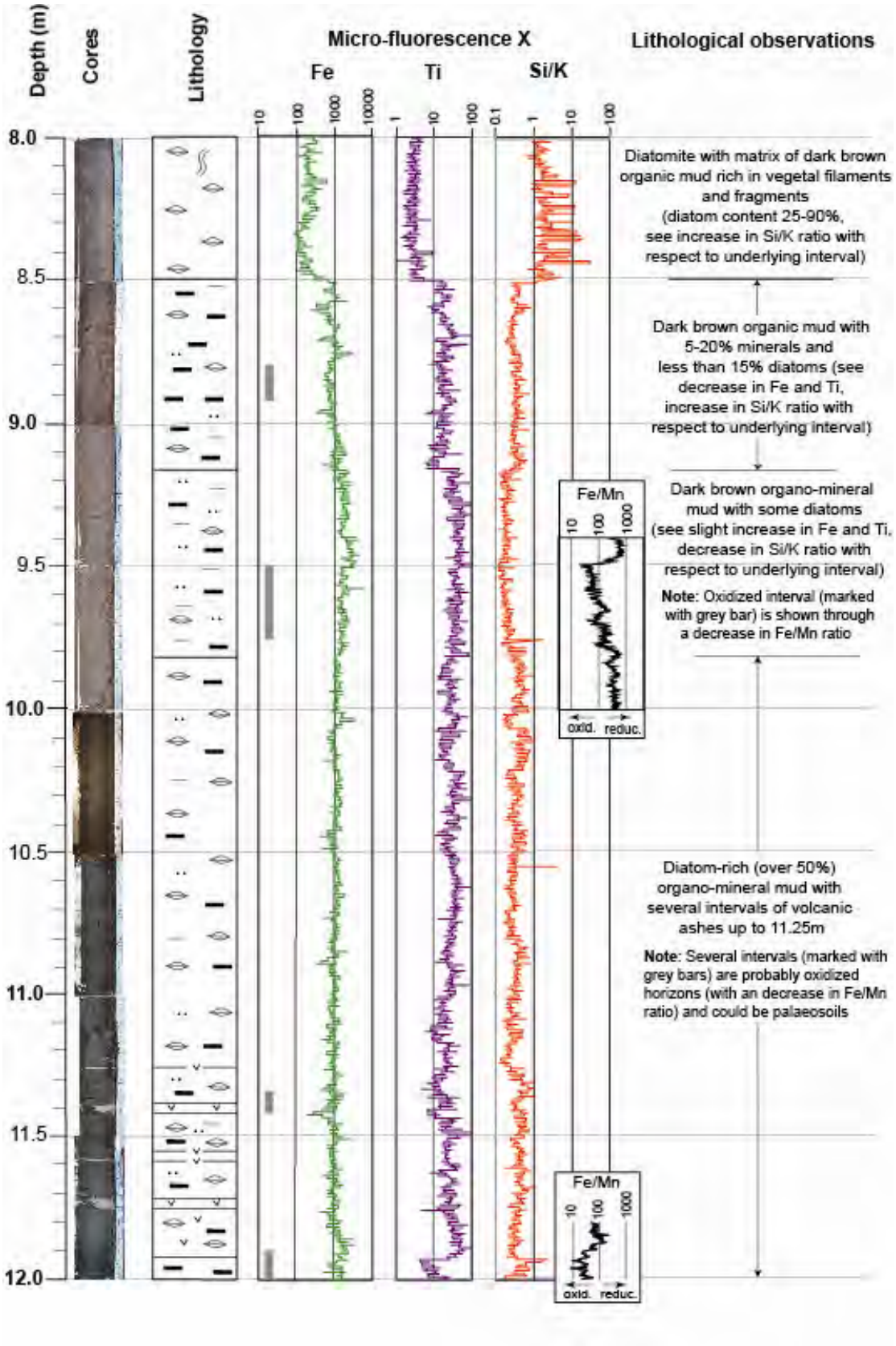

Fig. 4.1b. Lithology of interval 12 - 8 m in core LLG-5. See Fig. 4.1a for lithological legend.

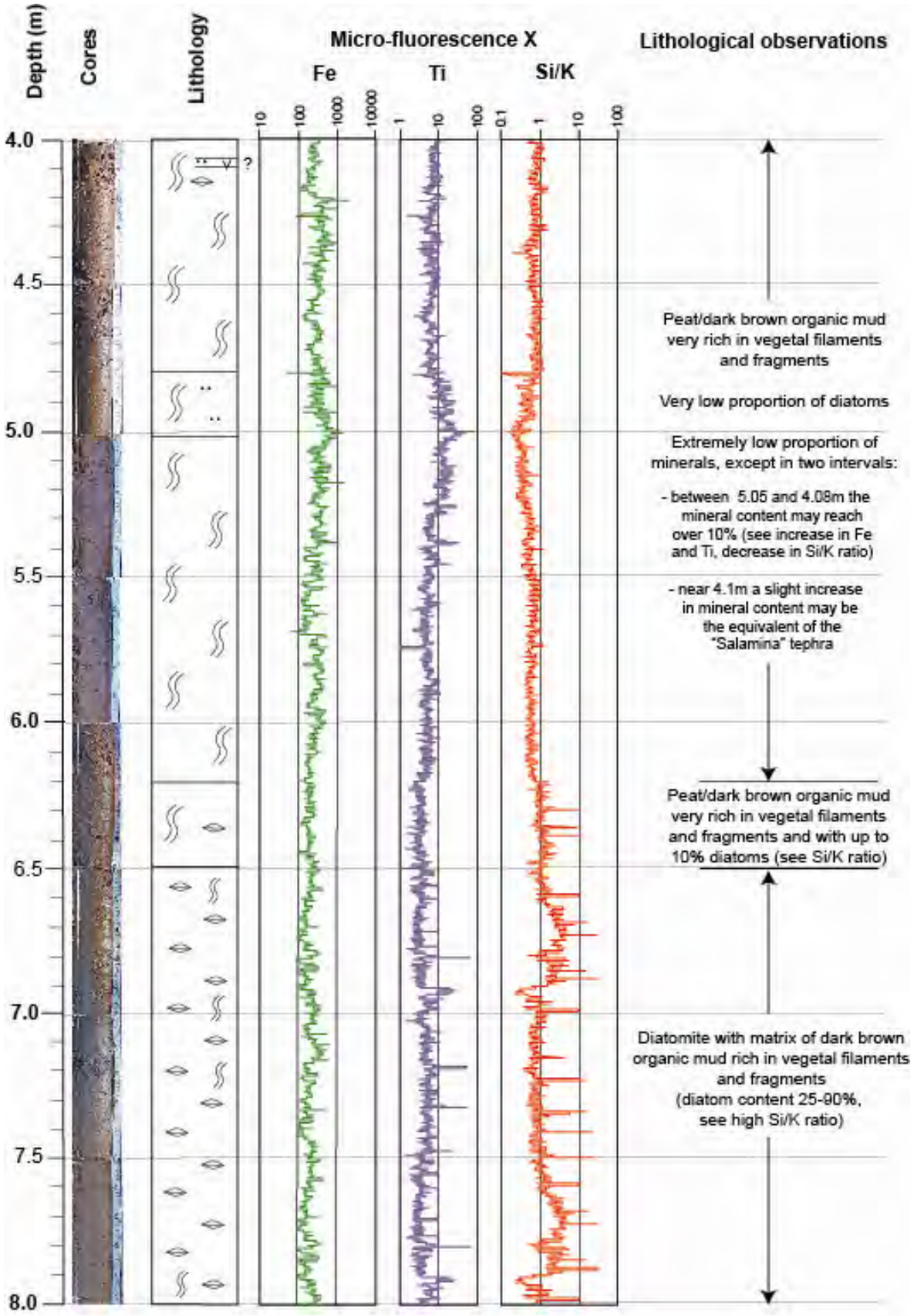

Fig. 4.1c. Lithology of interval 8 - 4 m in core LLG-5. See Fig. 4.1a for lithological legend.

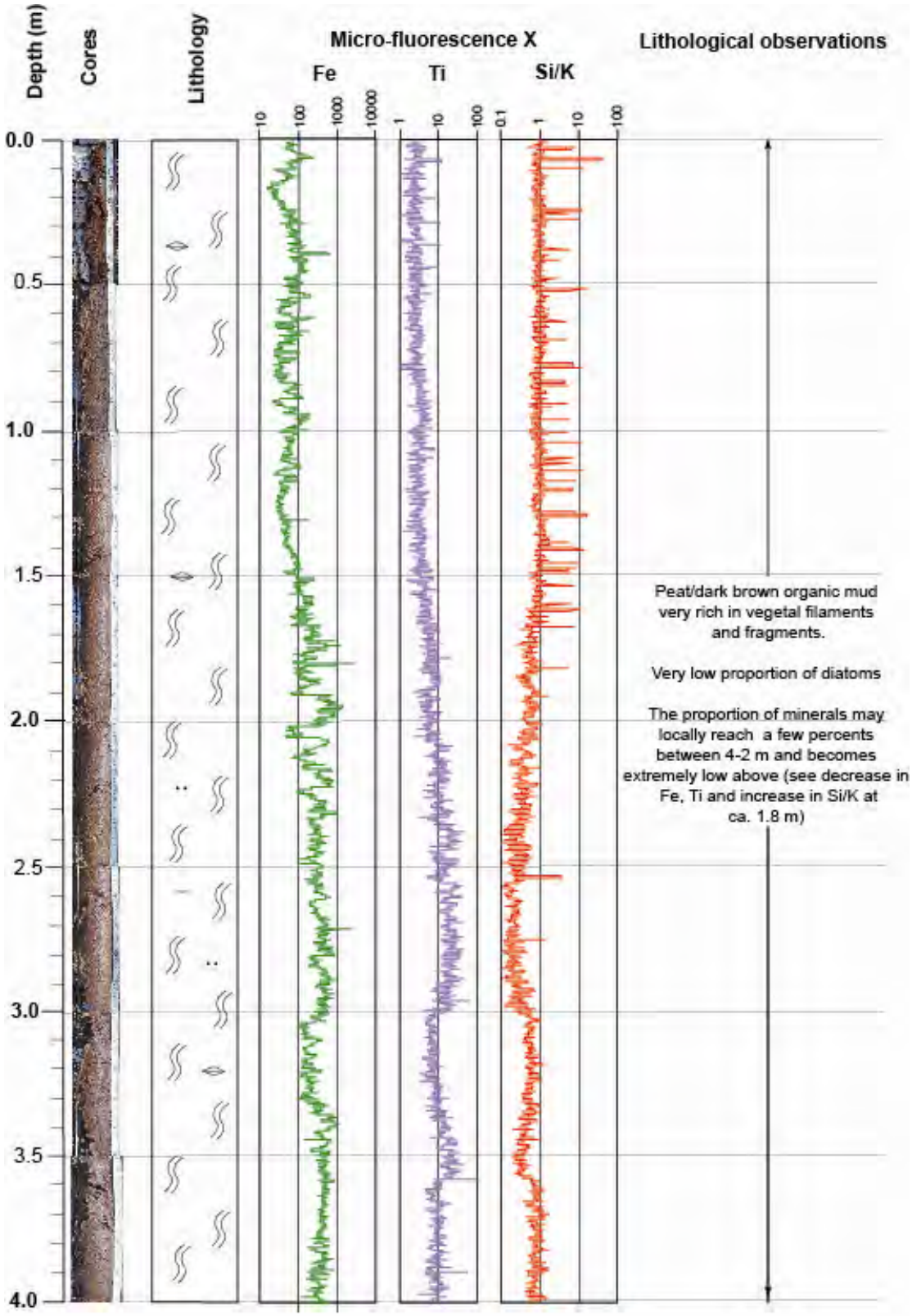

Fig. 4.1d. Lithology of interval 4 - 0 m in core LLG-5. See Fig. 4.1a for lithological legend.

4.2.2. CORRELATION OF CORES LLG-2 TO LLG-9 (FIG. 4.2)

Apart from core LLG-1 taken on the flank of the basin (Fig. 3.2) cores 2 to 9 were recovered in the central part of the basin and are all distant from one another by less than 20 m. Cores 5-9 are concentrated in the deepest part of the depression.

A very precise lithological correlation can be established between cores LLG-2 and LLG-5 (Fig. 4.2). The former has been studied by (Parra, 2005; Parra et al., 2010b) and the latter in the present study. This correlation is particularly important because it will permit to link palynological data obtained in LLG-2 with geochemical data obtained in LLG-5. Moreover, most of the AMS ^{14}C datings come from LLG-5 and the upper part of LLG-2 (see chapter 4.3 below). Correlations with the other cores were made visually and with high-resolution photographs. The sedimentary infill of the Llano Grande depression can be subdivided into three packages from base to top (labeled 1, 2 and 3 in Fig. 4.2):

1) The lowermost interval is made entirely of light-coloured mineral mud with some organic matter in its upper part. It contains numerous intervals with dark laminae that are reminiscent of glacial varves. In LLG-5, coarse mineral grains were encountered at the base, testifying to the proximity of the basement. The upper boundary of this interval is clearly identified as an unconformity. It marks the transition to a dark-coloured organic-rich mineral mud and is located between 12.3 and 12.7 m in all the cores that penetrated it.

2) The organo-mineral interval can be subdivided into two parts. The lower part contains high percentages of diatoms. In its basal part it contains several intercalations of volcanic ashes. These have been tentatively correlated by Parra et al. (2010a) with eruptive stages called Canalones and Romerales by Thouret et al. (1995). According to the age model established for the Llano Grande mire,(see paragraph 2.3), they are dated between 15,000 and 17,000 cal yr BP. Moreover, within this same basal part, two levels of oxidation/paleosoils are encountered. The lowermost one is particularly easy to identify through its black colour (see Figs. 4.1a and b). The upper part of the organo-mineral interval is relatively poor in diatoms and the transition occurs in all cores at a depth comprised between 9.8 and 9.5 m. In LLG-2, this diatom-poor organo-mineral interval contains indications of an oxidized horizon (paleosoil, Parra et al. (2010b). Without detailed analyses, it is difficult to precisely identify such an interval in the other cores. In LLG-5, the relation Fe/Mn might be an indicator (see Fig. 4.1a, b and text above).

The top of the organo-mineral interval is another important marker for the correlation of the cores. It marks a sudden transition to a sediment made essentially of vegetal filaments and fragments with little mineral content apart from diatoms. This change occurs between 8.5 m (LLG-5) and 7.43 m (LLG-2). Nevertheless, although this transition is rapid, there is no indication in any of the cores of an unconformity at this level. The stratification remains horizontal and there are no indications of a major hiatus. The difference in depth between LLG-2 and LLG-5 indicates the existence of a microtopography in the basin or can be explained by differential compaction of underlying sediments. The two cores are distant of less than 11 meters.

3) The lower part of the vegetal-rich upper interval is very rich in diatoms which can locally form up to 90% of the sediments (see Figs. 4.1b and c), thereby forming a true diatomite. The diatom-rich sediment changes suddenly upwards to peat or organic mud extremely rich in vegetal filaments and fragments. This limit occurs in all the cores at ca. 6 m (5.94 m in LLG-2 and 6.2 m in LLG-5). The upper 6 m or so of all cores are identical. Within this interval, the only marker is a few cm-thick intercalation of volcanic ashes situated at around 4 m. It is clearly visible in LLG-2 and LLG-9 and interpreted in LLG-5 (see above). This interval has been previously interpreted as the "Salamina" tephra related to the eruption of the Cerro Bravo volcano and dated at between 6,500 and 7,200 ^{14}C yr BP (Parra, 1991; Parra et al., 2010b) i.e., 7,400 to 8,000 cal yr BP. According to the age model obtained in Llano Grande (see paragraph 4.3), this ash layer appears slightly younger with an age of ca. 6,000 cal yr BP.

This threefold subdivision corresponds to major paleoenvironmental changes. The lower interval made of laminated clays can be interpreted as periglacial clays. This is supported by the datations obtained in LLG-4 and LLG-8 (Fig. 4.2)**.** They probably correspond to the phase of glacier melting. This type of environment is encountered in present-day superpáramo lakes like those in the Sierra Nevada del Cocuy (N. Parra, pers. comm.), where there is hardly any vegetation. The overlying organo-mineral interval without vegetal fiber corresponds to the Tardiglacial (see paragraph 4.3). It can be interpreted as an environment of a few-meter deep páramo black lakes. The latter contain mineral mud associated to the deglaciation and mixed with organic matter from the growing vegetation. The upper interval corresponds to the Holocene period during which the Llano Grande Laguna was infilled mainly by vegetal fragments and little minerals. It was occupied by marshes, peat bogs and very shallow, brackish páramo black lakes (Parra et al., 2010b).

Apart from the limit between glacial clays and the beginning of the organic-rich sedimentation, the whole Tardiglacial and Holocene sequence in Llano Grande does not present any indication of unconformities or significant hiatus in the sedimentation. The numerous datations obtained throughout this sequence confirm the continuity of the deposition (Fig. 4.2 and paragraph 4.3**).** The various correlation lines shown in figure 6 can therefore be considered as **time lines**. This is particularly important when correlating LLG-2 and LLG-5 and establishing the age model for the sediments (see paragraph 4.3).

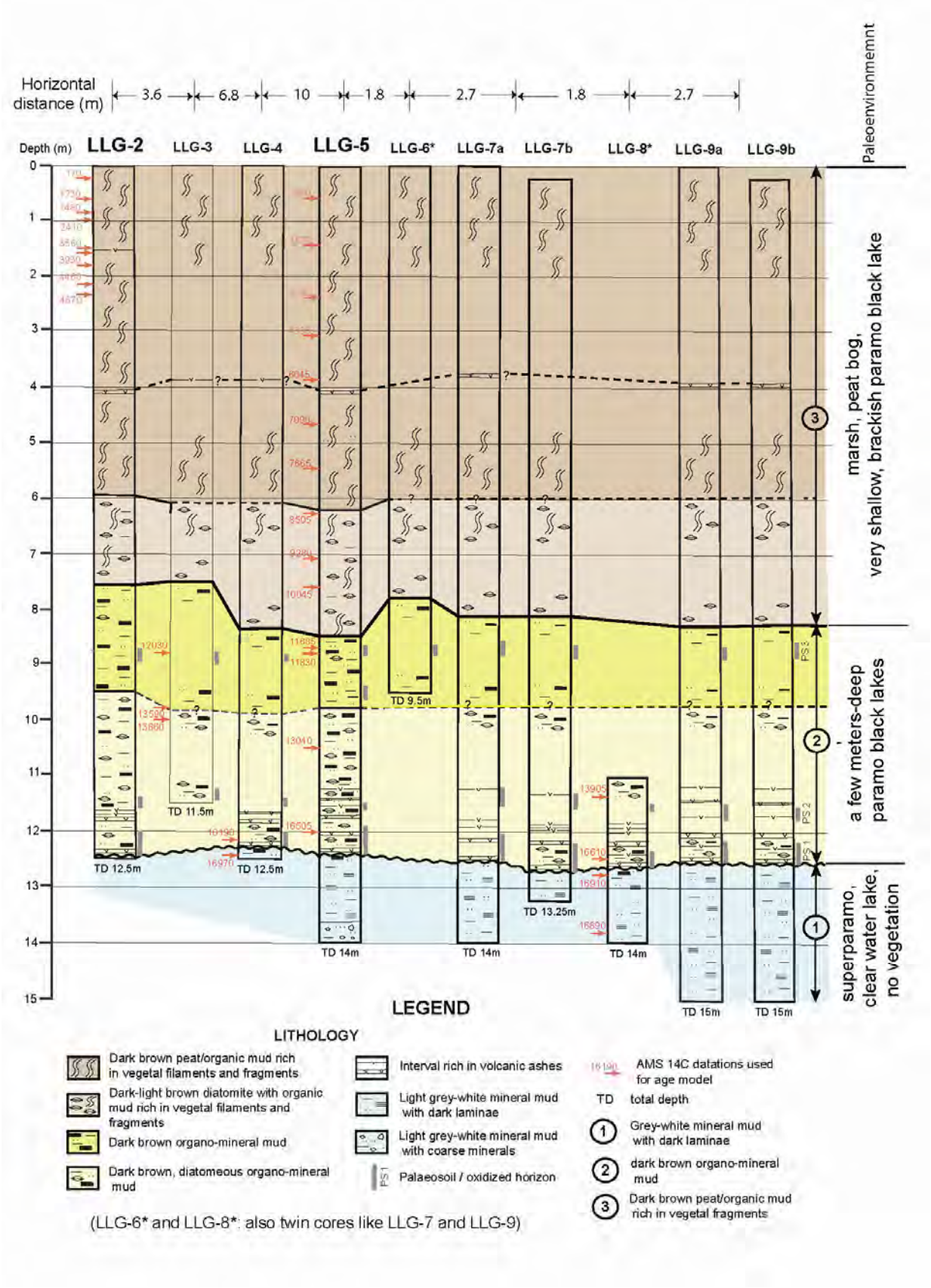

Fig. 4.2. Correlation of Llano Grande cores 2 to 9. The lithology is well studied in cores 2 (Parra, 2005; Parra et al. 2010b) and 5 (this study). The other cores have been studied visually and in photos.

4.3 RADIOCARBON DATINGS AND AGE MODEL

4.3.1. ESTABLISHING THE AGE MODEL

The core LLG-2 was the first one to be radiocarbon dated in the framework of the studies undertaken by Parra (2005) and Velásquez (2005). Out of the thirty-three ^{14}C analyses performed in LLG-2, 25 were carried out using the standard method and 8 using the Accelerator Mass Spectrometry (AMS) method. The AMS datings were concentrated in the first 2.5 meters (Fig. 4.2).

In the framework of the present study, another 29 AMS datings were obtained, principally in LLG-5. Therefore, a total of 37 AMS datings is available for the whole Tardiglacial-Holocene sequence in Llano Grande (Table 4.1). Consequently, it has been decided not to take into consideration the less reliable standard ^{14}C datings available in LLG-2. Among all the available AMS datings, some have been further discarded because they give too low values (oxidized horizons, contamination by shallower roots, not enough organic carbon, see Table 4.1). Finally, the 30 AMS datings shown in Table 4.2 have been kept to establish the age model described below. These data are plotted in Figure 4.3. All but three are concentrated in the organic-rich sediments corresponding to intervals 2 and 3 of figure 4.2. Of these three samples from core LLG-8 taken in the periglacial clays (interval 1 in Fig. 4.2), two are very close to the unconformity separating intervals 1 and 2. They were taken in organic-rich clays and confirm that the age of the unconformity is close to 17,000 cal yr BP.

The third sample was taken more than one meter below the unconformity in core LLG-8 (depth 1370-1380 cm, Table 4.1), in a zone were organic matter becomes scarce. Vegetal remains had to be concentrated from the clays prior to dating. The age obtained is also very close to 17,000 cal yr BP (Table 4.1). Because of scarcity of organic matter, this age is probably slightly underestimated but indicates that the sedimentation rate of the (peri)glacial clays has been very rapid. This last sample has not been considered in the model, the aim of which was to produce a mean to convert in time the results of palynology and geochemistry obtained in intervals 2 and 3 of cores LLG-2 and LLG-5, respectively. Consequently 30 datations have been used in the model (Table 4.2).

Figure 4.2 shows the main correlation lines linking the various cores. As mentioned above these can be considered as **time lines** because no hiatus has been observed in any of the cores. The cores are all located very close to each other in the deeper central part of the depression (Fig. 3.2). In all of them the studied interval 2+3 has the same thickness. Only a small variation in depth is observed between cores LLG-2 and LLG-5 at the limit of intervals 1 and 2. Nevertheless, for the reasons exposed above, this line can be taken as a time line.

All AMS datings have been plotted with respect to their depth (Fig. 4.3), and a polynomial function has been adjusted to provide a depth vs. age curve, which has been labeled LLG-5, because most of the datings come from LLG-5 grey (curve in Fig. 4.3). Nevertheless, in order to find the best adjustment, two polynomial functions had to be used to accommodate the very low sedimentation rate of the upper 1.5m of the cores. In this upper part, datings from LLG-2 complemented by those of LLG-5 give a very accurate function (Fig. 4.3).

Core	Interval (cm)	av. depth (cm)	Age yr BP	Deviation (±)	cal yr BP (Intcal04) 2σ	Deviation (±)	δC13 (o/oo PDB)	C14 Lab	Lithology	Remarks
LLG-2	19-21	20	130	30	170	110	-25	Poz-235	peat	
LLG-5	50-53	51.5	770	40	700	40	-27.6	Beta-259645	fibrous organic mud	
LLG-2	58-61	59.5	1280	30	1230	60	-25	Poz-238	fibrous organic mud	
LLG-2	76-80	78	1600	30	1480	70	-25	Poz-237	peat	
LLG-2	94-98	96	2370	35	2410	75	-25	Poz-238	fibrous organic mud	
LLG-2	139-148	143.5	3340	35	3560	85	-25	Poz-251	fibrous organic mud	
LLG-5	140-142	141	3330	40	3570	110	-24.3	Beta-259646	fibrous organic mud	
LLG-2	175-178	176.5	3630	35	3930	80	-25	Poz-232	peat	
LLG-2	211-214	212.5	4030	35	4490	70	-25	Poz-250	fibrous organic mud	
LLG-2	228-230	229	4120	40	4670	150	-25	Poz-239	fibrous organic mud	
LLG-5	230-233	231.5	3890	40	4290	130	-25.7	Beta-259647	fibrous organic mud	
LLG-5	300-303	301.5	3910	40	4335	95	-26.2	Beta-259648	fibrous organic mud	
LLG-5	380-383	381.5	5230	40	6045	125	-24.7	Beta-259649	fibrous organic mud	
LLG-5	460-463	461.5	6170	50	7090	150	-25.6	Beta-259650	fibrous organic mud	
LLG-5	540-543	541.5	6830	50	7665	85	-25.3	Beta-259651	fibrous organic mud	
LLG-5	620-623	621.5	7730	50	8505	95	-26.3	Beta-259652	fibrous organic diatom. mud	
LLG-5	700-703	701.5	8280	50	9280	160	-25	Beta-259653	fibrous organic diatom. mud	
LLG-5	746-748	747	8050	50	8900	130	-26.4	Beta-246335	fibrous organic diatom. mud	too low value
LLG-5	752-754	753	8910	50	10045	155	-26.1	Beta-246336	fibrous organic diatom. mud	
LLG-5	866-868	867	10080	50	11685	295	-24.8	Beta-246337	organo-mineral mud	
LLG-5	872-874	873	10150	50	11830	220	-25.6	Beta-246338	organo-mineral mud	
LLG-3	874-876	875	10280	60	12030	215	-29.1	Poz-21086	organo-mineral mud	
LLG-5	960-963	961.5	9370	60	10580	150	-27.6	Beta-259654	oxidized organo-mineral mud	too low value
LLG-3	974-976	975	11740	70	13590	170		Poz-21087	organo-mineral mud	
LLG-3	994-996	995	11980	70	13860	150		Poz-21088	organo-mineral diatom. mud	
LLG-5	1046-1048	1047	11120	60	13040	140	-27	Beta-246339	organo-mineral diatom. Mud	
LLG-5	1110-1112	1111	9330	60	10505	195	-24.8	Beta-259655	oxidized organo-mineral mud	too low value
LLG-8	1130-1134	1132	11950	100	13905	105	-26.6	Beta-286835	organo-mineral mud	
LLG-8	1130	1130	11205	75	13160	80	-26.7	Beta-287418	plant remains	root contamination
LLG-8	1185	1185	11940	120	13890	120	-27.5	Beta-286836	plant remains	root contamination
LLG-5	1197-1200	1198.5	13850	70	16505	365	-27	Beta-259656	organo-mineral mud	
LLG-4	1212-1214	1213	13590	90	16190	430		Poz-21090	organo-mineral mud	
LLG-4	1237-1239	1238	14210	90	16970	460		Poz-21091	organo-mineral mud	
LLG-5	1242-1247	1246	10900	60	12875	65	-24	Beta-259658	wh-blk lamin. clay	not enough C
LLG-8	1240-1243	1241.5	13940	70	16610	180	-28.9	Beta-278833	organo-mineral mud	
LLG-8	1266-1274	1270	14170	70	16910	175	-27.8	Beta-278834	organo-mineral mud	
LLG-8	1370-1380	1375	14130	70	16890	200	-23.2	Beta-278835	concentrated plant material	below studied zone

Table 4.1. AMS ^{14}C datations available in the Llano Grande wet zone. Those highlighted in grey have not been considered for the age model because of too low values for various reasons. The deepest value at 1370 - 1380 cm being in the glacial clays, it has not been used in the model.

Another function was obtained using data from 150 to 1280 cm. These two functions merge perfectly at 148 cm and form the continuous grey curve in figure 4.3. This curve is that to be used to convert the µXRF data from depth to age. Because all palynological data have been obtained from the core LLG-2 and because there are some differences in the depth of time lines with respect to core LLG-5 (Fig. 4.2)**,** some adjustments need to be made to properly convert palynological data in core LLG-2 from depth to age. These adjustments correspond to the black curve in figure 4.3 valid from 405 to 1249 cm in LLG-2.

There is no change in depth between the two cores down to 405 cm (volcanic ashes, time line labeled “a” in Fig. 4.3). Depth differences between LLG-2 and LLG-5 occur for the time lines labeled “b”, “c” and “d”. The time line labeled “e” is at the same depth in both cores. Consequently, the age of time lines “b”, “c” and “d” was established using the LLG-5 age model in grey. Then, this age was plotted with respect to the depth of time lines “b”, “c” and “d” in LLG-2, and a linear time function was obtained for each segment (see black line in Fig. 4.3 between 405 and 1249 cm). To convert palynological data of LLG-2 from depth to age, one has to use the LLG-5 grey function down to 405 cm, then the four linear functions defining the depth vs. age curve in black between 405 and 1249 cm (Fig. 4.3).

Core	Interval (cm)	av. depth (cm)	Age yr BP	Deviation (±)	cal yr BP (Intcal04) 2σ	Deviation (±)	δC13 (o/oo PDB)	C14 Lab	Lithology
LLG-2	19-21	20	130	30	170	110	-25	Poz-235	peat
LLG-5	50-53	51.5	770	40	700	40	-27.6	Beta-259645	fibrous organic mud
LLG-2	58-61	59.5	1280	30	1230	60	-25	Poz-238	fibrous organic mud
LLG-2	76-80	78	1600	30	1480	70	-25	Poz-237	peat
LLG-2	94-98	96	2370	35	2410	75	-25	Poz-238	fibrous organic mud
LLG-2	139-148	143.5	3340	35	3560	85	-25	Poz-251	fibrous organic mud
LLG-5	140-142	141	3330	40	3570	110	-24.3	Beta-259646	fibrous organic mud
LLG-2	175-178	176.5	3630	35	3930	80	-25	Poz-232	peat
LLG-2	211-214	212.5	4030	35	4490	70	-25	Poz-250	fibrous organic mud
LLG-2	228-230	229	4120	40	4670	150	-25	Poz-239	fibrous organic mud
LLG-5	230-233	231.5	3890	40	4290	130	-25.7	Beta-259647	fibrous organic mud
LLG-5	300-303	301.5	3910	40	4335	95	-26.2	Beta-259648	fibrous organic mud
LLG-5	380-383	381.5	5230	40	6045	125	-24.7	Beta-259649	fibrous organic mud
LLG-5	460-463	461.5	6170	50	7090	150	-25.6	Beta-259650	fibrous organic mud
LLG-5	540-543	541.5	6830	50	7665	85	-25.3	Beta-259651	fibrous organic mud
LLG-5	620-623	621.5	7730	50	8505	95	-26.3	Beta-259652	fibrous organic diatom. mud
LLG-5	700-703	701.5	8280	50	9280	160	-25	Beta-259653	fibrous organic diatom. mud
LLG-5	752-754	753	8910	50	10045	155	-26.1	Beta-246336	fibrous organic diatom. mud
LLG-5	866-868	867	10080	50	11685	295	-24.8	Beta-246337	organo-mineral mud
LLG-5	872-874	873	10150	50	11830	220	-25.6	Beta-246338	organo-mineral mud
LLG-3	874-876	875	10280	60	12030	215	-29.1	Poz-21086	organo-mineral mud
LLG-3	974-976	975	11740	70	13590	170		Poz-21087	organo-mineral mud
LLG-3	994-996	995	11980	70	13860	150		Poz-21088	organo-mineral diatom. mud
LLG-5	1046-1048	1047	11120	60	13040	140	-27	Beta-246339	organo-mineral diatom. Mud
LLG-8	1130-1134	1132	11950	100	13905	105	-26.6	Beta-286835	organo-mineral mud
LLG-5	1197-1200	1198.5	13850	70	16505	365	-27	Beta-259656	organo-mineral mud
LLG-4	1212-1214	1213	13590	90	16190	430		Poz-21090	organo-mineral mud
LLG-4	1237-1239	1238	14210	90	16970	460		Poz-21091	organo-mineral mud
LLG-8	1240-1243	1241.5	13940	70	16610	180	-28.9	Beta-278833	organo-mineral mud
LLG-8	1266-1274	1270	14170	70	16910	175	-27.8	Beta-278834	organo-mineral mud

Table 4.2. The 30 AMS ^{14}C datations used to establish the age model of the Llano Grande wet zone.

4.3.2. LLANO GRANDE SYNTHETIC LITHOLOGICAL SECTION IN TIME AND SEDIMENTATION RATES

The age model of figure 4.3 shows that the studied section in Llano Grande from 1250 cm to surface corresponds to an interval spanning the Lateglacial and Holocene. The synthetic lithological section in calibrated time established from the age model (Fig. 4.4) indicates that the mineral-rich lower section characterizes the Lateglacial period with a significant input of siliciclastic erosion products until approximately 11,400 cal yr BP. From 11,400 cal yr BP, the sedimentation was dominated by organic matter associated with the development of marshes, peatbogs and brackish páramo lakes with very little mineral input.

The age model permits the calculation of sedimentation rates (Fig. 4.4)**.** The top bottom of the glacial clays is at ca. 17,000 cal yr BP. The infill of the deepest part of the depression was probably very rapid with the melting of the ice. The age dating in LLG-8 more than one meter below the unconformity confirms the very high sedimentation rate, most probably of over 1m/1000yr. The period between ca. 16,700 and 11,400 cal yr BP corresponds to an active erosion phase with an important mineral input into the depression. Sedimentation rates varied between 0.7 and 1.1 m/1000yr. From 11,400 cal yr BP, organic sedimentation dominated. Until ca. 3,200 cal yr BP the rate of accumulation of organic matter was high, varying between 0.6 to 0.85 m/1000yr. During the last 3,000 years, sedimentation was dominated by the formation of peat and sedimentation rates dropped to 0.5 m/1000yr.

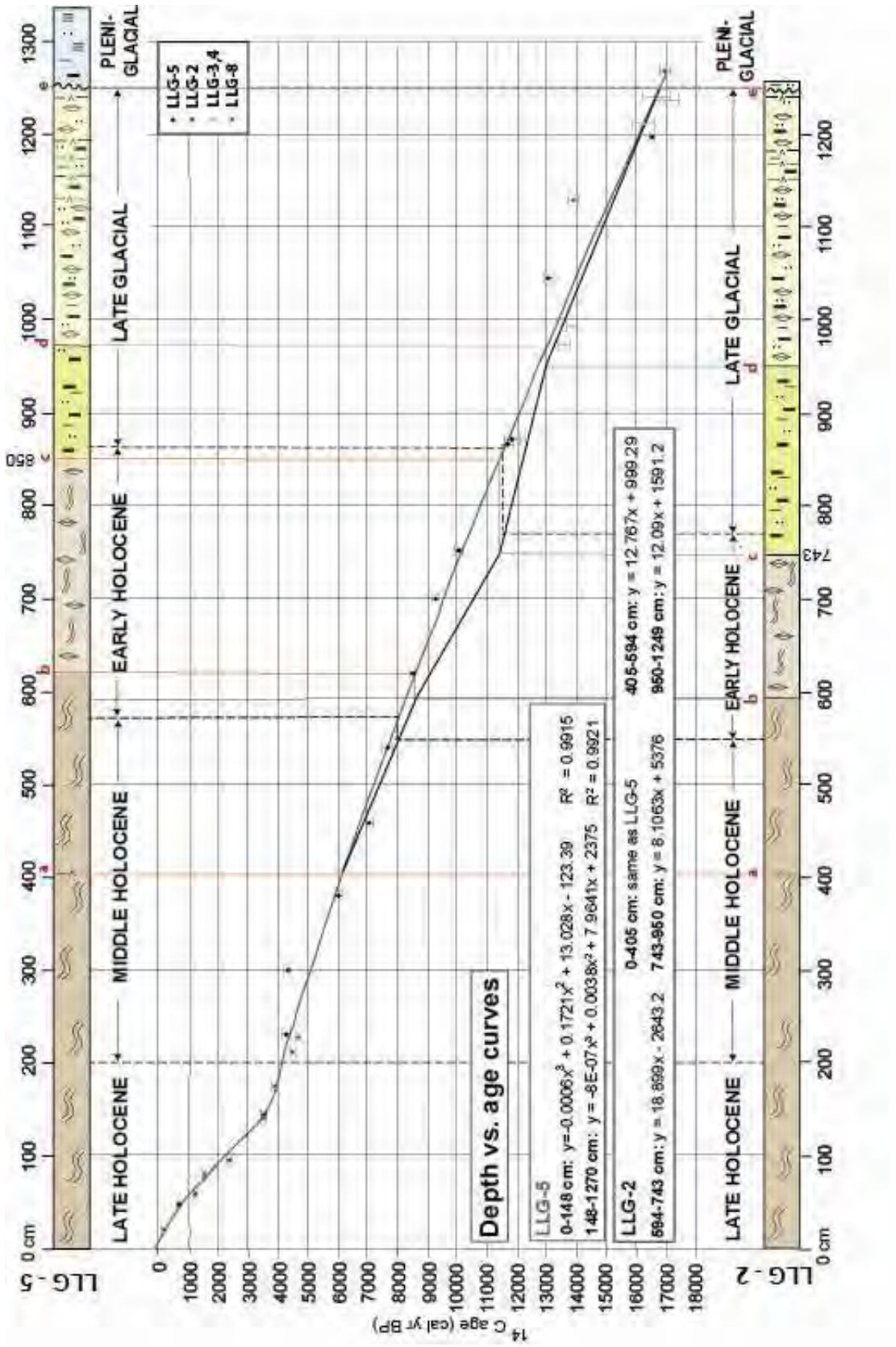

Fig. 4.3. Age model for the Llano Grande wet zone: the grey curve is to be used to convert µXRF data of LLG-5 from depth to age (cal yr BP), and the black curve to convert palynological data of LLG-2 from depth to age (cal yr BP) in interval 405 - 1249 cm. Letters a to e in red correspond to lithological limits that are time lines (see Fig. 4.2).

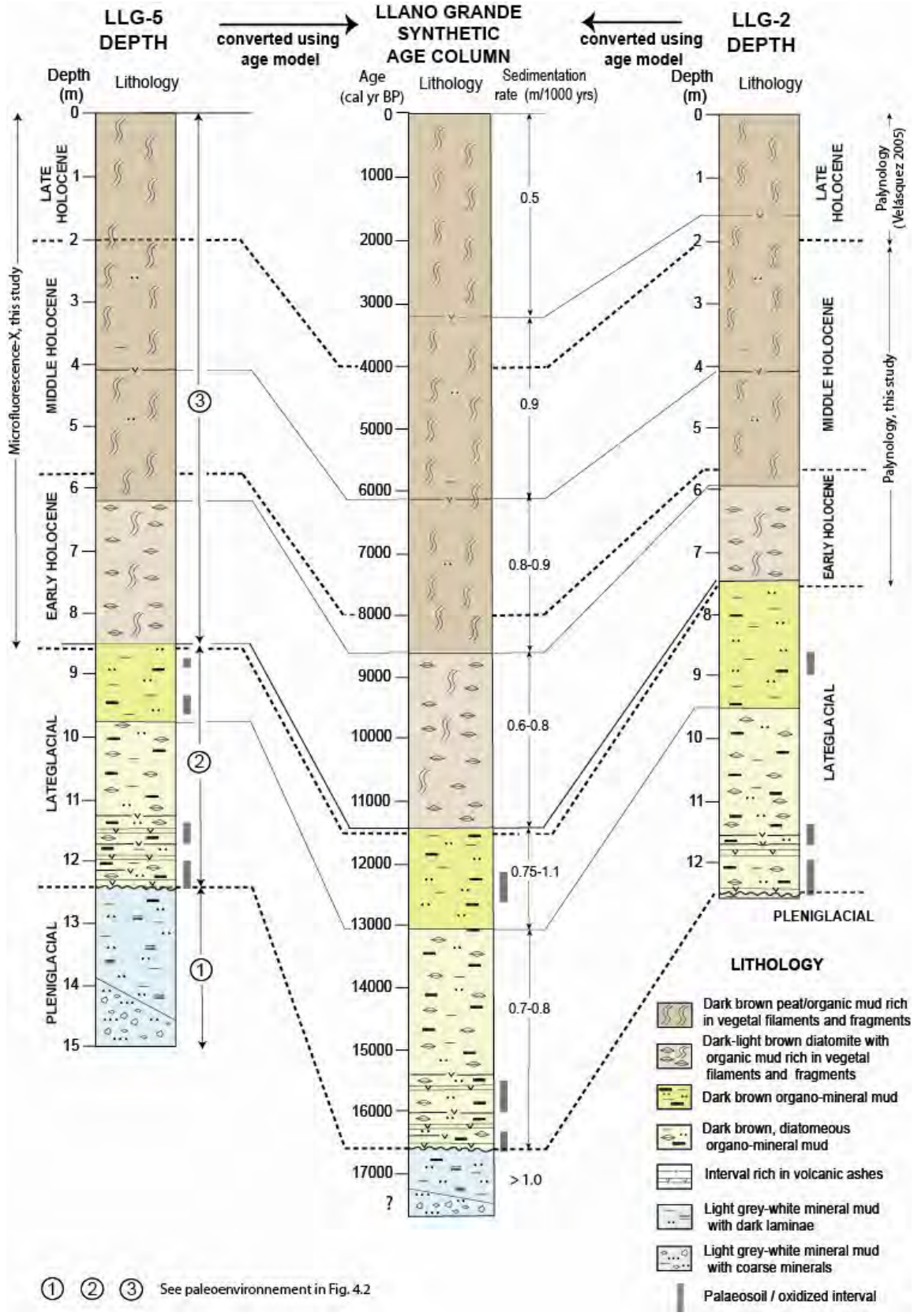

Fig. 4.4. Synthetic lithological column in time for the Llano Grande wet zone and estimation of sedimentation rates.

Obviously, these sedimentation rates need to be also analyzed in relation with the intensity of precipitations that can be derived from the palynological (see chapter 4.4) and geochemical proxies (see chapter 4.5) used in the project.

The age model of figure 4.3 and the correlation in figure 4.4 show that the interval studied by palynology in this research, i.e., from 220 cm to 754 cm in LLG-2, spans the whole Early and Middle Holocene. The interval studied by Velásquez (2005), i.e., 0-220 cm in LLG-2, spans the Late Holocene. According to the age model of figure 4.3, the deepest sample studied in LLG-2 at 754 cm is dated at 11,490 cal yr BP, which corresponds in LLG-5 to a depth of 857 cm. Therefore, our study covers the major lithological change from a mineral-rich sediment (paleoenvironment 2) to an organic- and filament-rich sediment (paleoenvironment 1). This change is located at 743 cm in LLG-2 and 850 cm in LLG-5 and is dated at ca. 11,400 cal yr BP (Fig. 4.3). Consequently, the age scale of all diagrams shown in this research will start at 11,500 cal yr BP.

4.4. PALYNOLOGY

4.4.1. REGIONAL VEGETATION CHANGE

Here we present the description of results for regional vegetation in a wide area around the Llano Grande mire, in the zone of the Páramo de Frontino for the period between 4,300 and 11,500 cal yr BP. The palynological results of taxa included in the pollen sum have been plotted with respect to an age scale in cal yr BP (Fig. 4.5). This period corresponds to the 220-754 cm interval in core LLG-2 (see age model above).

Over this interval, 203 samples have been studied, which corresponds to a time resolution of ca. 35 years. In part 5, these data will be combined with those of Velásquez (2005) who studied the interval 0-220 cm (0 - 4,300 cal yr BP, i.e., the Late Holocene) with a resolution of ca. 20 years. The pollen diagram shows taxa *included in the pollen sum* for each vegetation belt, i.e., subandean forest (7 taxa), Andean forest (18 taxa) and páramo vegetation (15 taxa), which represent the regional vegetation. Others groups (see Appendix A2) were identified, such as Pteridophytes (9 taxa), algae (4 taxa), diatoms and other 10 taxa which had low proportions.

Based on CONISS cluster analysis we recognize 5 periods/zones and 10 subzones which are described below (Fig. 4.5). **In these results, the relative change in the average percentage of a species/vegetation belt with respect to the previous period will be expressed in % change (%CH). All percentages of taxa in parentheses correspond to average values over the period described.**

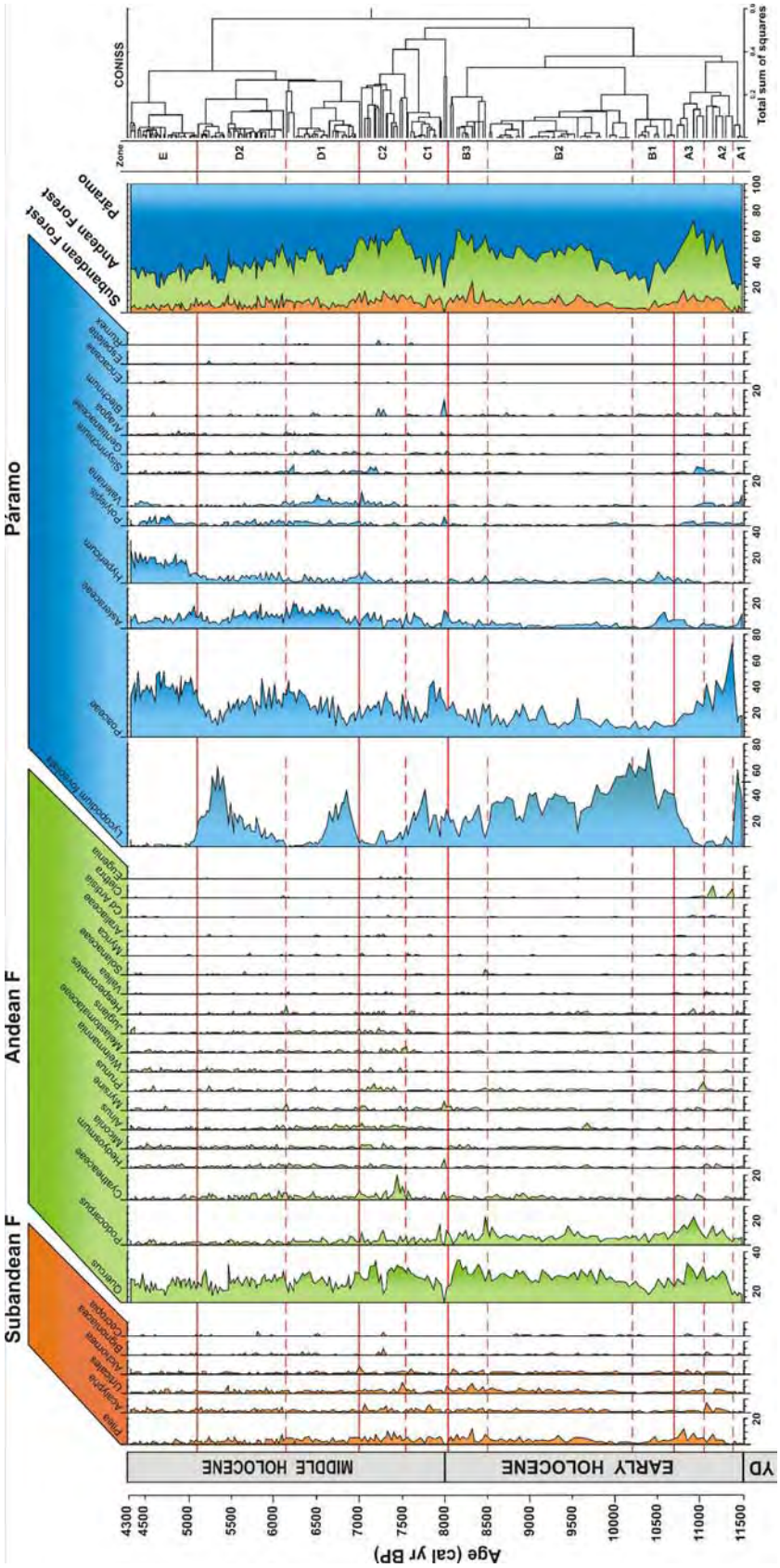

Fig. 4.5. Pollen diagram for taxa *included in the pollen sum* of LLG-2 core from 220 to 754 cm. Data are plotted with respect to an age scale in cal yr BP. From left to right: records in percents of selected taxa (included in the sum) grouped within their respective vegetation belt. On the right hand side, summary of the distribution of vegetation belts in percents, palynological zones and CONISS dendrogram. (YD=Younger Dryas equivalent).

POLLEN ZONE A (11,488 - 10,700 CAL YR BP)

Period 1: Subzone A1 (11,488 - 11,400 cal yr BP): 4 samples

This period corresponds to the highest proportion of páramo vegetation over the whole Early and Middle Holocene record, with an average value of 78.6%. Consequently, forest vegetation (subandean and Andean forests) exhibits its minimum proportions of the whole record with an average value of 21%. This period probably marks the end of the Younger Dryas (YD) equivalent.

The subandean forest represents only 3.1% and is mainly made of *Pilea* (1.6%), *Acalypha* and Urticales. The Andean forest is dominated by *Quercus* (7.1%) and *Podocarpus* (5.4%). Cyatheaceae have an average value of 1.9%. Páramo vegetation is represented mainly by *Lycopodium foveolata* (43.9%) and Poaceae (21.7%). Asteraceae (5.1%) and *Valeriana* (3.8%) are moderaly represented. *Polylepis* has an average value below 2%.

Period 2: Subzone A2 (11,400 - 11, 050 cal yr BP): (6 samples)

The subandean forest and the Andean forest vegetation show their highest relative increase of the whole Early and Middle Holocene (173%CH and 104%CH respectively). Consequently, this coincides with the maximum relative decrease (-31%CH) of páramo vegetation in the whole record. During the whole period, there is no significant dominance of forest (46%) or páramo (54%) vegetation. Poaceae show the highest relative increase in the Early-Middle Holocene with 98.6%CH.

In the subandean forest, *Pilea* (3%) and *Acalpyha* (2.4%) present an important relative increase but remain with low values. In the Andean forest, *Quercus* (18.3%) increases significantly and becomes the most abundant tree, together with *Podocarpus* (8.3%). *Clethra* (2.9%) and *Hedyosmum* (1.5%) present low values. The páramo vegetation is dominated mainly by Poaceae (43%) which has a relative increase of 98%CH. On the other hand, *Lycopodium foveolata* has a considerable relative decrease (-92%CH). *Polylepis* and *Sysyrinchium* increase but their average value remains below 2%. Asteraceae decreases considerably (-68%CH) down to an average value of 1.6%.

Period 3: Subzone A3 (11,050 - 10,700 cal yr BP): (6 samples)

During this period, the forest vegetation (subandean and Andean forests) reaches its maximum proportion of the whole Early and Middle Holocene. It increases significantly (30%CH) to reach a maximum value of 71% and an average value of 59%. This period also coincides with the highest proportion of Andean forest in the whole record (48%).

In the subandean forest, *Pilea* (43%) presents an important relative increase (113%CH) which makes it the dominant element. *Acalypha* shows its highest relative decrease (-53%CH) in the record. Urticales increase (49%CH) but keep a low average value (2%). *Quercus* (22%, 24%CH) and *Podocarpus* (13%, 67%CH) increase together and dominate the Andean forest. Cyatheaceae, *Miconia* and *Prunus* increase but keep average values below 2%. Other taxa with low average values (<2%) such as *Morella* and *Hesperomeles* present their highest relative increase of the whole record (254%CH and 86%CH

respectively). *Hedyosmum* presents its highest relative decrease in the record (-63%CH) to reach a very low average value of 0.5%.

In the páramo vegetation, Poaceae (20%) and *Lycopodium foveolata* (10%) are dominant. Their behaviour is opposite, whereas *Lycopodium foveolata* presents a relative increase of 195%CH, Poaceae decrease (-53%CH). Asteraceae (108%CH) and *Sisyrinchium (*65.9%CH) increase significantly, V*aleriana* decreases towards the end of the period and disappears. Gentianaceae appear for the first time in the studied record.

POLLEN ZONE B (10,700 - 8,050 CAL YR BP)

Period 4: Subzone B1 (10,700 - 10,200 cal yr BP): (9 samples)

This period is characterized by the highest relative increase in páramo vegetation during the Early-Middle Holocene (average value 68% and 67%CH). Consequently, the average value of the subandean forest decreases to 5.5% (-51.7%CH) and that of the Andean forest to 26.3% (-45%CH). This period shows the poorest representation of tree elements of Andean forest during the Early and Middle Holocene. This is illustrated by the highest relative decrease in average value of many taxa such as *Pilea* (-57%CH) and Urticales (-60%CH) in the subandean forest and *Quercus* (-40%CH), *Podocarpus* (-47%CH), *Hedyosmum* (-61%CH), Melastomataceae (-50%CH) and *Miconia* (-52%CH) in the Andean forest.

In the subandean vegetation, all elements have low average values. It is dominated by *Pilea (*2.8%), *Acalypha (*0.9%) and Urticales (0.8%). In the Andean forest, *Podocarpus* and *Quercus* remain the dominant taxa but their proportion is extremely reduced. Cyatheaceae decrease significantly (-57%CH) and *Clethra* disappears. The páramo vegetation is dominated by *Lycopodium foveolata* (50%) and Poaceae (9.3%). Their behaviour is opposite: whereas *Lycopodium foveolata* presents a relative increase of 396%CH, Poaceae continue to decrease (-53%CH). Asteraceae and *Hypericum* increase together and have average values of 4.1% and 2.9% respectively. Although Ericaceae increase considerably (166%CH), their average value is extremely low (0.4%). *Sisyrinchium* and *Polylepis* decrease considerably.

Period 5: Subzone B2 (10, 200 - 8,500 cal yr BP): (35 samples)

The lower part of this subzone continues to be dominated by páramo vegetation until 9,800 cal yr BP with an average value of 67%. From then on, it starts to decrease and the forest vegetation (subandean and Andean forests) becomes more important. Until the end of the period both vegetation belts are co-dominant with no significant differences in their proportions (forest average value of 47% and páramo average value of 53%). In general terms, the proportion of forest vegetation significantly increases with respect to the previous period. The subandean forest shows an important relative increase of 49.7%CH and the Andean forest of 36.1%CH. Urticales and *Hedyosmum* show their highest relative increase of the whole studied interval (138%CH and 186%CH respectively), whereas in the páramo vegetation *Hypericum* shows its highest relative decrease (-51%CH).

*Pilea (*3.3%) and Urticales (1.8%) increase together and dominate the subandean forest. *Acalypha* and *Alchornea* also increase but remain at values below 2%. The Andean forest is dominated by *Quercus* (20.5%) which increases markedly and by *Podocarpus* (6.7%). Cyatheaceae also have an important relative increase (77%CH). Taxa such as *Alnus, Juglans*, *Hedyosmum, Miconia,* and *Myrsine* increase but their average value remains below 1%. The páramo vegetation continues to be dominated by *Lycopodium foveolata* (although it shows a relative decrease of -36.5%CH) and Poaceae, which show an opposite behaviour (+46%CH). Asteraceae (-46%CH) and *Hypericum* (-51%CH) decrease and *Valeriana* starts to increase. *Espeletia* makes its first appearance in the column with a very low value of 0.04%.

Period 6: Subzone B3 (8,500 - 8,050 cal yr BP): (12 samples)

The forest vegetation continues to increase and there is a co-dominance between forest (54.4%) and páramo vegetation (45.6%). There is an overall relative increase in forest vegetation (23%CH), but the subandean vegetation increases (47%CH) in greater proportion than the Andean forest (17%CH). Near the end of the period (8,100 cal yr BP) the páramo vegetation starts to increase again.

Pilea (5.4%) and Urticales (3.2%) increase together and continue to dominate the subandean forest. At the same time, *Acalypha* and *Alchornea* also increase but their average value remains below 2%**.** The Andean forest consists mainly of *Quercus* (25%) and *Podocarpus* (8%), which both increase with respect to the previous period. Cyatheaceae are constant. Tree elements in low proportions such as *Miconia, Myrsine* and *Vallea* increase significantly, whereas *Alnus* and *Weinmannia* decrease. In the páramo vegetation *Lycopodium foveolata* and Poaceae dominate with similar average values of 18%, although within the period their behaviour is opposite: while *Lycopodium foveolata* decreases (-50.3%CH), Poaceae increases (up to 38%CH). Asteraceae increase considerably (84%CH). On the other hand, *Hypericum* increases but keeps low proportions (2%). *Espeletia* disappears again.

POLLEN ZONE C (8,050 - 7,000 CAL YR BP)

Period 7: Subzone C1 (8,050 - 7,580 cal yr BP): (13 samples)

The páramo vegetation dominates with an average value of over 60% and decreases at the end of the period. The AP% decreases (-30%CH) and most of its elements are poorly represented or absent during the period.

In the subandean forest, *Pilea* (3.2%) with a relative decrease of –34%CH and *Acalypha* (2.3%) with a relative increase of 27%CH are the most important taxa, whereas Urticales decrease considerably (-47%CH). In the Andean forest, *Quercus* (16.7%) and *Podocarpus* (5.2%) are dominant but decrease. Taxa with low average values such as *Myrsine* (1.6%) and *Alnus* (0.8%) increase, while Cyatheaceae (1.6%), *Miconia* (0.7%) and *Vallea* (0.2%) decrease. In the páramo vegetation, *Lycopodium foveolata* (24.2%) and Poaceae (25.3%) increase together and are the dominant taxa. Asteraceae increase significantly (35%CH) to reach an average value of 5.5%. *Polylepis* and *Blechnum* also increase but their average

value remains below 2%. *Hypericum* strongly decreases (-47%CH), as well as *Valeriana* which almost disappears.

Period 8: Subzone C2 (7,580 - 7,000 cal yr BP): (18 samples)

The forest vegetation has an significant relative increase in this period (43.5%CH).The Andean forest becomes more diverse because of the increased importance of some taxa such as *Juglans*, Melastomataceae, *Miconia* and *Prunus.* Elements of the Andean forest such as Melastomataceae, *Miconia and Prunus* show their major representation of the whole Early and Middle Holocene record although with low average values (below 2%). The average value of the páramo vegetation is reduced from 60 to 43% (-28.4%CH).

The main taxa in the subandean vegetation are *Pilea* (5.1%) and Urticales (2.4%) which increase together and are dominant, whereas *Achalypha* is slightly reduced. *Alchornea* increases (42%CH) but has an average value below 2%. In the Andean vegetation, *Quercus* increases to 23.1% (38%CH) and is dominant together with Cyatheaceae (5.1%). The latter partly replace *Podocarpus* (4.5%) which presents a small relative reduction of -13.3%CH. *Alnus* increases considerably (160%CH), although its average value is only of 2.2%. Although they keep low average values, taxa such as *Juglans* (196%CH), Melastomataceae (147%CH), and *Prunus* (190%CH) become more important. Poaceae have a small relative decrease (-9%CH) and dominate the páramo vegetation, whereas *Lycopodium foveolata* decreases significantly (-74%CH). Asteraceae, *Hypericum, Valeriana* and *Sisyrinchium* increase and *Polylepis* and *Blechnum* decrease considerably (both -49%CH).

POLLEN ZONE D (7,000 - 5,100 CAL YR BP)

Period 9: Subzone D1 (7,000 - 6,120 cal yr BP): (29 samples)

During this period, the páramo vegetation regains importance and increases from an average value of 43% in the previous zone to 59% (36%CH). Forest vegetation (subandean and Andean forests) decreases down to near 30%.

With low proportions, *Pilea* (3.8%), Urticales (1.34%) and *Acalypha* (1.21%) dominate the subandean forest. *Alchornea* has an average value below 1%*. Quercus* (17%) and *Podocarpus* (3.2%) decrease together (-30%CH) and still dominate the Andean forest. Cyatheaceae present an important relative decrease (-48%CH) to reach an average value of 2.7%. Taxa important in the previous period, such as Melastomataceae and *Prunus,* decrease significantly*. Alnus* also decreases but in minor proportion (1.8%), *Hedyosmum* increases significantly (36.6%CH) but remains at a low average value (1.6%). Páramo vegetation is mainly dominated by Poaceae which has only a small increase of 6.8%CH. *Lycopodium foveolata (*94%CH) and Asteraceae increase significantly together (77%CH) and become dominant elements with average values of 12% for both. Moreover, from about 6,600 cal yr BP until the end of the period *Lycopodium foveolata* decreases to reach a low average value of 2.8%, whereas Poaceae increase. *Hypericum* and *Valeriana* increase together (about 37%CH) but present low average values of 2.6% and 2.7% respectively. Others elements such as Gentianaceae (379%CH) and *Polylepis* (217%CH) increase significantly but keep average values below 2%.

Period 10: Subzone D2 (6,120 - 5,100 cal yr BP): (39 Samples).
This subzone is still dominated by páramo vegetation which reaches an average value of 63.5% (7.2%CH). Although Poaceae show a small decrease (-0.5%CH) and *Lycopodium foveolata* increases considerably (82%CH), their behavior presents a tendency to be inversely proportional. The relative decrease in forest vegetation is not so significant (-10%CH), but most of its elements are poorly represented or absent during the period.

In the subandean forest, the three dominant taxa are *Pilea* (-26%CH), *Acalpyha* (37%CH) and Urticales (14%CH). *Alchornea* shows its major relative decrease of the whole record (-42%CH). In the Andean forest *Quercus* does not show a significant change (-1.3%CH) and is the most abundant taxon with an average value of 17%. *Podocarpus* decreases significantly (-40%CH) with an average value of 1.9%, but remains a co-dominant element with Cyatheaceae (2.8%). Other taxa with average values below 2%, such as *Miconia* and *Weinmannia* increase and other ones such as *Alnus, Juglans* and *Myrsine* display the most important relative decrease of the whole record (-50%CH). In the páramo vegetation, *Lycopodium foveolata* increases considerably (82%CH) and dominates with Poaceae with almost equal average values of 25%, although their behaviour remains opposite. Although Asteraceae show an important relative decrease (-26.7%CH), it continues be an important element (8.6%). *Hypericum* starts to be more important (53%CH), *Polylepis* decreases (-17%CH), Gentianaceae, *Valeriana and Sisyrinchium* decrease significantly and have average values inferior to 1%.

POLLEN ZONE E (5,100 - 4,300 CAL YR BP)

Period 11: Zone E (5,100 - 4,310 cal yr BP): (22 samples)
This period corresponds to the second highest proportion of páramo vegetation in the whole record with an average value of 69.6%. This implies a relative decrease in forest vegetation (-16%CH). The subandean forest exhibits a more important relative decrease (-28%CH) than the Andean forest (-14.2%CH).

Taxa of the subandean forest decrease considerably and have average values lower than 2%. *Pilea* decreases (-42%CH, average value 1.6%) and dominates with *Acalypha* (-13%CH, average value 1.4%) and Urticales (-37%CH, average value1%). In the Andean forest, *Quercus* decreases (-16.2%CH) and dominates with *Podocarpus,* which only slightly decreases (-1.7%CH). Cyatheaceae show a significant decrease (-47%CH), Alnus a decrease of -11%CH and *Hedyosmum* remains stable. Taxa such as Melastomatacae, *Miconia*, *Prunus, Weinmannia* and *Vallea* have average values below 1%. In this subzone, páramo vegetation is characterized by the highest average proportion of Poaceae (38.4%) in the Early and Middle Holocene. On the contrary, *Lycopodium foveolata* shows its highest relative decrease (-93%CH) and minimun average value of 1.5%. It is replaced by *Hypericum* (313%CH) with an average value of 16.8% and thereby becomes a dominant element of this vegetation belt. Asteraceae decreases slightly (-13%CH), whereas *Polylepis* increases (83%CH). Other elements such as *Valeriana* and *Aragoa* increase but their average value is below 1%.

4.4.2. LOCAL VEGETATION CHANGE

Here we present the description of results of local vegetation in and around the Llano Grande mire for the period between 11,500 and 4,300 cal yr BP. The palynological results of aquatic vegetation have been plotted with respect to an age scale in cal yr BP **(**Fig 4.6). This period corresponds to the 220-754 cm interval in core LLG-2 (see age model above). Over this interval, 203 samples have been studied, which corresponds to a time resolution of ca. 35 years. In part 5, these data will be combined with those of Velásquez (2005) who studied the interval 0-220 cm (0 - 4,300 cal yr BP, i.e., the Late Holocene) with a time resolution of ca. 20 years.

The pollen diagram showing changes in aquatic vegetation in the lake has been calculated on the basis of the local pollen sum. This sum includes aquatics reflecting deeper water (*Isoetes*), shallow water (Apiaceae, Cyperaceae, *Lachemilla* and *Ranunculus*) and cushion vegetation (*Plantago*). The lateral distribution model can be seen in figure 2.4. When we refer to the family Apiaceae, this includes taxa of Apiaceae as well as *Hydrocotyle* found in the record.

Based on CONISS cluster analysis we have recognized 6 periods/zones and 9 subzones indicated in figure 4.6**. In these results, the relative change in the average percentage of a species/vegetation belt with respect to the previous period will be expressed in % change (%CH). All percentages of taxa in parentheses correspond to average values over the period described.**

POLLEN ZONE A (11,488 - 11,400 CAL YR BP)

Period 1: Zone A1 (11, 488 - 11,400 cal yr BP): (4 samples)

This subzone is characterized by high proportions of submerged vegetation with an average value of 56.9%, which decreases sharply toward the end of the period. The marsh vegetation is also important with an average value of 41.6%.. Cushion vegetation is almost absent with an average value of 1.4%

Marsh vegetation is dominated mainly by Cyperaceae (36.8%) and Apiaceae (3.6%). *Ranunculus* shows very low proportions (1.4%). Cushion vegetation represented by *Plantago* is almost absent with an average value of 1.4%.

POLLEN ZONE B (11,400 - 7,980 CAL YR BP)

Period 2: Subzone B1 (11,400 - 10,200 cal yr BP): (21 samples)

Marsh vegetation is the dominant element in this period with very high proportions and exhibits its highest relative increase of the Early and Middle Holocene (130.4%CH). Consequently, the submerged vegetation presents its highest relative decrease in the record (-95%CH). Cushion vegetation shows an oscillating behaviour but with a very low average value (1.6%).

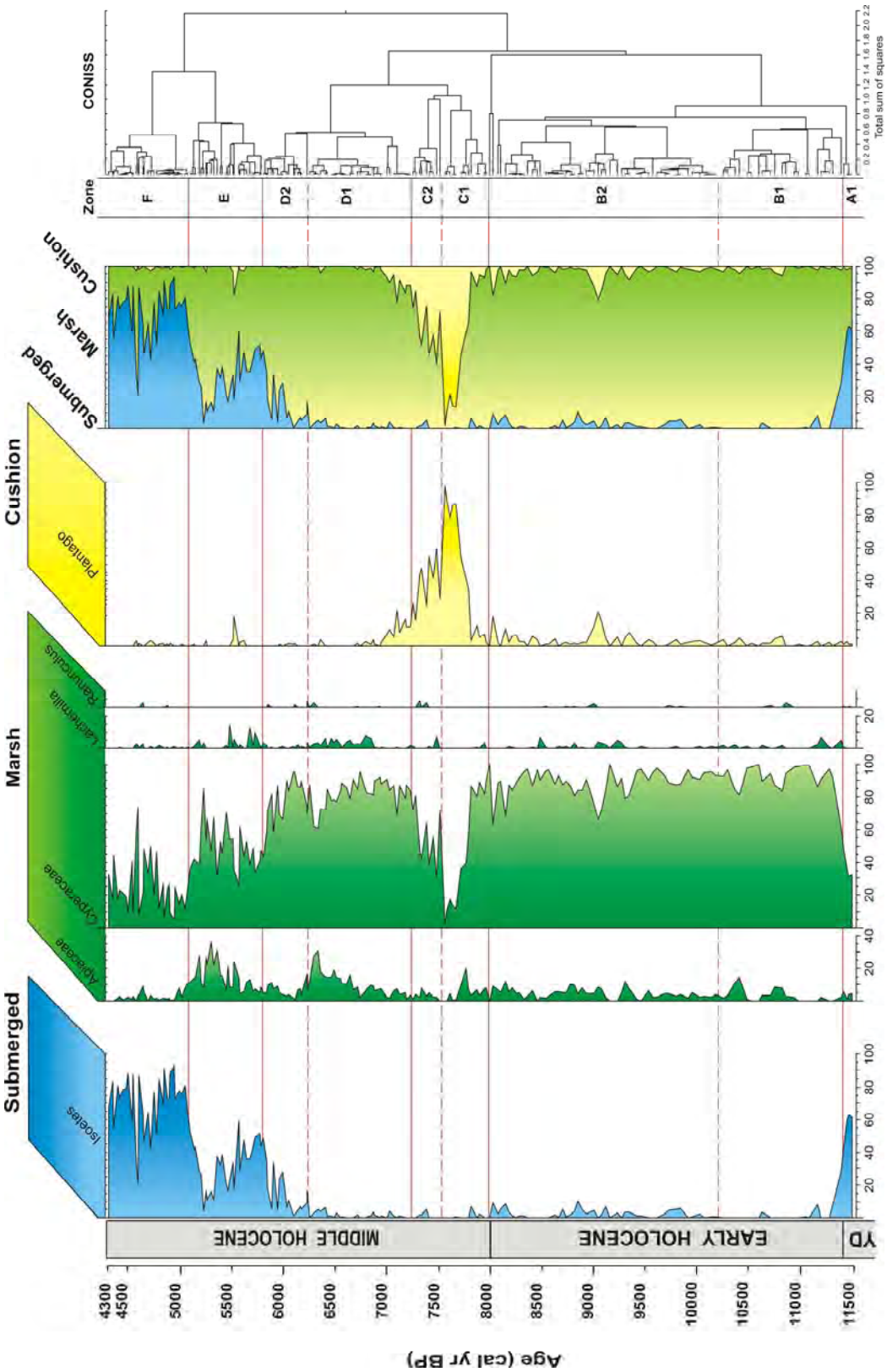

Fig. 4.6. Pollen diagram of aquatic vegetation in LLG-2 core from 220 to 752 cm. Data are plotted with respect to an age scale in cal yr BP. From left to right: records in percents of selected taxa (local vegetation) grouped within their local vegetation zone (see Fig. 2.8). On the right hand side, summary of the distribution of vegetation groups in percents, palynological zones and CONISS dendrograma. (YD= Younger Dryas equivalent).

Marsh vegetation is mainly dominated by Cyperaceae (91.5%) which present their highest relative increase in the record (148%CH). Apiaceae are also significantly present but have a relative decrease of -20%CH. Although *Lachemilla* shows an important relative increase (153.2%CH), it has a low average value of 1.2%. *Ranunculus* has a relative decrease of -47%CH. Cushion vegetation increases (15%CH) but its average value is only of 1.6%.

Period 3: Subzone B2 (10,200 - 7,980 cal yr BP): (49 samples)
Marsh vegetation continues to dominate this period with essentially Cyperaceae and secondarily Apiaceae (the latter show an important relative increase of 46.6%CH). *Lachemilla* and *Ranunuculus* decrease considerably and even disappear. Although the submerged vegetation does not present significant differences in its average value, its behaviour is characterized by some intervals with important increases. Cushion vegetation continues to show an oscillating behaviour in this period with a relative increase of 119%CH.

POLLEN ZONE C (7,980 - 7,240 CAL YR BP)

Period 4: Subzone C1 (7,980 - 7,530 cal yr BP): (13 samples)
In general terms, there is a co-dominance between marsh (53.2%) and cushion vegetation (46%). In the basal part of this period the marsh vegetation is abundant until around 7,820 cal yr BP when it starts to decrease and is replaced by cushion vegetation. This marks the highest relative increase in cushion vegetation (1119%CH) of the whole record with an average value of 46%.

Submerged vegetation shows a relative decrease of -66%CH and its minimum average value of the whole record (0.8%). Marsh vegetation decreases significantly (-43.5%CH) and is composed mainly of Cyperaceae with a significant relative decrease (-46%CH), whereas Apiaceae increase (17%CH) and become a dominant element.

Period 5: Subzone C2 (7 530 - 7 240 cal yr BP): (9 samples)
This period is dominated by marsh (60.8%) and cushion vegetation (38%), the latter showing a relative decrease of -17%CH. Marsh vegetation becomes more important in this period (14.4%CH). Cyperaceae increase relatively (17.8%CH) and dominate this vegetation together with Apiaceae (-43.1%CH). *Lachemilla* shows an important relative increase (210%CH) but keeps a very low average value of 1.1%, wheras *Ranunculus* reappears with a low average value of 0.8%. Although the submerged vegetation increases relatively (40%CH), it still has a very low average value (1.1%).

POLLEN ZONE D (7,240 - 5,800 CAL YR BP)

Period 6: Subzone D1 (7,240 - 6,240 cal yr BP): (31samples)
This subzone is characterized by the almost total dominance of marsh vegetation (56.2%CH, average value 95%), represented mainly by Cyperaceae (46%CH, average value 82%) and secondarily by Apiaceae which have their maximum relative increase of the whole record (234%CH) and become a more important taxon with an average value of 10.2%. In a similar

way, *Lachemilla* increases to reach its maximum average value of the whole record (2.5%). As a consequence, cushion vegetation shows it maximum relative decrease of the whole record (-90%CH). The submerged vegetation increases relatively (28%CH) but keeps a low average value.

Period 7: Subzone D2 (6,240 - 5,800 cal yr BP): (17 samples)

It is characterized by the highest relative increase in submerged vegetation of the whole record (1027%CH) and the near-disappearance of cushion vegetation (0.4%, relative decrease of -90%CH). The marsh vegetation is dominated by Cyperaceae (76.8%) and Apiaceae (6.2%) which decrease relatively of -6.3CH and -39.5%CH respectively. *Lachemilla* decreases significantly (-63.8%CH) and is poorly represented (0.9%).

POLLEN ZONE E (5,800 - 5,090 CAL YR BP)

Period 8: Zone E (5,800 - 5,090 cal yr BP): (27 samples)

The submerged vegetation continues to increase and doubles its proportion. Although marsh vegetation decreases relatively overall (-20.7%CH), it shows two clear peaks of abundance and is still dominant. It is characterized by a relative decrease in Cyperaceae (-35.2%CH, average value 49.7%) and a significant relative increase in Apiaceae (138.7%CH, average value 14.8%) and *Lachemilla* (150.8%CH, average value 2.34%). Cushion vegetation increases significantly but keeps a low average value of 1.1%.

POLLEN ZONE F (5,090 - 4,300 CAL YR BP)

Period 9: Zone F (5,090 - 4,300 cal yr BP) (31 samples)

This zone is characterized by having the highest proportion of submerged vegetation in the whole record (70.4%). Marsh vegetation shows a major decrease (-56.7%CH) and its lowest average value (29%) of the whole record. It is dominated by Cyperaceae and Apiaceae with average values of 25.7 and 2.5% respectively, the lowest in the whole record. *Lachemilla* also decreases significantly (-76%CH) and reaches a very low average value of 0.6%. Cushion vegetation decreases (-52%CH) and is poorly represented (0.6%).

4.5. MICRO-X-RAY FLUORESCENCE (µXRF)

4.5.1. GENERAL RESULTS

The µXRF data presented here were recorded in the LLG-5 core and cover the time interval 11,500 - 0 cal yr BP. This corresponds to the cored interval 8-857 cm. Over this interval, ultra high-resolution analyses of the following major elements were carried out: Al, Si, Mn, Ca, K, Ti and Fe (Fig. 4.7). Some 16540 points were measured for a period of time of 11,500 years, which gives a time resolution of less than a year. The records of the seven measured elements are presented in figure 4.7 with a 12-point moving average, which corresponds to a ca. decadal moving average. Iron is by far the most abundant of all. For the six others,

values from 0 - 3,700 cal yr BP are extremely low, most often below the reliability level of ca. 7 cps. This interval is dominated by peat and coincides with a significant decrease in precipitations (see below) and sedimentations rates (Fig. 4.4). Aluminium is below the reliability level throughout the studied section and can not be used. Silicium is also low throughout, but picks up from ca. 5,600 cal yr BP and can be used as paleoenvironmental marker in the lower part of the section (see below).

Among the five other elements, all show an increase prior to ca. 4,000 cal yr BP (Fig. 4.7), directly linked to precipitations. The most commonly used elements as precipitation proxies are Ti and Fe (see methods above), Ti being the most conservative of the two. The behaviour of potassium is extremely similar to that of Ti. K is another conservative element and in the interval 4,000 - 11,500 cal yr BP, his similarity with Ti confirms their value as precipitation proxies, even in zones of lower concentration (prior to 7,500 cal yr BP). Although less conservative and overall noisier (potential redox reactions), Fe can also be used as a precipitation proxy in the Holocene section at Llano Grande, in the light of its overall good correlation with Ti (see below). This is particularly important for the last 3,500 cal yr BP, during which measured Ti values are very low and only Fe values can be used with reliability as a precipitation proxy.

The two remaining elements, i.e., Mn and Ca, also show an overall trend that has similarities with that of K, Ti and Fe. But Mn is not a conservative element and does not show high-amplitude variations. Nevertheless, it may be used as a paleoenvironmental indicator in association with Fe (see below). In the very cold environment of the Páramo de Frontino, organisms with carbonate shells should be absent. Consequently, Ca should be essentially derived from plagioclases and its abundance linked to erosion. Although its overall variation resembles that of K, Ti and Fe, some trends are nevertheless difficult to explain: in particular, whereas Ti, K and Fe indicate an overall increase in precipitations from 11,400 until ca. 4,500 cal yr BP, Ca values indicate an overall decreasing trend. Subsequently, this element will not be considered in the discussion.

To summarize, µXRF data in this research will be used mainly as a precipitation proxy (Ti and Fe, see paragraph 4.5.2). Accessorily, they can contribute to paleoenvironmental interpretation (Si/K, Fe/Mn, see paragraph 4.5.3). Obviously, these data also contribute to the lithological description of the cores (see lithological description of core LLG-5 in chapter 4.2).

4.5.2. PRECIPITATION PROXIES (TI AND FE, FIG. 4.8)

The end of the mineral-rich sedimentation at ca. 11,400 cal yr BP marks the end of a very humid period corresponding to the Northern Hemisphere Younger Dryas, both elements show very high values throughout this period, as confirmed by ongoing research in the Late Glacial period (C. Monsalve, pers. comm.).

The transition from mineral-rich to organic-rich sedimentation in the basal Holocene coincides with a sudden transition to much drier conditions. The Early and Middle Holocene show an

overall increase in precipitations with a maximum of the whole Holocene in the interval spanning from ca. 5,000 to 4,000 cal yr BP. Nevertheless, both curves show that this increase is not linear but present variations. In the Early Holocene and lower part of the Middle Holocene (11,400 - 7,000 cal yr BP) the increase is marked by low amplitude variations and terminates with a more humid period just before 7,000 cal yr BP. At around 7,000 cal yr BP, a rapid decrease in precipitations is followed by another increase that culminates at ca. 5,500 cal yr BP. This is followed by a well-marked, short drier period between ca. 5,500 and 5,000 cal yr BP. As already mentioned, the interval 5,000 to 4,000 cal yr BP coincides with the maximum of rainfall in the whole Holocene.

A rapid transition to drier conditions is shown by both curves in the lower partfof the Late Holocene until ca. 3,300 cal yr BP. Above this level, Ti values are very low and only Fe data should be taken into consideration, keeping in mind that this element is not as conservative as Ti. Nevertheless, both elements show that most of the Late Holocene period has been drier than the rest of the Holocene. Variations in Fe concentration in the interval 3,300-0 cal yr BP suggest an alternation of drier and more humid periods, the latter spanning approximately from 2,300 to 1,800 and from 1,500 to 600 cal yr BP.

These data will be compared and discussed in part 5 below in relation with the information obtained from the local aquatic vegetation (chapter 4.4)

4.5.3. PALAEOENVIRONMENTAL PROXIES (SI/K AND FE/MN RATIOS, FIGS. 4.9 TO 4.11)

As explained above in part 3, the Si/K ratio can be used as a proxy for the abundance of diatoms in a sediment and therefore complements the lithological information (see chapter 4.2). In Llano Grande, this ratio is not reliable in the upper part of the section where Si and/or K values are too low (Fig. 4.9). It can not be used in the interval 6,000 - 0 cal yr BP. Diatoms are rather scarce down to 8,500 cal yr BP, as confirmed by the lithological observations. Between 8,500 and 11,400 cal yr BP, the Si/K ratio confirms the richness in diatoms observed under the microscope but also shows that their abundance is not evenly distributed. Three decreasing-upwards cycles are present. When compared with Ti data (Fig. 4.10), the Si/K data show an inverse correlation with the rainfall, i.e., the highest proportions of diatoms coincide with the lowest rainfall. This is probably a direct influence of dilution brought in by increased erosion associated to higher precipitations.

In some cases (see above in part 3), the Fe/Mn ratio can be used as a paleoenvironmental indicator of the redox potential of lakes. Figure 4.11 shows the variations of this ratio over the studied interval. Fe content is everywhere considerably higher than that of Mn. Over the last 4,000 years, the ratio is unreliable because of too low Mn values. Between 11,500 and 4,000 cal yr BP, variations in Mn have very low amplitudes, so that the Fe/Mn ratio appears to reflect essentially the variations in Fe. Consequently, without any other evidence, it is difficult to interpret these variations as the signature of changes in the redox potential. The situation is different in the Late Glacial part of the LLG-5 core, where evidences of oxidizing conditions (lower Fe/Mn ratio) are supported by lithological interpretation of paleosoils (see chapter 4.2 above).

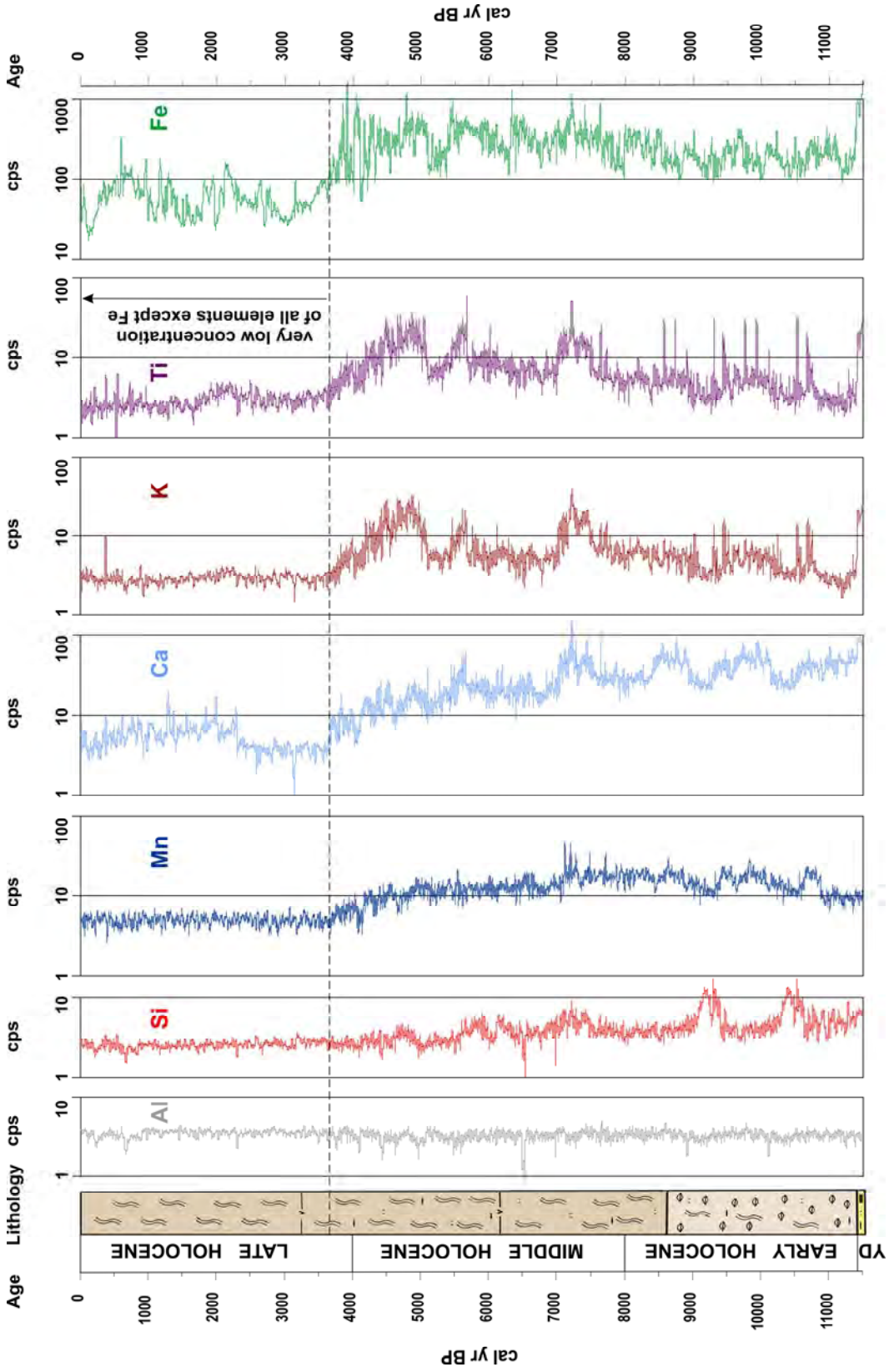

Fig. 4.7. µXRFdata for the seven elements measured in LLG-5. Elements are expressed in counts per second (cps) plotted in log scale with a 12 pt moving average. See text for explanations. (YD= Younger Dryas equivalent).

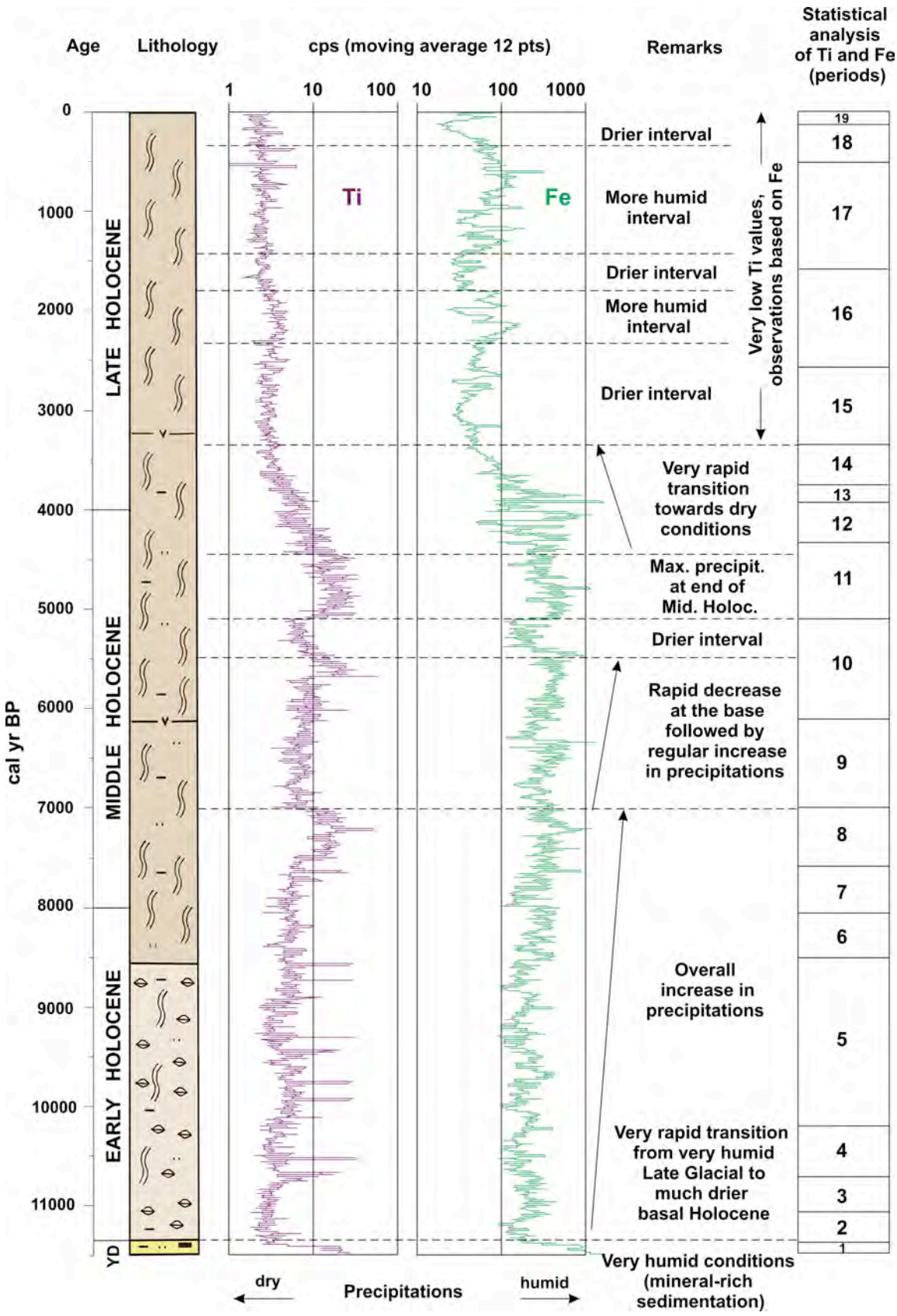

Fig. 4.8. µXRFdata of Ti and Fe used as precipitation proxies. See text for explanations. The column at the right hand side refers to the statistical analysis presented in appendix A3. (YD=Younger Dryas equivalent).

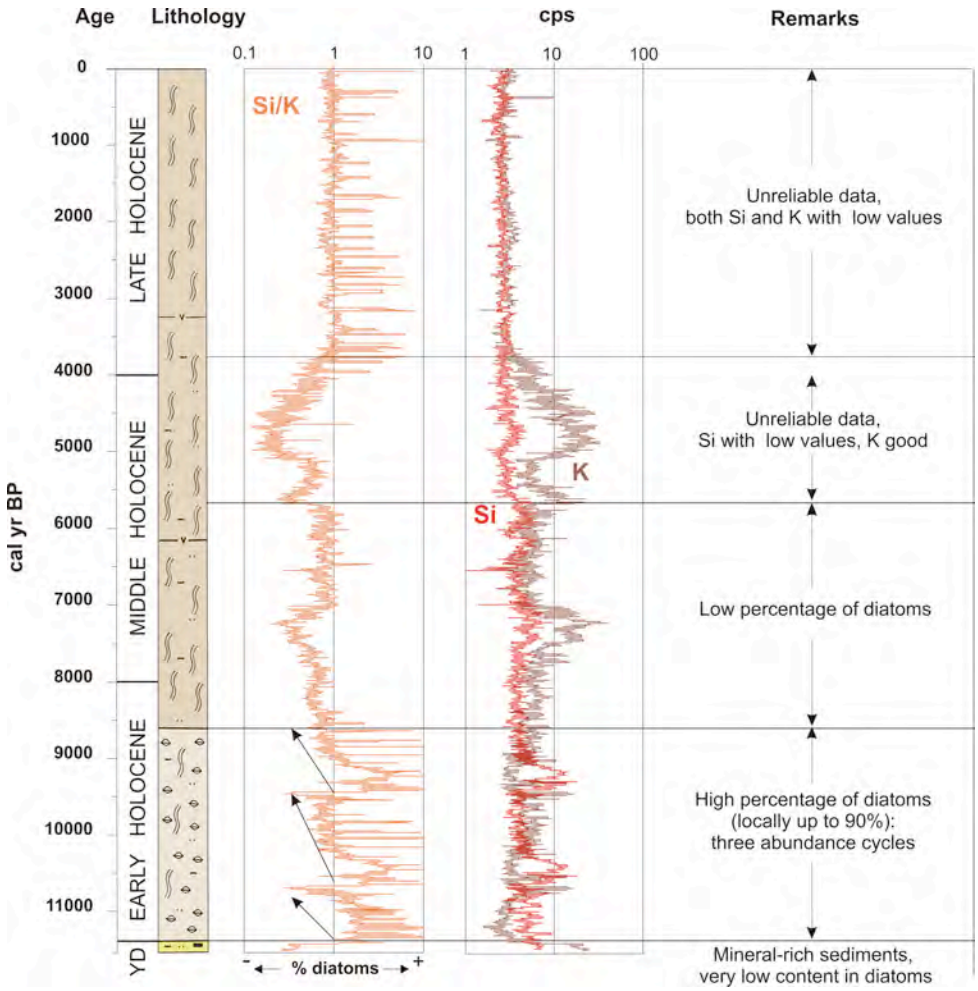

Fig. 4.9. Use of Si/K ratio as indicator of diatom-rich sediments. Curves are displayed in log scale with a moving average of 12 pt (decadal moving average). (YD=Younger Dryas equivalent).

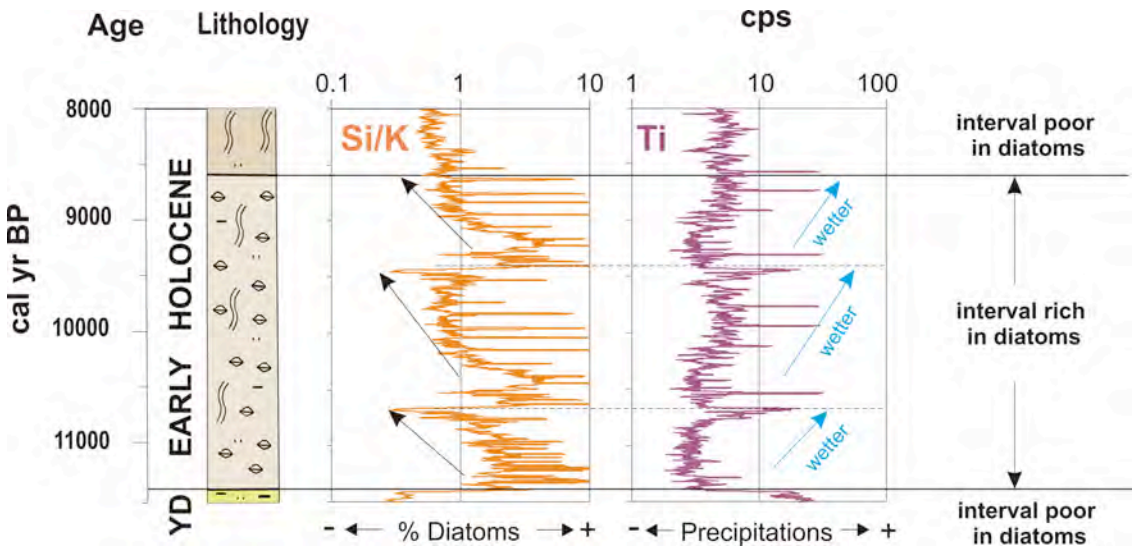

Fig. 4.10. In the interval 11,400 - 8,500 cal yr BP, geochemical proxies indicate that diatom-richest intervals seem to be associated with lower precipitations (see interpretation in text). (YD=Younger Dryas equivalent).

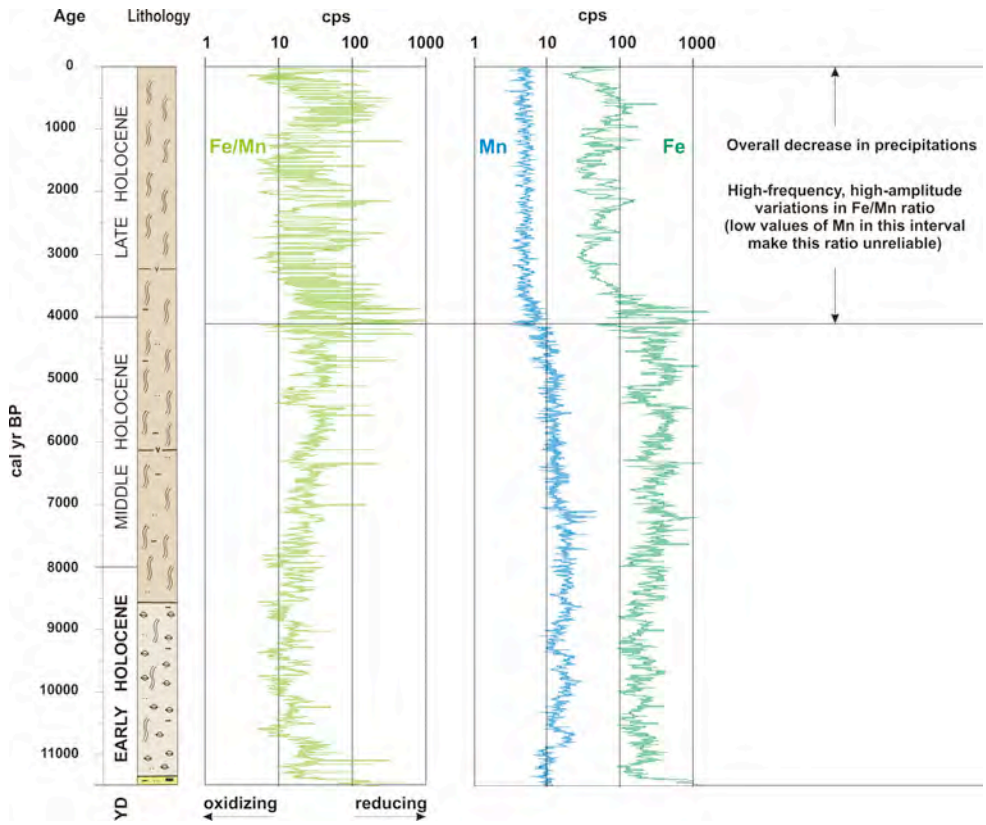

Fig. 4.11. Use of Fe/Mn ratio as potential indicator of oxidizing/reducing conditions. See text for explanation. Curves are displayed in log scale with a moving average of 12 pt (decadal moving average). (YD=Younger Dryas equivalent).

4.5.4 Statistical analysis of Fe and Ti data (see Appendix A3)

4.5.4.1 Introduction

The Fe and Ti signals from core LLG-5 have been analyzed according to the procedure described in chapter 3.5. In a first phase, various tests have been carried out on the signal, in particular checking for and removing the outliers. Both signals have then been analyzed for intervals of increasing and decreasing trends and for periods of stability. These results are shown in Appendix A3, where the signals are broken down according to the palynological zonation (time periods 1 to 19).

In a second phase, spectral and wavelet analysis has been performed on the Fe and Ti signal. The basic aims of wavelet analysis are both to determine the frequency (or scale) content of a signal and to assess the temporal variations in this frequency content.

The spectral analysis results presented below are shown for three main time periods: (1) the end of the Late Glacial and the whole Holocene between 12,000 cal yr BP and the present-day; (2) the interval 12,000 - 10,000 cal yr BP spanning the Younger Dryas-Early Holocene boundary at ca. 11,400 cal yr BP; (3) the interval 5,000 cal yr BP until the present-day spanning the late Middle and Late Holocene.

4.5.4.2. Ti signal

(Late Glacial)-Holocene period: 12,000 - 0 cal yr BP (Fig. 4.12)

In general terms, events during the Holocene can be identified through the significant increase in the variance of the high frequencies which are very sensitive to changes.

The low frequencies, such as the millennial bands (1,000, 2,000 years) are present with high variance values throughout the whole period. On the other hand, the high frequencies (periodicities of 64, 32, and ENSO band from 4 to 8 years are intermittent and could be indicative of a fast response to any change in the conditions.

As seen above in the lithology, there is a major temporal change at ca. 11,400 cal yr BP with a transition from a mineral-rich sedimentation to an organic-rich sedimentation. This marks the transition from the Late Glacial to the Early Holocene. Therefore, as mentioned in part 5 below, the interval 12,000 - 11,400 cal yr BP corresponds to the Younger Dryas equivalent (YD). The YD is characterized by a high variance in the high frequencies such as the ENSO band. From ca. 11,400 until 7,615 cal yr BP all frequencies (except those in the millennium band) decrease in variance and become intermittent.

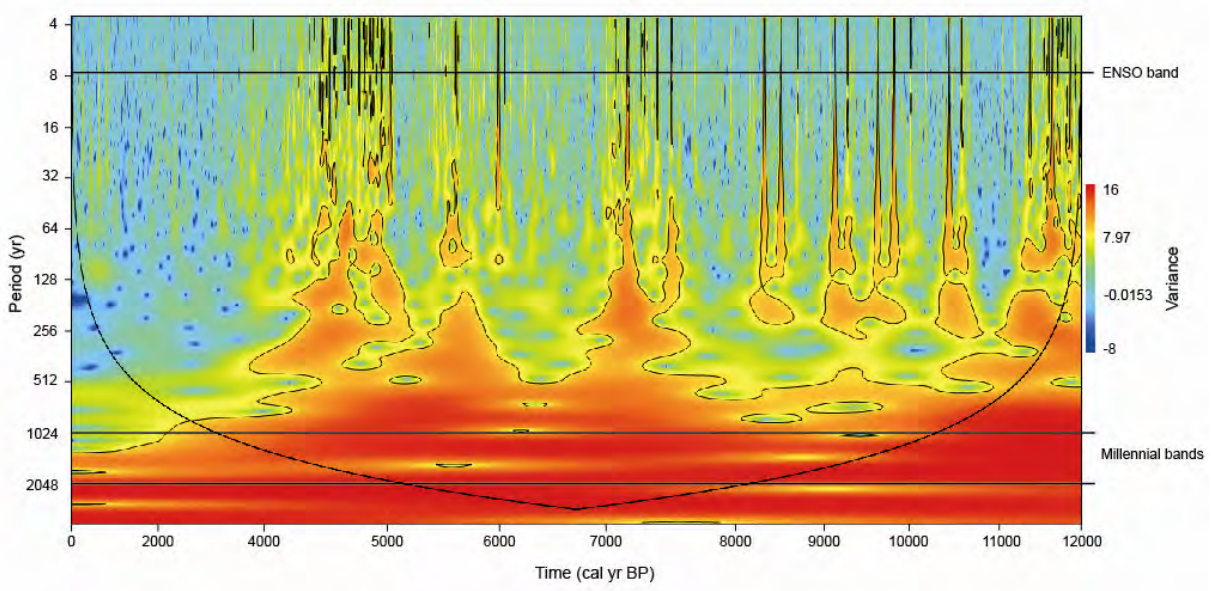

Fig. 4.12. Late Glacial) - Holocene (12,000 - 0 cal yr BP) wavelet spectrum for the Ti signal in the LLG-5 record calculated using Morlet wavelet on the time series of red colour intensity.

From ca. 7,620 till 7,100 cal yr BP occurs a temporal change with a significant increase in the variance of all frequencies. Then the variance decreases with a quiet period until ca. 5,790 cal yr BP for frequency bands higher than 512 yrs. Between 5,790 and 5,480 cal yr BP occurs another change which causes an increase in the variance of the high frequencies. Between 5,480 and 5,190 cal yr BP all frequencies higher than 256 years decrease in varianceThe last important change in the Holocene occurs between ca. 5,200 and 4,880 cal yr BP where the variance of all cyclical components increases considerably, in particular the most sensitive high frequencies of the 8 and 4 yrs bands. From ca. 4,880 cal yr BP the

variance of all frequencies begins to decrease gradually until the present-day. The spectrum is only affected by small changes in the signal which are perceived mainly by the higher frequency components (i.e. the 64, 32, 16, 8 and 4 year band).

Transition Late Glacial (Younger Dryas) to Early Holocene: 12,000 - 10,000 cal yr BP (Fig. 4.13)

This interval spans the transition from the Late Glacial (Younger Dryas) to the Early Holocene. It is during this period that the highest change in variance in the Ti signal takes place during the whole Holocene. The end of the Younger Dryas is marked by the high variance of almost all cyclical components (both high and low frequencies). The structural change occurring at ca 11,403 cal yr BP affects significantly the comportment of the high frequencies components such as 64, 32, 8 and 4 years. The impact on the lower frequency bands is not very clear because their variance remains high. After this change a period of calm is evidenced in all frequency bands until ca. 10,813 cal yr BP. From this date until 10,690 cal yr BP a period of temporal change is marked by an increase in the variance of all cyclical components particularly in the band between 4 and 8 years (ENSO band).

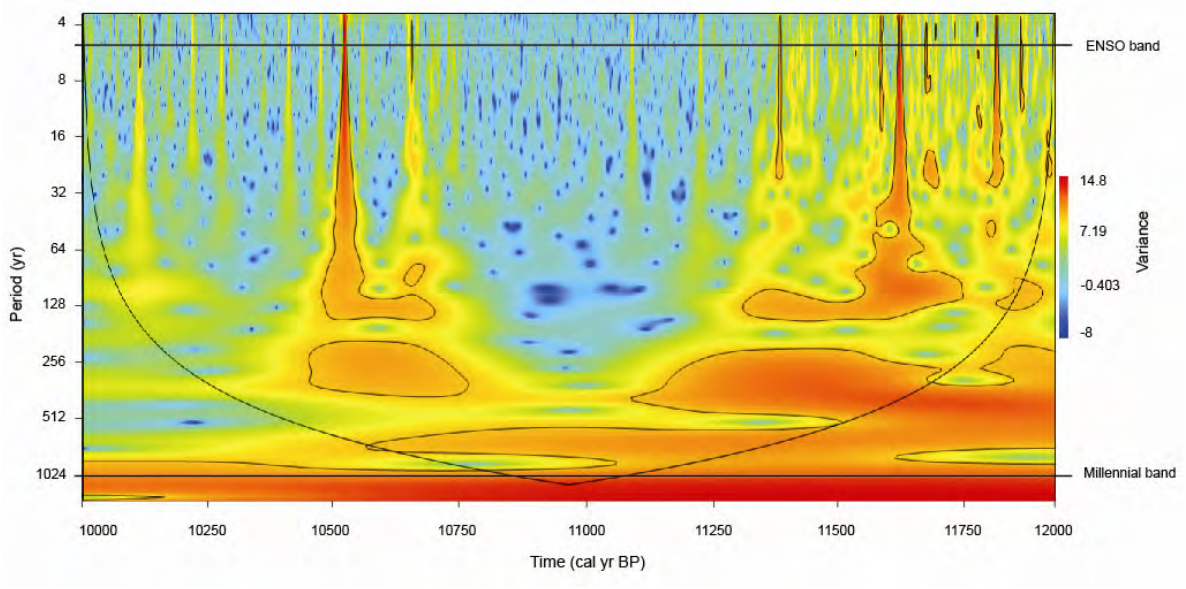

Fig 4.13. Transition Younger Dryas-early Holocene (12,000 - 10,000 cal yr BP) wavelet spectrum for Ti signal in the LLG-5 record calculated using Morlet wavelet on the time series of red colour intensity.

This change is followed by a period of stability until 10,180 cal yr BP, where all cyclical components display less differences in variance. This period is only interrupted by a short temporal change between 10,450 and 10,500 cal yr BP, which is particularly affecting the higher frequencies. At the end of the period, another change triggers an increase in the variance of the higher frequency components (2, 16, 8 and 4 years).

Throughout the investigated period, the millennial band always presents evidence of a high variance.

Late Middle Holocene- present day period: 5,000 - 0 cal yr BP (Fig. 4.14)

The spectral results show important changes which mark the transition from Middle to Late Holocene. As mentioned above in paragraph 4.5.2 (Fig. 4.8), it should be noted that from ca. 3,300 cal yr BP the Ti signal becomes very low and may not be reliable.

The spectral analysis shows that the start of this period is characterized by a high variance in all cyclical components and mainly in the high frequencies. This could be due to the temporal change started at around 5,190 and lasting until 4,875 cal yr BP and to the following period of stable average values but with high variance between 4,875 and 4,710 cal yr BP.

The stable period in average values between 4,310 and 4,230 cal yr BP could have caused the increase in variance in the frequency components, especially in the 32 and 16 year bands. From 4,195 cal yr BP the signal starts to have a gradual decrease and between 4,160 and 4,010 cal yr BP a period of stability in average values is established and this coincides with the progressive decrease in variances, which is best perceived by the millennial band.

Since this important change at 4,010 cal yr BP, the signal continues to decrease gradually until the present day and presents low variance values in all its cyclical components. It is important to note the effect on the millennial band which shows a significant decrease in its variance. Although the higher frequencies become more stable, they are still affected by spontaneous or temporal events which can alter the signal.

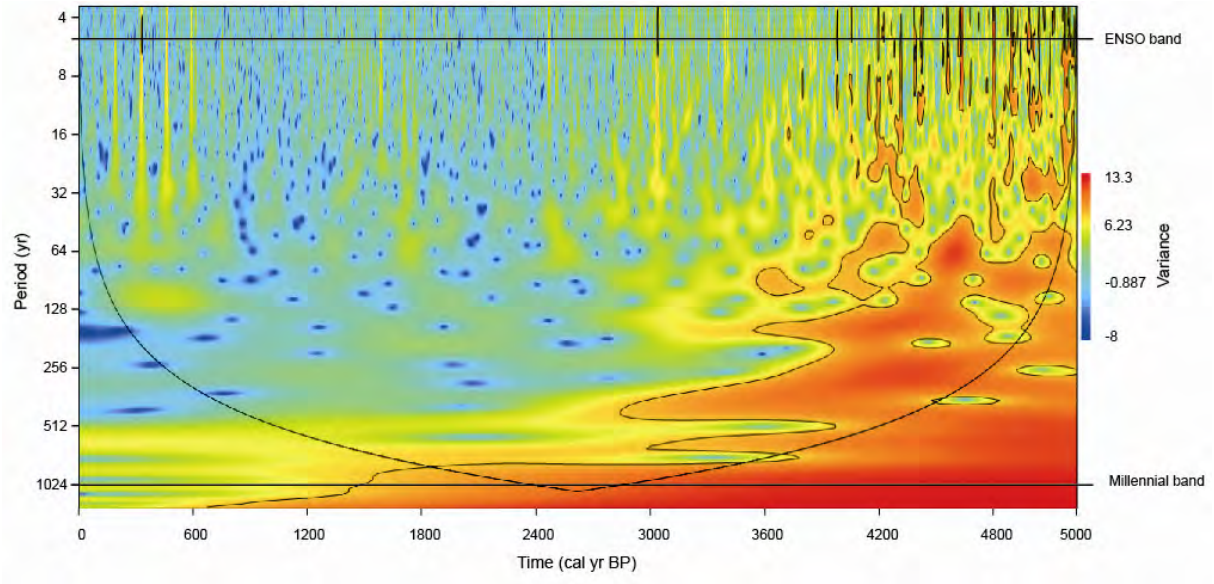

Fig 4.14. Late Middle Holocene to present-day (5,000 - 0 cal yr BP) wavelet spectrum for Ti signal in the LLG-5 record calculated using Morlet wavelet on the time series of red colour intensity.

In summary, this period starts with a high variance in all cyclical components until 4,010 cal yr BP. It is followed by a gradual decrease until the present day which is more perceived by the millennial band, whereas the higher frequencies are still sensible to temporal changes which affect the signal comportment.

4.5.4.3. Fe signal

As mentioned above in paragraph 4.5.2, the Fe signal is more sensitive to environmental changes and this is evidenced by its variance values being higher than those of the Ti signal when showing most important changes. The results of spectral analyses for Fe will be described in the same way as for the Ti signal, i.e., for the whole Holocene, and then for the transition Younger Dryas to Early Holocene and the period late Middle Holocene to present-day

(Late Glacial) - Holocene period: 12,000 - 0 cal yr BP (Fig. 4.15)

In general terms, the high variability of this signal does not allow to identify any dominance among the different cyclical components, therefore this causes problem for an accurate interpretation. The signal behaviour is characterized by a high variability in the variance of all components which exhibit intermittently high values in variance during the whole Holocene.

The Younger Dryas (YD) presents the same characteristic as those described for the Ti signal, i.e., high variances displayed by all components (the low as well as the high frequencies) until the marked structural change of the signal to a lower level which occurred at 11,403 cal yr BP. This change could be the trigger to the decrease in variance which affects all cyclical components and extends until ca. 11,300 cal yr BP. It is followed by intermittently high variance behavior of all cyclical components with some temporal changes which are more perceived by the high frequencies components such as 8 and 4 years.

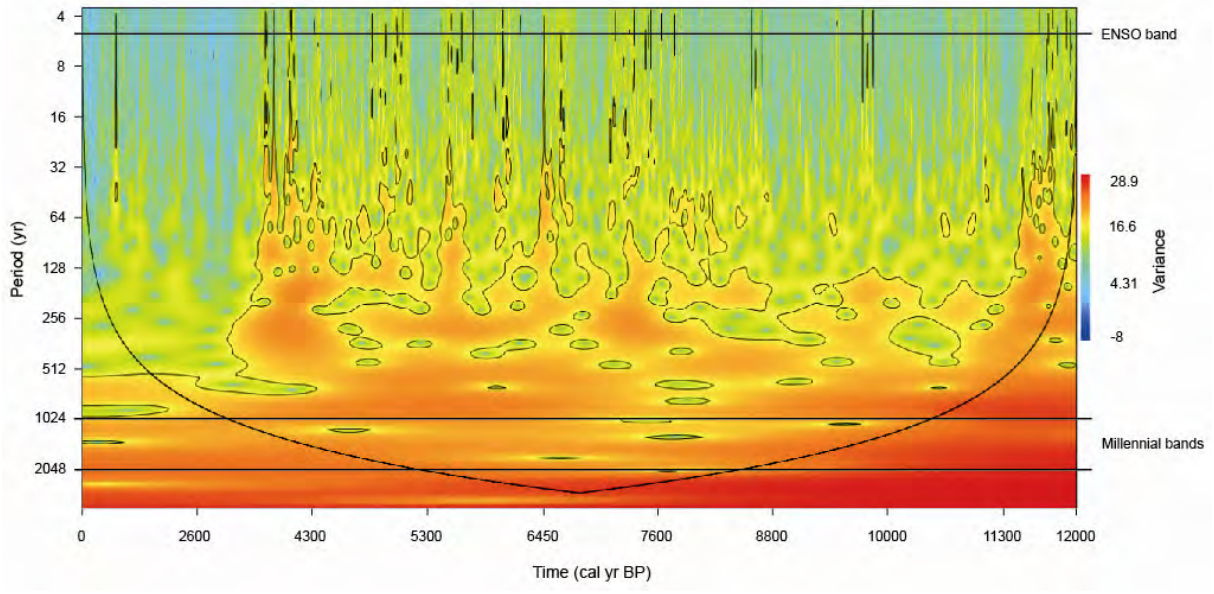

Fig 4.15. (Late Glacial) - Holocene (12,000 - 0 cal yr BP) wavelet spectrum for the Fe signal in the LLG-5 record calculated using Morlet wavelet on the time series of red colour intensity.

A temporal change between 8,550 and 8,390 cal yr BP is reflected by a decrease in variance in the millennial bands, causing an opposite effect in the high frequency components, especially in the 128 year band but also extending to higher frequencies in a lower proportion. The most important increase in the variance of all cyclical components starts at around 7,790 until 7,290 cal yr BP affecting significantly the 8 and 4 year bands (ENSO band). The variance of these components decreases until 6,770 cal yr BP but the lower frequency components still have high variance.

An increase in the variance of all cyclical components could be the response of the signal structural change with an increasing trend starting at 6,670 and lasting until 6,520 cal yr BP. It is followed by a decreasing trend which alters the high frequency components higher than the 64 year band. During the period 6,520 - 5,380 cal yr BP, where the Fe signal is marked by an increasing trend, high variances are dominant in all cyclical components. A quieter period from 5,380 until 5,120 cal yr BP is marked mainly in the high frequency bands such as 16, 8 and 4 years.

The period between 5,000 and 4,000 cal yr BP is characterized by a high variance over short time periods in the high-frequency bands. All cyclical components are affected especially from 4,200 cal yr BP. The major impact is registered from 4,120 up to 4,010 cal yr BP where an event triggered a rapid increase in the signal values, as well as in its variance, producing a significant effect over the 16, 8 and 4 years periods.
A quieter period is established from 3,800 cal yr BP, extending until the present-day and only affected by some insignificant temporal changes in the signal which are always detected by the high frequencies.

Transition Late Glacial (Younger Dryas) to Early Holocene: 12,000 - 10,000 cal yr BP (Fig. 4.16)

The late Younger Dryas period is characterized by having the highest values of variance in the whole 12,000 - 0 cal yr BP time interval (see Fig. 4.15). Therefore, performing an accurate analysis of the signal is not easy. At the same time, it is important to consider the high sensibility of this element which could be the cause of this pattern. Similarly to the Ti signal, the Fe signal displays the structural change occurring at 11,403 cal yr BP. It is supported by a meaningful decrease in variance of all cyclical components. From this date until 11,250 cal yr BP a quieter period influences all cyclical components. From then on, the behaviour of the spectrum becomes intermittent in its variance showing short relatively calm periods alternating with high variance values until 10,000 cal yr BP.

It is important to note that high frequencies are very sensitive to the instability of the signal. This means that a slight change in the signal is registered by high variances in the 8 and 4 year band during the whole transition YD - Early Holocene.

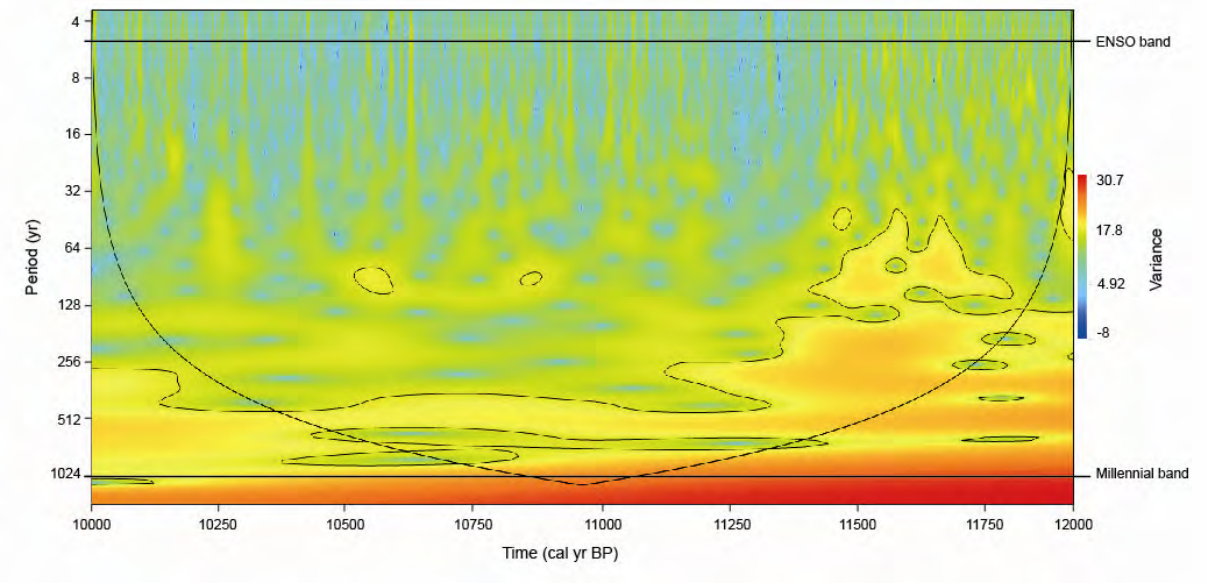

Fig 4.16. Transition Younger Dryas-Early Holocene (12,000 - 10,000 cal yr BP) wavelet spectrum for the Fe signal in the LLG-5 record calculated using Morlet wavelet on the time series of red colour intensity.

Late Middle Holocene - present day period: 5,000 - 0 cal yr BP (Fig. 4.17)

The spectrum analysis for the Fe signal shows clearly the transition from Middle to Late Holocene by its high intensity in variance for all its cyclical components. The period starts with high variance and keeps it up until 3,665 cal yr BP.

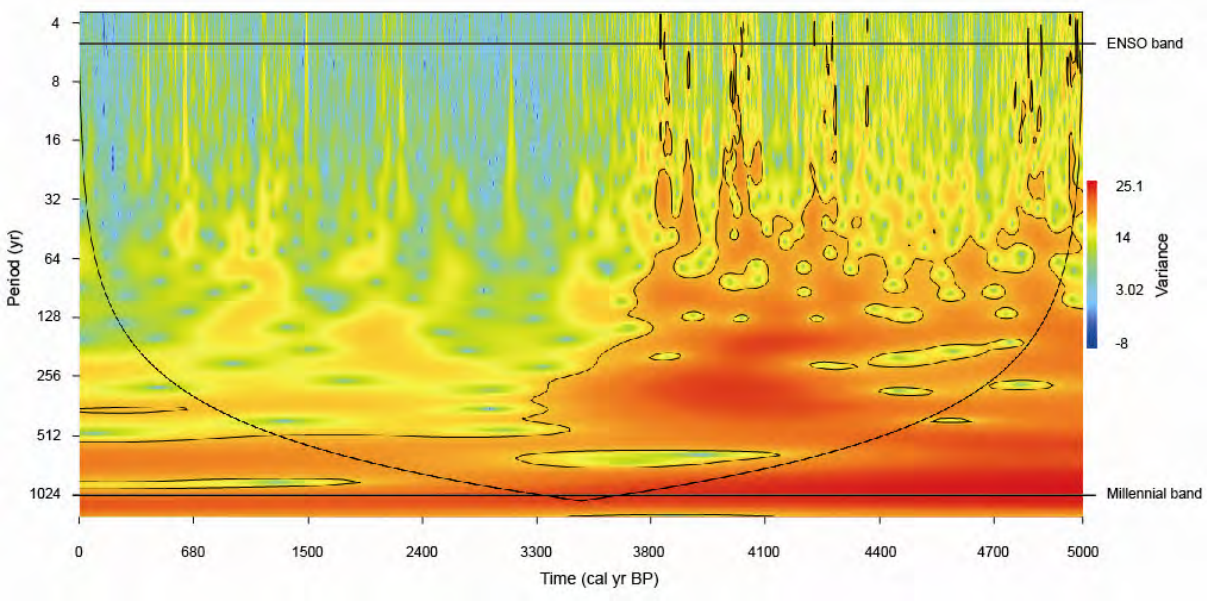

Fig 4.17. Late Middle Holocene - present–day (5,000 - 0 cal yr BP) wavelet spectrum for the Fe signal in the LLG-5 record calculated using Morlet wavelet on the time series of red colour intensity.

The most important changes in variance are marked by some major events such as (1) the structural change in the Fe signal with a decreasing trend between 4,890 and 4,710 cal yr BP; (2) structural changes with increasing and decreasing trend periods from 4.120 extending until 4,010 cal yr BP and (3) structural change with increasing and decreasing trend periods between 3,915 up to 3,815 cal yr BP. These periods of highest variance influence considerably the high frequencies mainly in the 8 and 4 year bands.

At around 3,800 cal yr BP a significant decrease in the signal triggers a gradual decrease in its variance. It becomes more stable in variance for all its cyclical components. From this time until 260 cal yr BP the signal is only perturbed by frequents short events which are only

CHAPTER 5

INTERPRETATION AND DISCUSSION

5. INTERPRETATION AND DISCUSSION

5.1. INTRODUCTION

The structure of this part 5 is the following: in the first part (**chapter 5.2**) we explain the models used to convert the palynological data into parameters that can be used as climatic proxies (temperature and rainfall). In the second part (**chapter 5.3**), we will discuss and interpret in terms of climate and environment both the results of palynology obtained in the core LLG-2 and those of geochemistry in the core LLG-5; **in paragraph 5.3.2** we discuss the Early and Middle Holocene period (i.e., time interval 4,300 to 11,500 cal yr BP) and in **paragraph 5.3.3**. we will integrate the palynological results obtained from core LLG-2 by Velásquez (2005) for the time period 4,300 cal yr BP till present-day (i.e., depth interval 0-220 cm) and our geochemical data obtained from LLG-5 for the same time period. This will allow an interpretation for the whole Holocene period. In a third part, we will make some considerations on the value of the climatic proxies used and the interpreted climatic changes in Llano Grande (**chapter 5.4**). In the final part (**chapter 5.5**), we will discuss these results with respect to existing regional data and try to interpret the mechanisms that might have influenced the climate in the Páramo de Frontino over the last 11,500 cal years BP.

5.2. USE OF POLLEN DATA AS CLIMATIC AND ENVIRONMENTAL PROXIES

5.2.1. ESTIMATION OF THE MEAN ANNUAL TEMPERATURE (MAT) FROM POLLEN DATA

Individual taxa within their own ecological group are responding to climate and environmental conditions. The addition of a larger number of such characteristic ecological groups forms vegetation belts, which may shift vertically. The altitudinal migration of vegetation belts in the tropics seems to depend essentially from temperature. Nevertheless, it may also be influenced by precipitations. However, the impact of the latter is not very well known, because there are very few studies and it is not possible to obtain reliable conclusions.

We use the definition of shifting Upper Forest Line (UFL) developed by Van der Hammen and González (1960a, 1963 and 1964) as the main parameter for reconstructing paleotemperatures. UFL is a very useful tool to reconstruct the Mean Annual Temperature (MAT) (see Groot et al., 2011).

This concept has been widely applied (e.g., Hooghiemstra, 1984 and 1989 Hooghiemstra and Ran, 1994; Van der Hammen and Hooghiemstra, 1995; Mommersteeg, 1998; Van't Veer and Hooghiemstra, 2000; Wille et al., 2001; Torres, 2005; Bogotá-Angel, 2011; Groot et al., 2011). Nevertheless, this method is only an approximation to attempt paleotemperature reconstructions. Consequently, it is important to keep in mind that, besides temperature, there might be other factors that can influence changes in UFL. The latter are insufficiently known to fine-tune environmental reconstructions (Scheffler et al., 2006).

Van der Hammen and González (1960a and 1963) defined the Upper Forest Line (UFL) as the uppermost and mainly continuous boundary between the about 5 m or taller forest

vegetation and the dwarf forest belt. Isolated forest patches, small dwarf forest at higher altitudes and wind-protected valleys should not be taken into account.

In the Colombian Andes the uppermost forest limit migrated from an elevation of ca. 2000 m amsl during the Last Glacial Maximum (LGM) to 3200 - 3400 m amsl under modern conditions (Nesbitt and Young, 1982). In recent times , the highest forest line recorded lies at 3800-3900 m amsl and the lowest one at 3200-3300 m amsl (Hooghiemstra, 1984). Local differences in altitude of the UFL can be caused by local environmental conditions, such as winds, topography, temperature distribution and amount of precipitations.

In order to establish the UFL in Colombia, many studies of recent pollen rain at different altitudes have been carried out in the Eastern Cordillera (Van der Hammen and González, 1960b; Grabandt, 1980) as well as investigations on Late Glacial and Holocene pollen records from the Eastern Cordillera at different altitudes (between 3500 and 2000 m amsl; Nesbitt and Young, 1982) . They have given an insight in the relationship between the altitudinal position of the UFL and the percentage of arboreal pollen (%AP) in the records. Lapse rate can be expressed as temperature variation per 100 m vertical change in altitude. Lapse rates of UFL with respect to temperature variations have been estimated in several studies in Colombia. Similarly, the decrease or increase in %AP is related to lower and higher altitudinal positions of the forest line, respectively. It is estimated that each UFL shift of 100 m corresponds to a variation of 5 %AP. This is assuming that the seasonal variations in mean monthly temperature remained as small as today (Groot et al., 2011).

In the Páramo de Frontino the present-day UFL can be estimated at 3450 m amsl (Rangel et al., 1999; Velásquez, 2005). The palynological data of Velásquez (2005) in Llano Grande show that the present-day %AP is of ca. 53% at 3460 m amsl. In the Páramo de Frontino, the present-day soil temperature (MAT) at 3400 m amsl has been measured by Velásquez (2005) at 8.3 °C. We will use this value as present-day MAT in Llano Grande. Because there are no detailed studies in the Western Cordillera about lapse rates, we will use a lapse rate of 0.65°C for each 5% change in %AP (Groot et al., 2011). Therefore, using these parameters we can convert the %AP curve to a MAT curve with the following relation (1)

$$\mathbf{MAT} = 8.3\left[\frac{(\%\mathbf{AP} - 53)}{5}\right]\mathbf{X}(0.65) \qquad \textbf{(1)}$$

Where:
MAT = Mean annual temperature (°C),
%AP = % arboreal pollen
53 = present-day %AP at 3460 m asml (altitude of Llano Grande)
Values of 0.65 and 5 = lapse rate value of 0.65°C for each 5% change in %AP

As we will see below, our record starts at the end of the Younger Dryas (YD) equivalent (Fig. 5.1). With the relation (1), the MAT at the end of the YD is estimated at 4-4.5°C lower than today. The order of magnitude of this value seems in line with that of ca. 5°C interpreted in Fuquene (Eastern Cordillera) by Groot et al. (2011).

5.2.2 ESTIMATION OF THE ALTITUDE OF THE UPPER FOREST LINE (UFL)

Shifts in the past UFL position can be estimated from the change in arboreal pollen percentages (%AP), which reflect the proportional changes in forest and páramo vegetation in the record. Using the assumption that a change of 5%AP corresponds to a shift of 100 of the UFL and taking a present-day UFL at 3450 m amsl and a present-day %AP of 53% at 3 460 m asml in Llano Grande, we can calculate the UFL using the relation (2):

$$\mathbf{UFL} = 3450 + \left[\frac{(\%\mathbf{AP} - 53)}{5}\right] \mathbf{X} (100) \qquad \textbf{(2)}$$

Where:
UFL = Upper forest line in meters
%AP = % arboreal pollen
3450 = present-day altitude (m amsl) of UFL
Values of 53 = present-day %AP at 3460 m asml (altitude of Llano Grande)
Values of 5 and 100 = each 5% change in %AP corresponds to an UFL shift of 100 m

Zone	Subzone	Interval (cm)	Period (cal yr BP)	Duration (cal yr BP)	Mean % AP	Mean % Páramo pollen	Mean MAT (°C) at 3'460 m amsl	Mean UFL position (m amsl)
E	E	299-220	5,100-4,310	790	30.3	69.7	5.3	2 996
D	D2	395-300	6,120-5,100	1020	36.7	63.4	6.1	3 125
	D1	470-396	7,000-6,120	880	40.7	59.3	6.7	3 204
C	C2	515-471	7,580-7,000	580	57.7	43.3	8.7	3 524
	C1	551-516	8,050-7,580	470	39.5	60.5	6.5	3 180
B	B3	588-552	8,500-8,050	450	54.4	45.6	8.4	3 479
	B2	681-589	10,200-8,500	1 700	44.1	55.9	7.1	3 273
	B1	706-680	10,700-10,200	500	31.9	68.1	5.5	3 028
A	A3	724-707	11,050-10,700	350	59.3	40.7	9.1	3 576
	A2	744-725	11,400-11,050	350	45.9	54.1	8.0	3 404
	A1	754-745	11,488-11,400	488	21.3	78.7	4.1	2 817

Table. 5.1. Main characteristics of the palynological subzones in core LLG-2 during the Early and Middle Holocene. Climate variability is characterized in terms of time period, mean %AP, mean % páramo vegetation, mean annual temperature (MAT) at 3460 m and mean position of upper forest line (UFL).

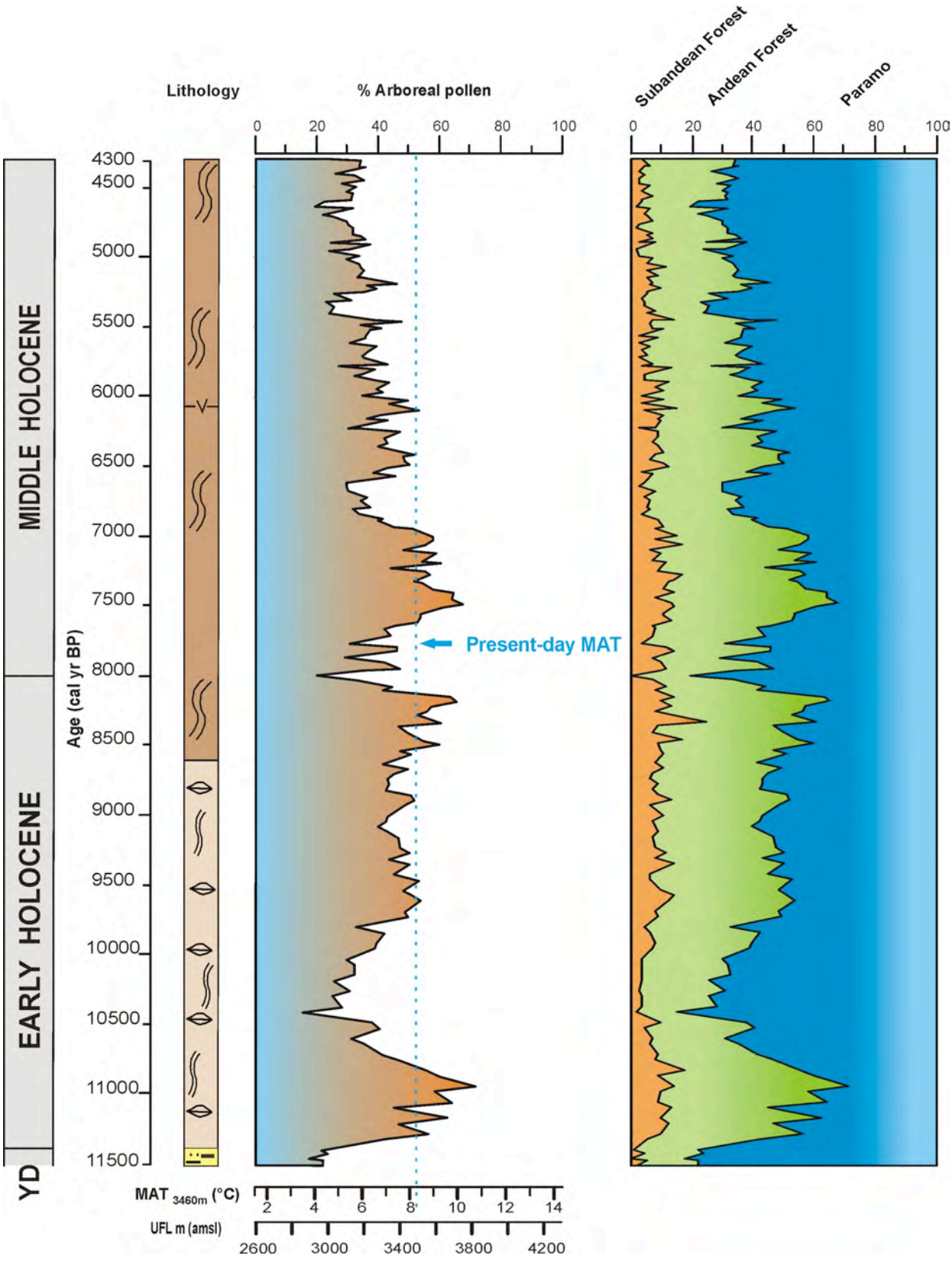

Fig. 5.1. Estimation of mean annual temperature (MAT) and altitude of upper forest line (UFL) during the Early and Middle Holocene in LLG-2, based on %AP. The diagram on the right hand side shows the palynological results reflecting the main vegetation belts (Fig. 4.5). The diagram on the left hand side represents the percentage in arboreal pollen (%AP) with the scales for MAT and altitude of UFL estimated using the models defined in the text. (YD = Younger Dryas equivalent).

Figure 5.1 shows the interpreted MAT and altitude of the UFL during the Early and Middle Holocene in LLG-2, using the relations (1) and (2). Table 5.1 shows the main characteristics of the palynological subzones defined in the core LLG-2 for this same time interval (see chapter 4.4).

5.2.3. ESTIMATION OF WATER DEPTH IN THE LLANO GRANDE LAKE

Variations in the water depth are reflected by changes in the proportion of different types of aquatic vegetation. Changes in water depth of the Llano Grande lake have been estimated using the proportions of aquatic vegetation observed during the Early and Middle Holocene.

The ecology of the modern aquatic and marsh vegetation in the Páramo de Frontino has been studied by Parraet al. (2010c) (see fig. 2.8). We use this model and the palynological results for local pollen (those *"not included in the sum"*) to estimate water depth. This local pollen includes aquatics reflecting deep water plants (*Isoëtes*), marsh vegetation (Apiaceae, Cyperaceae, *Lachemilla* and *Ranunculus*) and cushion vegetation (*Plantago*).

In Colombia the fossil pollen record of the aquatic and swamp vegetation has been widely used (Hooghiemstra, 1984 and 1989; Mommersteeg, 1998; Van't Veer and Hooghiemstra, 2000; Torres, 2005; Haberzettl et al., 2006; Bogotá-Angel, 2011; Groot et al., 2011). Applying the model developed by Parra et al. (2010c) in the Páramo de Frontino shown in figure 2.8, we use the relation (3) below to estimate the water depth of the Llano Grande lake. In the marsh vegetation, we have taken only the Cyperaceae which make up the near-totality of this vegetation group.

$$\mathbf{WATERDEPTH} = \frac{(\%\textbf{\textit{Isoëtes}} \times 60) + (\%\textbf{Cyperaceae} \times 10) + (\%\textbf{\textit{Plantago}} \quad 0.1)}{100} \qquad \textbf{(3)}$$

Where:
Water depth = depth of water (cm) in Llano Grande lake
Values of 60, 10 and 0.1 = average water depth in cm corresponding to respective taxa according to the model of figure 2.8.

Using relation (3), the results obtained for aquatics in the Early and Middle Holocene of LLG-2 (Fig. 4.6) can be converted into an estimated water depth curve for the Llano Grande lake (Fig. 5.2).

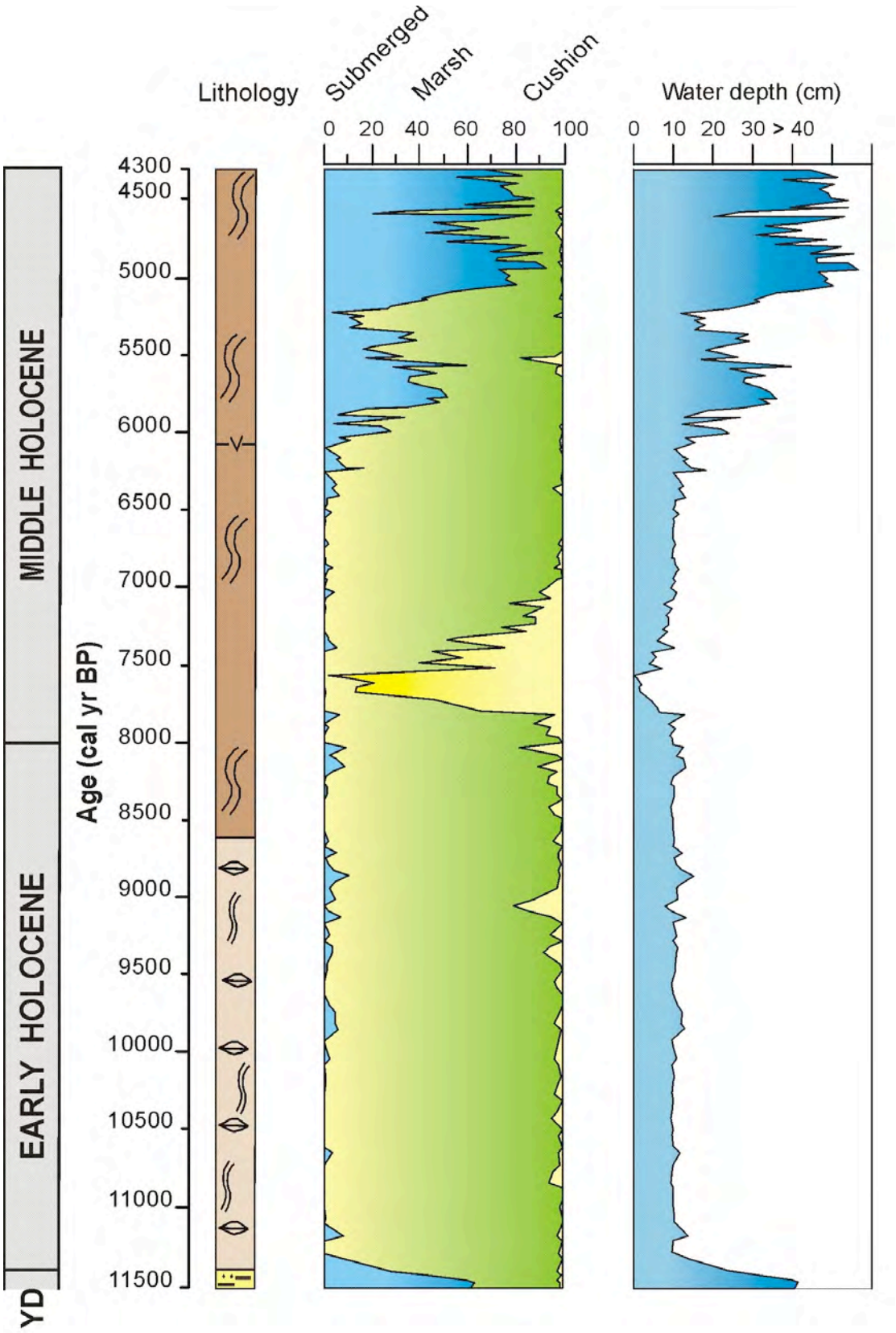

Fig. 5.2. Estimation of water depth in the Llano Grande lake (right hand side diagram) during the Early and Middle Holocene using the model defined in the text. This diagram is based on the palynological results obtained for the aquatic vegetation (see Fig. 4.6). (YD = Younger Dryas equivalent).

5.3. CLIMATIC AND ENVIRONMENTAL RECONSTRUCTION FOR THE EARLY AND MIDDLE HOLOCENE

5.3.1. INTRODUCTION

In this chapter 5.3, we analyze and compare the climatic signature given by the various proxies used in this study: palynological proxies for temperature and humidity as defined above (MAT derived from UFL, humidity derived from aquatics) and geochemical proxies for rainfall derived from µXRF (titanium and iron).

In the first phase (paragraph 5.3.2), we concentrate on the Early and Middle Holocene and analyze the record with respect to the pollen zonation we have established (see Fig. 4.5). In a second phase (paragraph 5.3.3) we integrate the palynological data of Velásquez (2005) for the Late Holocene, in order to cover the whole Holocene period with palynological and geochemical data.

Variations in Ti and Fe can be used as indices of past regional hydrological changes, with higher values reflecting increased rainfall (see part 3; e.g., Peterson and Haug, 2006). It will be particularly interesting to compare this high resolution proxy with the humidity index (or water depth) provided by aquatics. Because of its much higher resolution (subyearly), µXRF data has to be considered as much more accurate than the palynological proxy which has a decadal (20-40 years) resolution. Moreover, we will use some of the information provided by the statistical analysis of the Ti and Fe signal (paragraph 4.4.2 and Appendix A3).

5.3.2. EARLY TO MIDDLE HOLOCENE (see Fig. 5.3)

5.3.2.1. Pollen zone A (11,488 - 10,700 cal yr BP)

This zone is subdivided into three subzones.

Period 1: Subzone A1 (11,488 - 11,400 cal yr BP)

Regional vegetation

Subandean and Andean forests are poorly represented. The subandean forest represents only 3.1% and is mainly made of *Pilea.* Low values of Urticales taxa (dry indicator) may suggest wet conditions. The Andean forest is composed of *Quercus* and *Podocarpus*. The páramo vegetation reaches its highest proportions of the whole Early and Middle Holocene record. It is dominated by *Lycopodium foveolata* and shows a significant representation of open vegetation elements such as Asteraceae and Poaceae. The relative importance of wet páramo elements such Asteraceae, *Valeriana* and *Lycopodium foveolata* are indicative of a wet páramo vegetation.

Local vegetation

High percentages of *Isoëtes* suggest deep water conditions in the lake (>40 cm) and are indicative of wet local conditions.

Rainfall proxy (µXRF)
This period is characterized by high proportions of Ti and Fe indicating high rainfall. Both elements decrease rapidly near the end of the period at ca. 11,403 cal yr BP, suggesting a rapid transition to drier conditions. The Morlet wavelet spectrum for Ti shows a high variance in the high frequencies such as the ENSO band (see Figs. 4.12, 4.13 and 5.4).

Environmental conditions
This period is characterized by the highest average proportion of páramo vegetation over the whole record (78%), and consequently the lowest average value of %AP (21.3%). The UFL shows its lowest estimated average altitude (ca. 2820 m amsl) of the whole record. The estimated MAT of 4.3°C is the lowest of the whole record, with a temperature ca. 4°C colder than today at 3 460 m amsl.

The landscape was mainly dominated by a wet páramo vegetation represented by *Lycopodium foveolata* and open vegetation (Poaceae and Asteraceae). The local vegetation is mainly represented by *Isoëtes* indicating a significant water depth in the Llano Grande lake. These very wet conditions are confirmed by high values of Fe and Ti implying high precipitation levels during this period. The high mineral input in the sediments confirms these observations. This cold and wet period is interpreted (see chapter 5.5 below) as the final part of the Younger Dryas equivalent (El Abra stadial in Colombia, see van't Veer et al., 2000).

Period 2: Subzone A2 (11,400 - 11,050 cal yr BP)
Regional vegetation
The forest vegetation (subandean and Andean forests) displays its most important increase of the whole record. The subandean forest is composed mainly of *Pilea* and *Acalypha.* There is a considerable increase in taxa indicative of dry conditions, such as *Acalypha* and Urticales, although with low values. The Andean forest remains dominated by *Quercus* and *Podocarpus,* and *Hedyosmum* has a very low average value. *Weinmannia* decreases. Páramo vegetation is mainly represented by Poaceae which show a significant increase. On the other hand, *Lycopodium foveolata* decreases and *Polylepis* increases (but its average value remains low). The taxa indicative of wetter conditions, such as Asteraceae, and *Lycopodium foveolata,* decrease significantly suggesting dry páramo vegetation.

Local vegetation
Marsh vegetation has its highest relative increase in the Early and Middle Holocene (130.4%CH), suggesting a low water level. The almost absence of *Isoëtes* also points to drier conditions.

Rainfall proxy (µXRF)
Overall, the proportions in Ti and Fe considerably decrease during this period, which points to much lower rainfall than in the previous period. Both indicators display an abrupt change to a lower level between 11,405 up to 11,403 cal yr BP. Both signals have a decreasing trend till 11,200 cal yr BP, followed by a period of stability in Ti and an increase in Fe until the end of the period. The Morlet wavelet spectrum for Ti shows a period of calm in all frequency bands (see Figs. 4.12, 4.13 and 5.4).

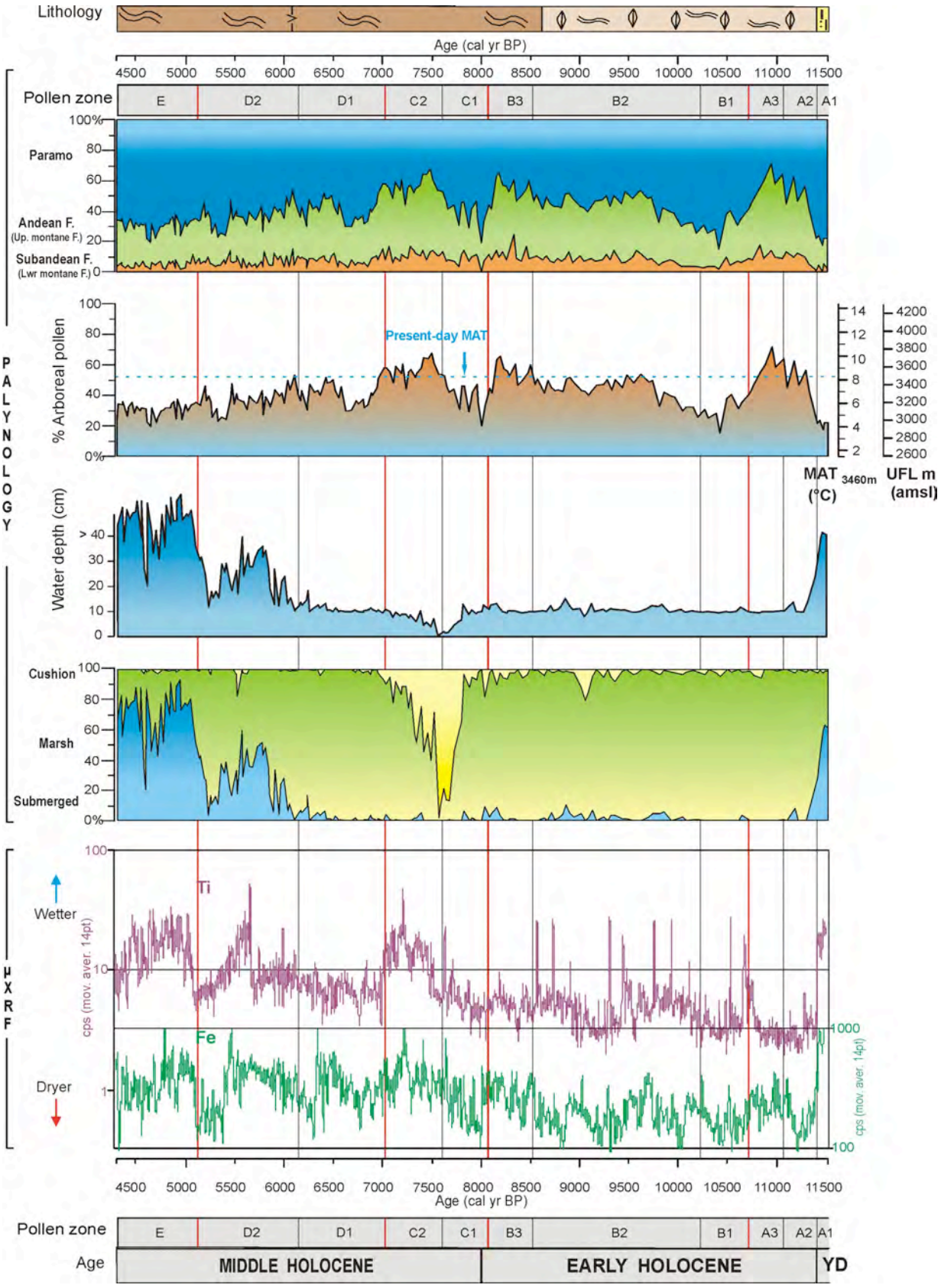

Fig. 5.3. Comparison of palynological climatic proxies (MAT and UFL derived from %AP) and μXRF rainfall proxies (Ti and Fe). These proxies are discussed in the text with respect to the pollen (sub) zones defined in figure 4.5. (YD = Younger Dryas equivalent).

Environmental conditions

The %AP shows its highest relative increase of the whole Early and Middle Holocene (114%CH) and reaches an average value of 45.9%. This indicates that the UFL might have migrated upslope up to ca. 3400 m amsl, close to the present-day UFL. The estimated MAT increases considerably to reach 8°C, which is close to present-day MAT at the site.

The subandean and Andean forests show their most important increase of the whole Early and Middle Holocene. The forest vegetation was mainly composed of tall elements such as *Quercus* and *Podocarpus* and in minor proportions *Pilea, Acalypha* and Urticales. Vegetation around the forest line may have been partly composed of *Polylepis* shrubs. The high proportion of taxa indicative of dry conditions such as Poaceae and Urticales, together with the decrease in "wetter" taxa such as Cyatheaceae*, Weinmannia, Lycopodium foveolata* and Asteraceae suggests dry conditions. Aquatics are dominated by marsh vegetation indicating a very low level of water in the lake (water depth of ca. 12 cm, i.e., a decrease of -69%CH). This is confirmed by the geochemical rainfall proxies.

All proxies indicate that Period 2 was much drier and much warmer than the conditions prevailing at the end of the Younger Dryas equivalent (Period 1).

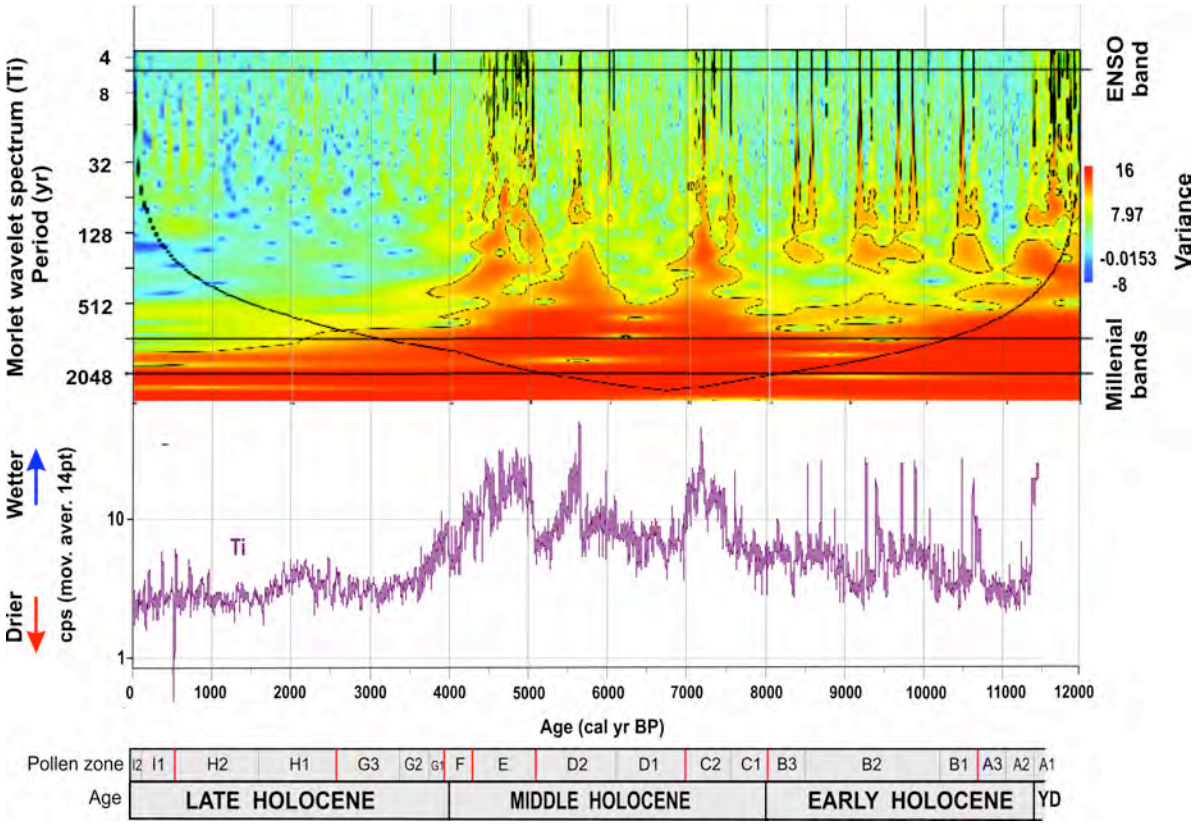

Fig. 5.4. Comparison between the Morlet wavelet spectrum of Ti (see Fig. 4.12), the Ti µXRF signal (see Figs. 5.3 and 5.5) and the pollen zones for the whole Holocene. (YD = Younger Dryas equivalent).

Period 3: Subzone A3 (11,050 - 10,700 cal yr BP)

Regional vegetation

The subandean forest remains represented by *Pilea* and Urticales, whereas *Acalypha* decreases. *Quercus* and *Podocarpus* increase and dominate the Andean forest. Low average values of *Hedyosmum, Weinmannia* and Melastomataceae suggest the presence of a dry forest type during almost this whole period, with an increasing trend towards the end of the period. The páramo vegetation is dominated by Poaceae, but *Lycopodium foveolata* becomes more important, especially towards the end of the period. Asteraceae and *Sisyrinchium* increase significantly and other páramo taxa are present but in low proportions (*Polylepis* and *Hedyosmum*)

Local vegetation

The total absence of *Isoëtes* and the high proportion of marsh vegetation point to a very low lake level. Marsh vegetation is composed mainly of Cyperaceae, with Apiaceae becoming more important at the end of the period. Cushion vegetation is also present at the end of the period.

Rainfall proxy (µXRF)

During almost the whole period, the Fe and Ti signals remain stable with low values indicating that low precipitation conditions prevailed. The more conservative Ti signal shows an increase from ca. 10,810 cal yr BP until the end of the period suggesting a short period of increased precipitations. The Morlet wavelet spectrum for Ti shows a period of calm in all frequency bands until ca. 10,810 cal yr BP, when the variance of all cyclical components increase, particularly in the ENSO band between 4 and 8 years (see Figs. 4.12, 4.13 and 5.4).

Environmental conditions

The %AP shows its highest value of 59.3% for the whole Early and Middle Holocene, which indicates the highest estimated UFL and MAT at ca 3575 m amsl and 9.1 °C respectively. This would mean an UFL ca. 125 m and a MAT ca. 0.8 °C higher than in the present-day.

The subandean and Andean forests show their most important proportions of the whole Early and Middle Holocene. The Llano Grande wet zone was surrounded by forest vegetation mainly composed by tall taxa such as *Quercus* and *Podocarpus,* which become more important than in the previous period, and by *Pilea* and Urticales as lower-sized forest. Vegetation around the forest line may be partly composed by *Polylepis* and Asteraceae shrubs. High proportions of “dry” taxa such as Poaceae and Urticales together with low values of “wet” taxa such as *Hedyosmum, Weinmannia,* Melastomataecae seem to suggest dry conditions.

These rather dry conditions are confirmed by the high proportions of marsh vegetation, the increase in *Plantago* and the absence of *Isoëtes*. This indicates a very low water depth as in the previous period (ca. 10 cm). Overall, Fe as well as Ti values keep low values, inferring low precipitations and little variability until 10,810 cal yr BP when the Ti signal shows a short

period of increase in precipitations. Therefore, proxies show that period 3 might have been slightly warmer and as dry as the previous one.

5.3.2.2. Pollen zone B (10,700 - 8,050 cal yr BP)

This zone is subdivided into three subzones.

Period 4: Subzone B1 (10,700 - 10,200 cal yr BP)

Regional vegetation

Overall, the forest vegetation in Period 4 shows the most important decrease during the whole of the Early and Middle Holocene. Consequently, it shows the poorest representation of Andean forest tree elements. The vegetation structure for the two forest belts has not significantly changed, but it presents the highest relative decrease in average values of many taxa such as *Pilea* and Urticales in the subandean forest, and *Quercus, Podocarpus, Hedyosmum*, Melastomataceae and *Miconia* in the Andean forest. Moreover, the structure of páramo vegetation changes, with the increase and dominance of *Lycopodium foveolata* and the decrease in Poaceae. Asteraceae and *Hypericum* increase together and dominate with low values. *Polylepis* decreases and disappears at the end of the period.

L*ocal vegetation*

Marsh vegetation remains dominant in the aquatic vegetation. It is composed mainly of Cyperaceae. Apiaceae become more important at the end of the period. Cushion vegetation presents a slight decrease with respect to the end of Period 3.

Rainfall proxy (µXRF)

Both Fe and Ti signals show a decrease between ca. 10,700 and 10,655 cal yr BP. Both signals then keep overall low stable values. Towards the end of the period both show an increasing trend. The Fe signal may display short-term variations not registered in the Ti signal (change in redox conditions? see chapter 3.4). The Morlet wavelet spectrum for Ti displays overall a period of stability where all cyclical components display little differences in variance. A short temporal change occurs between 10,450 and 10,500 cal yr BP affecting particularly the high frequencies. Towards the end of the period, the increase observed in the Ti signal corresponds to an increase in the variance of the higher frequency bands (see Figs. 4.12, 4.13 and 5.4).

Environmental conditions

The %AP decreases significantly to 32% indicating an estimated downslope shift of the UFL to ca 3030 m amsl and an estimated decrease in MAT from 9.1 to 5.5°C, i.e., 2.8°C lower than today. This would mean a ca. 500 m downward shift of the Andean vegetation belt. *Polylepis* shrubs disappear around the forest line. The structure of the páramo vegetation changes and shows a high dominance of *Lycopodium foveolata* and in minor proportions Poaceae. Asteraceae and *Hedyosmum* show similar lower proportions.

The aquatic vegetation composed by marsh vegetation and some *Plantago* points to a low water level in the mire, similar to Period 3 (ca. 10 cm water depth). Overall, the geochemical rainfall proxies do not change significatly with respect to the previous period, hence low precipitation regimes characterize this period.

Therefore, an important change occurred in this period, where the vegetation suggests much colder conditions than in Period 3, whereas both palynological and geochemical proxies indicate dry conditions close to those in Period 3.

Period 5: Subzone B2 (10,200 - 8,500 cal yr BP)

Regional vegetation

The lower part of this subzone continues to be dominated by páramo vegetation until 9,800 cal yr BP when the latter starts to decrease and the forest vegetation (both subandean and andean forests) becomes more important. This increase in forest vegetation is significant with respect to the previous Period 4.

The vegetation structure for the two forest belts does not display significant changes. *Pilea* and Urticales are the most important elements in the subandean forest and *Quercus* dominates strongly the Andean forest together with *Podocarpus*. The low representation of *Hedyosmum*, Cyatheaceae, *Weinmannia* and Melastomataceae may indicate a dry forest but this could be compensated by high proportions of *Quercus.* Therefore, no clear humidity information can be drawn from this information. Páramo vegetation continues to be dominated by *Lycopodium foveolata* (although it shows a relative decrease of -36.5%CH) and Poaceae. Asteraceae and *Hypericum* decrease.

L*ocal vegetation*

Marsh vegetation remains dominant among the aquatic vegetation. It is composed mainly of Cyperaceae. *Isoëtes* increases significantly but remains at relatively low values. Cushion vegetation continues to show an oscillating behaviour during this period with a significant relative increase.

Rainfall proxy (µXRF)

Over this period, both Ti and Fe show up-and-down variations, the Fe signal being considerably noisier, which can be expected from this element less conservative than Ti. Detailed statistical variations in the curves can be found in Appendix A3. The more conservative Ti clearly shows a lower and upper part of the period wetter than Period 4, with an intermediate drier interval (ca. 9,500 - 9,000 cal yr BP). Overall, the average rainfall is higher than during Period 4. The Morlet wavelet spectrum for Ti displays an overall decrease in variance for most frequencies (except those in the millennial bands) with some short intermittent periods of increase (see Figs. 4.12 and 5.4).

Environmental conditions

The %AP increases significantly (38%CH) to reach an average value of 44.1%, which can be interpreted as an upslope shift of the UFL to ca 3270 m amsl and an increase in MAT from 5.5 to 7.5°C. The latter estimated temperature is 0.8°C lower than today. Dry subandean and Andean vegetation belts were mainly composed by *Quercus, Podocarpus, Pilea* and Urticales. The páramo vegetation is still dominated by *Lycopodium foveolata* (although in minor proportions) and accompanied by Poaceae which are increasing, possibly an indication of drier páramo conditions.

In the local vegetation, the high dominance of marsh species and the increase in *Plantago* indicates a low water level, although the increase in *Isoëtes* could be an indicator of slightly wetter conditions compared with Period 4. These characteristics suggest that the water level in the mire is still low, but probably slightly higher than in Period 4 (estimated water depth of ca. 11 cm).

The Ti signal confirms the observations made on local vegetation. It clearly shows an overall level of precipitations higher than in the previous period, with a drier interval in the middle.

Therefore, Period 5 can be described from these proxies as a relatively dry and warm period.

Period 6: Subzone B3 (8,500 - 8,050 cal yr BP)

Regional vegetation

During this period, the forest vegetation continues to increase, with a slight dominance of forest (54.4%) over páramo vegetation (45.6%). As in Period 5, there is an overall increase in forest vegetation but the subandean vegetation increases in greater proportion than the Andean forest. Near the end of the period (at 8,100 cal yr BP), the páramo vegetation starts to increase again.

Higher values of *Pilea* and Urticales may indicate a relatively high altitudinal position of the subandean forest. The increase in *Alchornea and* Urticales suggests relatively dry conditions. The Andean forest is still dominated by *Quercus* and *Podocarpus.* Although in low proportions, tree elements such as *Miconia, Myrsine* and *Vallea* increase significantly, whereas *Alnus* and *Weinmannia* decrease. The structure of the páramo vegetation changes. While *Lycopodium foveolata* decreases, Poaceae increase. Dry conditions seem to be confirmed by the decrease in wet elements such as V*aleriana* and the increase of *Hypericum* (dry indicator).

Local vegetation

Marsh vegetation continues to dominate this period with essentially Cyperaceae and secondarily Apiaceae (the latter showing an important increase of 46.64%CH). *Lachemilla* and *Ranunculus* decrease considerably and even disappear. Submerged vegetation does not present significant differences in average value and remains poorly represented as in Period 5. Cushion vegetation increases over the period.

Rainfall Proxy (µXRF)

The Fe signal remains noisier than the Ti one. Consequently, we prefer to use that of the more conservative Ti, which shows a relative stability and an average close to the upper part of Period 5. The Morlet wavelet spectrum for Ti displays a similar picture to that of period 5, with overall low variance for most frequencies (except those in the millennial bands) with some short intermittent periods of increase (see Figs. 4.12 and 5.4).

Environmental conditions

The %AP continues to increase in this period to reach an average value of 54.4% which indicates that the UFL may have moved upslope to ca. 3480 m amsl. An estimated increase

of 1°C in MAT with respect to the previous period suggests a value of 8.5°C at the LLG site. This period is most similar to present-day conditions both in terms of temperature and UFL. The site LLG-2 was surrounded by an Andean forest belt represented by *Quercus* and *Podocarpus,* and lower down the dry subandean forest was mainly composed by *Pilea* and Urticales. Above the UFL, open dry páramo vegetation was dominated by Poaceae and *Lycopodium foveolata.* Asteraceae were present close to the forest line at the base of the páramo vegetation belt.

A very low water table is inferred from the high percentages of marsh, the increase in cushion vegetation and the decrease in *Isoëtes.* These characteristics indicate a low water level in the mire, not significantly different from Period 5 (ca. 11 cm).

The Ti signal shows that the intensity of precipitations is stable with respect to Period 5.

Therefore, palynological and geochemical proxies suggest that Period 6 is warmer than the previous one, but that relatively dry conditions are continuing.

5.3.2.3. Pollen zone C (8,050 - 7,000 cal yr BP)

This zone is subdivided into two subzones

Period 7: Subzone C1 (8,050 - 7,580 cal yr BP)

Regional vegetation

Forest pollen decreases significantly during this period indicating a lower altitudinal position of the UFL. The structure of the subandean forest belt changes with a decrease in *Pile*a and Urticales and a considerable increase in *Acalypha.* The Andean forest is still dominated by *Quercus* and *Podocarpus*. Taxa with low average values such as *Myrsine* and *Alnus* increase, whereas Cyatheaceae, *Miconia* and *Vallea* decrease. In the páramo vegetation, both *Lycopodium foveolata* and Poaceae increase and are the dominant taxa. *Polylepis* and *Blechnum* also increase but their average value remains low.

Local vegetation

Overall, there is a dominance of mash and cushion vegetation. In the basal part of the period, marsh vegetation is abundant until around 7,820 cal yr BP, then it decreases rapidly to be replaced by cushion vegetation. This represents the highest relative increase of the whole record in cushion vegetation. *Isoëtes* is almost absent.

Rainfall proxy (µXRF)

Both the Ti and Fe signals show low values in the lower part of the period, with a slight increase in the upper part. Overall, the average value is not higher than in Period 6. The Morlet wavelet spectrum for Ti displays overall low variance for most frequencies (except those in the millennial bands, see Fig. 4.12 and 5.4).

Environmental conditions

A rapid downward shift of the UFL is indicated by the decrease in arboreal pollen. The % AP value of 39.5% indicates that the UFL moved downslope to an estimated altitude of ca. 3180

m amsl. The estimated MAT of 6.5°C indicates a decrease of 2°C with respect to the previous period. The dry Andean forest belt is dominated by *Quercus*, *Podocarpus, Acalypha* and Pilea. *Polylepis* and Asteraceae shrubs are present close to the UFL and suggest dry conditions. The páramo vegetation composed of Poaceae and *Lycopodium foveolata* reaches lower altitudes suggesting colder conditions.

This period is marked in its upper part by the major increase in cushion vegetation and the almost absence of *Isoëtes.* This suggests that the mire becomes nearly dry towards the end of the period

The Fe and Ti signals suggest drier conditions than in the previous period until ca. 7,790 cal yr BP. In the upper part both signals suggest a slight increase in precipitations.

Therefore, the considerable lowering of the UFL points to cold conditions (ca. 1.7°C colder than today) during Period 7. The regional and mainly local vegetation composition suggests very dry conditions especially near the end of the period. Dry conditions are also inferred from geochemical proxies, although both tend to show a slight increase in rainfall during the last 200 years of the period, during which the cushion vegetation is at its maximum.

The latter observation raises the problem of the lag time necessary for the vegetation to react to changing conditions: whereas the Ti and Fe signals are synchroneous with precipitations in such a small drainage basin as Llano Grande, it may take some time for the vegetation to readjust, particularly if the change in precipitation is small, as suggested by the geochemical records.

Period 8: Subzone C2 (7,580 - 7,000 cal yr BP)

Regional vegetation

The forest vegetation increases significantly during this period, indicating an upslope shift of the UFL. The subandean forest resembles that of Period 6 with *Pilea* and Urticales as the dominant taxa. In the Andean forest, *Quercus* is still the major constituent. Cyatheaceae are also important and partly replace *Podocarpus* suggesting a wet forest. The latter is confirmed by the increase in *Weinmmania,* Melastomataceae and *Hedyosmum.* This vegetation belt becomes more diverse because of the increased importance of some taxa such as *Alnus*, *Juglans*, *Miconia* and *Prunus.* Poaceae strongly dominate the páramo vegetation, whereas *Lycopodium foveolata* decreases significantly. Asteraceae, *Hypericum* and *Sisyrinchium* increase.

Local vegetation

This period is characterized by a gradual change in the dominance between marsh and cushion vegetation. Cushion vegetation has the highest percentages at the base of the subzone, but gradually decreases towards the top and is replaced by marsh vegetation. This implies an increase in the water depth of the mire.

Rainfall proxy (µXRF)
This period is characterized by the highest signals of both Ti and Fe since the base Holocene. The signals increase until between 7,295 and 7,230 cal yr BP and then show a decreasing trend until the end of the period (see Appendix A3. The Morlet wavelet spectrum for Ti displays a significant increase in the variance of all frequencies; particularly the higher frequencies (see Figs. 4.12 and 5.4).

Environmental conditions
The increase in %AP with an average value of 56.7% indicates that UFL moved upslope to an estimated altitude of ca. 3525 m amsl. An estimated MAT of ca 8.7°C indicates an increase of 2.2°C with respect to the previous period, i.e., a considerable warming.

The subandean forest is mainly composed of *Pilea* and Urticales, whereas a wide Andean forest belt develops around the Llano Grande lake, becoming richer in taxa. It is mainly dominated by *Quercus* and Cyatheaceae. The increase in *Weinmmania,* Melastomataceae and *Hedyosumum* suggests wet conditions. A slight increase in *Alnus* and *Morella* could indicate an expansion of the marsh forest possibly due to the warmer climatic conditions. The zone of the UFL is occupied by Asteraceae shrubs, whereas open páramo vegetation dominated by Poaceae is situated at higher altitudes
This period is characterized by a gradual increase in the water depth of the lake. At the base, cushion vegetation has very high percentages meaning that the mire might be close to dryness. Cushion vegetation gradually decreases towards the top of the period and is replaced by mash vegetation, indicating that the mire becomes inundated. The average water depth for this period is estimated at ca. 7 cm. The Fe and Ti signals confirm this shift towards more humid conditions with a maximum of rainfall between ca. 7,295 and 7,230 cal yr BP.

Therefore, Period 8 is much warmer than the previous one, with estimated UFL and MAT respectively 65 m and 0.4°C higher than today. The increase in marsh vegetation and rainfall in the upper part of the period suggests a change to wetter conditions than in the previous period.

5.3.2.4. Pollen zone D (7,000 - 5,100 cal yr BP)
This zone is subdivided into two subzones

Period 9: Subzone D1 (7,000 - 6,120 cal yr BP)
Regional vegetation
Lower proportions of subandean elements suggest that this type of vegetation colonized lower altitudes with respect to Period 8. This belt is still dominated by *Pilea*, Urticales and *Acalypha*. In the Andean forest, *Quercus*, *Podocarpus, Alnus and* Cyatheaceae decrease together but remain the dominant taxa. The low percentages of *Alnus* and *Myrsine* suggest a narrow marsh forest. Although they have low proportions, *Hedyosmum* and *Myrsine* increase significantly, which may suggest slightly wetter conditions. The páramo vegetation is mainly dominated by Poaceae. *Lycopodium foveolata* and Asteraceae increase significantly and become important elements with average values of 12% for both. The overall increase in

Lycopodium foveolata, together with an increase in *Hypericum* and *Valeriana* may also suggest slightly wetter conditions. Nevertheless, from about 6,600 cal yr BP until the end of the period this trend seems to be counterbalanced by a decrease in *Lycopodium foveolata* and a gradual increase in Poaceae.

Local vegetation

This subzone is characterized by the almost total dominance of marsh vegetation (95%), represented mainly by Cyperaceae and secondarily by Apiaceae. *Lachemilla* increases to reach its maximum average value of the whole record. Although it keeps a low average value, the submerged vegetation gradually increases toward the top of the period.

Rainfall proxy (µXRF)

The Fe signal displays an unstable behaviour during this period with alternating intervals of increase and decrease (see Appendix A3). The signal of the more conservative Ti does not present significant changes over the whole period. In average, both elements indicate wetter conditions than during periods 2 to 7, but drier than those prevailing in Period 8 (Fig. 5.3). The Morlet wavelet spectrum for Ti displays a quiet period where the variance of frequency bands higher than 512 years decreases significantly (see Figs. 4.12 and 5.4).

Environmental conditions

During this period the %AP decreases to an average of 40% indicating a downslope shift of the UFL to an estimated altitude of ca. 3205 m amsl. The estimated MAT of 6.7°C indicates a decrease of ca 2°C compared to the previous period.

The subandean forest decreases indicating an altitudinal lowering of this belt. A rather wet Andean forest dominated by *Quercus, Podocarpus* and Cyatheaceae is inferred. The moderate presence of *Alnus* and *Myrsine* suggests a narrow marsh forest. Asteraceae and *Polylepis* shrubs are present close to the forest line. An important páramo vegetation is indicated by the high proportions of Poaceae, *Lycopodium foveolata, Hypericum* and *Valeriana.*

The increase in marsh vegetation and decrease in cushion vegetation indicates that the mire is inundated by a slightly thicker water layer than in the lower part of Period 8. The slight increase in *Isoëtes* towards the end of period confirms the presence of a thin water layer.

These rather low-water conditions (estimated water depth of ca. 7 cm) are confirmed by geochemical proxies which indicate lower rainfall than in Period 8, but a higher average than during periods 2-7. Drier páramo conditions suggested by the gradual increase of elements such as Poaceae, *Hypericum* and Asteraceae after 6,615 cal yr BP are not supported by geochemistry.

Therefore, the increase in páramo vegetation corresponds to a lowering of the UFL and MAT (estimated values at respectively 245 m and 1.6°C lower than today). The mire is constantly under a thin layer of water with an average rainfall higher than during periods 2-7, but lower than that of Period 8.

Period 10: Subzone D2 (6,120 - 5,100 cal yr BP)

Regional vegetation

The elements of forest vegetation show a continuous regular decrease during this period. The lower altitudinal position of the subandean forest is confirmed by the low values of *Pilea*, Urticales and *Acalypha*. In the Andean forest, *Quercus* is the most abundant taxon. *Podocarpus* decreases significantly but remains a dominant element with Cyatheaceae. Other taxa with low proportion such as *Miconia* and *Weinmannia* increase and *Alnus* loses significance. In the páramo vegetation, *Lycopodium foveolata* increases gradually in a considerable way and dominates together with the Poaceae and present similar average values of ca. 25%, although their behaviour remains opposite. Although Asteraceae show a decrease they continue to be an important element. *Hypericum* starts to be more important. *Polylepis* decreases.

Local vegetation

The submerged vegetation increases significantly in the central part of the period, suggesting a deepening of the lake (Fig. 5.3). Marsh vegetation decreases relatively overall, but is still dominant. It varies in the opposite way to the submerged vegetation and shows two peaks of abundance in the lower and upper part of the period. It is mainly composed of Cyperaceae and Apiaceae. Cushion vegetation increases slightly but keeps a low average value of 1.1%

Rainfall proxy (µXRF)

This period presents a high variability in the behaviour of both signals as described in Appendix A3. Overall, both signals increase in the central part of the period indicating a maximum of precipitation which fits with the increase in water depth of the lake derived from aquatics (Fig. 5.3). The Morlet wavelet spectrum for Ti shows low variance in frequency bands higher than 512 years until 5,790 cal yr BP (Fig. 5.4). Between this date and 5,480 cal yr BP, a change causes an increase in the variance of the high frequencies. This interval coincides with the maximum of precipitations observed in the signal. From 5,480 cal yr BP until the end of the period, all frequencies higher than 256 years decrease in variance (Figs. 4.12 and 5.4).

Environmental conditions

The UFL keeps getting lower than in the previous period (average %AP down to 36.7%), with an estimated average altitude shifted downslope to ca. 3125 m amsl, i.e. a decrease of ca. 80 m with respect to the previous period. Consequently, the estimated MAT of ca. 6.1°C shows temperatures 0.6°C cooler than during Period 9.

Relatively high proportions of *Weinmannia,* Cyperaceae and Melastomataceae suggest a wet Andean forest mainly dominated by *Quercus and Podocarpus*. Asteraceae and *Polylepis* shrubs are situated close to the forest line. The Llano Grande lake is surrounded by a wide páramo vegetation belt dominated by *Lycopodium foveolata*, Poaceae and *Hypericum.*

A deeper lake level is inferred in the central part of the period from the high proportions of *Isoëtes.* The average water depth of the lake is estimated at ca. 24 cm, i.e., quite deeper than in the previous period (ca. 7 cm). This trend is corroborated by the geochemical proxies which show increased rainfall in the same central part of the period.

Therefore, palynological and geochemical proxies tend to demonstrate that Period 10 was colder and wetter than the previous one. The estimated UFL (3125 m amsl) and MAT (~ 6.1°C) are respectively 325 m and ca. 2.2 ˚C lower than today.

5.3.2.5. POLLEN ZONE E (5,100 - 4,300 CAL YR BP)

Period 11: Zone E (5, 100 - 4,300 cal yr BP)

Regional vegetation

The decrease in forest vegetation continues during this period, which corresponds to the second highest proportion of páramo vegetation of the whole record. The composition of forest vegetation does not change significantly, only its proportions do change. The subandean forest is very limited and is mainly composed by *Pilea*, Urticales and *Acalypha.* The Andean forest is dominated by *Quercus* and *Podocarpus.* Cyatheaceae show a significant decrease. Important elements such as *Hedyosmum,* Melastomataceae, *Weinmannia*, *Miconia* and *Mysrine* remain stable. The páramo vegetation presents changes in composition. Poaceae have their highest average proportion. By contrast, *Lycopodium foveolata* shows its highest relative decrease and a minimum average value of 1.5%. It is replaced by *Hypericum* which becomes a co-dominant element of this vegetation belt. Asteraceae decrease slightly but continue to be an important element, whereas *Polylepis* increases.

Local vegetation

This zone is characterized by the highest proportion of submerged vegetation in the whole record. Marsh vegetation shows a major decrease. It is dominated by Cyperaceae and Apiaceae. Cushion vegetation decreases and is poorly represented (0.6%).

Rainfall proxy (µXRF)

This zone is characterized by exhibiting an unstable comportment of Fe as well as Ti (see Appendix A3 for details). Overall, both Ti and Fe show a considerable increase with respect to the upper part of period 11. From about 4,700 cal yr BP both signals show an overall decrease. The Morlet wavelet spectrum for Ti shows an important change between ca. 5,200 and 4,880 cal yr BP, where the variance of all cyclical components increases considerably, and particularly the most sensitive frequencies of the ENSO band (Fig. 5.4). This corresponds to the increase observed in both signals (Fig. 5.5). After 4,880 cal yr BP, the variance of all frequencies begins to decrease gradually (Figs. 4.12, 4.14 and 5.4).

Environmental conditions

This period corresponds to the second highest proportion of páramo vegetation in the Early and Middle Holocene. A decrease in %AP down to 30% indicates a downslope shift of the UFL to ca. 2995 m amsl, which means a lowering of ca. 130 m with respect to the previous period. An estimated MAT of about 5.3°C characterizes this period.

The subandean vegetation is dominated by *Pilea*, Urticales and *Acalypha* taxa. *Quercus* and *Podocarpus* dominated the Andean forest. Cyatheaceae, Melastomataceae, *Weinmannia*, *Miconia* and *Myrsine* were also present. The vegetation around the UFL was partly

composed by Asteraceae and *Polylepis* shrubs. Around Llano Grande, a wide open páramo was established, dominated by Poaceae and co-dominated by *Hypericum.* Dry conditions in the páramo are confirmed by the significant decrease in *Lycopodium foveolata.*

The highest proportion of *Isoëtes* indicates the deepest lake level and this is confirmed by the decrease in marsh elements. The estimated water depth is deeper than 40 cm, a significant increase compared to the previous period (ca. 24 cm), implying heavier precipitations during this period.

Geochemical proxies confirm the high level of rainfall, particularly in the lower half of the period. An overall decreasing trend characterizes the upper part.

Except for the Younger Dryas, this period is marked by the lowest UFL of the whole Early and Middle Holocene record. The UFL is estimated at 2995 m, i.e., 455 m lower than the present-day forest line. The estimated MAT (ca. 5.3°C) indicates a temperature ca. 3°C lower than today. Consequently, this period can be interpreted as the coldest and wettest (in terms of rainfall) of the whole Early and Middle Holocene. Although palynological and geochemical proxies point to important rainfall and a deeper lake, it is important to note that the palynological signature of the páramo is dry, its vegetation being dominated mainly by Poaceae and *Hypericum.*

5.4. CLIMATIC AND ENVIRONMENTAL RECONSTRUCTION FOR THE LATE HOLOCENE

In this part, we will cover the Late Holocene using the palynological results of Velásquez (2005) and adding our geochemical results. We will use the palynological zonation proposed by Velásquez (2005) and apply to his palynological data the same models to estimate the UFL and MAT. This will give us a picture of climatic variations for the whole Holocene derived from palynological and geochemical proxies (Fig. 5.5).

5.4.1. POLLEN ZONE F (4,300 - 3,925 CAL YR BP)

Period 12: Zone F (4,300 - 3,925 cal yr BP)
This period corresponds to pollen zone 1 of Velásquez (2005).

Regional vegetation
The subandean forest is represented by *Acalypha, Alchornea* and Urticales. *Quercus* dominates the Andean forest together with *Alnus, Podocarpus*, Cyatheaceae, *Juglans, Hedyosmum* and *Myrsine.* Close to the UFL a *Polylepis* forest is developed. The proportions of *Lycopodium foveolata* are still low and Poaceae decrease considerably in the páramo vegetation.

Local vegetation
The aquatic vegetation is still dominated by *Isoëtes* but the latter shows a considerable decrease towards the top of the period, whereas the marsh vegetation mainly made of

Cyperaceae and Apiaceae increases. *Lachemilla* has a very important increase in this period. Although the cushion vegetation shows an increase, its proportion remains low and it is locally absent.

Rainfall proxy (µXRF)
Both signals show a high variability during this period (see Appendix A3). If one considers the conservative Ti, the signal overall decreases rapidly during the period pointing to a decrease in rainfall. The Morlet wavelet spectrum for Ti shows a gradual decrease in the variance of all frequencies (Figs. 4.12, 4.14 and 5.4).

Environmental conditions
The %AP increases to reach an average value of 42%. This indicates an estimated upslope shift of the UFL to ca. 3215 m amsl, i.e. about 220 m higher than during the previous period. The estimated MAT is of ca. 7°C, i.e., an increase of some 1.7 °C compared to Period 11.

The aquatic vegetation exhibits a considerable decrease, whereas marsh vegetation increases. This seems to indicate a decrease in water depth of Llano Grande lake back to a depth of ca. 37 cm.

Geochemical proxies indicate a decrease in rainfall with respect to the previous period. This confirms the shallower water depth estimated from aquatic plants.

Therefore, period 12 is marked by a warming up trend and drier conditions than those in the previous period.

5.4.2. POLLEN ZONE G (3,925 - 2,580 CAL YR BP)
This zone corresponds to pollen zone 2 of Velásquez (2005) and is subdivided into three subzones.

Period 13: Subzone G1 (3,925 - 3,750 cal yr BP)
This period correspond to subzone 2A of Velásquez (2005).

Regional vegetation
The forest vegetation increases considerably and co-dominates with the páramo vegetation. The subandean forest is mainly composed of Urticales, *Pilea, Acalypha* and *Alchornea*. The Andean forest is dominated by *Quercus*, Cyateacheae, *Podocarpus, Hedyosumum, Myrsine, Miconia,* and *Weinmannia.* Poaceae *and Lycopodium foveolata* dominate the páramo vegetation, and Asteraceae and *Hypericum* are also present.

Local vegetation
The submerged vegetation decreases significantly and is replaced by cushion vegetation which has an average value of about 32%. Marsh vegetation does not show important changes but *Lachemilla* decreases considerably (-38% CH).

Rainfall proxy (µXRF)
It is important to note that from this period onwards, the signals of both Ti and Fe show much less fluctuations than in the previous periods (see Appendix A3). In this period, both signals show a rapidly decreasing trend indicating a diminishing rainfall. The Morlet wavelet spectrum for Ti shows a gradual decrease in the variance of all frequencies (Figs. 4.12, 4.14 and 5.4).

Environmental conditions
The increase of the %AP up to 52% indicates an estimated UFL at ca 3430 m amsl, i.e. a slight upslope shift of around 14 m with respect to the previous period. The relative importance of *Quercus* accompanied by the relative low proportions of *Weinmannia* is indicative of an oak-dominated high Andean forest (Quercetum). The estimated MAT of 8.1°C is ca. 1.1°C higher than in the previous period.

In the aquatic vegetation, *Plantago* increases considerably, whereas *Isoëtes* decreases. This suggests a lower lake level estimated at ca. 20 cm water depth, i.e. some 17 cm lower than in the previous period. This interpretation is supported by both Ti and Fe signatures which show a diminution of the rainfall

Therefore, this period is interpreted as warmer and drier than the previous one.

Period 14: Subzone G2 (3,750 - 3,340 cal yr BP)
It corresponds to subzone 2B of Velásquez (2005).

Regional vegetation
The forest vegetation continues to increase to reach an average value of 55.7%. The composition of the subandean and Andean forests does not present important changes. The páramo vegetation is mainly dominated by *Lycopodium foveolata,* whereas Poaceae decrease considerably, suggesting wetter páramo vegetation during this period. The lower part of the páramo belt was occupied by Asteraceae shrubs.

Local vegetation
In the lower part of the period, *Isoëtes* increases sharply to reach an average value of around 61%. Marsh vegetation decreases and is still dominated by Cyperaceae and Apiaceae. *Plantago* decreases. In the upper part of the period, the trend reverses itself with a sharp decrease in submerged vegetation.

Rainfall proxy (µXRF)
As in period 13, both signals show much less fluctuations (see Appendix A3). Both signals indicate the continuation of the decreasing trend observed in period 13 pointing to a decrease in rainfall. The Morlet wavelet spectrum for Ti shows a gradual decrease in the variance of all frequencies (Figs. 4.12, 4.14 and 5.4). The Morlet wavelet spectrum for Fe (Fig. 4.17) is perturbed by frequent short events only perceived by high frequencies, especially in the 8 and 4 year band (ENSO band, Fig. 4.17)

Environmental conditions

A gradual increase of the forest elements marks this period. The increase of %AP up to 55.7% indicates an upslope shift of the UFL to ca. 3500 m amsl, i.e., 75 m higher than in the previous period. The estimated MAT of ca. 8.6°C shows slightly warmer temperature (0.5°C) than in period 13.

The high proportions of submerged vegetation (and the decrease in cushion vegetation) in the early part of the period give an estimated average water depth of ca. 40 cm for the period, although there is a rapid decrease in the late part of the period, at the end of which the water depth is down to below 20 cm.

Both Fe and Ti signals indicate a progressive diminution of the rainfall.

Therefore, pollen indicates a warmer period than the previous one. Although it is much wetter at the beginning than the previous one, it ends up with much drier conditions.

Period 15: Subzone G3 (3,340 - 2,580 cal yr BP)

It correspond to subzone 2C of Velásquez (2005)

Regional vegetation

The forest vegetation reaches its maximum values of the whole Holocene with an average value of 77%. Consequently the páramo vegetation reaches its minimum value. All elements of the subandean as well as Andean forest reach their highest record. Páramo vegetation is mainly dominated by Poaceae and *Lycopodium foveolata,* but the latter decreases considerably. *Valeriana* and *Sisyrinchium* become more important.

Local vegetation

Submerged vegetation decreases sharply during this period, replaced by cushion vegetation which has an average value of around 33%. Marsh vegetation substantially increases and is mainly dominated by Cyperaceae which increase significantly, while Apiaceae and *Lachemilla* decrease.

Rainfall proxy (µXRF)

Both signals do not show significant variations. They have very low average values, the lowest since the beginning of the Holocene (that of Ti is below the threshold of reliability). This indicates very low rainfall. The Morlet wavelet spectrum for Ti continues to show a gradual decrease in the variance of all frequencies (Figs. 4.12, 4.14 and 5.4). The Morlet wavelet spectrum for Fe (Fig. 4.17) is perturbed by frequent short events only perceived by high frequencies, especially in the 8 and 4 year bands (ENSO band, Fig. 4.17).

Environmental conditions

The páramo vegetation is at very high altitude. The increase of the %AP up to 77% indicates an estimated UFL at ca. 3930 m amsl, i.e. an upslope shift of around 427 m with respect to the previous period. The relative importance of *Quercus* accompanied by the relative low proportions of *Weinmannia* is indicative of an oak-dominated high Andean forest.

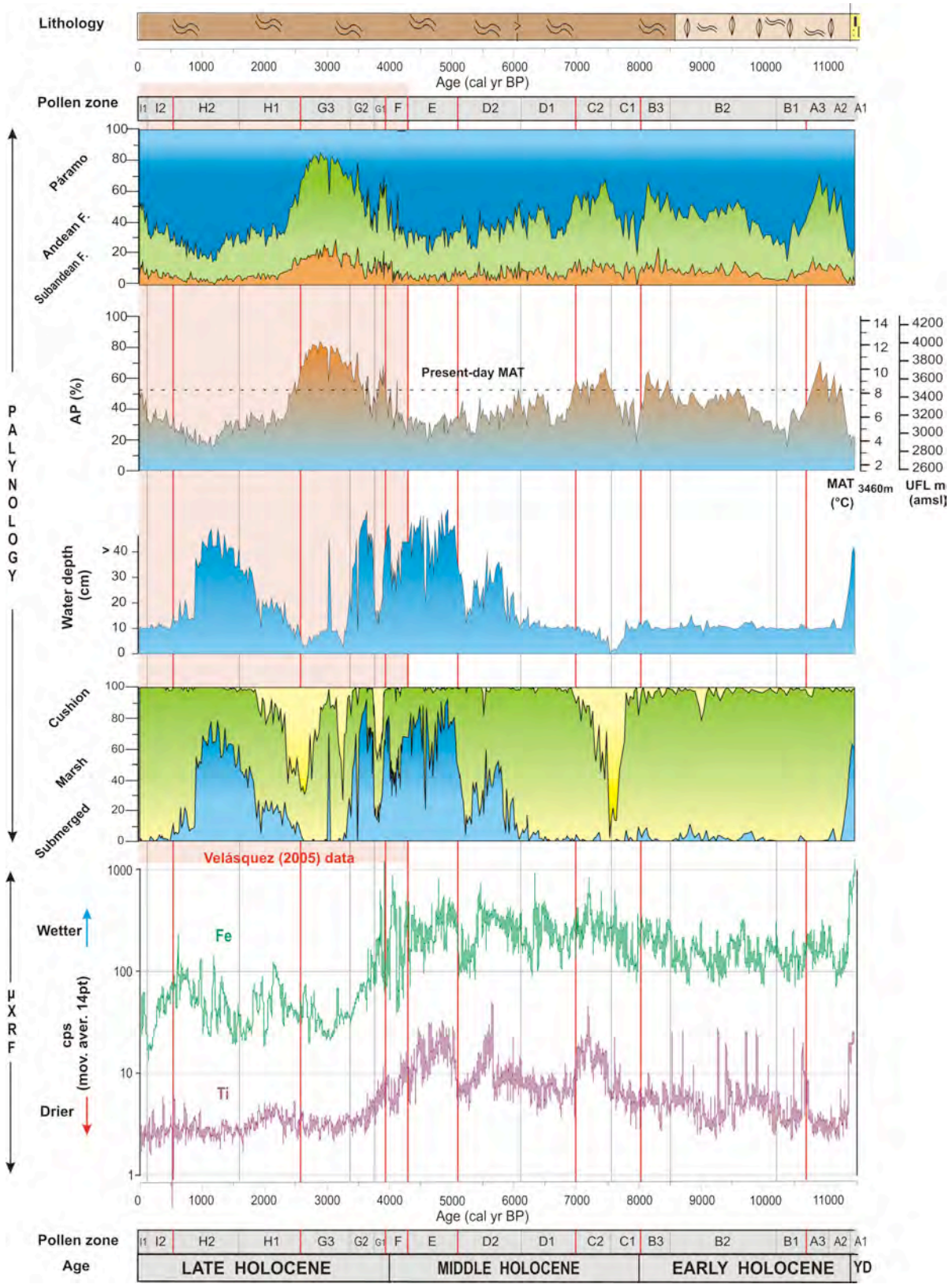

Fig. 5.5. Comparison of palynological climatic proxies (MAT and UFL derived from %AP) and μXRF rainfall proxies (Ti and Fe) for the whole Holocene. This figure is an extension of figure 5.3 including Velásquez's (2005) palynological data for the Late Holocene. See discussion in the text. (YD = Younger Dryas equivalent).

The estimated MAT of 11.4°C is ca.2.8°C higher than in the previous period. This suggests a temperature of about 3°C higher than today.

Marsh vegetation and *Plantago* increase considerably, whereas *Isoëtes* is poorly represented. This indicates a considerable decrease in lake level with an estimated average water depth of ca. 8 cm, i.e., more than 30 cm lower than in the previous period.

Both Fe and Ti signals confirm these suggested dry conditions. Their very low signal points to low rainfall regimes.

Consequently, this period is interpreted as much warmer than the present-day conditions with a UFL ca. 440 m higher than today. Both aquatic vegetation and geochemical proxies indicate very dry conditions. Therefore, in this case, temperature is the most likely factor to explain this rapid upslope shift of the UFL. One can certainly not invoke increased precipitations, because both palynology and geochemistry indicate very dry conditions.

5.4.3. POLLEN ZONE H (2,580 - 520 CAL YR BP)

This pollen zone corresponds to pollen zone 3 of Velásquez (2005) and is subdivided into two subzones.

Period 16: Subzone H1 (2,580 - 1,600 cal yr BP)

It correspond to subzone 3A of Velásquez (2005)

Regional vegetation

Overall, the subandean and Andean forest vegetation does not present important changes in its composition, but its proportion decreases considerably and the páramo vegetation has an increase of 175% CH. The páramo vegetation presents important changes in the proportions of its elements: Poaceae increase initially and then become stable. They co-dominate with *Lycopodium foveolata* which presents an opposite behaviour. Asteraceae and *Hypericum* increase progressively to reach their maximum value towards the end of the period

Local vegetation

Plantago decreases gradually and almost disappears at the end of the period, whereas *Isoëtes* presents a significant increase to reach ca. 50% at the end of the period. Marsh vegetation exhibits a slight decrease and changes in its composition, with an increase in Apiaceae and decrease in Cyperaceae.

Rainfall proxy (µXRF)

During this period both signals remain low overall (that of Ti is below the threshold of reliability), the Fe having a more unstable behaviour. Nevertheless, both signals seem to show slightly higher values in an interval spanning ca. 2,500 -1,900 cal yr BP (see Appendix A3). The Morlet wavelet spectrum for Ti continues to show a gradual decrease in the variance of all frequencies (Figs. 4.12, 4.14 and 5.4). The Morlet wavelet spectrum for Fe (Fig. 4.17) is perturbed by frequent short events only perceived by high frequencies, especially in the 8 and 4 year band (ENSO band, Fig. 4.17)

Environmental conditions

A significant drop in the proportion of arboreal taxa suggests a much lower position of the UFL estimated at ca. 3125 m amsl. This is ca. 810 m lower than during the previous period. The estimated MAT of 6.1°C is ca 5.3°C colder than during the previous period.

The local vegetation shows increasingly wet conditions throughout this period. A progressive increase in *Isoëtes* is accompanied by a decrease in *Plantago.* Mash vegetation is co-dominant and composed of Cyperaceae and Apiaceae. The water depth in the mire is estimated at an average of ca 20 cm, i.e., some 11 cm higher than during the previous period. The estimated water depth increases throughout the period from less than 10 cm to ca. 30 cm at the end.

Both Fe and Ti signals show a low level of rainfall, with a slight increase in the central part of the period.

The considerable decrease (-53%CH) in forest vegetation and the expansion of dry páramo vegetation indicate much colder conditions than during the previous period. Although geochemical proxies indicate low rainfall regimes, aquatic plants suggest that the water depth increases throughout the period.

Period 17: Subzone H2 (1,600 - 520 cal yr BP)

It corresponds to subzone 3B of Velásquez (2005)

Regional vegetation

The páramo vegetation continues to increase and forest vegetation decreases. The composition of the subandean forest does not change. The Andean vegetation shows a gradual decrease in *Quercus* and the other taxa do not present significant differences in their dominance. The páramo vegetation exhibits a different composition with the highest proportions of *Espeletia frontinoensis* in the whole record. *Hypericum,* Asteraceae *a*nd *Lycopodium foveolata* decrease together, the latter almost disappearing. *Aragoa* is more relevant in this period.

Local vegetation

In general terms, *Isoëtes* dominates this period and increases to reach an average of 43% (previous period 23.3%). It starts to decrease at around 1,000 cal yr BP until the end of the period. Marsh vegetation is mainly dominated by Cyperaceae and Apiaceae and *Lachemilla* decreases considerably. Plantago is almost absent during this period.

Rainfall proxy (µXRF)

The Ti signal is very low, below the threshold of reliability. That of Fe is also low overall, but shows a lot of unstability. It tends to be slightly higher between ca. 1,480 and 1,200 cal yr BP and between ca. 1,000 cal yr BP and the end of the period (see Appendix A3). The Morlet wavelet spectrum for Ti displays a very low variance in all frequencies (Figs. 4.12, 4.14 and 5.4).

The Morlet wavelet spectrum for Fe (Fig. 4.17) is perturbed by frequent short events only perceived by high frequencies, especially in the 8 and 4 year band (ENSO band, Fig. 4.17)

Environmental conditions
The percentages of arboreal pollen decrease considerably indicating an estimated UFL at ca. 2870 m amsl. This corresponds to a downslope shift of ca. 250 m with respect to the previous period. The estimated MAT of 4.5°C is ca 1.6°C lower than during the previous period.

Forest vegetation has lower proportions of *Quercus.* The low percentages of Cyatheaceae, *Hedyosmum, Weinmmania* and Melastomataceae may indicate a relatively dry forest type. Close to the UFL grew stem rossetes of *Espeletia* and Asteraceae shrubs. The páramo vegetation expanded and was dominated by Poaceae. The gradual decrease in *Hedyosmum* and *Lycopodium foveolata* and the higher proportions of Poaceae could indicate a dry páramo.

The gradual increase in *Isoëtes* accompanied by the decrease in marsh vegetation up to 1,000 cal yr BP seems to indicate a higher lake level. From 1,000 cal yr BP this behaviour is sharply reversed with a much lower lake level at the end of the period. An average water depth ca 31 cm is estimated for this period, i.e., some 12 cm higher than in the previous period.

Although the Fe signal shows rapid periods of increase and decrease, it always keeps low values which indicate low intensity of rainfall. This is confirmed by the extremely low Ti signal.

Therefore, this period is interpreted as colder than the previous one. Conditions are wetter in the lower part and become drier from 1,000 cal yr BP.

5.4.4. POLLEN ZONE I (520 CAL YR BP - PRESENT DAY)

This zone corresponds to pollen zone 4 of Velásquez (2005) and is subdivided into two subzones.

Period 18: Subzone I1 (520 - 130 cal yr BP)
It correspond to subzone 4A of Velásquez (2005)

Regional vegetation
Although the páramo vegetation still dominates during this period, it decreases gradually towards the end of the period. Consequently, the forest vegetation increases to reach an average value of 33.8%. The subandean forest is characterized by a progressive increase of its elements such as Urticales, *Pilea Alchornea* and *Acalypha.* The Andean forest is dominated by *Quercus*, Cyatheaceae, *Alnus* and Solanaceae. There is a gradual increase in taxa such as *Hedyosmum, Mysrine, Weinmannia, Prunus and Hesperomeles.* For first time in the record, Ericaceae present high proportions in the páramo vegetation and co-dominate

with Poaceae. *Polylepis* increases and *Espeletia* decreases. Asteraceae still have low values.

Local vegetation

The trend towards a lower water table is inferred from the major expansion of marsh vegetation which has an increase of 73%CH during this period. This is accompanied by a significant decrease in submerged vegetation (*Isoëtes*).

Rainfall proxy (µXRF)

Both Fe and Ti signals have low values (that of Ti is below the threshold of reliability). The Fe signal shows a decreasing trend overall. The Morlet wavelet spectrum for Ti shows a very low variance in all frequencies. The high frequencies might be affected by spontaneous or temporal events which can alter the signal (Figs. 4.12, 4.14 and 5.4; Appendix A3) . The Morlet wavelet spectrum for Fe (Fig. 4.17) is perturbed by frequent short events only perceived by high frequencies, especially in the 8 and 4 year band (ENSO band, Fig. 4.17) until 260 cal yr BP. After that there is a loss in variance of all cyclical components, even the high frequency ones.

Environmental conditions

The forest vegetation expands slightly and its structure does not show important changes. An increase in %AP with an average value of 33.8% indicates an upslope shift of the UFL to an estimated altitude of 3065 m amsl, i.e., ca. 195 m higher than in the previous period. The estimated MAT of ca. 5.8°C shows a increase of ca. 1.2°C for this period.

The gradual increase in Urticales and *Acalpyha* may indicate a drier subandean forest. *Quercus* and Cyatheaceae dominated the Andean forest and the low proportions of *Hedyosmum* and Melastomataceae could suggest dry conditions. In the high part of the forest vegetation there existed a dwarf forest of *Polylepis*. The páramo vegetation expanded and was mainly represented by Poaceae and Ericaceae. This together with the poor representation of wet páramo vegetation (*Valeriana* and the almost absent *Lycopodium foveolata*) suggest a dry páramo vegetation

The general trend to shallower water depth started in the previous period continues as shown by the aquatic vegetation. The estimated average water depth of ca. 11 cm is much lower than in the previous period (ca. 21 cm). The lake is surrounded by dry páramo vegetation with a large input of Poaceae pollen. The very low values of Fe and Ti are indicative of very low rainfall.

Therefore, all proxies indicate warmer and drier conditions than during the previous period.

Period 19: Subzone I2 (130 - 0 cal yr BP)
It correspond to subzone 4B of Velásquez (2005)

Regional vegetation
The forest vegetation increases to reach a balance with the páramo vegetation with average values of 47% and 53% respectively. The composition of the subandean forest does not show significant changes. In the Andean forest, there is an increase in *Eugenia* towards the top of the record, whereas *Morella, Weinmannia, Hedyosmum and Myrsine* increase and finally decrease gradually towards the end of period. The páramo vegetation is still dominated by the same taxa with an overall decreasing trend.

Local vegetation
Isoëtes is absent throughout most of the period. The marsh vegetation is dominated by Cyperaceae. *Plantago* is absent.

Rainfall proxy (µXRF)
Both Fe and Ti signals have very low values (that of Ti is below the threshold of reliability). Both signals show a slight increase during the last 20 years (see Appendix A3). The Morlet wavelet spectrum for Ti shows a very low variance in all frequencies. The high frequencies might be affected by spontaneous or temporal events which can alter the signal (Figs. 4.12, 4.14 and 5.4; Appendix A3). The Morlet wavelet spectrum for Fe (Fig. 4.17) shows very low variance of all cyclical components.

Environmental conditions
The increase in forest vegetation taxa indicates that the UFL gets closer to the lake. An average %AP value of 47.8% suggests an upslope shift of the UFL to ca. 3350 m amsl, i.e., some 280 m higher compared to the previous period. An estimated MAT of ca. 7.6°C is 1.8°C warmer than during the previous period.

The Andean forest vegetation does not show significant changes in its structure. It records for the first time the presence of *Eugenia.* The relative importance of *Quercus* together with the relatively low proportions of *Weinmannia* are indicative of an oak-dominated high Andean forest (Quercetum). In general, the páramo vegetation continues being dominated by Poaceae and Ericaceae. The presence of *Polylepis, Hypericum* and Poaceae are indicative of a dry páramo, which becomes wetter towards the end of the period as shown by the gradual increase in *Lycompodium foveolata*

The substantial decrease in *Isoëtes* and the dominance of marsh vegetation indicate a trend to a lower water level in the lake with an estimated water depth of ca. 10 cm. This is supported by the expansion of the marsh forest suggested by the relatively important proportions of *Morella* and *Alnus*.

Fe and Ti signals remain very low indicating low rainfall. Therefore, this period can be considered as warmer and drier with respect to the previous two periods.

5.5. CONSIDERATIONS ABOUT HOLOCENE CLIMATE IN LLANO GRANDE

5.5.1. CLIMATE PROXIES

The temperature proxy in this study is derived directly from the proportion of arboreal pollen (%AP), using the concept of migration of the upper forest line (UFL) with respect to a lapse rate, as explained above in paragraph 5.2.1. This allows an estimation of the Mean Annual Temperature (MAT) over the last 11,500 years.

Proxies for humidity/precipitations used in this study are derived both from palynology and µXRF. When comparing these, one has to keep in mind the very different time resolution of the two sources of data: for palynology, it is approximately of 35 years in the Early and Middle Holocene, and of 20 years in the Late Holocene, whereas µXRF has a sub-yearly resolution. Consequently, geochemistry is much more accurate and can be confidently used and studied statistically (see chapter 3.4 and paragraph 4.5.4). µXRF measures the amount of chemical elements (in minerals) brought in the basin by runoff waters. Therefore, this signal gives an "instantaneous" indication of the amount of rainfall in the drainage basin. Nevertheless, it gives no clue about how these precipitations are distributed over the year (intensity of precipitations over shorter or longer periods). In the terrestrial pollen record, some taxa in the different vegetation belts can be used as indicators of wetter or drier conditions, but variations in their relative proportions should be used with caution. Using the local aquatic vegetation (paragraph 5.2.3) gives a good approach to the estimation of the water depth in the lake/mire and can be compared directly with the amount of rainfall estimated with µXRF (Fig. 5.5).

Although variation scales are not comparable, there is a good correlation between µXRF and aquatics data in the late Younger Dryas equivalent and over most of the Holocene until ca. 2,500 cal yr BP, i.e., until pollen zone G3 (Fig. 5.5). There might be slight offsets between the µXRF signal and the response of the aquatics, but this can be attributed to the lag time the vegetation might need to react to changing humidity conditions. This good correlation demonstrates the validity of using local vegetation (aquatics) as a rainfall proxy. The link with humidity indicators in the terrestrial pollen is not always obvious and the latter might give a different signal from that given by aquatics and µXRF. A good example is the pollen zone E (5,100 - 4,310 cal yr BP) where both aquatics and µXRF point to high rainfall and deep water depth (Fig. 5.5), whereas terrestrial pollen indicates a very dry signature in the páramo. Therefore, to explain these differences, one would have to introduce other parameters that are difficult to master (e.g. evapotranspiration, orography, influence of climatic parameters such as ENSO, etc…). It is precisely in this pollen zone E that Ti and Fe signals show the highest variability, probably associated to a strong ENSO (see below in chapter 5.6).

In the last 2,500 years, the signature of µXRF and aquatics tends to differ, particularly in the pollen subzones H1 and H2. Whereas the Fe and Ti signals show very low rainfall, aquatics point to a deeper lake, especially in subzone H2 (Fig. 5.5). µXRF clearly demonstrates that the overall amount of rainfall is much lower than in the Early and Middle Holocene. Nevertheless, the amount of water in the mire apparently becomes more important. All this might be indicative of an important change in the yearly climate, for example a change in the

temporal distribution of the rainfall (seasons). As demonstrated below in chapter 5.6, the Late Holocene is marked by the southward migration of the ITCZ, which must have influenced the seasonal regime in the Páramo de Frontino.

5.5.2. CLIMATE CHANGES

Both geochemical and palynological proxies demonstrate that the Holocene record in the Páramo de Frontino is marked by rapid and very significant changes in temperature and precipitations (Fig. 5.5). Temperatures may have varied (up or down) of a few degrees centigrade over less than a century.

After a cold and wet Younger Dryas equivalent, the base of the Holocene becomes very warm and dry before returning to colder and dry conditions at around 10,000 cal yr BP. Between 9,500 and 7,000 cal years BP an overall warm and dry interval can be interpreted as “Holocene thermal maximum”, although it might be interrupted by colder breaks (e.g. at around 8,000 cal yr BP with a peak in dryness). During this warm interval, average temperatures were slightly below, but close to, present-day MAT. Most of the rest of the Middle Holocene until ca. 4,000 cal yr BP is much colder with estimated average temperatures some 2°C lower than today. From ca. 6,000 cal yr BP, conditions become much wetter, with a peak in rainfall between 5,000 and 4,000 cal yr BP. Between 4,500 and 3,500 cal year BP, the amount of rainfall decreases considerably and become much lower than in the Early and Middle Holocene, giving a dry signature for the Late Holocene. A rapid increase in arboreal pollen characterizes the lower part of the Late Holocene, leading to estimated temperatures some 3°C higher than today associated with very dry conditions. From ca. 2,500 cal yr BP, the forest lines drops again considerably and, until ca. 130 cal yr BP, the Late Holocene has estimated average temperatures at least 2°C lower than today with a minimum between ca. 1,400 and 750 cal yr BP where temperature might have been 4°C lower than today, like in the final part of the Younger Dryas equivalent. During the last 200 years the temperature is estimated to have risen by some 2°C.

We shall now attempt to correlate this local high-resolution Holocene climate record of the Páramo de Frontino with more regional data.

5.6. REGIONAL CORRELATIONS

5.6.1. INTRODUCTION

Results presented above are the first record at such a high resolution (both for palynology and μ XRF) in the whole of tropical South America. With such a resolution, it becomes important to try to distinguish purely local variations from a more regional signal. The Páramo de Frontino is a high-altitude site in the northwestern termination of the Western Cordillera, and its Holocene paleoclimatic signature will be influenced by both Atlantic and Pacific oceans. When comparing with other South American tropical records, one has to pay particular attention to the location of those, because the topography of the Andes plays an

important role, in particular when analyzing humidity records. Moreover, the quality and accuracy of the data may differ considerably from one record to the other, as well as the quality of the age model.

Figure 5.6 presents a correlation of basic paleoclimatic interpretations (essentially temperature and humidity) between Llano Grande and eighteen other sites in Colombia, Venezuela, Ecuador, Peru and Central America. These sites are geographically located in figures 5.7 and 5.8. They are organized in different latitudinal/geographical zones.

- Latitude 5° - 11° N

Site 1: Vélez et al. (2006) analyzed a transect of four locations in Colombia. The northernmost one is Lake Fuquene in the high plain of Bogotá (Eastern Cordillera) that can be coupled with data from El Abra (Van't Veer et al., 2000) at altitudes of 2570 - 2580 m amsl. Humidity information can be derived from pollen, but the resolution is well over 100 years.
Site 2: The Laguna de Los Anteojos lies at 3920 m amsl on the western flank of the Mérida Andes in Venezuela. Core data have been studied by sedimentology, geochemistry (Ti XRF data) and palynology spanning the interval 14,500 - 9,500 cal yr BP (Late Glacial and Early Holocene). The pollen record has a resolution of ca. 150 years (Stansell et al., 2010).
Site 3: The Laguna Verde Alta is a very high altitude site (4215 m amsl) also located in the Mérida Andes of Venezuela (Rull et al. 2005). Its pollen record spans the Late Glacial to recent and has a time resolution of over 200 years.
Site 4: Although not a continental site, the marine Cariaco Basin in Venezuela is a very important data point for the tropics (Haug et al., 2001; Peterson and Haug, 2006). It provides a fluorescence-X record at a time resolution of 4-5 years over the Late Glacial and Holocene. Ti and Fe are proxies for precipitations in the coastal ranges of Venezuela and give an interesting comparison data point with the microfluorescence data of Llano Grande. Sea surface temperatures (SST) in the Cariaco Basin have been derived from the Mg/Ca values in surface-dwelling planktonic foraminifera (Lea et al., 2003). Although their time resolution is only of ca. 170 years, they can be used for comparison with the temperature model derived from palynology in Llano Grande.

- Latitudes 0°-5° N

This group of sites corresponds essentially to low altitude locations in Colombia.

Site 5: This site analyzed by Vélez et al. (2006) is located in the rain forest on the Pacific coast (50 m amsl). Data from lithology, diatoms and pollen cover the Late Holocene with a time resolution of less than 50 years.
Site 6: This site is in the Patia valley between the Western and Central cordilleras at 760 m amsl. No accurate climatic reconstruction is possible, except for a very clear humid period at the end of the Early Holocene and at the base of the Middle Holocene (Vélez et al., 2006).
Site 7: pollen records from eight sites in the Popayan area with altitudes ranging between 1300 and 1750 m amsl were investigated by Wille et al. (2001). The time resolution is of ca. 130 years. These data give climatic information over the Late Glacial and early Holocene.

Site 8: The study of Berrio et al. (2002) provides the first information of dry vegetation history in the Cauca Valley. Two pollen records are used in association with sediment and charcoal data. Over most of the record the time resolution is above 100 years.
Site 9: Pollen data over the last 8,700 years were analyzed in Laguna Loma Linda (310 m amsl) in the transitional zone between the lowland savannas (Llanos Orientales) and the Amazonian rainforest (Behling and Hooghiemstra, 2000). The time resolution of the pollen data is of ca. 125 years.
Site 10: This is the last site used by Vélez et al. (2006). It lies in the eastern lowland savannas (Llanos Orientales) at an altitude of 290 m amsl, close to Laguna Loma Linda (site 9). The original study was done by Wille et al. (2003). The pollen record has an average time resolution of ca. 50 years over the Holocene. It highlights variations of humidity at submillenium timescale that could be related to ENSO variability.
Site 11: Two cores recovered from wetlands in the Ecuadorian Amazon (altitude 220 m amsl) were analyzed for pollen, charcoal and loss-on-ignition (Weng et al., 2002). Pollen data have a time resolution of over 200 years. They show an alternation of dry and wet periods at millenium timescales

- Latitudes 0°-10° S

Site 12: The Laguna Pallcacocha in southern Ecuador lies at a very high altitude of 4060 m amsl, 500m east of the western Andean continental divide. Its sedimentary record is strongly influenced by ENSO variability, as shown by trends derived from statistical analysis (Moy et al., 2002). This laguna together with Laguna Chorreras located 4 km east at 3700 m amsl have been studied by palynology (Hansen et al., 2003) in the Late Glacial and Holocene. Unfortunately the time resolution is low (160 to 400 years).
Site 13: The Laguna Rabadilla de Vaca lies in southern Ecuador at 3012 m amsl in the páramo vegetation zone. It lies close to the eastern Andean divide and is strongly influenced by easterly trade winds from the Amazon. It has been investigated by multiple proxies: pollen, charcoal, X-ray fluorescence and magnetic susceptibility (Niemann et al., 2009). Although the time resolution of the pollen data is low (ca. 220 years) and it is quite far south with respect to Llano Grande, the high altitude and the XRF data make it an interesting site for comparison.
Site 14: The Lake Compuesta is situated in the Western Cordillera of the Peruvian Andes at 3950 m amsl. It has been analyzed using pollen, charcoal, magnetic susceptibility and bulk density (Weng et al. 2006). The time resolution of pollen data is very low (ca. 500 years), but general climatic trends can be derived from the vegetation.
Site 15: Ice cores were taken from the Huascaran Glacier in the north-central Andes of Peru at 6050 m amsl (Thompson et al., 1995). The oxygen isotope ratio $\delta^{18}O$ is a proxy that provides indications on temperature variations.

- Central America

Three locations have been selected to the northwest of Frontino:
Site 16: The closest one to Frontino is a crater lake near sea-level in the Pacific coastal plain of Panama, where pollen and phytolith records have been studied (Piperno and Jones,

2003). The time resolution of pollen is low (ca. 350 years) and human impact affects the Middle and Late Holocene record.

Site 17: Pollen records from cores taken in two bogs of the Costa Rican Cordillera de Talamanca (altitudes 2310 and 2700 m amsl) provide climate information over the Holocene with a time resolution of ca. 200 years (Islebe et al., 1995).

Site 18: Pollen and isotope measurements were carried out on a core from Lake Tzib (at sea-level) in central eastern Yucatan, Mexico (Carrillo-Bastos et al., 2010). They cover the last 7,900 cal yr BP, but pollen time resolution is low (ca. 300 years).

5.6.2. CORRELATIONS

We have tried to summarize the data of figure 5.6 in four maps corresponding to the end of the Younger Dryas equivalent (ca. 11,500 cal yr BP, Fig. 5.7A), the Early Holocene (11,500 - 8,000 cal yr BP, Fig. 5.7B), the Middle Holocene (8,000 - 4,000 cal yr BP, Fig. 5.8A) and the Late Holocene (4,000 - 0 cal yr BP, Fig. 5.8B). Moreover, in figure 5.9, we have compared the data from Cariaco and Llano Grande because both contain high-resolution XRF data. On this same figure we have also added data of the Laguna de los Anteojos in Venezuela (a high-altitude site in the Mérida Andes with XRF data) and the Laguna Rabadilla de Vaca in Ecuador (a high-altitude site with both pollen and XRF data).

- End of Youger Dryas equivalent (ca. 11,500 cal yr BP, Fig. 5.7A)

Our data in Llano Grande begin very close to 11,500 cal yr BP. There is a major climatic transition at ca. 11,400 cal yr BP with a rapid change from very wet to dry, and from cold to warm conditions (Figs. 5.3 and 5.5). This lowermost cold phase corresponds to the termination of the South American equivalent of the Younger Dryas (YD) cooling equivalent. In Colombia, it is referred to as the « El Abra stadial » (Van't Veer et al., 2000). In this study, we shall refer simply to the YD. Most of the YD will be analyzed in the thesis of C. n this study, we shall refer simply to the YD. Most of the YD will be analyzed in the thesis of C. Monsalve who is studying the Late Glacial in Llano Grande. The explanations for this abrupt global temperature shift favour either tropical (Clement et al., 2001) or high latitude (Broecker, 2006) ocean-atmosphere systems as the dominant driving mechanisms. Whatever the initial cause of the YD, the tropics must have played an important role in modulating the climate system during and at the termination of the event (Stansell et al., 2010). In this respect, Llano Grande is an important high-resolution data point for the YD in Central and tropical South America, where its upper boundary is still unsufficiently known (Van't Veer et al., 2000).

In tropical South America, the YD cold period is observed in several sites (Figs. 5.6 and 5.7A). It is normally registered as a dry period, except in the high altitude sites of Frontino in Colombia and Laguna Los Anteojos in the Mérida Andes of Venezuela in the north, and of Laguna Rabadilla de Vaca and Pallcacocha/Chorreras in southern Ecuador (Fig. 5.6A). There is a striking difference between Frontino and the Cariaco Basin where XRF data show respectively a very wet and a very dry YD (Fig. 5.9).

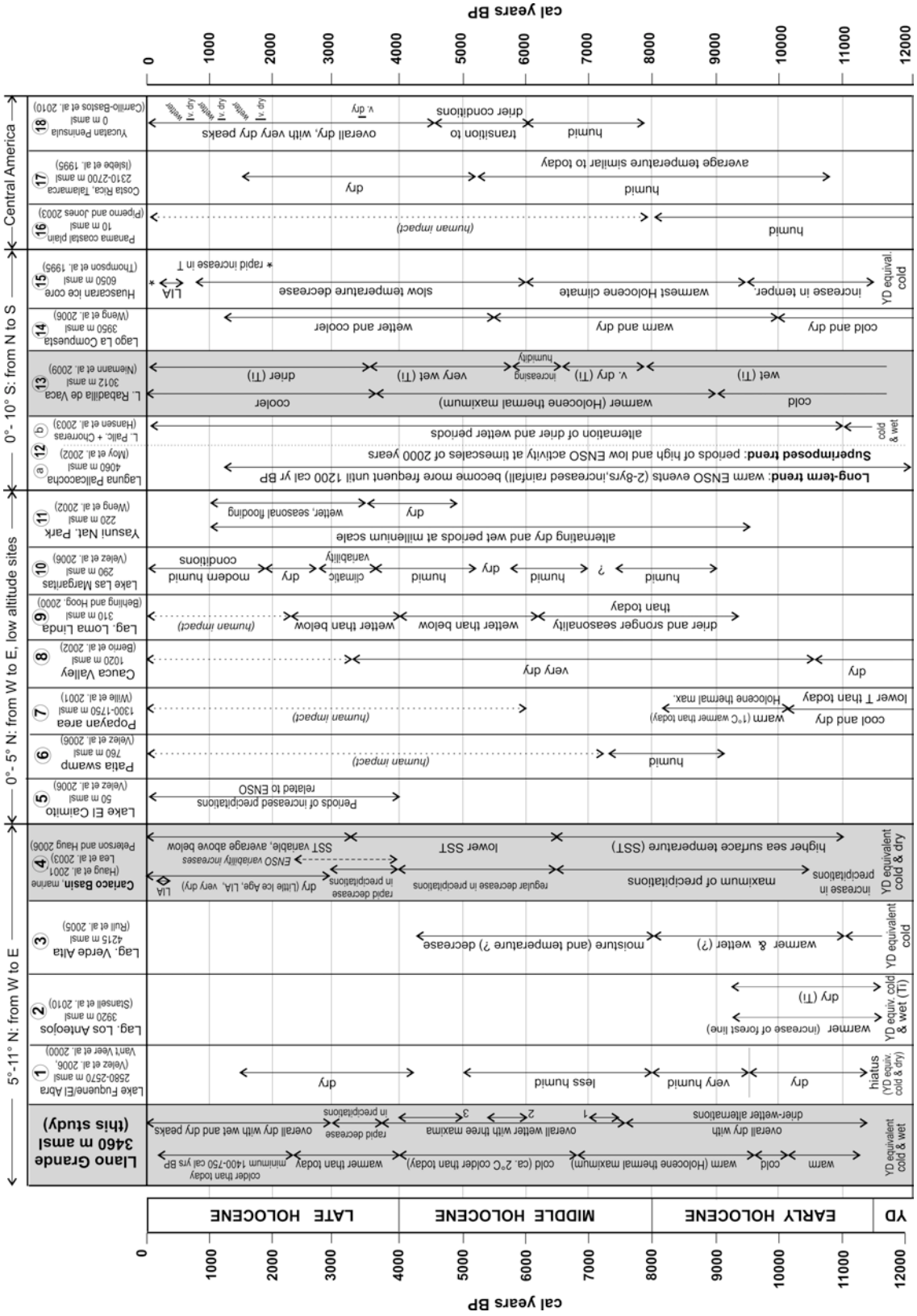

Fig. 5.6. Major palaeoclimatic trends derived from various studies in NW South America and Central America. See figures 5.7 and 5.8 for site location and text for explanation.

- Early Holocene (11,500 - 8,000 cal yr BP, Fig. 5.7B)

Most of the sites with temperature data show a marked increase during the course of the Early Holocene. This is interpreted by the various authors as the beginning of the “Holocene thermal maximum”. In Cariaco and Llano Grande the overall increase is significant from the beginning of the Early Holocene, but shows rapid changes during this period (Fig. 5.9). Humidity records are more contrasted and depend highly of the geographical location. The most striking feature is observed between Frontino, the Laguna Los Anteojos (Mérida Andes) and the Cariaco Basin, where Ti XRF data are available : at the first two locations conditions become dry, whereas by contrast, the Cariaco Basin becomes gradually wetter (Fig. 5.9). The two Central American sites (Panama and Costa Rica) show wet conditions similarly to the Cariaco Basin. Other sites further south in Colombia, Ecuador and Peru seem to show wetter conditions on the Amazon Basin side.

- Middle Holocene (8,000 - 4,000 cal yr BP, Fig. 5.8A)

Most of the records with temperature information in Colombia, Venezuela, Ecuador and Peru (Fig. 5.6) show a temperature decrease at some point during this interval, which is interpreted as the end of the “Holocene thermal maximum” (Frontino, Mérida Andes, Cariaco, Rabadilla de Vaca, Lago la Compuesta, Huascaran Glacier). Frontino and Cariaco show a significant cooling between 6,000 and 4,000 cal yr BP (Fig. 5.9).

Humidity variations are more difficult to compare, because the accuracy of the proxy used may differ considerably. It is interesting to observe the overall decrease in precipitation in Cariaco between 7,000 and 4,000 cal yr BP (the maximum is between 10,000 and 7,000 cal yr BP). Moisture is also decreasing in the Mérida Andes of Venezuela (Laguna Verde Alta). The evolution towards dry conditions in the upper part of the Middle Holocene is also registered in Costa Rica and Yucatan. By contrast, the Llano Grande location shows an overall increase in precipitations with a maximum between ca. 5,000 and 4,500 cal yr BP. Superimposed on this overall trend are shorter term significant variations with periodicities ranging from the millenium bands to much higher frequencies, in particular in the ENSO band (Figs. 5.4 and 5.9). In the Laguna Rabadilla de Vaca (southern Ecuador), the maximum of precipitations occurs also in the upper part of the Middle Holocene, between 6,000 and 3,500 cal yr BP (Fig. 5.9). Nevertheless, this site is quite exposed to Amazonian air masses and comparison with northern Colombia is complex. East of the Andes in the Amazon Basin, the Middle Holocene is marked by alternations of wet and dry periods, maybe becoming wetter towards the top (in Colombia).

In the Pacific, warm ENSO events (lasting 2 - 8 years), with increased rainfall, become more and more frequent (Moy et al., 2002). In Llano Grande, the same trend can be observed: the Morlet wavelet spectrum for Ti (Fig. 5.4) displays an increase in high variance events through the Middle Holocene and more specially in the ENSO band. This increase culminates in the interval ca. 5,000 - 4,000 cal yr BP.

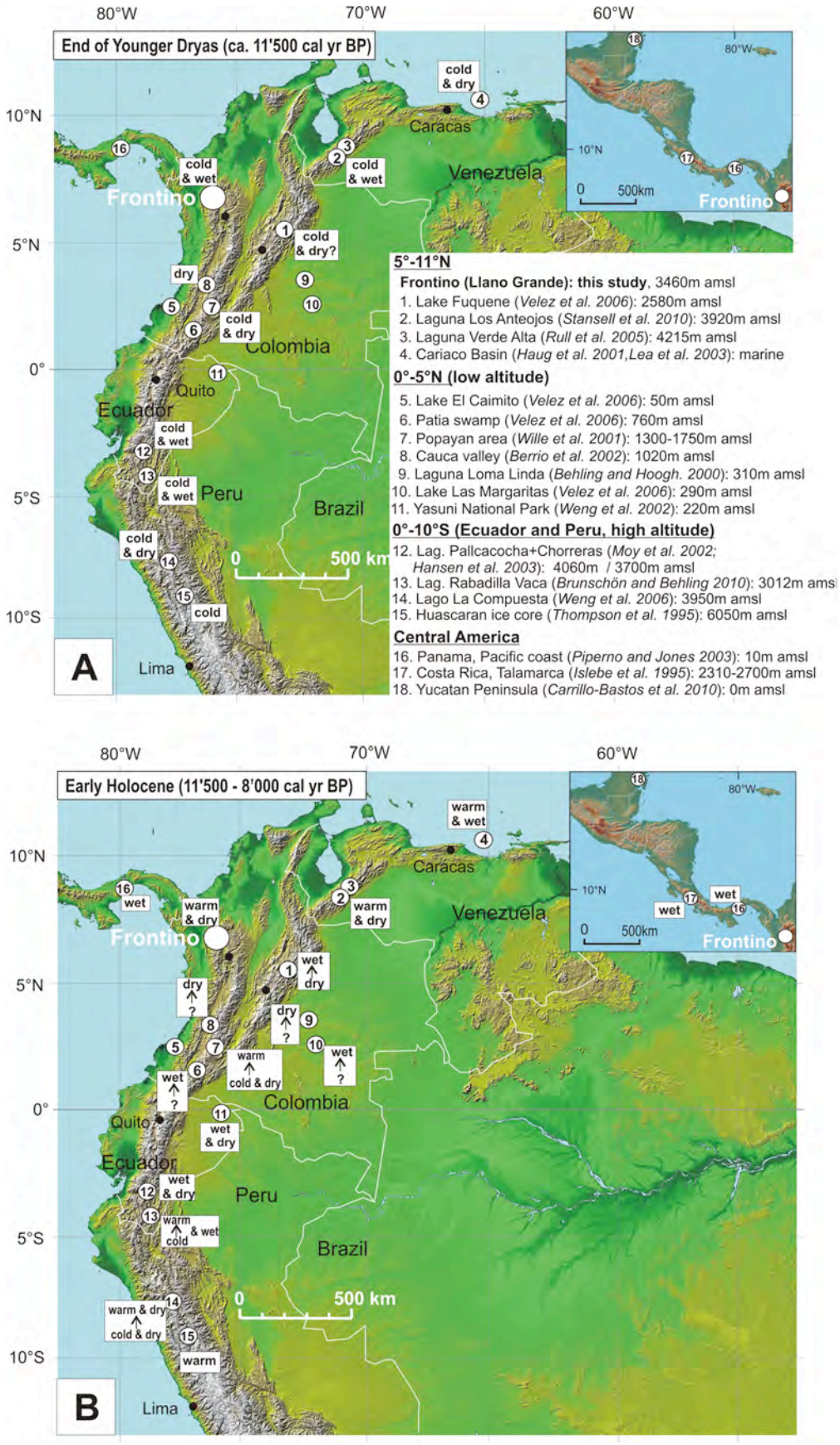

Fig. 5.7. Summary of temperature and precipitations in selected sites of Central/northern South America: A) at the end of the Younger Dryas; B) during the Early Holocene.

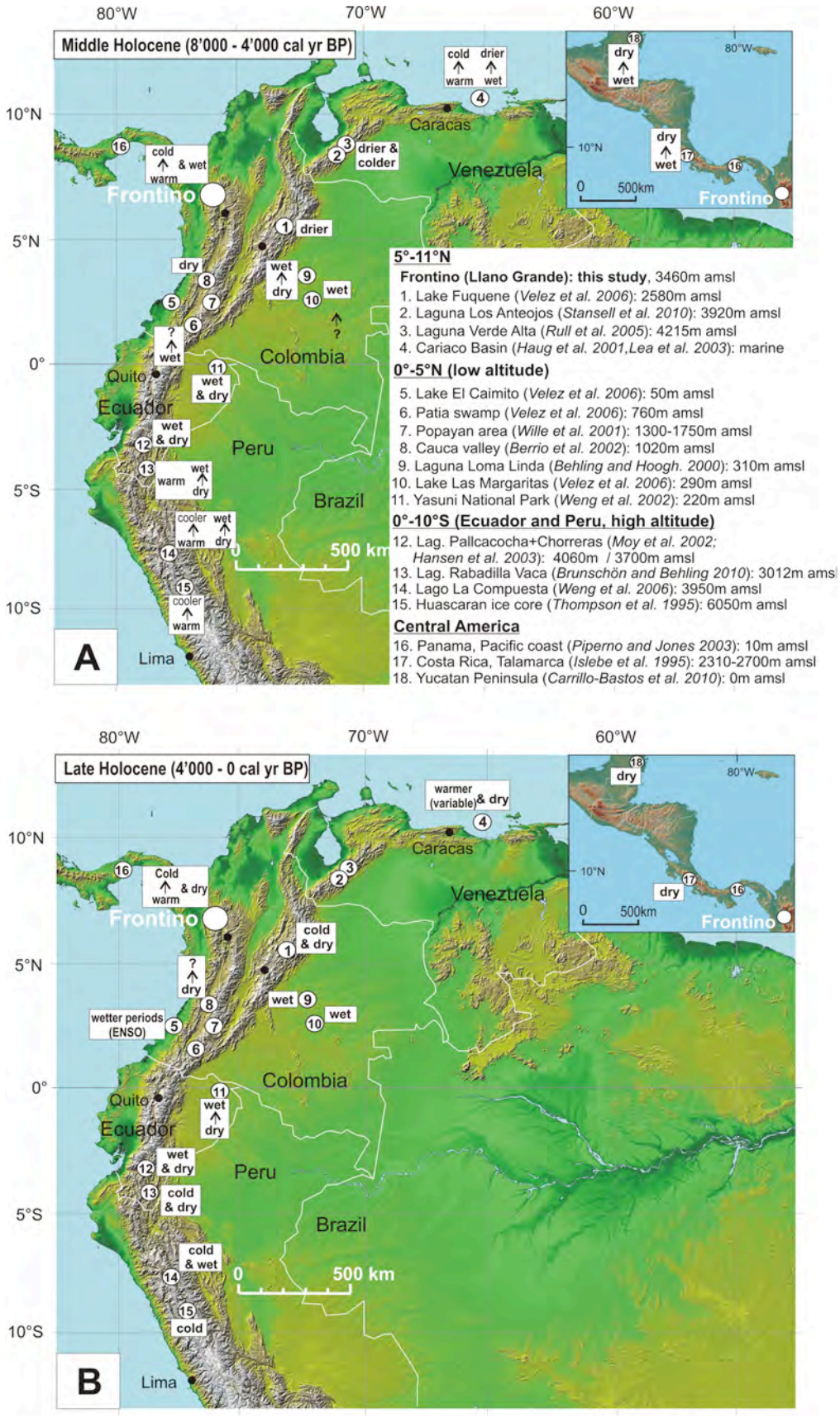

Fig. 5.8. Summary of temperature and precipitations in selected sites of Central/northern South America: A) during the Middle Holocene; B) during the Late Holocene.

- Late Holocene (4,000 - 0 cal yr BP)

The detailed reconstruction of the climatic conditions and vegetation in Llano Grando during the Late Holocene have been presented by Velásquez (2005). The purpose of our study is not to duplicate this work, but to incorporate the new µ XRF data to obtain an overall evaluation (see Fig. 5.5).

In terms of temperature, the Llano Grande record is particular, because the temperature model based on the arboreal pollen shows a significant period of warming between 4,000 and 2,500 cal yr BP. This increase in arboreal pollen is accompanied by very dry conditions (Fig. 5.9). This temperature increase can not be confirmed in the Colombian Andes because of lack of detailed study. In southern Ecuador (Laguna Rabadilla de Vaca) and in Peru (Lago La Compuesta, Huascaran Glacier), the Late Holocene is interpreted as a cold period, except for the last hundreds of years where temperatures are rising (Fig. 5.6). After 2,500 cal yr BP, temperatures in Llano Grande drop rapidly with a low at ca. 1,200 cal yr BP. It increases rapidly over the last 200 years (Fig. 5.9). The interval referred to as « Medieval Anomaly » (or Medieval Warm Period, MWP) in Europe corresponds in Llano Grande to the coldest interval of the Late Holocene. The period equivalent to the « Little Ice Age » (LIA) shows a slight decrease in temperature (Fig. 5.9).

Humidity data show overall dry conditions in Llano Grande (although with more pronounced oscillations than in Cariaco as shown by µXRF and palynology data, Fig. 5.9). Ti data over the last 3,500 cal years BP may be too low to be reliable and one has to consider the Fe data. One has to remember that the latter have a tendency to be noisier because they may be subject to redox changes in the sediments. Nevertheless, their good similarity with Ti data lower in the record and with the palynological humidity proxy tends to confirm the validity of this proxy in the uppermost 3,500 years of the record. Similar, overall dry conditions in the Late Holocene are also observed in the Cariaco Basin and Central America (Fig. 5.8B). XRF data in Llano Grande and Cariaco show a rapid decrease in precipitations after 4,500 cal yr BP. In Llano Grande this is associated with a high variance in the high frequency ENSO band (Fig. 5.4). During the Medieval Anomaly both areas record a slight increase in rainfall. Finally, during the LIA, both Cariaco and Llano Grande show drier conditions. On the Pacific side, the increase in wetter periods is associated with the increased frequency of ENSO events (lake El Caimito, Laguna Pallcacocha). The influence of ENSO events can also be interpreted in Llano Grande from the Morlet wavelet spectrum for Fe (Fig. 4.17): between 3,800 and 260 cal yr BP, although the Fe signal (the Ti signal is too low to be reliable) is very stable in variance, it is only perturbed by frequent short event in the ENSO band.

5.6.3. DISCUSSION

It is now recognized that Holocene climatic variability has been quite important and that Holocene climatic history could be the key to understanding and predicting responses in the current climate change debate. In tropical regions, in particular in northern South America where this study is located, one of the most important oceanic-atmospheric systems regulating present-day and past climatic variations is the Atlantic ITCZ driven by high latitude

forcing in the northern Atlantic. Changes in its mean position best explain precipitation variations in tropical South America (Petersen and Haug, 2006). Nevertheless, it is now demonstrated that this Atlantic-driven mechanism interacts in western northern South America with another oceanic-atmospheric system characterizing the tropical Pacific, i.e., the ENSO. These two mechanisms are today the best explanations for the large and abrupt climate changes characterizing the latest Quaternary. Petersen and Haug (2006), using the record of riverine input of sediments to the Cariaco Basin (Venezuela) as a basis, give a good review of the existing data in favour of high-latitude vs. tropical forcing mechanisms. They conclude that both mechanisms are important, but the degree to which each contributes is perhaps timescale dependent. They highlight the need to obtain more high-resolution paleoclimate records in areas exposed to ITCZ and ENSO influences.

In this respect, the Llano Grande record presented here is ideally located because the Páramo de Frontino is exposed to the influence of both oceans. It is very well dated, has a continuous sedimentary record and has not been influenced by human impact. Moreover, the proxies used, i.e., palynology and µXRF, have a resolution at respectively decadal and sub-yearly timescales. Therefore, we will try to analyze our results with respect to the existing data and interpretations and attempt to correlate our observations within the existing climatic mechanisms mentioned above, trying to interpret them in a more regional way. Nevertheless, the lack of other high-resolution studies using the same proxies is a limiting factor. In particular, there are not other high-altitude records in the Western Cordillera of Colombia. Because of its high-resolution XRF data, the Cariaco Basin (although in the Caribbean Sea) remains the best accurate comparison point (Fig. 5.9) as rainfall proxy in northern South America. For the YD and Early Holocene, XRF data are also available from the Laguna Los Anteojos in the Mérida Andes of Venezuela (Stansell et al., 2010) and for the whole Holocene from the Laguna Rabadilla de Vaca en Ecuador (Fig. 5.9).

As far as **temperature** is concerned, the resolution of the high-altitude Llano Grande record is not matched by any other record in northwestern South America (Fig. 5.9). Our model obtained from palynology fits the overall picture known in this zone. A cold YD equivalent (El Abra stadial in Colombia, see Van't Veer et al., 2000) is present, with a temperature decrease of possibly 4°C or more lower than today. This figure can be compared with that of ca. 5°C in the Eastern Cordillera of Colombia (Groot et al., 2011), of 3°C suggested by van't Veer et al. (2000) for Costa Rica, Guatemala and Colombia, and that of 2.2-2.9°C in the Venezuelan Andes (Stansell et al., 2010). An abrupt increase in temperature marks the base of the Early Holocene. An interval of overall higher temperatures straddles the Early and Middle Holocene and can be referred to as the « Holocene thermal maximum ». It is also interpreted in most of the sites used for comparison (Fig. 5.6), although its actual duration seems to vary from site to site (a reality or data affected by resolution, age model, etc…?). The upper part of the Middle Holocene (6,000 - 4,000 cal yr BP) in Frontino is considerably colder with a temperature decrease possibly down to 3°C lower than today. This colder period seems to match a colder interval observed from SST in the Cariaco Basin (Fig. 5.9, Lea et al., 2003). Colder conditions are also observed in high-altitude sites of Peru (Fig. 5.8A).

In the Late Holocene, the temperature model of Llano Grande (Fig. 5.9) suggests a temperature maximum centered at ca. 3,000 cal yr BP. This observation can not be correlated with other records, except in the SST curve of the Cariaco Basin which also shows a high at around 3,000 cal yr BP (but with an extremely low time resolution). In the upper part of the Late Holocene, much colder conditions are interpreted in Llano Grande, except for the last two hundred years following the Little Ice Age (LIA). In the time interval coinciding with the Medieval Anomaly the temperature model suggests conditions as cold as during the YD. In high-altitude sites of Ecuador and Peru cold conditions are also encountered (Fig. 5.8B). A correlation between the Late Glacial-Holocene XRF data of Cariaco and the low-resolution, poorly dated pollen record of Lake Fuquene (Van der Hammen and Hooghiemstra, 1995) has been attempted by Petersen and Haug (2006). The increase in páramo vegetation over the last thousands of years suggests that cold conditions also prevailed in Fuquene.

In terms of **precipitations**, our µXRF data (supported by the palynological proxy, Fig. 5.9) show a very aprupt change between a wet YD and a much drier early Holocene. Although less abrupt, the same transition can be observed to the northeast in the Mérida Andes of Venezuela at the high-altitude Laguna Los Anteojos (Stansell et al., 2010, Fig. 5.9). By contrast, XRF data show the opposite in the Cariaco Basin (Haug et al., 2001, Petersen and Haug, 2006): the YD is dry and the transition to a wet Early Holocene is gradual. In the Yucatan Peninsula (Lake Peten Itza), Hodell et al. (2008) also observe a dry YD followed by the return to wetter conditions in the early Holocene. Both in Cariaco and Yucatan, authors explain the dry conditions of the YD through the latitudinal displacement towards the south of the mean position of the ITCZ during the last glacial maximum. With the warming phase of the early Holocene, the ITCZ migrated northwards resulting in wetter conditions at both sites.

The latitudinal position of Frontino is not too different from that of Cariaco. If its precipitation regime at the YD-Early Holocene transition would have been directly influenced by the ITCZ, one would expect a similar signal to that encountered in Cariaco (similarly to what happens in the late Middle and Late Holocene, see below). Moreover, the abrupt YD-Early Holocene transition looks quite different from the gradual change observed in the Late Holocene. Therefore, we postulate that in Frontino the moisture regime in the YD and Early Holocene might have been more under the influence of the Pacific Ocean (ENSO, Choco Jet). The Morlet wavelet spectrum for Ti (Fig. 5.4) shows very high variances in the high frequency bands (in particular the ENSO band) for the last 600 years of the YD (Fig. 5.4 and 4.13). In the Early Holocene, all frequencies decrease in variance, becoming intermittent with some short events affecting the high frequencies (ENSO band). The influence of external forcing (solar activity) with millenial-scale fluctuations may also have played a role, as has been demonstrated in the Pacific Ocean during the Early Holocene (Marchitto et al., 2010). High frequencies in the millennial bands are also observed in Llano Grande (Fig. 5.4).

Cariaco and Frontino exhibit contrasting rainfall patterns during the Early and Middle Holocene (Fig. 5.9). In Cariaco, increasing rainfall in the lower part of the Early Holocene is followed by a precipitation maximum coinciding with the Holocene thermal maximum between ca. 10,000 and 6,000 cal yr BP (Fig. 5.9; Haug et al., 2001; Petersen and Haug, 2006). This is consistent with the postulated northward migration of the ITCZ after the YD.

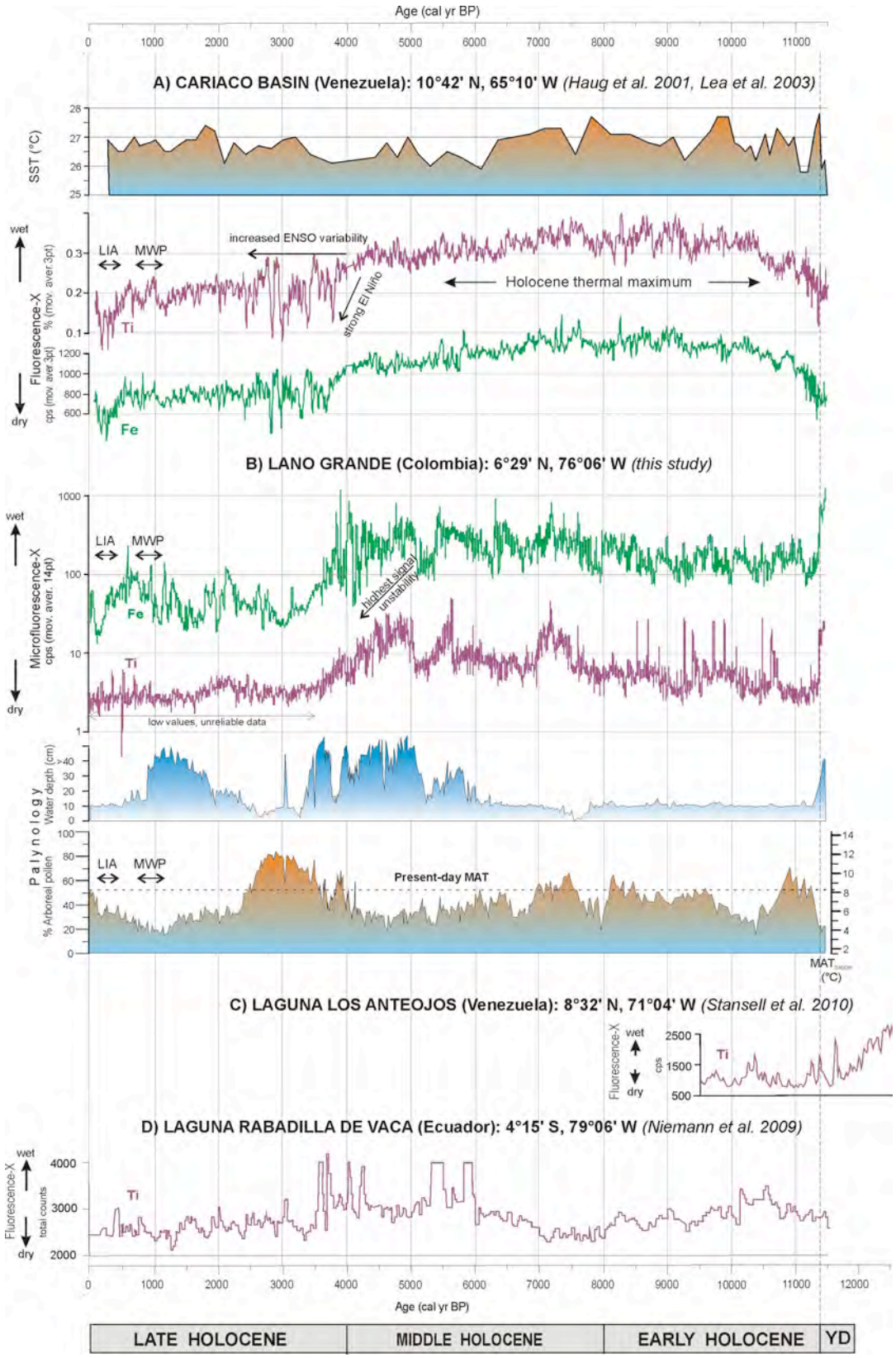

Fig. 5.9. Comparison of climatic proxies in the Holocene in several South American sites : A) Cariaco Basin : sea surface temperatures (SST) and fluorescence-X data used as proxy for rainfall ; B) Llano Grande (this study) : microfluorescence-X data used as rainfall proxy and palynological data used as humidity and temperature proxies ; C) Laguna Los Anteojos (Venezuela) : fluorescence-X data used as rainfall proxy ; D) Laguna Rabadilla de Vaca : fluorescence-X data used as rainfall proxy. (LIA = Little Ice Age; MWP = Medieval Warm Period or Medieval Anomaly; YD= Younger Dryas equivalent).

The correlation of this wet and warm interval in Cariaco with La Niña-like wet conditions in the eastern equatorial Pacific (Marchitto et al., 2010) is an argument to interpret the existence of already existing ENSO teleconnections at that time (Stott et al., 2002). From 7,000 cal yr BP, the intensity of precipitations in Cariaco starts to decrease regularly until 4,000 cal yr BP and drops abruptly afterwards (Fig. 5.9). This is interpreted as reflecting the southward migration of the ITCZ leading to dry Late Holocene conditions in the Cariaco Basin (Haug et al., 2001; Petersen and Haug, 2006).

The picture in Frontino is different. µXRF data show an overall increase in precipitations through the Early and Middle Holocene with a maximum of precipitations centered over 5,000 - 4,500 cal yr BP. Superimposed on this general trend, both Ti and Fe data show oscillations at millenial and submillenial timescales. The Morlet wavelet spectrum for Ti shows continuous high variance in the millennial bands during this period. In the high-frequency bands (in particular the ENSO band), intervals of high variance are very intermittent but increase in number, particularly in the Middle Holocene. We can tentatively interpret these data as reflecting the dual signature of the ITCZ and ENSO: the overall increase in rainfall would be the result of theF southward migration of the ITCZ, whereas the higher frequency cycles would be linked to ENSO. Our observations in Frontino can be correlated with those of Moy et al. (2002), who have interpreted in the Laguna Pallcacocha in Ecuador that warm ENSO events became more frequent throughout the Holocene, with a superimposed trend showing periods of high and low ENSO activity at timescales of 2,000 years. Orbitally-driven external forcing with a 1,000/2,500 years cyclicity (Debret et al., 2009 ; Marchitto et al., 2010) may also be an important factor.

The comparison of rainfall record in Cariaco and Frontino over the last 5,000 years is most interesting (Fig. 5.9), because it highlights the dual influence of ITCZ and ENSO over the climate of both areas. XRF data in both areas illustrate the rapid trend towards dry conditions in the Late Holocene. This is associated with the southward shift of the ITCZ, as demonstrated by Haug et al. (2001) and Petersen and Haug (2006). This was accompanied by an increase in ENSO activity, probably related to a precessional control (Clement et al., 2000), leading to the prevalence of El Niño events in the Late Holocene. In lake sediments from Ecuador, Rodbell et al. (1999) showed that modern ENSO periodicities were established only after about 5,000 years ago. Haug et al. (2001) related these observations to precessionally forced insolation changes. The latter would have directly forced the southward migration of the ITCZ, but also increased the prevalence of El Niño through the Holocene. This would have further amplified the southward shift of the ITCZ while adding a higher frequency component to its latitudinal variations. It is interesting to note that statistical analysis of µXRF data in Llano Grande indicates that it is in the interval 5,100 - 4,300 cal yr BP (period 11, Figs. 4.8 and 5.9 and pollen zone E in Figs. 5.3 and 5.5, see also Appendix A3) that both Ti and Fe signals show the highest unstability of the whole Holocene. Time series analysis confirms that this period had high variances in both signals, particularly in the high frequency bands such as the ENSO (Figs. 5.4 and 4.15). Between 3,800 and 260 cal yr BP, although the Fe signal is very stable in variance, it is only perturbed by frequent short event in the ENSO band.

CHAPTER 6

CONCLUSIONS

6. CONCLUSIONS

6.1. AIMS AND METHODS

The Llano Grande Holocene section studied here has been recovered from cores taken in the Páramo de Frontino at the altitude of 3460 m at the northwestern termination of the Western Cordillera in the Colombian Andes. This site is ideally located to study the influence of both Atlantic and Pacific oceans on the climate behaviour at this location during the Holocene. Moreover, this zone is remote and has never been anthropogenically disturbed.

The ca. 14 m thick section has been precisely dated through 30 AMS C^{14} analyses which provide an accurate age model covering a time period from 17,000 cal yr BP until present and demonstrate the absence of hiatuses. This study covers the last 11,500 years, i.e., the whole Holocene.

Palynology and microfluorescence-X (µXRF) have been used as climatic proxies. Palynology provides information on the variations of regional and local vegetation. The variations in the relative proportion of arboreal pollen indicate altitudinal changes in the upper forest line. This can be used to estimate fluctuations in the mean annual temperature (MAT) over time. Changes in the local aquatic vegetation are an indication for variations in water depth of the lake/mire. The latter can be compared with µXRF data which are a measure of the mineral erosion in the local drainage basin. In the Páramo de Frontino wet environment, the amount of minerals deposited in the lake is directly related to precipitations, and µXRF can be used as a rainfall proxy. Both Ti and Fe signals have been used in this respect.

In this study, the detailed palynological data covers the Early and Middle Holocene (11,500 – 4,300 cal yr BP) with a ca. 35 years time resolution. It can be merged with existing palynological data of Velásquez (2005) who covered the period 4,300-0 cal yr BP with a time resolution of ca. 20 years. The palynological data can subsequently be studied in relation with µXRF analyses. The latter have been carried out over the whole Holocene with a sub-yearly resolution. Therefore, for the first time in tropical South America, this research presents an interpretation of Holocene climate variations with a decadal to yearly time resolution using both palynological and geochemical proxies (Fig. 5.5).

6.2. LLANO GRANDE RESULTS

The end of the Younger Dryas equivalent (El Abral stadial in Colombia) corresponds in the cores to a lithological change from organo-mineral mud to organic mud. This limit is dated at ca. 11,400 cal yr BP. The studied uppermost part of the YD is cold and wet. An abrupt change occurs at the base of the Holocene, which becomes very warm and dry before returning to colder and dry conditions at around 10,000 cal yr BP. Between 9,500 and 7,000 cal yr BP an overall warm and dry interval can be interpreted as “Holocene thermal maximum”, although it might be interrupted by colder breaks. For example, at around 8,000 cal yr BP a cold peak associated with dry conditions is observed. It might be an expression of the 8.2 kyr event well-known in the North Atlantic (Alley and Agustsdottir, 2005; Rohling and

Pälike, 2005; Cheng et al., 2009). The time shift might be due to the age model or might correspond to a real lag time associated to the tropics response to this event. During the warm interval of the "Holocene thermal maximum", mean annual temperatures are estimated to have been slightly below, but close to, the present-day MAT. Most of the rest of the Middle Holocene until ca. 4,000 cal yr BP is much colder with estimated mean annual temperatures some 2°C lower than today. From ca. 6,000 cal yr BP, conditions become much wetter, with a maximum in rainfall between 5,000 and 4,000 cal yr BP. Between 4,500 and 3,500 cal yr BP, the amount of rainfall decreases considerably and becomes much lower than in the Early and Middle Holocene for the rest of the Late Holocene. The lower part of the Late Holocene shows estimated temperatures some 3°C higher than today associated with very dry conditions. From ca. 2,500 cal yr BP, the forest line drops again considerably and, until ca. 130 cal yr BP, the Late Holocene has estimated mean annual temperatures at least 2°C lower than today with a minimum between ca. 1,400 and 750 cal yr BP where temperature might have been 4°C lower than today, like in the final part of the Younger Dryas equivalent. During the last 200 years the temperature is estimated to have risen by some 2°C.

The combination of palynology with µXRF has permitted the comparison of both methods as proxies for rainfall, although one has to keep in mind the difference in time resolution between the two methods. There is a good correlation between µXRF and aquatics data in the late Younger Dryas equivalent and over most of the Holocene until ca. 2,500 cal yr BP, i.e., until pollen zone G3 (Fig. 5.5). There might be slight offsets between the µXRF signal and the response of the aquatics, but this can be attributed to the lag time the vegetation might need to react to changing humidity conditions. This good correlation demonstrates the validity of using local vegetation (aquatics) as a rainfall proxy. In the last 2,500 years, the signature of µXRF and aquatics tends to differ, particularly in the pollen subzones H1 and H2 (Fig. 5.5). µXRF clearly demonstrates that the overall amount of rainfall is much lower than in the Early and Middle Holocene. Nevertheless, the amount of water in the mire apparently becomes more important. All this might be indicative of an important change in the yearly climate, for example a change in the temporal distribution of the rainfall (seasons). The Late Holocene is marked by the southward migration of the ITCZ, which must have influenced the seasonal regime in the Páramo de Frontino.

6.3. REGIONAL COMPARISONS

This research has demonstrated that the Holocene record in the Páramo de Frontino is marked by rapid and very significant changes in temperature and precipitation. Temperatures may have varied (up or down) of a few degrees centigrade over less than a century. Although the lack of other studies with a similar time resolution is a limiting factor, these results can been compared with existing regional information in northwestern South America/Central America, in order to attempt to interpret the climate driving mechanisms in the Holocene of the Páramo de Frontino (north western of South America).

In tropical regions, in particular in northern South America where this study is located, one of the most important oceanic-atmospheric systems regulating present-day and past climatic variations is the Atlantic ITCZ driven by high latitude forcing in the northern Atlantic.

Nevertheless, it is now demonstrated that this Atlantic-driven mechanism interacts in western northern South America with another oceanic-atmospheric system characterizing the tropical Pacific, i.e., the ENSO. These two mechanisms are today the best explanations for the large and abrupt climate changes characterizing the latest Quaternary. Petersen and Haug (2006) have highlighted the need to obtain more high-resolution paleoclimate records in areas exposed to ITCZ and ENSO influences. In this respect, the Llano Grande record presented here is ideally located because the Páramo de Frontino is exposed to the influence of both oceans. It is very well dated, has a very good resolution, has a continuous sedimentary record and has not been influenced by human impact. Nevertheless, the lack of other high-resolution studies using the same proxies is a limiting factor.

The temperature model obtained from palynology fits the overall picture known in this zone. A cold YD equivalent is comparable with data in the Eastern Cordillera of Colombia, in Costa Rica, Guatemala and in the Venezuelan Andes. Everywhere, an abrupt increase in temperature marks the base of the Early Holocene. Overall, the observed « Holocene thermal maximum » is interpreted in most of the sites used for comparison. But its definition remains loose and its actual duration and detailed interpretation may vary from site to site. The upper part of the Middle Holocene in Frontino is considerably colder, which seems to match a colder interval observed from sea surface temperature (SST) in the Atlantic basin of Cariaco (Venezuela). Colder conditions are also observed in high-altitude sites of Peru. In the early Late Holocene, the temperature maximum observed in Llano Grande can not be correlated with other records, except in the SST curve of the Cariaco Basin which also shows a high. In the upper part of the Late Holocene, conditions are much colder in Llano Grande, except for the last two hundred years. Cold conditions also prevailed in the Colombian Eastern Cordillera and in high-altitude sites of Ecuador and Peru.

Because of its high-resolution XRF data, the Cariaco Basin (in the Caribbean Sea) is to date the only accurate comparison point as rainfall proxy in northern South America. This comparison permits an attempt to analyse the variable influence of Atlantic vs. Pacific climate mechanisms in the Páramo de Frontino. Two types of patterns may be distinguished, one for the late YD-Early Holocene (1), the other one for the Middle and Late Holocene (2).

(1) During the late YD and Early Holocene, Cariaco and other Central American sites show a gradual transition from a dry YD to wet conditions, demonstrating the northward migration of the ITCZ following the last glacial period. This contrasts with the sharp transition in Frontino from a wet YD to a dry Early Holocene. The latter suggests that Frontino climate might have been more under the influence of the Pacific Ocean (ENSO, Choco Jet, among others) or local climatic conditions (e.g., orographic parameters), and less affected by the ITCZ at that time. Time series analysis demonstrates very high variances in the high frequency bands (in particular the ENSO band) for the last 600 years of the YD. In the Early Holocene, all frequencies decrease in variance, becoming intermittent with some short events affecting the high frequencies (ENSO band). The influence of external forcing (solar activity) with millenial-scale fluctuations may also have played a role, as has been demonstrated in the Pacific Ocean during the Early Holocene. High frequencies in the millennial bands are also observed in Llano Grande.

(2) In Cariaco, increasing rainfall in the lower part of the Early Holocene is followed by a precipitation maximum coinciding with the Holocene thermal maximum between ca. 10,000 and 6,000 cal yr BP. This is consistent with the postulated northward migration of the ITCZ after the YD. The correlation of this wet and warm interval in Cariaco with La Niña-like wet conditions in the eastern equatorial Pacific is an argument to interpret the existence of already existing ENSO teleconnections at that time. From 7,000 cal yr BP, the intensity of precipitations in Cariaco starts to decrease regularly until 4,000 cal yr BP and drops abruptly afterwards (Fig. 5.9). This is interpreted as reflecting the southward migration of the ITCZ leading to dry Late Holocene conditions in the Cariaco Basin.

In Frontino, µXRF data show an overall increase in precipitations through the Early and Middle Holocene with a maximum of precipitations centered over 5,000-4,500 cal yr BP. Superimposed on this general trend, both Ti and Fe data show oscillations at millenial and submillenial timescales. Time series analyses display continuous high variance in the millennial bands during this period. In the high-frequency bands (in particular the ENSO band), intervals of high variance are very intermittent but increase in number, particularly in the Middle Holocene. We can tentatively interpret these data as reflecting the dual signature of the ITCZ and ENSO: the overall gradual increase in rainfall in the Middle Holocene in Frontino would be the result of the southward migration of the ITCZ, whereas the higher frequency cycles would be linked to ENSO. Orbitally-driven external forcing with a1,000-2,500 years cyclicity may also be an important factor.

The comparison of rainfall record in Cariaco and Frontino over the last 5,000 years is most interesting, because it highlights the dual influence of ITCZ and ENSO over the climate in both areas. XRF data in both areas illustrate the rapid trend towards dry conditions in the Late Holocene. This is associated with the southward shift of the ITCZ. This was accompanied by an increase in ENSO activity, leading to the prevalence of El Niño events in the Late Holocene (Petersen and Haug, 2006). Haug et al. (2001) related these observations to precessionally forced insolation changes. The latter would have directly forced the southward migration of the ITCZ, but also increased the prevalence of El Niño through the Holocene. This would have further amplified the southward shift of the ITCZ while adding a higher frequency component to its latitudinal variations. It is interesting to note that, in the interval 5,100 - 4,300 cal yr BP in Llano Grande, time series analysis demonstrates that this period had high variances in both signals, particularly in the high frequency bands such as the ENSO. Between 3,800 and 260 cal yr BP, although the Fe signal is very stable in variance, it is only perturbed by frequent short event in the ENSO band.

To summarize, our study provides a new record illustrating the potential teleconnections existing between tropical Pacific and Caribbean (Atlantic) Sea climatic conditions.

REFERENCES

REFERENCES

Alley, R.B., and A.M. Ágústsdóttir. 2005. The 8k event: cause and consequences of a major Holocene abrupt climate change. *Quaternary Science Reviews*. 24:1123-1149.

Arellano, P.H., and J.O. Rangel. 2008. Patrones en la distribución de la vegetación en áreas de páramo de Colombia: heterogeneidad y dependencia espacial. *Caldasia* 30(2):355-411.

Arnold, J.R., and W.F. Libby. 1949. Age determination by radiocarbon content: checks with samples of known age. *Science*. 110:678:680.

Bakker, J., M. Moscol Olivera, and H. Hooghiemstra. 2008. Holocene environmental change at the upper forest line in northern Ecuador. *The Holocene*. 18:877-893.

Barnett, T.P. 1981. On the Nature and Causes of Large-Scale Thermal Variability in the Central North Pacific Ocean. *Journal of Physical Oceanography*. 11:887-904.

Barnett, T.P., D.W. Pierce, M. Latif, D. Dommenget, and R. Saravanan. 1999. Interdecadal interactions between the tropics and midlatitudes in the Pacific Basin. *Geophys. Res. Lett.* 26:615-618.

Barss, M.S., and G.L. Williams. 1973. Palynology and nanofossil processing techniques. *Geological Survey of Canada*. 73-26:1-25.

Batten, D.J., and L. Morrison. 1983. Methods of palynological preparation for palaeo-environmental, source potential and organic maturation studies. *Bulletin Norwegian Petroleum Directorate*. 2:35-53.

Baliunas, S., P. Frick, D. Sokoloff, and W. Soon. 1997. Time scales and trends in the central England temperature data (1659-1990): A wavelet analysis. *Geophys. Res. Lett.* 24:1351-1354.

Beck, J.W., D.A. Richards, R.L. Edwards, B.W. Silverman, P.L. Smart, D.J. Donahue, S. Hererra-Osterheld, G.S. Burr, L. Calsoyas, A.J. Timothy , Jull, and D. Biddulph. 2001. Extremely Large Variations of Atmospheric 14C Concentration During the Last Glacial Period. *Science*. 292:2453-2458.

Behling, H., and H. Hooghiemstra. 2000. Holocene Amazon rainforest–savanna dynamics and climatic implications: high-resolution pollen record from Laguna Loma Linda in eastern Colombia. *Journal of Quaternary Science*. 15:687-695.

Benninghoff, W.S. 1962. Calculation of the pollen and spore density in sediments by addtion of exotic pollen in known quantites. *Pollen Spores*. 4:332-333.

Bergman, J.W., H.H. Hendon, and K.M. Weickmann. 2001. Intraseasonal Air–Sea Interactions at the Onset of El Niño. *Journal of Climate*. 14:1702-1719.

Berrío, J.C., H. Hooghiemstra, R. Marchant, and J.O. Rangel. 2002. Late-glacial and Holocene history of the dry forest area in the south Colombian Cauca Valley. *Journal of Quaternary Science*. 17:667-682.

Bogotá-Angel, R.G. 2011. Pleistocene centennial-scale vegetational, environmental and climatic change in the Colombian Andes: based on biotic and abiotic proxy analyses from Lake Fúquene sediments. Ph D Thesis. Institute for Biodiversity and Ecosytems Dynamic (IBED). University of Amsterdam. 144 pp.

Bonny, A.P. 1972. A method for determining absolute pollen frequencies in lake sediments *New Phytologist*. 71:393-405.

Bradbury, J.P., B. Leyden, M. Salgado-Labouriau, W.M. Lewis, C. Schubert, M.W. Binford, D.G. Frey, D.R. Whitehead, and F.H. Weibezahn. 1981. Late Quaternary Environmental History of Lake Valencia, Venezuela. *Science*. 214:1299-1305.

Bradley, R.S. 1999. Paleoclimatology. Reconstructing climates of the Quaternary. Second Edition. International Geophysiques Series Vol 24.University of Massachusetts. Amherst, Massachusetts. 613pp.

Broecker, W.S. 2006. Was the Younger Dryas Triggered by a Flood? *Science*. 312:1146-1148.

Brown, C.A. 1960. Palynological Techniques. C. A Brown, Baton Rouge, (Eds). USA. 188pp.

Brunschön, C., and H. Behling. 2010. Reconstruction and visualization of upper forest line and vegetation changes in the Andean depression region of southeastern Ecuador since the last glacial maximum - A multi-site synthesis. *Review of Palaeobotany and Palynology*. 163:139-152.

Bryant, V.M.J., and J.H. Wrenn. 1998. New developments in palynomorph sampling, extraction and analysis. American Association Stratigraphic Palynologists. Contrib Series. 33. 155pp

Burleigh, R. 1981. W. F. Libby and the development of radiocarbon dating. *Antiquity*. 55:96-98.

Buytaert, W., R. Celleri, B.D. Bievre, F. Cisneros, G. Wyseure, J. Deckers, and R. Hofstede. 2006. Human impact on the hydrology of the Andean paramos. *Earth-science reviews*. 79:53-72.

Carrillo-Bastos, A., G.A. Islebe, N. Torrescano-Valle, and N.E. González. 2010. Holocene vegetation and climate history of central Quintana Roo, Yucatán Península, Mexico. *Review of Palaeobotany and Palynology*. 160:189-196.

Chaves, C.B., and A. Jaramillo. 1998. Regionalización de la temperatura del aire en Colombia. *CENICAFE*. 49:224-230.

Cheng, H., D. Fleitmann, R.L. Edwards, X. Wang, F.W. Cruz, A.S. Auler, A. Mangini, Y. Wang, X. Kong, S.J. Burns, and A. Matter. 2009. Timing and structure of the 8.2 kyr B.P. event inferred from δ18O records of stalagmites from China, Oman, and Brazil. *Geology*. 37:1007-1010.

Cleef, A.M. 1981. The vegetation of the Páramos of the Colombian Cordillera Oriental. Ph D Thesis, State University of Utrecht. 320pp.

Cleef, A.M., and H. Hooghiemstra. 1984. Present vegetation of the area og the high plain of Bogotá. *Dissertationes Botanicae*. 79:42-66.

Cleef, A.M., J.O. Rangel, S. Salamanca, C.L. Ariza, and G.B.A. Van. Reenen. 2005. La vegetación del páramo del Macizo de Tatamá, cordillera Occidental de Colombia. *In* La cordillera Occidental Colombiana, transecto Tatamá. *Estudios de Ecosistemas Tropoandinos*. Van der Hammen,T., J.O. Rangel, and A,M. Cleef, (Eds). Berlin-Suttgart. 6:377-468.

Clement. A.C. 1999. Orbital controls on the El Nino/Southern Oscillation and the tropical climate. *Paleoceanography*. 14:441-456.

Clement, A.C., M.A. Cane, and R. Seager. 2001. An Orbitally Driven Tropical Source for Abrupt Climate Change. *Journal of Climate*. 14:2369-2375

Cuatrecasas, J. 1958. Aspectos de la vegetación natural de Colombia. *Revista Academia Colombiana de Ciencias Exactas, Físicas y Naturales*. 10(40):221-264.

Debret, M., D. Sebag, X. Crosta, N. Massei, J.R. Petit, E. Chapron, and V. Bout-Roumazeilles. 2009. Evidence from wavelet analysis for a mid-Holocene transition in global climate forcing. *Quaternary Science Reviews*. 28:2675-2688.

Deser, C., and M.L. Blackmon. 1995. On the Relationship between Tropical and North Pacific Sea Surface Temperature Variations. *Journal of Climate*. 8:1677-1680.

Doher, L.I. 1980. Palynomorph preparation procedures currently used in the paleontology and stratigraphic laboratories. United State Geological Survey. *United State Geological Survey, Circular*. 830:1-29.

Emanuel, K.A. 1994. Atmospheric convection. Oxford University Press. New York, United States. 580pp.

Engle, R.F. 1982. Autoregressive conditional heteroscedasticity with estimates of the variance of United Kingdom inflation. *Econometrica* 50:987-1008.

Ertdman, G. 1960. The acetolysis method. *Svensk. Bot.Tidskr*. 54:561-564.

Espinal, L.S. 1992. Geografía ecológica de Antioquia. Zonas de vida. Universidad Nacional de Colombia. Medellín. 146pp.

Espinal, S., J. Boeke, and J. McElroy. 1983. Notas sobre la flora del páramo de Frontino (Urrao). *Gallencia*. 13:85-88.

Faegri, K., and J. Iversen. 1964. Textbook of Pollen Analysis. Second edition. Blackwell Scientific Publications. Oxford. 237pp.

Fama, E.F. 1963. Mandelbrot and the Stable Paretian Distribution. *Journal of Business*. 36:420-429.

Fama, E.F. 1965. The Behavior of Stock Market Prices. *Journal of Business*. 38:34-105.

Farge, M. 1992. Wavelet Transforms and their Applications to Turbulence. *Annual Review of Fluid Mechanics*. 24:395-458.

Figlewski, S. 1979. Subjective information and and market efficiency in a betting market. *Journal of Political Economy*. 96:246-273.

Flórez, M.T., and L.N. Parra. 1999. Atlas de los fitolitos de la vegetación de Belmira y Frontino, Departamento de Antioquia. Ed Gráficas Montoya. Medellín. 56 pp.

Fox, J., and R. Andersen. 2005. Using the R Statistical Computing Environment to Teach Social Statistics Courses. Department of Sociology, McMaster University. 36pp

Gamage, N., and W. Blumen. 1993. Comparative Analysis of Low-Level Cold Fronts: Wavelet, Fourier, and Empirical Orthogonal Function Decompositions. *Monthly Weather Review*. 121:2867-2878.

Gan, M.A., V.E. Kousky, and C.F. Ropelewski. 2004. The South America Monsoon Circulation and Its Relationship to Rainfall over West-Central Brazil. *Journal of Climate*. 17:47-66.

García, B., and J. Londoño. 1984. Aspectos generales del páramo de Frontino como ecosistema. Universidad Nacional de Colombia, Sede Medellín. 115 pp.

García, B., and J. Londoño. 1985. El clima en Colombia. Colombia sus gentes y regiones *Revista del Instituto Geografico Agustín Codazzi*. 3:315.

Giese, B.S., and J.A. Carton. 1999. Interannual and Decadal Variability in the Tropical and Midlatitude Pacific Ocean. *Journal of Climate*. 12:3402-3418.

González, E.A., T. Van der. Hammen, and R.F.Flint. 1965. Late Quaternary glacial and vegetational sequence in Valle de Lagunillas, Sierra Nevada de Cocuy, Colombia. *Leidse Geol. Mededel*. 32:157-182.

Gordon, A.D., and H.J.B. Birks. 1972. Numerical methods in Quaternary Palaeoecology I. Zonation of pollen diagrams *New Phytologist*. 71:961-979.

Goslar, T., M. Arnold, E. Bard, T. Kuc, M.F. Pazdur, M. Ralska-Jasiewiczowa, K. Rozanski, N. Tisnerat, A. Walanus, B. Wicik, and K. Wieqkowski. 1995. High concentration of atmospheric ^{14}C during the Younger Dryas cold episode. *Nature*. 377:414-417.

Grabandt, R.A.J. 1980. Pollen rain in relation to arboreal vegetation in the Colombian Cordillera Oriental. *Review of Palaeobotany and Palynology*. 29-147.

Graham, N.E. 1994. Decadal-scale climate variability in the tropical and North Pacific during the 1970s and 1980s: observations and model results. *Climate Dynamics*. 10:135-162.

Gray, J. 1965a. Palynological Techniques. *In* Handbook of paleontological techniques. Kummel B., and D. Raup, (Eds). W. H. Freeman and Co, San Francisco. 471-481.

Gray, J. 1965b. Techniques in Palynology. *In* Handbook of paleontological techniques. Kummel B., and D. Raup, (Eds). W.H Freeman and Co, San Francisco. 530-587.

Grimm, E.C. 1987. CONISS: a FORTRAN 77 program for stratigraphically constrained cluster analysis by the method of incremental sum of squares. *Computers & Geosciences*. 13:13-35.

Groot, M.H.M., R.G. Bogotá-Angel, L.J. Lourens, H. Hooghiemstra, M. Vriend, J.C. Berrio, E. Tuenter, J. Van der Plicht, B. Van Geel, M. Ziegler, S.L. Weber, A. Betancourt, L. Contreras, S. Gaviria, C. Giraldo, N. González, J.H.F. Jansen, M. Konert, D. Ortega, O. Rangel, G. Sarmiento, J. Vandenberghe, T. Van der Hammen, M. Van der Linden, and W. Westerhoff. 2011. Ultra-high resolution pollen record from the northern Andes reveals rapid shifts in montane climates within the last two glacial cycles. *Climate of the Past*. 7:299-316.

Gu, D., and S.G.H. Philander. 1995. Secular Changes of Annual and Interannual Variability in the Tropics during the Past Century. *Journal of Climate*. 8:864-876.

Haberzettl, T., H. Corbella, M. Fey, S. Janssen, A. Luecke, C. Mayr, C. Ohlendorf, F. Schaebitz, G.H. Schleser, M. Wille, S. Wulf, and B. Zolitschka. 2007. Lateglacial and Holocene wet-dry cycles in southern Patagonia; chronology, sedimentology and geochemistry of a lacustrine record from Laguna Potrok Aike, Argentina. *Holocene*. 17:297-310.

Haberzettl, T., M. Wille, M. Fey, S. Janssen, A. Lücke, C. Mayr, C. Ohlendorf, F. Schäbitz, G.H. Schleser, and B. Zolitschka. 2006. Environmental change and fire history of southern Patagonia (Argentina) during the last five centuries. *Quaternary International*. 158:72-82.

Haney, R.L. 1980. A Numerical Case Study of the Development of Large-Scale Thermal Anomalies in the Central North Pacific Ocean. *Journal of Physical Oceanography*. 10:541-556.

Hansen, B.C.S., D.T. Rodbell, G.O. Seltzer, B. León, K.R. Young, and M. Abbott. 2003. Late-glacial and Holocene vegetational history from two sites in the western Cordillera of southwestern Ecuador. *Palaeogeography, Palaeoclimatology, Palaeoecology*. 194:79-108.

Hastenrath, S. 1991. Climate dynamics of the tropics. D. Kluwer, (Eds). 488pp.

Hastenrath, S. 1999. Equatorial Mid-Tropospheric Easterly Jet over the Eastern Pacific. *Journal of the Meteorological Society of Japan*. Vol.77 (3):701-709.

Hastenrath, S., and L. Heller. 1977. Dynamics of climatic hazards in northeast Brazil. *Quarterly Journal of the Royal Meteorological Society*. 103:77-92.

Haug, G., K.A. Hughen, D.M. Sigman, L.C. Peterson, and U. Roehl. 2001. Southward migration of the Intertropical Convergence Zone through the Holocene. *Science*. 293:1304-1308.

Haug, G.H., D. Günther, L.C. Peterson, D.M. Sigman, K.A. Hughen, and B. Aeschlimann. 2003. Climate and the Collapse of Maya Civilization. *Science*. 299:1731-1735.

Helmke, J.P., H.A. Bauch, U. Röhl, and A. Mazaud. 2005. Changes in sedimentation patterns of the Nordic seas region across the mid-Pleistocene. *Marine geology*. 215:107-122.

Hendon, H.H., M.C. Wheeler, and C. Zhang. 2007. Seasonal Dependence of the MJO–ENSO Relationship. *Journal of Climate*. 20:531-543.

Hessler, I., L. Dupont, R. Bonnefille, H. Behling, C. González, K.F. Helmens, H. Hooghiemstra, J. Lebamba, M.-P. Ledru, A.-M. Lézine, J. Maley, F. Marret, and A. Vincens. 2010. Millennial-scale changes in vegetation records from tropical Africa and South America during the last glacial. *Quaternary Science Reviews*. 29: 2882–2899.

Hodell, D.A., F.S. Anselmetti, D. Ariztegui, M. Brenner, J.H. Curtis, A. Gilli, D.A. Grzesik, T.J. Guilderson, A.D. Müller, M.B. Bush, A. Correa-Metrio, J. Escobar, and S. Kutterolf. 2008. An

85-ka record of climate change in lowland Central America. *Quaternary Science Reviews*. 27:1152-1165.

Hooghiemstra, H. 1984. Vegetational and climatic history of the High Plain of Bogotá, Colombia: a continuous record of the last 3.5 million years. *Dissertationes Botanicae*. 79:1-368.

Hooghiemstra, H. 1989. Quaternary and upper-pliocene glaciations and forest development in the tropical andes: Evidence from a long high-resolution pollen record from the sedimentary basin of Bogotá, Colombia. *Palaeogeography, Palaeoclimatology, Palaeoecology*. 72:11-26.

Hooghiemstra, H., and E.T.H. Ran. 1994. Late and middle pleistocene climatic change and forest development in Colombia: pollen record Funza II (2-158 m core interval). *Palaeogeography, Palaeoclimatology, Palaeoecology*. 109:211-246.

Houze, R.A., Jr. 2004. Mesoscale convective systems. *Rev. Geophys.* 42:RG4003.

Hughen, K., S. Lehman, J. Southon, J. Overpeck, O. Marchal, C. Herring, and J. Turnbull. 2004. 14C Activity and Global Carbon Cycle Changes over the Past 50,000 years. *Science*. 303:202-207.

Hsieh, D.A. 1995. Nonlinear Dynamics in Financial Markets: Evidence and Implications. *Financial Analysts Journal*. July-August:55-62.

Hyde, H.A., and D.A. Williams. 1944. The right word. *Pollen Analysis Circular*. No 8:6pp.

IDEAM, I.d.H., Meteorología y Estudios Ambientales. 2001. El Medio ambiente en Colombia. Ministerio del Medio Ambiente. Républica de Colombia, Santa Fé de Bogotá. 543pp.

Islebe, G.A., H. Hooghiemstra and K. Van der Borg. 1995. A cooling event during the Younger Dryas Chron in Costa Rica. *Palaeogeography, Palaeoclimatology, Palaeoecology.* 117:73-80.

Jackson, S.T. 1999. Techniques for analysing unconsilidated lake sediments. *In* Fossil plants and spores: modern techniques. Jones,T.P., and N.P. Rowe, (Eds). Geological Society, London. 274-278.

Jansen, J.H.F., S.J. Van der Gaast, B. Koster, and A.J. Vaars. 1998. CORTEX, a shipboard XRF-scanner for element analyses in split sediment cores. *Marine geology*. 151:143-153.

Jaramillo, D., and L.N. Parra. 1993. Aspectos biofísicos generales del Páramo de Frontino. *Revista ICNE.* 4(2): 81-96.

Jenkins, R., and J.L. de Vries. 1970. Practical X-ray Spectrometry. MacMillan. London. 190pp.

Jojoa, L.M. 2007. Recostrucción palinológica de la vegetación y el clima durante el Holoceno medio en el sector Llano Grande, Páramo de Frontino, Antioquia Colombia). Tesis pregrado en Biología. Universidad de Nariño. Facultad de Ciencias Exactas. Departamento de Biología. San Juan de Pasto. 88pp.

Jones, T.P., and N.P. Rowe. 1999. Fossil plants and spores: Modern techniques. The Geological Society, London. 396pp.

Jowsey, P.C. 1966. An improved peat sampler. *New Phytologist*. 65:245-248.

Kessler, W.S. 2001. EOF Representations of the Madden-Julian Oscillation and Its Connection with ENSO. *Journal of Climate*. 14:3055-3061.

Kessler, W.S., and R. Kleeman. 2000. Rectification of the Madden-Julian Oscillation into the ENSO Cycle. *Journal of Climate*. 13:3560-3575.

Klein, J., J. Lerman, P. Damon, and E. Ralph. 1982. Calibration of radiocarbon dates: tables based on the consensus data of the Workshop on Calibrating the Radiocarbon Time Scale. *Radiocarbon*. 24(2):103-150.

Koinig, K., W. Shotyk, A.F. Lotter, C. Ohlendorf, and M. Sturm. 2003. 9000 years of geochemical evolution of lithogenic major and trace elements in the sediment of an alpine lake; the role of climate, vegetation, and land-use history. *Journal of paleolimnology*. 30:307-320.

Koutavas, A., and J. Lynch-Stieglitz. 2005. Variability of the marine ITCZ over the eastern Pacific during the past 30,000 years: Regional Perspective and Global Context. *In* The Hadley Circulation: Present, Past and Future. Díaz, H.F, and R.S. Bradley, (Eds). Kluwer Academic Publishers. 347-369.

Kuhry, P. 1988. Palaeobotanical-palaeoecological studies of tropical high Andean peatbog sections (Cordillera Oriental, Colombia). *Dissertationes Botanicae 116,* J. Cramer, Berlin-Stuttgart. 241 pp.

Kuhry, P., J.B. Salomons, P.A. Riezebos, and T. Van der Hammen. 1983. Paleoecología de los últimos 6.000 años en el área de la laguna del Otún-El Bosque. *In* Studies on Tropical Andean Ecosystems/Estudios de Ecosistemas Tropoandinos 1: La Cordillera Central Colombiana transecto Parque de los Nevados. Van der Hammen, T., P.A.Pérez, and P.Pinto, (Eds). Cramer (Borntraeger), Berlin-Stuttgart.

Larkin, N.K., and D.E. Harrison. 2001. Tropical Pacific ENSO Cold Events, 1946–95: SST, SLP, and Surface Wind Composite Anomalies. *Journal of Climate*. 14:3904-3931.

Larkin, N.K., and D.E. Harrison. 2002. ENSO Warm (El Niño) and Cold (La Niña) Event Life Cycles: Ocean Surface Anomaly Patterns, Their Symmetries, Asymmetries, and Implications. *Journal of Climate*. 15:1118-1140.

Latif, M., and T.P. Barnett. 1996. Decadal Climate Variability over the North Pacific and North America: Dynamics and Predictability. *Journal of Climate*. 9:2407-2423.

Lau, K.M., and H. Weng. 1995. Climate Signal Detection Using Wavelet Transform: How to Make a Time Series Sing. *Bulletin of the American Meteorological Society*. 76:2391-2402.

Lau, K.M. 2005. El Nino Southern Oscillation connection. *In* Intraseasonal Variability in the Atmosphere-Ocean Climate System. Lau W. K. M., and D. Waliser, (Eds). Praxis Publishing. 271-305.

Lea, D.W., D.K. Pak, L.C. Peterson, and K.A. Hughen. 2003. Synchroneity of Tropical and High-Latitude Atlantic Temperatures over the Last Glacial Termination. *Science*. 301:1361-1364.

Lenters, J.D., and K.H. Cook. 1999. Summertime Precipitation Variability over South America: Role of the Large-Scale Circulation. *Monthly Weather Review*. 127:409-431.

Leyden, B.W. 2002. Pollen evidence for climatic variability and cultural disturbance in the Maya lowlands. *Ancient Mesoamerica* 13:85-101.

Liu, Z., L. Wu, R. Gallimore, and R. Jacob. 2002. Search for the origins of Pacific decadal climate variability. *Geophys. Res. Lett.* 29:1404.

Lobato, I.N., and C. Velasco. 2007. Efficient Wald Tets for fractional unit roots. *Econometrica*. 2:575-589.

López, M.E., and W.E. Howell. 1967. Katabatic Winds in the Equatorial Andes. *Journal of the Atmospheric Sciences*. 24:29-35.

Lozano, G., L.N. Parra, R. Segecin, and J.J. Ramírez. 1999. Inferencias paleolimnológicas del Holoceno basadas en diatomeas de la laguna Puente Largo, Páramo de Frontino, Antioquia. Ed Gráficas Montoya. Medellín. 57-116.

Lozano, G., and R. Schnetter. 1976. Estudios ecológicos en el Páramo de Cruz Verde, Colombia. II Las comunidades vegetales. *Caldasia*. 11(54):54-68.

Madden, R.A., and P.R. Julian. 1971. Detection of a 40–50 Day Oscillation in the Zonal Wind in the Tropical Pacific. *Journal of the Atmospheric Sciences*. 28:702-708.

Madden, R.A., and P.R. Julian. 1972. Description of Global-Scale Circulation Cells in the Tropics with a 40-50 Day Period. *Journal of the Atmospheric Sciences*. 29:1109-1123.

Madden, R.A., and P.R. Julian. 1994. Observations of the 40-50-Day Tropical Oscillation.A Review. *Monthly Weather Review*. 122:814-837.

Maddox, R.A. 1980. Mesoscale Convective Complexes. *Bulletin of the American Meteorological Society*. 61:1374-1387.

Maher, L.R.J. 1972. Absolute pollen diagram of Redrock lake, Boulder County, Colorado. *Quaternary Research*. 2:531-553.

Maher, L.R.J. 1981. Statistics for microfossil concentration measurements employing samples spiked with marker grains. *Review of Palaeobotany and Palynology*. 32:153-191.

Mallat, S.G. 1989. Multiresolution approximations and wavelet orthonormal bases of $L^2(R)$. *Trans. Amer. Math. Soc*. 315:69-87.

Mandelbrot, B.B. 1963. The variation of certain speculative prices. *Journal of Business*. XXXVI. 392-417.

Mantua, N.J., and S.R. Hare. 2002. The Pacific Decadal Oscillation. *Journal of Oceanography* Volume 58, Number 1:35-44.

Mantua, N.J., S.R. Hare, Y. Zhang, J.M. Wallace, and R.C. Francis. 1997. A Pacific Interdecadal Climate Oscillation with Impacts on Salmon Production. *Bulletin of the American Meteorological Society*. 78:1069-1079.

Marchant, R., J.C. Berrío, H. Behling, A. Boom, and H. Hooghiemstra. 2006. Colombian dry moist forest transitions in the Llanos Orientales. A comparison of model and pollen-based biome reconstructions. *Palaeogeography, palaeoclimatology, Palaeoecology*. 234:28-44.

Marchant, R., H. Behling, J.C. Berrio, A. Cleef, J. Duivenvoorden, H. Hooghiemstra, P. Kuhry, B. Melief, E. Schreve-Brinkman, B. Van Geel, T. Van der Hammen, G. Van Reenen, and M. Wille. 2002. Pollen-based biome reconstructions for Colombia at 3000, 6000, 9000, 12 000, 15 000 and 18 000 ^{14}C yr ago: Late Quaternary tropical vegetation dynamics. *Journal of Quaternary Science*. 17:113-129.

Marchant, R., H. Behling, J.C. Berrio, A. Cleef, J. Duivenvoorden, H. Hooghiemstra, P. Kuhry, B. Melief, B. Van. Geel, T. Van der. Hammen, G.V. Reenen, and M. Wille. 2001. Mid- to Late-Holocene pollen-based biome reconstructions for Colombia. *Quaternary Science Reviews*. 20:1289-1308.

Marchitto, T.M., R. Muscheler, J.D. Ortiz, J.D. Carriquiry, and A. Van Geen. 2010. Dynamical Response of the Tropical Pacific Ocean to Solar Forcing During the Early Holocene. *Science*. 330:1378-1381.

Marshall, A.G., O. Alves, and H.H. Hendon. 2009. A Coupled GCM Analysis of MJO Activity at the Onset of El Niño. *Journal of the Atmospheric Sciences*. 66:966-983.

Martínez, I., L. Keigwin, T.T. Barrows, Y. Yokoyama, and J. Southon. 2003. La Niña-like conditions in the eastern equatorial Pacific and a stronger Choco jet in the northern Andes during the last glaciation. *Paleoceanography*. 18:1033.

Martínez, R., D. Ruíz, M. Andrade, L. Blacutt, D. Pabón, E. Jaimes, G. León, M. Villacís, J. Quintana, E. Montealegre, and C. Euscátegui. 2011. Synthesis of the climate of the tropical Andes. *In* Climate change and biodiversity in the tropical Andes. Herzog S.K., R. Martínez, P.M. Jorgensen and H. Tiessen, (Eds). Inter-American Institute for Global Change (IAI), 97-109. Paris, France.

Matthews, J. 1969. The assessment of a method for the determination of absolute pollen frequencies *New Phytologist*. 68:161-166.

Mazaud, A., C. Laj, E. Bard, M. Arnold, and E. Tric. 1992. A geomagnetic calibration of the radiocarbon time-scale. *In* The Last Deglaciation : Absolute and Radiocarbon Chronologies, NATO/ASI Series 1,2 . Bard, E., and W.S. Broecker, (Eds). Springer Verlag, Berlin. 163-169.

Mejía, F., O. Mesa, G. Poveda, J. Vélez, H. Hoyos, R. Mantilla, J. Barco, A. Cuartas, M. Montoya, and B. Botero. 1999. Distribución espacial y ciclos anual y semi-anual de la precipitación en Colombia. Serie del Posgrado en Recursos Hidráulicos No.16. Universidad Nacional de Colombia.

Mesa, O.J., L.F. Carvajal, J.E. Salazar, and Poveda, G. 1997. Introducción al clima de Colombia. Ed Universidad Nacional de Colombia. 390pp.

Mestas-Nuñez, A.M., and D.B. Enfield. 1999. Rotated Global Modes of Non-ENSO Sea Surface Temperature Variability. *Journal of Climate*. 12:2734-2746.

Meyers, S.D., B.G. Kelly, and J.J. O'Brien. 1993. An Introduction to Wavelet Analysis in Oceanography and Meteorology: With Application to the Dispersion of Yanai Waves. *Monthly Weather Review*. 121:2858-2866.

Minobe, S. 1997. A 50-70 year climatic oscillation over the North Pacific and North America. *Geophys. Res. Lett.* 24:683-686.

Mitchell, T.P., and J.M. Wallace. 1996. ENSO Seasonality: 1950-78 versus 1979-92. *Journal of Climate*. 9:3149-3161.

Mommersteeg, H. 1998. Vegetation development and cyclic and abrup climatic change during the Late Quaternary. Ph D Thesis. University of Amsterdam, Amsterdam. 191pp.

Monsalve, C.A. 2011. Caracterización climática entorno al Páramo del Sol, Municipio de Urrao, Antioquia-Colombia. 70pp. (Unpublished)

Moore, A.M., and R. Kleeman. 1999. Stochastic Forcing of ENSO by the Intraseasonal Oscillation. *Journal of Climate*. 12:1199-1220.

Moore, P.D., J.A. Webb, and M.E. Collinson. 1991. Pollen Analysis. Second edition. Blacweell Scientific Publications, (Eds). Oxford, London. 216pp.

Moy, C.M., G.O. Seltzer, D.T. Rodbell, and D.M. Anderson. 2002. Variability of El Nino/Southern Oscillation activity at millennial timescales during the Holocene epoch. *Nature*. 420:162-165.

Moscol-Olivera, M., J.F. Duivenvoorden, and H. Hooghiemstra. 2009. Pollen rain and pollen representation across a forest-páramo ecotone in northern Ecuador. *Review of Palaeobotany and Palynology*. 157:285-300.

Muñoz, P. 2007. Evolution paléoenvironnementale de l'Holocène récent dérivé de l'enregistrement palynologique dans une zone humide de moyenne montagne du département du Quindío (Colombie Centrale). Mémoire No 147 Master en sciences naturelles de l'environnement. Université de Genève. 86pp.

Nakamura, H., G. Lin, and T. Yamagata. 1997. Decadal Climate Variability in the North Pacific during the Recent Decades. *Bulletin of the American Meteorological Society*. 78:2215-2225.

Namias, J. 1959. Recent Seasonal Interactions between North Pacific Waters and the Overlying Atmospheric Circulation. *J. Geophys. Res.* 64:631-646.

Neelin, J.D., D.S. Battisti, A.C. Hirst, F.-F. Jin, Y. Wakata, T. Yamagata, and S.E. Zebiak. 1998. ENSO theory. *J. Geophys. Res.* 103:14261-14290.

Nesbitt, H.W., and G.M. Young. 1982. Early Proterozoic climates and plate motions inferred from major element chemistry of lutites. *Nature*. 299:715-717.

Newman, M., P.D. Sardeshmukh, and C. Penland. 2009. How Important Is Air-Sea Coupling in ENSO and MJO Evolution? *Journal of Climate*. 22:2958-2977.

Niemann, H., T. Haberzettl, and H. Behling. 2009. Holocene climate variability and vegetation dynamics inferred from the (11700 cal. yr BP) Laguna Rabadilla de Vaca sediment record, southeastern Ecuadorian Andes. *The Holocene*. 19:307-316.

Ogden, J.H. 1986. An alternative to exotic spore or pollen addition in quantitative microfossil studies. *Canadian Journal of Earth Sciences*. 23:102-106.

Ohlendorf, C., and M. Sturm. 2008. A modified method for biogenic silica determination. *Journal of paleolimnology*. 39:137-142.

Ospina, M. 1973. Bases para la planeación y desarrollo del Parque Nacional "Las Orquídeas" (Antioquia), Colombia.

Oster, R. 1979. Las precipitaciones en Colombia. *Colombia Geográfica*. Vol VI(2).

Pak, H., and J.R.V. Zaneveld. 1974. Equatorial Front in the Eastern Pacific Ocean. *Journal of Physical Oceanography*. 4:570-578.

Parra, L.N. 1991. Geología glacial del Páramo de Frontino. Universidad Nacional de Colombia. Medellín. 44pp (unpublished).

Parra, L.N. 2005. Análisis facial de alta resolución de sedimentos del Holoceno Tardío en el Paramo de Frontino, Antioquia. Ph D Tesis. Instituto de Ciencias Naturales. Universidad Nacional de Colombia. Bogotá. 215pp.

Parra, L.N., and A. Jaramillo. 1999. Análisis palinológico del núcleo Puente Largo Páramo de Frontino. Ed Gráficas Montoya. Medellín. 236pp.

Parra, L.N., O. Rangel, and T. Van der Hammen. 2010a. Geomorfología del Páramo de Frontino. *In* Colombia Diversidad Biótica X:Cambios global (natural) y climático(antrópico) en el páramo colombiano. Rangel-Ch, J.O. (Eds). Bogotá. Instituto de Ciencias naturales Bogotá. 1-14.

Parra, L.N., J.O. Rangel, and T. Van der Hammen. 2010b. Los sedimentos paramunos y la estratigrafía de la turbera Llano Grande, Páramo de Frontino (Antioquia, Colombia). *In* Colombia Diversidad Biótica X:Cambios global (natural) y climático(antrópico) en el páramo colombiano. Rangel-Ch, J.O. (Eds). Bogotá. Instituto de Ciencias Naturales Bogotá. 67-91.

Parra, L.N., J.O. Rangel, and T. Van der Hammen. 2010c. Modelo de facies para los humedales paramunos. *In* Colombia Diversidad Biótica X:Cambios global (natural) y climático(antrópico) en el páramo colombiano. Rangel-Ch, J.O. (Eds). Bogotá. Instituto de Ciencias Naturales Bogotá. 15-41.

Pearson, G., and M. Stuiver. 1986. High-precision calibration of the radiocarbon time scale, 500-2500 BC. *Radiocarbon*. 28(2B):839-862.

Pearson, G., and M. Stuiver. 1993. High-precision bidecadal calibration of the radiocarbon time scale, 500-2500 BC. *Radiocarbon.* 35(1):25-33.

Pennington, W., and A.P. Bonny. 1970. Absolute Pollen Diagram from the British Late-Glacial. *Nature*. 226:871-873.

Peterson, L., and G.H. Haug. 2006. Variability in the mean latitude of the Atlantic Intertropical Convergence Zone as recorded by riverine input of sediments to the Cariaco Basin (Venezuela). *Palaeogeography, Palaeoclimatology, Palaeoecology*. 234:97-113.

Philander, S.G.H. 1990. El Niño, La Niña and the Southern Oscillation. San Diego Academic Press. 293pp.

Philander, S.G.H., D. Gu, G. Lambert, T. Li, D. Halpern, N.C. Lau, and R.C. Pacanowski. 1996. Why the ITCZ Is Mostly North of the Equator. *Journal of Climate*. 9:2958-2972.

Phipps, D., and G. Playford. 1984. Laboratory techniques for extraction of palynomorphs from sediments. Vol. 11(1). Department of Geology, University of Queesland 1-23.

Pierce, D.W., T.P. Barnett, N. Schneider, R. Saravanan, D. Dommenget, and M. Latif. 2001. The role of ocean dynamics in producing decadal climate variability in the North Pacific. *Climate Dynamics*. 18:51-70.

Piperno, D.R., and J.G. Jones. 2003. Paleoecological and archaeological implications of a late Pleistocene/Early Holocene record of vegetation and climate from the Pacific coastal plain of Panama. *Quaternary research*. 59:79-87.

Poveda, G., A. Jaramillo., M.M. Gil., N. Quiceno., and R. Mantilla. 2001. Seasonality in ENSO Related Precipitation, River Discharges, Soil Moisture, and Vegetation Index (NDVI) in Colombia. *Water Resources Research*. 37:2169-2178.

Poveda, G., and O.J. Mesa. 1997. Feedbacks between Hydrological Processes in Tropical South America and Large-Scale Ocean-Atmospheric Phenomena. *Journal of Climate*. 10:2690-2702.

Poveda, G., and O.J. Mesa. 2000. On the existence of Lloró (the rainiest locality on Earth): Enhanced ocean-atmosphere-land interaction by a low level jet. *Geophys. Res. Lett.* 27:1675-1678.

Poveda, G., P.R. Waylen, and R.S. Pulwarty. 2006. Annual and inter-annual variability of the present climate in northern South America and southern Mesoamerica. *Palaeogeography, Palaeoclimatology, Palaeoecology*. 234:3-27.

Rangel, J.O. 1995-2010. Colombia diversidad biótica, vol. 1 to 10. Instituto de Ciencias Naturales, Universidad Nacional de Colombia. Rangel-Ch, J.O. (Eds). Bogotá.

Rangel, J.O., and M. Aguilar. 1995. Una aproximación sobre la diversidad climática en las regiones naturales de Colombia. *In* Colombia Diversidad Biótica 1. Editorial Guadalupe. Santafe de Bogotá.

Rangel , J.O., and C. Lozano. 1986. Un perfil de vegetación entre La Plata (Huila) y el volcán de Puracé. *Caldasia.* 14 (68-70):503-547.

Rangel, J.O., D. Sánchez, and C. Ariza. 1999. Fitosociología del Páramo de Frontino. In Tardiglacial y Holoceno del norte de la Cordillera Occidental de Colombia. Ed Gráficas Montoya. Medellín. 236pp.

Rangel , J.O., T. Van Der Hammen, and R. Jaramillo. 1982. Tipos de vegetación en el transecto Buritaca-La Cumbre Sierra Nevada de Santa Marta (entre 0 y 4100 m). *Colombia Geográfica.* 10:1-18.

Rasmusson, E.M., and T.H. Carpenter. 1982. Variations in Tropical Sea Surface Temperature and Surface Wind Fields Associated with the Southern Oscillation/El Niño. *Monthly Weather Review*. 110:354-384.

Riedinger, M.A., M. Steinitz-Kannan, W.M. Last,and M. Benner. 2002. A ~ 6100 ^{14}C yr record of El Niño activity from the Galápagos Islands. *Journal of paleolimnology*. 27:1-7.

Reimer, P., M. Baillie, E. Bard, A. Bayliss, J. Beck, C. Bertrand, P. Blackwell, C. Buck, G. Burr, K. Cutler, P. Damon, R. Edwards, R. Fairbanks, M. Friedrich, T. Guilderson, A. Hogg, K. Hughen, B. Kromer, G. McCormac, S. Manning, C. Bronk Ramsey, R. Reimer, S. Remmele, J. Southon, M. Stuiver, S. Talamo, F. Taylor, J. van der Plicht, and C. Weyhenmeyer. 2004. IntCal04 terrestrial radiocarbon age calibration, 0–26 cal kyr BP. *Radiocarbon.* 46(3):1029-1058.

Rivera, D. 2001. Páramos de Colombia. Editor Banco de Occidente, Santiago de Cali, Colombia. 204 pp.

Roberts, N. 1998. The Holocene: An environmental history. Second Edition. Blackwell Publishing. 316 pp.

Rodbell, D.T., G.O. Seltzer, D.M. Anderson, M.B. Abbott, D.B. Enfield, and J.H. Newman. 1999. An ~15,000-Year Record of El Niño-Driven Alluviation in Southwestern Ecuador. *Science*. 283:516-520.

Röhl, U., and L.J. Abrams. 2000. High-resolution, downhole and nondestructive core measurements from Sites 999 and 1001 in the Caribbean Sea: application to the Late Paleocene Thermal Maximum. Proc. Ocean Drill. Prog., Sci. Results 165. 191–203.

Rohling, E.J., and H. Palike. 2005. Centennial-scale climate cooling with a sudden cold event around 8,200 years ago. *Nature*. 434:975-979.

Roubik, D.W., and J.E. Moreno P. 1991. Pollen and spores of Barro Colorado Island. Monographs in Sytematic Botany, Missouri Botanical Garden 36. 268pp.

Ropelewski, C.F., and M.S. Halpert. 1987. Global and Regional Scale Precipitation Patterns Associated with the El Niño/Southern Oscillation. *Monthly Weather Review*. 115:1606-1626.

Ryan, P.D., D.A.T. Harper, and J.S. Whalley. 1995. PALSTAT, Statistics for palaeontologists. Chapman and Hall (now Kluwer Academic Publishers). 31pp.

Rybníčková, E., and K. Rybníček. 1971. The determination and elimination of local elements in pollen spectra from different sediments. *Review of Palaeobotany and Palynology*. 11:165-176.

Ruddiman, W.F. 2001. Earth's Climate: Past and Future. Freeman and Company, (Eds). New York. 464 pp.

Ruíz, D., M.P. Arroyave, A.M. Molina, J.F. Barros, M.E. Gutierrez, and P.A. Zapata. 2009. Signals of climate variability/change in surface water supply of high-mountain watersheds - case study: Claro River high mountain basin, Los Nevados Natural Park, Andean Central Mountain Range, Colombia. World Bank Group. 207pp.

Rull, V., M.B. Abbott, P.J. Polissar, A.P. Wolfe, M. Bezada, and R.S. Bradley. 2005. 15,000-yr pollen record of vegetation change in the high altitude tropical Andes at Laguna Verde Alta, Venezuela. *Quaternary research*. 64:308-317.

Salomons, J.B. 1986. Paleoecology of volcanic soils in the Colombian Central Cordillera (Parque nacional natural de Los Nevados). Van der Hammen, T. (Eds). The Quaternary of Colombia,13. Amsterdam, Holland.

Sánchez, D. 1998. Inventario florístico del páramo de Frontino (Urrao) Antioquia. *Revista Facultad Nacional de Agronomía*. 51(2):99-156.

Sánchez, D. 1999. Composición florística del Páramo de Frontino. In Tardiglacial y Holoceno del norte de la Cordillera Occidental de Colombia. Ed Gráficas Montoya. Medellín. 236pp.

Scheffler, K., D. Buehmann, and L. Schwark. 2006. Analysis of late Palaeozoic glacial to postglacial sedimentary successions in South Africa by geochemical proxies – Response to climate evolution and sedimentary environment. *Palaeogeography, Palaeoclimatology, Palaeoecology*. 240:184-203.

Scheibe, R. 1933. Geología del sur de Antioquia. *Comp.Est. Geol.Oficiales de Colombia.* Bogotá. 97-167.

Srinivasan, J., and G.L. Smith. 1996. Meridional Migration of Tropical Convergence Zones. *Journal of Applied Meteorology*. 35:1189-1202.

Stansell, N.D., M.B. Abbott, V. Rull, D.T. Rodbell, M. Bezada, and E. Montoya. 2010. Abrupt Younger Dryas cooling in the northern tropics recorded in lake sediments from the Venezuelan Andes. *Earth and Planetary Science Letters*. 293:154-163.

Stockmarr, J. 1971. Tablets with spores used in absolute pollen analysis. *Pollen and Spores*. 13:615-621.

Stockmarr, J. 1973. Determination of spore concentration with electronic particle counter. *Danmarks Geologiske Undersøgelse*. Årbok. 87-92.

Stott, L., C. Poulsen, S. Lund, and R. Thunell. 2002. Super ENSO and Global Climate Oscillations at Millennial Time Scales. *Science*. 297:222-226.

Strang, G., and T. Nguyen. 1997. Wavelets and Filter Banks. Wellesley-Cambridge Press, second edition. USA. 500 pp.

Stuiver, M. 1982. A high-precision calibration of the AD radiocarbon time scale. *Radiocarbon*. 24(1):1-26.

Stuiver, M., and B. Becker. 1993. High-precision decadal calibration of the radiocarbon time scale, AD 1950-6000 BC. *Radiocarbon.* 35(1):35-65.

Stuiver, M., T.F. Braziunas, B. Becker, and B. Kromer. 1991. Climatic, solar, oceanic, and geomagnetic influences on late-glacial and holocene atmospheric 14C12C change. *Quaternary research*. 35:1-24.

Stuiver, M., and H.A. Polach. 1977. Discussion: reporting of ^{14}C data. *Radiocarbon*. 19(3):355–363.

Stuiver, M., and P.J. Reimer. 1993. Extended ^{14}C data base and revised CALIB 3.0 ^{14}C age calibration program. *Radiocarbon*. 2:215-230.

Stuiver, M., P.J. Reimer, E. Bard, J.W. Beck, G.S. Burr, K.A. Hughen, B. Kromer, G. McCormac, J. va, and M. Spurk. 1998. INTCAL98 radiocarbon age calibration, 24,000-0 cal BP. *Radiocarbon.* 40(3):1041-1083.

Stuiver, M., and H.E. Suess. 1966. On the relationship between radiocarbon dates and true sample ages. *Radiocarbon*. 8:534-540.

Sturm, H. 1978. Zur Ökologie der andinen Paramoregion. Dr W Junk, Publishers, The Hague. *Biogeographica*, Vol XIV. 121pp

Subramanian, A.C., M. Jochum, A.J. Miller, R. Murtugudde, R.B. Neale, and D.E. Waliser. 2011. The Madden-Julian Oscillation in CCSM4. *Journal of Climate*. 24:6261-6282.

Talma, A.S., and J.C. Vogel. 1993. A simplified approach to calibrating ^{14}C dates. *Radiocarbon*. 2:317-322.

Tang, Y., and B. Yu. 2008. MJO and its relationship to ENSO. *J. Geophys. Res.* 113:D14106.

Tarbuck, E.J., and F.K. Lutgens. 2008. Earth: An introduction to Physical Geology. 9th Edition. Pearson Prentice Hall. 714pp.

Thompson, L.G. 2000. Ice core evidence for climate change in the Tropics: implications for our future. *Quaternary Science Reviews*. 19:19-35.

Thompson LG., E. Mosley-Thompson, M.E. Davis, P.N. Lin, K.A. Henderson, J. Cole-Dai, J.F Bolzan JF and K.B. Liu. 1995. Late Glacial Stage and Holocene tropical ice core records from Huascarán, Peru. *Science* 269:46-50.

Thouret, J.C., J.M. Cantagrel, C. Robin, A. Murcia, R. Salinas, and H. Cepeda. 1995. Quaternary eruptive history and hazard-zone model at Nevado del Tolima and Cerro Machin volcanoes, Colombia. *Journal of volcanology and geothermal research*. 66:397-426.

Thouret, J.C. and A. Pérez. 1983. Reseña geográfica. In Estudios de ecosistemas Tropoandinos, la Cordillera Central Colombiana, Transecto Parque de los Nevados (Intr y datos inic). Van der Hammen,T., P.P. Preciado, and P. Pinto, (Eds). 1:31-37.

Thouret, J.C., T. Van der Hammen, B. Salomons, and E. Juvigné. 1996. Paleoenvironmental Changes and Glacial Stades of the Last 50,000 years in the Cordillera Central, Colombia. *Quaternary research*. 46:1-18.

Torrence, C., and G. Compo. 1998. A practical guide to Wavelet Analysis. *Bulletin of the American Meteorological Society*. Vol 79(1):61-78.

Torres, V. 2005. Pliocene-Pleistocene evolution of flora, vegetation and climate: a palynological and sedimentological study of a 586 m core from the Bogotá Basin, Colombia. Ph D Thesis. Institute for Biodiversity and Ecosytems Dynamic (IBED). University of Amsterdam. 181pp.

Traverse, A. 1988. Paleopalynology. Unwin Hyman. Boston. 600pp.

Trenberth, K.E. 1991. General characteristics of El Niño-Southern Oscillation. *In* Teleconnections Linking Worldwide Climate Anomalies. Glantz, R.M., R. Katz, and N. Nicholls, (Eds). Cambridge.

Trenberth, K.E., and T.J. Hoar. 1996. The 1990-1995 El Nino Southern Oscillation event: Longest on record. *Geophysical research letters*. 23:57-60.

Trumbore, S.E. 2000. Radiocarbon Geochronology. *In* Quaternary Geochronology:methods and applications. American Geophysical Union, Reference Shelf. Stratton Noller, J.M., J.M. Sowers, and W.R. Lettis, (Eds). 4 : 41-60.

Tschudy, R.H. 1969a. Applied palynology. *In* Aspects of Palynology. Tschudy, R.H., and R.A. Scott, (Eds). Wiley-Interscience, New York, United States. 103-126.

Tschudy, R.H. 1969b. Relationship of palynomorphs to sedimentation *In* Aspects of Palynology. Tschudy, R.H., and R.A. Scott, (Eds). Wiley-Interscience New York, United States. 79-96.

Tschudy, R.H., and R.A. Scott. 1969c. Introduction. *In* Aspects of Palynology. Tschudy, R.H., and R.A. Scott, (Eds). Wiley-Interscience New York, United States. 1-4.

Van der Hammen, T. 1974. The Pleistocene change of vegetation and climate in tropical South America. *Journal of Biogeography*. 1:3-26.

Van der Hammen, T., J. Barelds, H. De Jong, and A.A. De Veer. 1980. Glacial sequence and environmental history in the Sierra Nevada del Cocuy (Colombia). *Palaeogeography, Palaeoclimatology, Palaeoecology*. 32:247-340.

Van der Hammen, T., and E. González. 1960a. Holoceno and Late Glacial climate and vegetation of páramo Palacio (Eastern Cordillera, Colombia, South America). *Geologie en Mijnbouw*. 39(12):737-746.

Van der Hammen, T., and E. González. 1960b. Upper Pleistocene and Holocene climate vegetation of the "Sabana de Bogotá", (Colombia, South America). *Leidse Geologische Mededelingen*. 25:126-315.

Van der Hammen, T., and E. González. 1963. Historia de clima y vegetación del Pleistoceno Superior y del Holoceno de la Sabana de Bogotá. *Boletín Geológico. Servicio Geológico Nacional*. (XI) 1-3:189-266.

Van der Hammen, T., and E. González. 1964. A pollen diagram from the Quaternary of the Sabana de Bogotá (Colombia) and its significance for the geology of the Northern Andes. *Geologie en Mijnbouw* 43(3):113-117.

Van der Hammen, T., and H. Hooghiemstra. 1995. Cronostratigrafía y correlación Plioceno y Cuaternario de Colombia. *Análisis Geográficos*. 24:51-67.

Van der Hammen, T., and H. Hooghiemstra. 2003. Interglacial–glacial Fuquene-3 pollen record from Colombia: an Eemian to Holocene climate record. *Global and Planetary Change*. 36:181-199.

Van der Hammen, T., O. Rangel, and A.M. Cleef. 2005. La Cordillera Occidental Colombiana transecto Tatamá. *Studies on Colombian Ecosystems. Estudios de Ecosistemas Tropoandinos, Vol 6. T.* Van der Hammen., J.O. Rangel, and A.M. Cleef, (Eds). Cramer-Borntraeger, Berlin-Stuttgart. 972 pp.

Van der Hammen, T., J.H. Werner, and H. van Dommelen. 1973. Palynological record of the upheaval of the Northern Andes: A study of the pliocene and lower quaternary of the Colombian Eastern Cordillera and the early evolution of its high-Andean biota. *Review of Palaeobotany and Palynology*. 16:1-122.

Van der Plas, G.W., E.J. De Boer, H. Hooghiemstra, F.B. Vincent Florens, C. Baider, and J. Van Der Plicht. 2012. *Mauritius* since the last glacial: environmental and climatic reconstruction of the last 38 000 years from Kanaka Crater. *Journal of Quaternary Science*. 27:159-168.

Van der Plicht, J. 2002. Calibration of the ^{14}C timescale: towards the complete datin range. *Netherlands Journal of Geosciences*. 81:85-96.

Van Geel, B., and T. Van der Hammen. 1973. Upper quaternary vegetational and climatic sequence of the fuquene area (Eastern Cordillera, Colombia). *Palaeogeography, Palaeoclimatology, Palaeoecology*. 14:9-92.

Van Geel, B., J. Van der Plicht, and H. Renssen. 2003. Major Δ14C excursions during the late glacial and early Holocene: changes in ocean ventilation or solar forcing of climate change? *Quaternary International*. 105:71-76.

Van't Veer, R., and H. Hooghiemstra. 2000. Montane forest evolution during the last 650 000 yr in Colombia: a multivariate approach based on pollen record Funza-I. *Journal of Quaternary Science*. 15:329-346.

Van't Veer,R., G.A. Islebe, and H. Hooghiemstra. 2000. Climatic change during the Younger Dryas chron in northern South America: a test of the evidence. *Quaternary Science Reviews*. 19:1821-1835.

Vareschi, V. 1970. Flora de los Páramos de Venezuela. Talleres gráficos Universidad de los Andes, Mérida-Venezuela. 425pp.

Velasco, I., and J.M. Fritsch. 1987. Mesoscale Convective Complexes in the Americas. *J. Geophys. Res.* 92:9591-9613.

Velásquez , C.A. 1999a. Atlas palinológico de la flora vascular paramuna de Colombia: Angiospermae. Colciencias, Universidad Nacional de Colombia,Medellín. 173pp.

Velásquez, C.A. 1999b. Análisis palinológico del núcleo Llano Grande Páramo de Frontino. *In* Tardiglacial y Holoceno del norte de la Cordillera Occidental de Colombia. Ed Gráficas Montoya. Medellín. 236pp.

Velásquez, C.A. 1999c. Sedimentación polínica reciente en el Páramo de Frontino. *In* Tardiglacial y Holoceno del norte de la Cordillera Occidental de Colombia. Ed Gráficas Montoya. Medellín. 236pp.

Velásquez, C.A. 2005. Paleoecología de alta resolución del Holoceno Tardío en el Páramo de Frontino Antioquia. Tesis doctoral Universidad Nacional de Colombia, Sede Medellín. 199pp.

Velásquez , C.A., K. Cabrera, L.N. Parra, and J.O. Rangel. 2004. Aspectos metodológicos a tener en cuenta en estudios paleoecológicos de alta resolución en los páramos andinos. *In* Memorias VIII Congreso Latinoamericano y II Congreso Colombiano de Botánica. Rangel, J.O., J. Aguirre, G. Andrade, and C. Giraldo, (Eds). 76-95.

Vélez, J.I., G. Poveda, and O.J. Mesa. 2000. Balances hidrológicos de Colombia. *In* Serie del Posgrado en Recursos Hidráulicos. Vol. No 16.

Vélez, M.I., M. Wille, H. Hooghiemstra, S. Metcalfe, J. Vandenberghe, and K. van der Borg. 2001. Late Holocene environmental history of southern Chocó region, Pacific Colombia; sediment, diatom and pollen analysis of core El Caimito. *Palaeogeography, Palaeoclimatology, Palaeoecology*. 173:197-214.

Waliser, D.E., and R.C.J. Somerville. 1994. Preferred Latitudes of the Intertropical Convergence Zone. *Journal of the Atmospheric Sciences*. 51:1619-1639.

Walker, M. 2005. Quaternary Dating Methods. John Wiley and Sons Ltd. England. 286pp.

Wang, B. 1995. Interdecadal Changes in El Niño Onset in the Last Four Decades. *Journal of Climate*. 8:267-285.

Wang, B., and Y. Wang. 1996. Temporal Structure of the Southern Oscillation as Revealed by Waveform and Wavelet Analysis. *Journal of Climate*. 9:1586-1598.

Wanner, H., J. Beer, J. Bütikofer, T.J. Crowley, U. Cubasch, J. Flückiger, H. Goosse, M. Grosjean, F. Joos, J.O. Kaplan, M. Küttel, S.A. Müller, I.C. Prentice, O. Solomina, T.F. Stocker, P. Tarasov, M. Wagner, and M. Widmann. 2008. Mid- to Late Holocene climate change: an overview. *Quaternary Science Reviews*. 27:1791-1828.

Ward, M.N. 1998. Diagnosis and Short-Lead Time Prediction of Summer Rainfall in Tropical North Africa at Interannual and Multidecadal Timescales. *Journal of Climate*. 11:3167-3191.

Waylen, P., and G. Poveda. 2002. El Niño–Southern Oscillation and aspects of western South American hydro-climatology. *Hydrological Processes*. 16:1247-1260.

Webb, T. 1980. The reconstruction of climatic sequences from botanical data. *Journal of Interdisciplinary History*. 10:749-772.

Weng, C., M.B. Bush, and J.S. Athens. 2002. Holocene climate change and hydrarch succession in lowland Amazonian Ecuador. *Review of Palaeobotany and Palynology*. 120:73-90.

Weng, C., M.B. Bush, J.H. Curtis, A.L. Kolata, T.D. Dillehay, and M.W. Binford. 2006. Deglaciation and Holocene climate change in the western Peruvian Andes. *Quaternary research*. 66:87-96.

Weng, H., and K.M. Lau, 1994: Wavelets, period doubling, and time-frequency localization with application to organization of convection over the tropical western Pacific. *J. Atmos. Sci*. 51:2523-2541.

White, W.B., and T.P. Barnett. 1972. A Servomechanism in the Ocean/Atmosphere System of the Mid-Latitude North Pacific. *Journal of Physical Oceanography*. 2:372-381.

Wille, M., H. Hooghiemstra, H. Behling, K. van der Borg, and A.J. Negret. 2001. Environmental change in the Colombian subandean forest belt from 8 pollen records: the last 50 kyr. *Vegetation History and Archaeobotany*. 10:61-77.

Wille, M., H. Hooghiemstra, B. van Geel, H. Behling, A. de Jong, and K. van der Borg. 2003. Submillennium-scale migrations of the rainforest-savanna boundary in Colombia: ^{14}C wiggle-matching and pollen analysis of core Las Margaritas. *Palaeogeography, Palaeoclimatology, Palaeoecology*. 193:201-223.

Williams, M., D. Dunkerley, P.D. Deckker, P. Kersahw, and J. Chappell. 1998. Quaternary environments. Second edition. Oxford University Press. New York. 329pp.

Wohlfarth, B., G. Skog, G. Possnert, and B. Holmquist. 1998. Pitfalls in the AMS radiocarbon-dating of terrestrial macrofossils. *Journal of Quaternary Science*. 13:137-145.

Wood, G.D., A.M. Gabriel, and J.C. Lawson. 1996. Palynological Techniques-Processing and Microscopy. *In* Palynology: principles and applications. Vol. vol. 1-3. Jansonius,J.M, and D.C. McGregor, (Eds). Dallas. American Association of Stratigraphic Palynologists Foundation. 29-50.

Yancheva, G., N.R. Nowaczyk, J. Mingram, P. Dulski, G. Schettler, J.F.W. Negendank, J. Liu, D.M. Sigman, L.C. Peterson, and G.H. Haug. 2007. Influence of the intertropical convergence zone on the East Asian monsoon. *Nature*. 445:74-77.Zhang, C. 2005. Madden-Julian Oscillation. *Rev. Geophys.* 43:RG2003.

Zhang, Y., J.M. Wallace, and D.S. Battisti. 1997. ENSO-like Interdecadal Variability: 1900–93. *Journal of Climate*. 10:1004-1020.

Zuluaga, J.E., and L. Mattsson. 1981. Glaciaciones de la Cordillera Occidental de Colombia, Páramo de Frontino. Departamento de Antioquia. Revista CIAF 6: 639-654.

APPENDICES

APPENDIX A1

REGIONAL CLIMATE IN NORTHERN SOUTH AMERICA

A1.1. MACROCLIMATIC PHENOMENAS (ITCZ, ENSO, PDO)

The atmospheric systems of the tropical Andes (between 25ºS and 10ºN) are affected by orography, the main regional circulation systems, and by oceanic currents. The main factors that influence the Andean climate are the presence of the Amazon forest to the east, the displacement of the ITCZ, and the presence of the trade winds to the north.

At high elevations, the subtropical jet stream and the permanent high pressure system of the South Pacific and South Atlantic are important. The topography of the tropical Andean mountain range itself with its two main branches, the Eastern Cordillera and the Western Cordillera, also modulates the formation of precipitation systems and temperature variations (Martínez et al., 2011).

A.1.1.1. SEASONAL VARIABILITY: *Intertropical Convergence Zone (ITCZ)*

The ITCZ is a circum-global atmospheric belt of intense moist convection and rainfall, marking the confluence of the northern and southern trade winds and the rising branch of the Hadley cell (Koutavas and Lynch-Stieglitz, 2005). The displacement of the ITCZ and the action of physical-geographical regional factors, such as orography determine the rainfall in Colombia.

The convecting system of the ITCZ acts to stabilize the tropical troposphere, which is heated from the ocean below, and plays an important role in the atmospheric energy cycle, particularly in the transport of heat to the extratropics. Furthermore, the extensive cloudiness associated with the ITCZ contributes significantly to the planetary albedo, and thus to the planetary energy balance (Waliser and Somerville, 1994). It regulates the hydrological cycle over the tropical continents and interacts tightly with the tropical oceans, notably with the seasonal appearance of the equatorial cold tongues in the Atlantic and Pacific (Koutavas and Lynch-Stieglitz, 2005).

The Atlantic ITCZ marks the dynamic boundary between the southeast and northeast Atlantic trade winds and is associated with a well organized zonal band of low pressure and high precipitation that occurs predominantly over the ocean basin and extends from South America to the west coast of Africa. Convection associated with the seasonal migration of the ITCZ plays a major role in controlling the patterns of rainfall over the adjacent continents (Hastenrath and Heller, 1977; Poveda and Mesa, 1997).

The hydrological annual cycle in tropical South America is largely controlled by the meridional oscillation of the ITCZ, though spatial variability is introduced by the presence of the Andes and the Amazon River basin, by the surrounding tropical Pacific and Atlantic Oceans, and by land-atmosphere feedbacks (Poveda et al., 2001).

Due to the strong linkage between variations in atmospheric and oceanic conditions the position of the ITCZ follows a seasonal cycle, with an abrupt shift from its northernmost position during boreal summer to its southernmost position during austral summer (Fig. 1.1). These variations of the ITCZ affect the rainfall distribution in equatorial and tropical regions, resulting in alternating wet and dry seasons (Hessler et al., 2010). Far from the equator the dry season (winter) is severe and the rainy season (summer) short. Near the equator, two short dry seasons occur (Ruddiman, 2001).

The annual migration of the ITCZ is influenced by the distribution of land and ocean (Hessler et al., 2010; Srinivasan and Smith, 1996). Over the ocean the ITCZ is well defined by the combination of convergence of trade winds and subsequent convection and heavy rainfall. Over land, the southern oscillation of the ITCZ across the equator responds to the seasonal insolation cycle and the near-surface convergence and convection become widely separated during the season of maximum excursion (northern- or southernmost ITCZ position (Hessler et al., 2010).

In South America during austral summer, when the ITCZ is located at its southernmost position, trade winds transport moisture from the equatorial Atlantic towards the Amazon basin causing the South American Summer Monsoon (Gan et al., 2004). These trade winds are channelled to the southeast to 20–23 °S by the Andean Cordillera (Lenters and Cook, 1999). During the winter season the ITCZ moves to its northernmost position at ~10 °N.

The ITCZ of the eastern equatorial Pacific generally migrates from a most southerly average position of about 3 °N in March to approximately 10 °N in September This broad band is associated with unstable rising air and extensive precipitation, as can be noted by the dominance of the September–November (SON) triad in Colombian rainfall in and west of the Andes (Velasco and Fritsch, 1987).

Areas to the south of the ITCZ in the Northern Hemisphere experience cross-equatorial westerly winds that form a low-level jet (Choco Jet), which, in combination with the topography of the Andes, are responsible for some of the wettest regions in the world along the Pacific coast of Colombia (mean annual precipitation in Chocó is in excess of 7000 mm. (Poveda and Mesa, 2000).

In Colombia and neighboring areas of the eastern Pacific Ocean, the ITCZ reaches its extreme meridional position between the months of January and February at about 2°N. Between March and May, the Pacific segment of the ITCZ moves to the north and is positioned between 2–7°N. The continental band joins the segment of the Atlantic Ocean between March and April to form a single system that is located between 5° S and 1°N in the east of the country. These two segments are joined by poorly organized convective zones on the Andean region.

Initially, between June and August, the Pacific segment is located near 8°N and ends at 10° N, entering the Caribbean region. The continental segment has a SW-NE orientation over the Colombian territory, and moves towards the north through Ecuador up to 8°N. Between

September and November, the Pacific segment begins its movement south to reach between 7-11°N. The continental band also begins moving towards the south from 8°N towards the Ecuador over the Orinoco and Amazon, slowly losing its inclination to coincide with the parallels. In this case the two segments of ITCZ are joined by convective zones (IDEAM, 2001).

Forcing during the northern hemisphere summer, when the ITCZ is in its northern position results in La Niña-like conditions and, conversely, forcing during winter, when the ITCZ is in its southern position, results in El Niño conditions (Clement, 1999).

A1.1.2. INTERANNUAL VARIABILITY: *El Niño Southern Oscillation (ENSO)*

Using the established definitions, El Niño is the warm ocean current frequently (every 3–4 years) observed in the eastern equatorial Pacific off the coast of Ecuador, and the Southern Oscillation (SO) refers to the varying bi-polar nature of atmospheric pressures in the western Pacific (low pressures) and the South Pacific sub-tropical anticyclone(Waylen and Poveda, 2002). It has a time scale of 2-7 years.

The general suite of environmental conditions associated with the two mean states has become known as El Niño (deepened thermocline in the eastern Pacific) and La Niña, anti-El Niño or El Viejo (shallower thermocline in eastern Pacific). Because the exact state of each unstable mean condition varies, no universally accepted definition of El Niño and La Niña can exist in terms of the dominant factors of sea-surface temperatures (SST) and atmospheric pressures (Waylen and Poveda, 2002).

ENSO has a very direct influence on weather conditions in some mid-latitude areas, and its effects have been linked to changes in storm tracks across North America, producing significant seasonal anomalies in temperature and precipitation (Ropelewski and Halpert, 1987). It is also thought to be a factor behind major drought events in the African Sahel region (Ward, 1998).

ENSO is the main forcing mechanism of Colombia's hydro-climatology at interannual timescales. It constitutes a complex of environmental changes that have differing influences throughout the study area, but which are loosely associated, statistically and physically, with the major regional precipitation-generating mechanisms (Waylen and Poveda, 2002).

The Equatorial Pacific has a region of relatively cool waters in the eastern Pacific referred to as the “cold tongue” and a wide area of very warm SST in the west referred to as the “warm pool” (Rasmusson and Carpenter, 1982; Philander, 1990; Larkin and Harrison, 2002). In general terms, an El Niño event is characterized by a warming of the cold tongue, an eastward shift of the warm pool, a weakening of the equatorial easterly winds and a flattening of the zonal thermocline slope (Rasmusson and Carpenter, 1982; Neelin et al., 1998).

During an El Niño event there is a shift in the center of convection from the western to the central Pacific. The accompanying Southern Oscillation, the “seesaw” of the atmospheric mass that produces a pressure gradient between the western and the eastern equatorial Pacific, is characterized by the Southern Oscillation Index (SOI). Negative values of the SOI are associated with warm events (El Niño), while positive values accompany cold events (La Niña) and a stronger Walker cell (west–east) circulation. ENSO is an aperiodic oscillation with a recurrence interval of between two and ten years, and an average of four (Trenberth, 1991), which appears to have become more frequent since the mid 1970’s (Trenberth and Hoar, 1996). La Niña is the opposite of El Niño and is associated with stronger zonal SST differences, stronger easterly winds, and a steeper thermocline (Philander, 1990; Larkin and Harrison, 2001).

Overall, during El Niño events, Colombia experiences droughts (reduced rainfall, soil moisture and river discharges) and evaporation, along with an increase in air temperature. The reverse is generally valid for La Niña. The impact of ENSO occurs earlier and is stronger in western and central Colombia than in the east (Poveda et al., 2001). A set of regional physical connections to ENSO are established and their varying local manifestations are viewed in the context of the dominant precipitation generating mechanisms and feedbacks at that location. In addition, some potential impacts of longer-lasting variations within the ocean-atmosphere system of the Atlantic are examined independently and in conjunction with ENSO (Poveda et al., 2006).

A1.1.3. DECADAL VARIABILITY: *Pacific Decadal Oscillation (PDO)*

Climate variability at decadal or interdecadal timescales is mostly represented by the PDO. The PDO is a pattern exhibited by the surface waters of the Pacific Ocean north of 20°N. The PDO shifts between warm and cool phases at inter-decadal timescales (Mantua et al., 1997). During a warm (or positive) phase, the west Pacific cools and part of the eastern Pacific warms. During a negative phase, the opposite pattern takes place. Decadal climate variations in the North Pacific Ocean have long been of interest and are an active field for scientific research (Namias, 1959; White and Barnett, 1972; Haney, 1980; Barnett, 1981) Despite this signal being most evident in the North Pacific, there is increasing evidence of its influence in South America (Mantua and Hare, 2002).

The Pacific Ocean has prominent SST variations on timescales that range from a few years to decades. This variability is often separated into two frequency bands: interannual variations with a characteristic timescale of a few years and decadal variations with a characteristic timescale of 10–20 yr. Still, the cause and mechanisms of the low-frequency climate variability in the North Pacific are not fully understood (Nakamura et al., 1997). Within the Pacific basin, interannual variability is dominated by ENSO, which has its largest signature in the tropics, particularly in the eastern tropical Pacific (Giese and Carton, 1999).

The interannual and decadal timescales in the Pacific interact with each other. (Wang, 1995; Mitchell and Wallace, 1996) describe decadal changes in the timing of ENSO events and (Graham, 1994), describes decadal variability in the tropics as having an ENSO-like

structure. Many of the climate anomalies associated with PDO are broadly similar to those connected with ENSO variations (El Niño and la Niña) though generally not as extreme (Latif and Barnett, 1996; Mantua et al., 1997; Minobe, 1997). Observations seem to suggest two important decadal variability modes in the Pacific: a decadal to bidecadal ENSO-like mode (Zhang et al., 1997) and a multidecadal North Pacific mode (Deser and Blackmon, 1995; Nakamura et al., 1997; Mestas-Nuñez and Enfield, 1999;). Modeling studies further suggest that the ENSO-like mode seems to originate mainly from the tropical Pacific region, whereas the North Pacific mode is generated predominantly in the North Pacific (Barnett et al., 1999; Pierce et al., 2001; Liu et al., 2002)

Overall, research suggests that three main characteristics distinguish PDO from ENSO: 1) 20th century PDO ”events” persisted for 20-to 30 years, whereas typical ENSO events persisted for 6 to 18 months; 2) the climatic fingerprints of PDO were most visible in the extratropics, especially in the North Pacific/North American sector, whereas secondary signatures existed in the tropics, and the opposite was true for ENSO; 3) the mechanisms causing PDO variability are not know, whereas causes for ENSO variability are relatively well-understood (Mantua et al., 1997; Zhang et al., 1997).

.

A1.2. MESOSCALE CONVECTIVE SYSTEMS (CHOCO JET, MJO)

Mesoscale convective systems (MCSs) are a cloud system that occurs in connection with a set of thunderstorms and produce a contiguous precipitation area ~100 km long scale at least in one direction. MCSs are the largest of the convective storms. They form when clouds occurring in response to convective instability amalgamate and organize themselves upscale into a single cloud system with a very large upper cirriform cloud structure and rainfall covering large contiguous rain areas. They account for a large proportion of precipitation in both the tropics and warmer mid-latitudes and they are an important link between atmospheric convection and the larger-scale atmospheric circulation. (Houze, 2004). The scale of an MCSs is huge in comparison to individual thunderstorms (Maddox, 1980).

A1.2.1. CHOCO JET

The southerly trade winds over the Eastern Pacific cross the Equator due to the predominant position of the ITCZ north of the Equator (Waliser and Somerville, 1994; Philander et al., 1996). The corresponding change of sign of the Coriolis acceleration, the predominant north-south coast orientation, the land-sea temperature and friction gradients contribute to explain the westerly winds prevailing once they enter the northern hemisphere (Hastenrath, 1991). The winds penetrate into western Colombia as a low-level westerly jet named "Choco Jet" (Chorro del Occidente Colombiano or western Colombian jet). The winds of the Choco jet are almost absent during February-March, attain their maximum velocity during October-November, and decrease onwards. The core of the Choco Jet is located at around 5°N throughout the year. These winds coming from the Pacific Ocean are colder and moister than the predominant upper easterly winds coming from the Atlantic and

the Caribbean. Pacific sea air is cooler and moister than the continental air (Poveda and Mesa, 2000).

The most important effect of The Choco Jet is a strong moisture advection from the Pacific Ocean into Colombia. The encounter of the low-level moisture–laden westerly jet and the easterly winds aloft, along with the effects of surface warming and orographic lifting produces a highly unstable atmospheric profile (Emanuel, 1994). The associated dynamics causes strong deep convection and high amounts of precipitation along the western flank of the Andes (Poveda and Mesa, 2000). The Choco Jet is bounded by the mid-tropospheric easterly jet that appears to emanate from the continent towards the Pacific Ocean. These two jets might be interacting to enhance upward motion throughout much of the troposphere, and thus contributing to development of deep convection (Hastenrath, 1999).

The Choco Jet it is associated with strong moisture transport over the eastern tropical Pacific and is highly intertwined with the development of MCSs (Maddox, 1980) over the Pacific Ocean which penetrate into Colombia and interact with the ITCZ. It is associated with the topographic gap that exists in the western branch of the Andes between 5°N and 5 °30'N, known as the Mistrató Pass, where mean heights decrease from around 3000 to 1500 m (Poveda and Mesa, 1997). It continues its interaction with high-level winds coming from the Atlantic thus influencing climate as far east as the western Amazon basin (Poveda and Mesa, 2000).

The Choco Jet, and its associated mesoscale convective cells, provoked an increase in snow precipitation over the Central Cordillera of Colombia and the advance of the Murillo glacier. In synchronicity with the intensified Choco Jet events, the ‘‘dry island’’ effect over the Eastern Cordillera of Colombia intensified, and the level of Fuquene Lake dropped (Martínez et al., 2003). The strength of the Choco Jet (centered at 5°N) is associated with the gradient of surface/air temperatures between western Colombia and the eastern equatorial Pacific (EEP) (El Niño 1 + 2 regions), thereby exhibiting strong annual and interannual variability, which contributes to explaining Colombia's hydro-climatology and its anomalies during ENSO (Poveda and Mesa, 2000).

Along with the stronger Choco Jet in the later part of the year, when the ITCZ is in its northerly position, the EEP is bathed by the cold, nutrient-rich Peru Current and the warm and less nutrient-rich Equatorial Countercurrent which meet along the Equatorial Front (Pak and Zaneveld, 1974). Because of the quasiperiodic disruption of the SST meridional pattern caused by the ENSO phenomenon in the EEP, the Choco Jet generally weakens causing dryness in the northern Andes (Poveda and Mesa, 2000).

A1.2.2. MADDEN–JULIAN OSCILLATION (MJO),

Madden and Julian made the pioneering discovery of a 40–50-day oscillation of the zonal winds in the tropics (Madden and Julian, 1971 and 1972). This discovery has led to numerous studies of a phenomenon now called the Madden–Julian oscillation (MJO), the dynamics of which are still not fully understood (Madden and Julian, 1994; Zhang, 2005).

The MJO is the dominant mode of intraseasonal variability in the tropical atmosphere (Subramanian et al., 2011) and is known to interact with a range of climate phenomena across different spatial and temporal scales (Lau, 2005).

The strength of the MJO varies from year to year, and some of this variability in the west Pacific has been linked to ENSO. For example, equatorial zonal wind variability on MJO time scales has been noted to affect the subsequent development of ENSO events (Bergman et al., 2001; Kessler, 2001; Hendon et al., 2007; Tang and Yu, 2008). MJO does not cause El Niño or La Niña, but they can change the development and intensity of the ENSO events (Kessler and Kleeman, 2000; Lau 2005; Marshall et al., 2009; Newman et al. 2009). The impact of ENSO on MJO variability is less clear (Subramanian et al., 2011). There seems to be a tendency to produce enhanced MJO activity during the warm events compared to cold ENSO events.

APPENDIX A2

Other fossil groups identified in the LLG-2 record but not shown in figure 4.5.

Group	Taxa
Pteridophytes	Aspleniaceae, *Elaphoglossum*, *Equisetum, Grammitis, Lophosoria, Polypodium, Selaginella,* Monolete psilate, Trilete echinate
Algae	*Botryococcus, Follicularia, Pediastrum*, *Zygnema*
Fungi	Diverse taxas
Diatoms	Diverse taxas
Other taxa	*Alternanthera*, Chenopodiaceae, *Croton, Drymis, Gunnera*, Mimosaceae, Myristicaceae. Piperaceae, *Ribes*, Rosaceae

APPENDIX A3

STATISTICAL ANALYSIS OF μXRF RAINFALL PROXY DATA (FE AND TI)

Based on a statistical analysis, we propose the following categories of significance levels in the counts par seconds (cps) for the Fe and Ti.

Element	Categories				
	Very Low	**Low**	**Medium**	**High**	**Very High**
Fe	< 582	582 - 1170	1170 - 2330	2330 - 3500	> 3500
Ti	<75	75-150	150-299	299-448	>448

Table A3.1. Categories of significance levels in Fe and Ti signal according to the cps

A detailed statistical analysis has broken down the Fe and Ti signal in different time periods with specific behaviour of the signal. Results for the Fe and Ti signal will be used in relation with the palynological zonation (see Figs. 5.3 and 5.4) and contribute to the interpretation of these time periods. The most important intervals showing increasing or decreasing trends or stability are described below

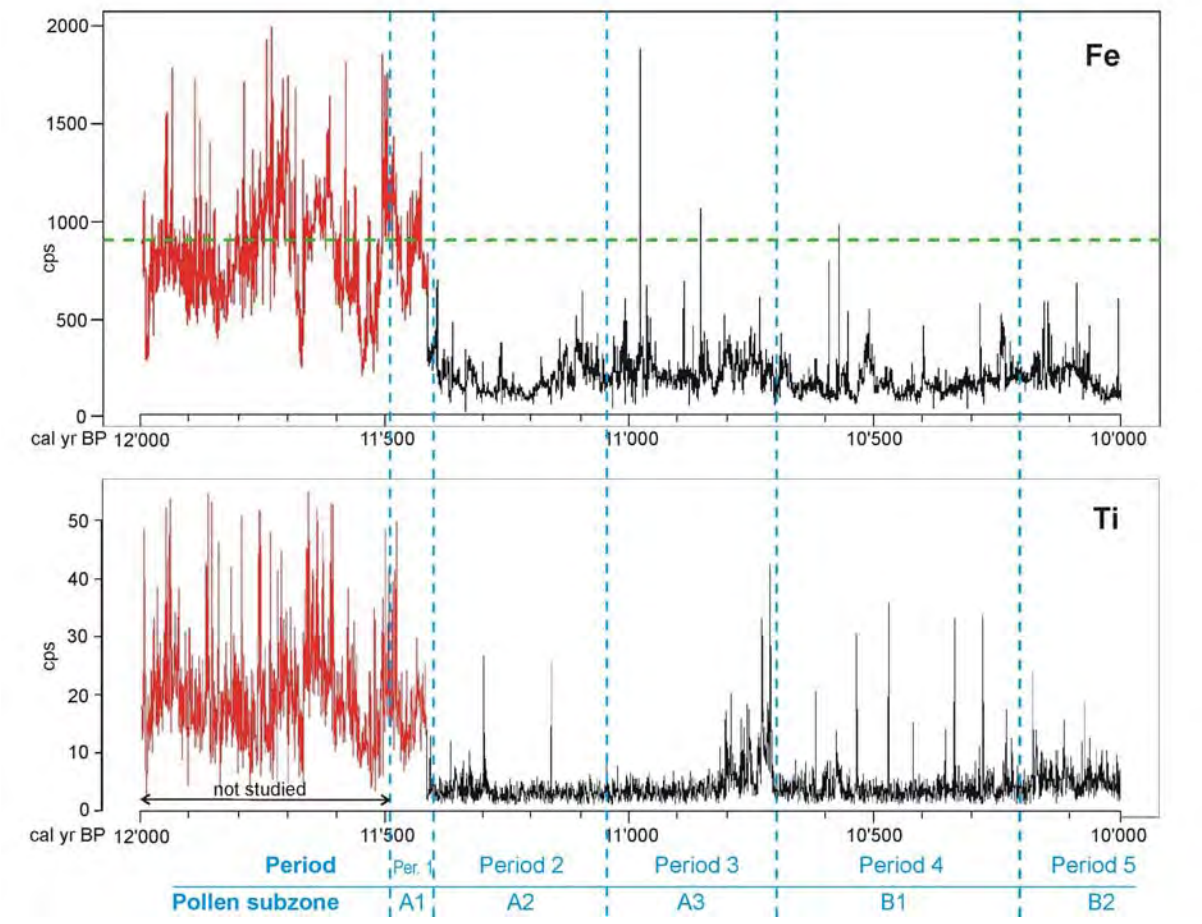

Fig. A3.1. Fe and Ti signal for interval 12,000 - 10,000 cal yr BP. Signal variations in each period are described in the text. The interval studied starts at 11,488 cal yr BP.

POLLEN ZONE A: 11,488 - 10,700 CAL YR BP

This pollen zone is divided into three subzones.

Period 1: Subzone A1 (11,488 - 11,400 cal yr BP)
From 11,500 until 11,403 cal yr BP both Fe and Ti show a stable average value of 900 and 20 cps respectively. They are characterized by a high variability in their behaviour.

Period 2: Subzone A2 (11,400 - 11,050 cal yr BP)

Fe signal
1. Structural change down to a lower level. Following an abrupt decrease between 11,405 and 11,403 cal yr BP, the signal displays a decreasing trend from 11,403 till 11,202 cal yr BP where the average value reaches 150 cps.
2. Increasing trend from 11,200 till 11,100 cal yr BP: the signal increases to reach an average value ca. 200 cps with a maximum value of 300 cps.
3. Period of stability between 11,100 and 10,660 cal yr BP with an average at around 250 cps.

Ti signal
1. The signal changes suddenly at ca. 11,403 cal yr BP, decreasing down to 3 - 3.3 cps.
2. The signal is stable with an average value at around 3 - 3.3 cps from 11,405 until 10,813 cal yr BP.

Period 3: Subzone A3 (11,050 - 10,700 cal yr BP)

Fe signal
Stable signal with an average value of around 250 cps from 11,100 cal yr BP until the end of the period.

Ti signal
Following a long period of stability with low average values similar to the previous subzone, the signal shows an slightly increasing trend from 10,813 up to 10,700 cal yr BP

POLLEN ZONE B : 10,700 - 8,050 CAL YR BP

This pollen zone is divided into three subzones

Period 4: Subzone B1 (10,700 - 10,200 cal yr BP)

Fe signal
1. The signal decreases rapidly between 11,660 and 10,655 cal yr BP.
2. It remains stable with an average value at around 150 cps from 10,655 to 10,530 cal yr BP.
3. A rapid up-and-down oscillation is displayed as follows:
   - Period of increasing trend: 10,530 - 10,505 cal yr BP.
   - Period of decreasing trend: 10,505 – 10,450 cal yr BP.
4. Between 10,450 till 10,085 cal yr BP the Fe shows a gradual increase.

Ti signal
1. Period of decreasing trend: 10,700 till 10,691 cal yr BP.

2. Period of stability with average values of around 3-3.3 cps from 10,691 till 10,182 cal yr BP.

Period 5: Subzone B2 (10,200 - 8,500 cal yr BP)

Fe signal

1. The period of gradual increase started in the previous subzone extends until 10,085 cal yr BP:
2. Decreasing trend from 10,085 until 10,025 cal yr BP.
3. Change to a lower average value of ca. 100cps between 10,025 and 9,990 cal yr BP.
4. Increase to reach an average value of 200 cps between 9,990 and 9,984 cal yr BP followed by a period of stability extending until 9,740 cal yr BP:
5. An up and down oscillation with the following periods
   - Increase from 9,740 till 9,690 cal yr BP. The average value reaches up to 550 cps.
   - Decrease from 9,690 till 9,575 cal yr BP. The average value reaches down to 180 cps.
6. A sudden increase from 9,575 till 9,573 cal yr BP, to reach average values up to 400 cps followed by a decreasing trend until 9,310 cal yr BP.
7. An up and down oscillation with the following periods
   - Increase from 9,310 till 9,280 cal yr BP.
   - Decrease from 9,280 till 9,230 cal yr BP.
8. Gradual increasing trend from 9,230 till 8,895 cal yr BP to reach a maximum value of 350 cps.
9. Decrease between 8,895 and 8,795 cal yr BP.
10. Stable interval with average value of ca. 180 cps between 8,795 and 8,550 cal yr BP.
11. An up and down oscillation with the following periods:
    - Increase from 8,550 till 8,510 cal yr BP.
    - Decrease from 8,510 till 8,390 cal yr BP.

Ti signal

1. Increase from 10,182 till 10,179 cal yr BP to reach an average value of 5.3 cps.
2. Stability in average value at around 5.3 cps between 10,179 and 9,605cal yr BP.
3. An up-and-down oscillation with the following periods
   - Increase from 9,605 till 9,495cal yr BP with a maximum value of 18 cps.
   - Decrease between 9,495 and 9,485 cal yr BP.
4. Stability with an average value of around 3.5 cps from 9,485 till 9,005 cal yr BP.
5. Slight increase between 9,005 and 9,000 cal yr BP.
6. The signal stabilizes from 9,000 until 7,615 cal yr BP with an average value of 5 cps.

Period 6: Subzone B3 (8,500 - 8,050 cal yr BP)

Fe signal

1. Continuation of gradual decrease started at 8,510 cal yr BP until 8,390 to reach a minimum value of ca 180 cps.
2. Slight increase between 8,390 and 8,385 cal yr BP.
3. Stability with average value of about 270 cps from 8,385 till 8,365 cal yr BP.
4. An up and down oscillation shaped as follows:
   - Rapid increase between 8,365 and 8,360 cal yr BP.
   - Period of stability with an average value of around 320 cps between 8,360 and 8,330 cal yr BP.
   - Rapid decrease with the average values down to 180 cps between 8,330 and 8,310 cal yr BP.
5. After a rapid increase, a period of stability with-an average value at around 320 cps extends from 8,310 till 8,000 cal yr BP.

Ti signal
The Ti signal is stable keeping an average value at around 5 - 5.3 cps.

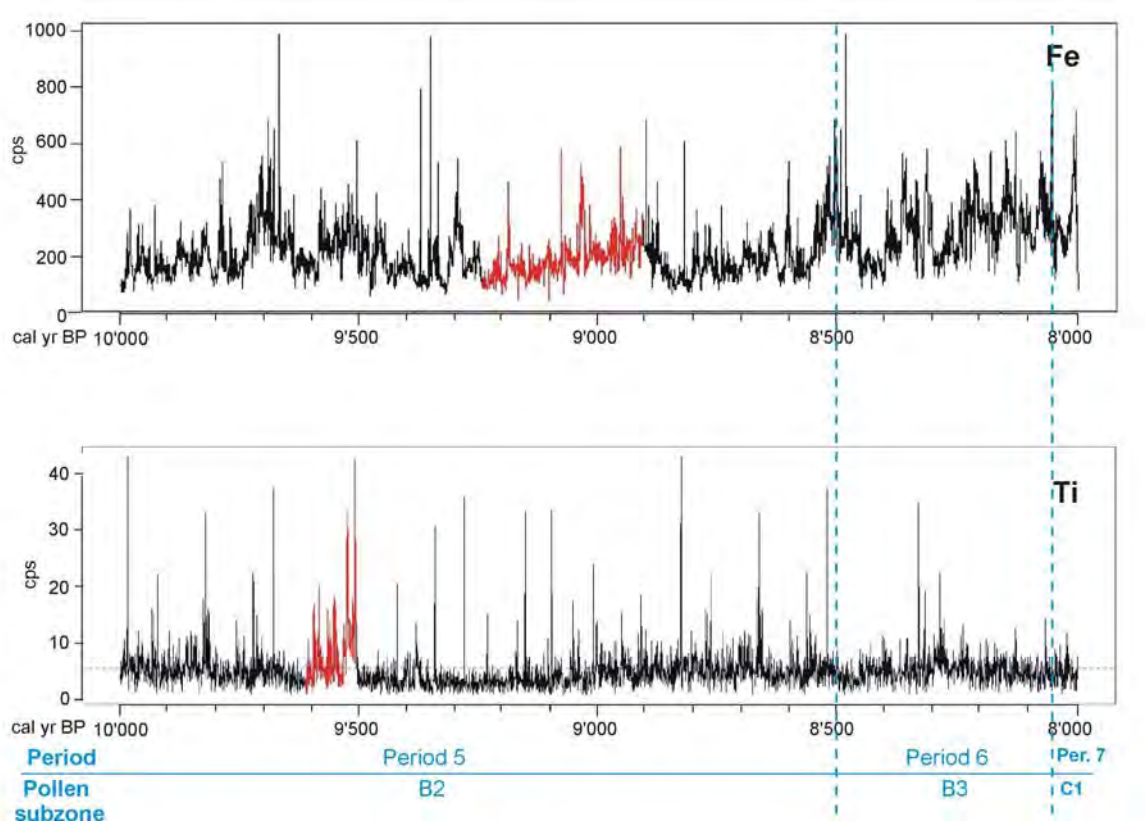

Fig. A3.2. Fe and Ti signal for interval 10,000-8'000 cal yr BP. Signal variations in each period are described in the text.

POLLEN ZONE C: 8,050 - 7,580 CAL YR BP
The pollen zone is divided into two subzones

Period 7: Subzone C1 (8,050 - 7,580 cal yr BP)

Fe signal
1. Stability with average value of around 320 cps continues from the previous period until 8,000 cal yr BP.
2. A rapid decrease between 8,000 till 7,997 cal yr BP followed by a stable interval with an average value of around 190 cps between 7,997 and 7,793 cal yr BP.
3. A rapid increase between 7,793 and 7,790 cal yr BP to reach an average value of around 350 cps.
4. A decreasing trend between 7,790 and 7,290 cal yr BP.

Ti signal
1. The period of stability started at 9,000 cal yr BP with an average value of around 5 cps continues until 7,615 cal yr BP.
2. Increasing trend from 7,615 until 7,295 cal yr BP

Period 8: Subzone C2 (7,580 - 7,000 cal yr BP)

Fe signal

1. An interval of stability with an average value of ca 350 cps continues until 7,290 cal yr BP.
2. A gradual increase from 7,290 till 7,230 cal yr BP to reach average values of ca. 650 cps.
3. A decrease between 7,230 and 7,130 cal yr BP.
4. An Increase between 7,130 and 6,910 cal yr BP.

Ti signal

1. The increasing trend started at 7,615 cal yr BP extends until 7,295 cal yr BP reaching values of up to 40 cps.
2. Decreasing trend between 7,295 and 7,095 cal yr BP to reach values of 5 cps.
3. Period of stability with average value of around 5 - 5.3 cps from 7,095 extending until 5 790 cal yr BP.

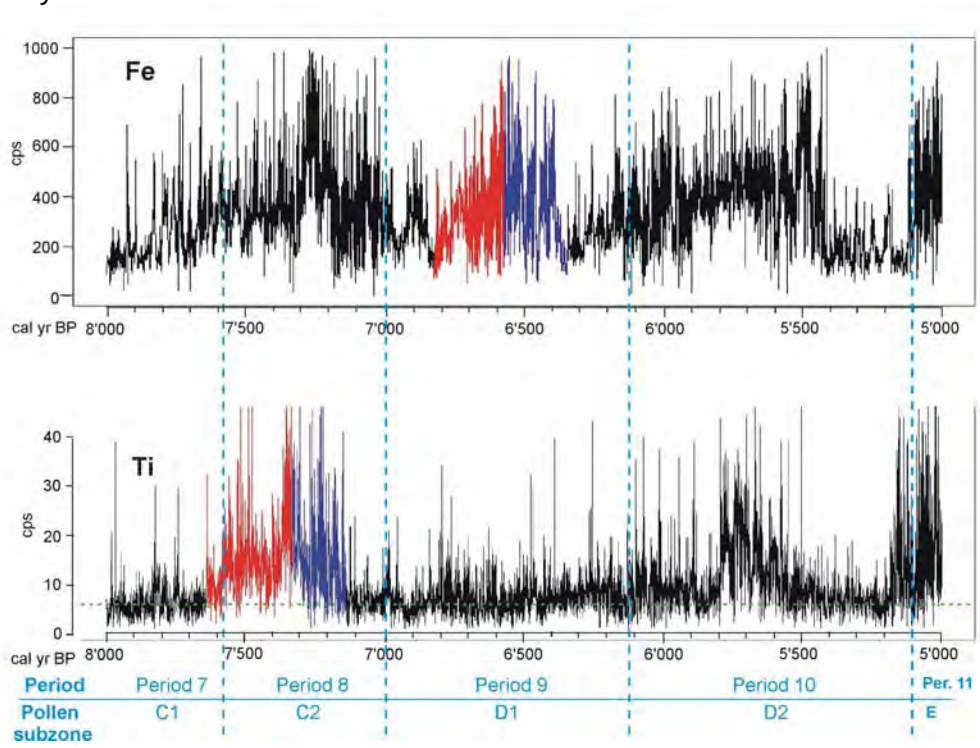

Fig. A3.3. Fe and Ti signal for interval 8,000 - 5,000 cal yr BP. Signal variations in each period are described in the text.

POLLEN ZONE D: 7,000 - 5,100 CAL YR BP

This pollen zone is divided into two subzones

Period 9: Subzone D1 (7,000 - 6,120 cal yr BP)

Fe signal

1. The decreasing trend started in the previous subzone continues until 6,910 cal yr BP.
2. An up-and-down oscillation shaped as follows:
   - An increase from 6,910 till 6,830 cal yr BP reaching a maximum value of around 500 cps.

- A decreasing trend between 6,830 and 6,770 cal yr BP.

3. Another oscillation characterized by:
   - A gradual increase between 6,770 and 6,520 cal yr BP. This interval is characterized by having higher values and being longer than the previous increase.
   - A gradual decrease from 6,520 to 6,290 cal yr BP.
4. An increasing trend extends from 6,290 until 6,110 cal yr BP and is characterized by a constant variance.

Ti signal

The Ti signal does not display significant changes: it continues having a stable behaviour with an average value of around 5 - 5.3 cps in the whole period.

Period 10: Subzone D2 (6,120 - 5,100 cal yr BP)

Fe signal

1. Increasing trend with an unsteady variance between 6,110 and 5,855 cal yr BP.
2. Stability with average value at around 450 cps from 5,855 till 5,465 cal yr BP.
3. Decrease down to 170 cps between 5,465 and 5,383 cal yr BP, followed by a period of stability from 5,383 to 5,120 cal yr BP.
4. An increase to reach values of around 450 cps between 5,120 and 5,095 cal yr BP.

Ti signal

1. Stability with average of around 5 - 5.3 cps is extending until 5,790 cal yr BP.
2. An up-and-down oscillation showing
   - An increase between 5,790 and 5,680cal yr BP to reach maximum values of around 35 cps.
   - A decreasing trend from 5,680 till 5,480 cal yr BP to reach minimum values of around 3 cps
3. Stability with average values of around 5 - 5.3 cps from 5,480 to 5,195 cal yr BP.
4. Increasing trend between 5,195 and 5100 cal yr BP.

POLLEN ZONE E: 5,100 - 4,310 CAL YR BP

Period 11: Zone E (5,100 - 4,310 cal yr BP)

This zone is characterized by exhibiting the most unstable behaviour in the Fe as well the Ti signal in the whole record. The main statistically significant intervals are described below.

Fe signal

1. Stability between 5,095 and 4,932 cal yr BP with average values of around 450 cps.
2. Overall change to a lower level marked by:
   - A decrease between 4,932 and 4,929 cal yr BP
   - An increase between 4,929 and 4,905 cal yr BP.
   - A decrease between 4,905 and 4,890 cal yr BP.
3. Overall change to a higher level marked by:
   - An increase between 4,890 and 4,885 cal yr BP.
   - A decrease between 4,885 and 4,797 cal yr BP.
   - An increase between 4,797 and 4,782 cal yr BP.
   - A decrease between 4,782 and 4,710 cal yr BP terminating with minimum values of around 150 cps.
4. An up-and-down oscillation showing :
   - An increase between 4,710 and 4,690 cal yr BP.
   - A decrease between 4,690 and 4,620 cal yr BP.

5. Stability with average values of around 300 cps from 4,620 to 4,395 cal yr BP.
6. An oscillation marked by:
   - A decrease between 4,395 and 4,335 cal yr BP.
   - An increase between 4,335 and 4,320 cal yr BP.
   - A decrease between 4,320 and 4,275 cal yr BP.

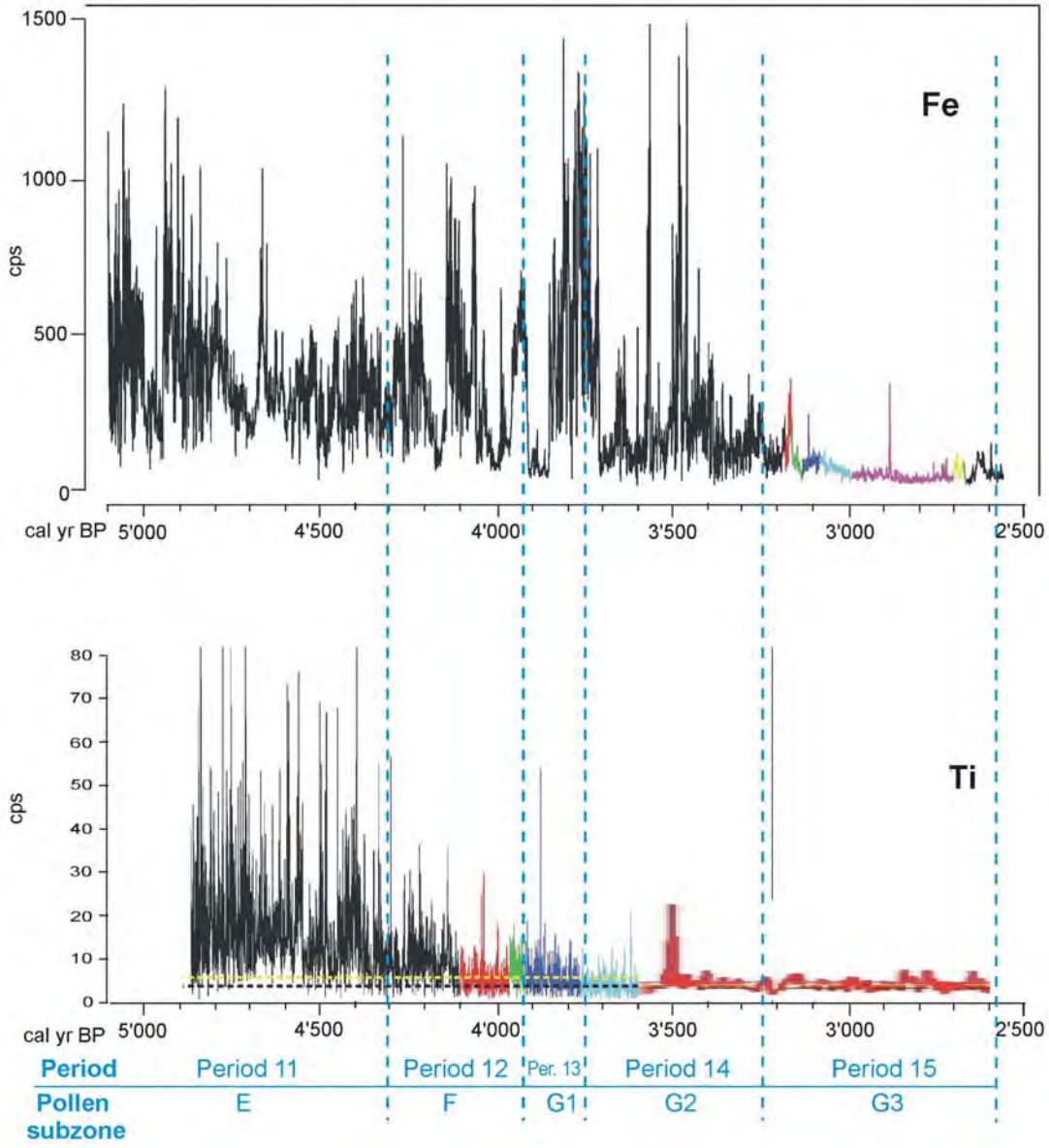

Fig. A3.4. Fe and Ti signal for interval 5'000-2'600 cal yr BP. Signal variations in each period are described in the text.

Ti signal

1. The increasing trend started at 5,195 cal yr BP is extending until 4,895 cal yr BP.
2. Decreasing trend between 4,895 and 4,875 cal yr BP.
3. Stability with an average value at around 16 cps from 4,875 until 4,800 cal yr BP.
4. Rapid decrease and increase respectively in the intervals 4,800 to 4,795 cal yr BP and 4,795 to 4,785 cal yr BP.
5. Stability with average values of around 16 - 18 cps from 4,785 till 4,716 cal yr BP.
6. Rapid decrease and increase respectively between 4,716 till 4,714 cal yr BP and 4,714 till 4,695 cal yr BP.

7. A series of ups-and-downs as follows:
   - Increase between 4,695 and 4,693 cal yr BP.
   - Decrease between 4,693 and 4,675 cal yr BP.
   - Increase between 4,675 and 4,655 cal yr BP.
   - Decrease between 4,655 and 4,640 cal yr BP
   - Increase between 4,640 and 4,570 cal yr BP.
   - Decrease between 4,570 and 4,560 cal yr BP.
8. A 4,560 - 4,425 cal yr BP interval showing:
   - Stability with average values of around 11 - 13 cps from 4,560 till 4,535 cal yr BP.
   - Increase between 4,535 till 4,475 cal yr BP to reach an average value of around 20 cps.
   - Decrease between 4,475 till 4,425 cal yr BP to reach a minimum value of around 5 cps.
9. Rapid increase from 4,425 till 4,422 cal yr BP followed by stability with average value of around 12 cps from 4,422 till 4,370 cal yr BP.
10. A series of rapid decreases and increases with average value of around 12 cps :
    - Decrease between 4,370 and 4,360 cal yr BP.
    - Increase between 4,360 and 4,350 cal yr BP0.
    - Decrease between 4,350 and 4,340 cal yr BP.
    - Increase between 4,340 and 4,330 cal yr BP.
    - Decrease between 4,330 and 4,320 cal yr BP.
    - Increase between 4,320 and 4,310 cal yr BP.
11. Stability with an average value of ca.12 cps from 4,310 till 4,230 cal yr BP.

POLLEN ZONE F: 4,310 - 3925 CAL YR B

This interval corresponds to pollen zone 1 in Velásquez (2005)

Period 12: Zone F (4,310 - 3 925 cal yr BP)

Fe signal

1. Oscillations observed in the previous time period continue :
   - Decrease between 4,320 and 4,275 cal yr BP.
   - Increase between 4,275 and 4,265 cal yr BP.
   - Rapid decrease between 4,265 and 4,260 cal yr BP.
2. Change to a lower variance and average value as follows:
   - Increase between 4,260 and 4,245 cal yr BP.
   - Decrease between 4,245 and 4,220 cal yr BP.
   - Increase between 4,220 and 4,205 cal yr BP.
   - Decrease between 4,205 and 4,195 cal yr BP.
   - Increase between 4,195 and 4,170 cal yr BP.
   - Decrease between 4,170 and 4,155 cal yr BP.
3. Change to a lower average value of 90 cps:
   - Decrease between 4,155 and 4,153 cal yr BP.
   - Stability with average value of around 90 cps between 4,153 and 4,120 cal yr BP.
4. A series of increases and decreases:
   - Increase between 4,120 and 4,090 cal yr BP.
   - Rapid decrease between 4,090 and 4,085 cal yr BP
   - Increase between 4,085 and 4,060 cal yr BP.
   - Decrease between 4,060 and 4,030 cal yr BP.
   - Increase between 4,030 and 4,015 cal yr BP.
5. Overall change to a lower level as follows:
   - Rapid decrease between 4,015 and 4,010 cal yr BP.
   - Increase between 4,010 and 3 980 cal yr BP.
   - Decrease between 3 980 and 3 975 cal yr BP.

- Stability with an average value of around 95 cps between 3 975 and 3 940 cal yr BP.

6. An up-and-down:
   - Increase between 3 940 and 3 930 cal yr BP.
   - Decrease between 3 930 and 3 915 cal yr BP.

Ti signal

1. The period of stability with an average value of around 12 cps started in the previous interval extends till 4,230 cal yr BP.
2. An interval where the variance considerably decreases:
   - Increase between 4,230 and 4,195 cal yr BP.
   - Decrease between 4,195 and 4,160 cal yr BP.
3. Change to a more quiet signal:
   - Stability with an average value of around 5.5 - 6 cps between 4,160 and 4,010 cal yr BP.
   - Increase between 4,010 and 4,006 cal yr BP.
   - Decreasing trend between 4,006 and 3 960 cal yr BP.
4. Stability with average value of around 5.5 - 6 cps from 3 960 till 3 795 cal yr BP.

POLLEN ZONE G: 3 925 - 2,580 CAL YR BP

This pollen zone is divided into three subzones

Period 13: Subzone G1 (3 925 - 3 750 cal yr BP)

Correspond to pollen subzone 2A in Velásquez (2005)

Fe signal

1. The decrease started in the previous interval extends until 3 915 cal yr BP.
2. An oscillation marked by:
   - Increase between 3,915 and 3,870 cal yr BP.
   - Decrease between 3,870 and 3,855 cal yr BP.
3. Stability with average value of around 245 cps between 3,855 and 3,810 cal yr BP.
4. An oscillation marked by:
   - Decrease between 3,810 and 3,802 cal yr BP.
   - Increase between 3,802 and 3,715 cal yr BP.

Ti signal

1. Stability period with average values of around 5.5 - 6 cps continues from 3,960 till 3,795 cal yr BP.
2. Decrease between 3,795 and 3,792 cal yr BP followed by period of stability with an average value of around 4 cps between 3,792 and 3,600 cal yr BP.

Period 14: Subzone G2 (3,750 - 3,340 cal yr BP)

Corresponds to pollen subzone 2B in Velásquez (2005)

Fe signal

1. Increase between 3,802 and 3,715 cal yr BP (continued from previous subzone).
2. Rapid decrease between 3,715 and 3,710 cal yr BP followed by period of stability with average value of around 95 cps between 3,710 and 3,685 cal yr BP.
3. Rapid oscillations as follows:
   - Increase between 3,685 and 3,660 cal yr BP.
   - Decrease between 3,660 and 3,640 cal yr BP.
   - Increase between 3,640 and 3,560 cal yr BP.
   - Decrease between 3,560 and 3,390 cal yr BP.

4. Change to lower values and period of stability with average value of around 60 cps between 3,390 and 2,820 cal yr BP.

Ti signal

1. The signal keeps its stability with an average value of around 4 cps till 3,600 cal yr BP.
2. Rapid decrease between 3,600 and 3,596 cal yr BP followed by period of stability with an average value of around 3.2 cps between 3,595 and 2,270 cal yr BP.

Period 15: Subzone G3 (3,340 - 2,580 cal yr BP)

Corresponds to pollen subzone 2C in Velásquez (2005)

Fe signal

1. The period of stability with an average value of around 60 cps extends till 2,820 cal yr BP.
2. Up-and-down oscillations as follows:
   - Increase between 2,820 and 2,765 cal yr BP.
   - Decrease between 2,765 and 2,745 cal yr BP.
   - Increase between 2,745 and 2,665 cal yr BP.
   - Decrease between 2,665 and 2,605 cal yr BP.
3. Period of stability with average value of around 60 cps between 2,605 and 2,345 cal yr BP.

Ti signal

The signal does not show significant changes and keeps stability with an average value of around 3.2 cps during the whole period.

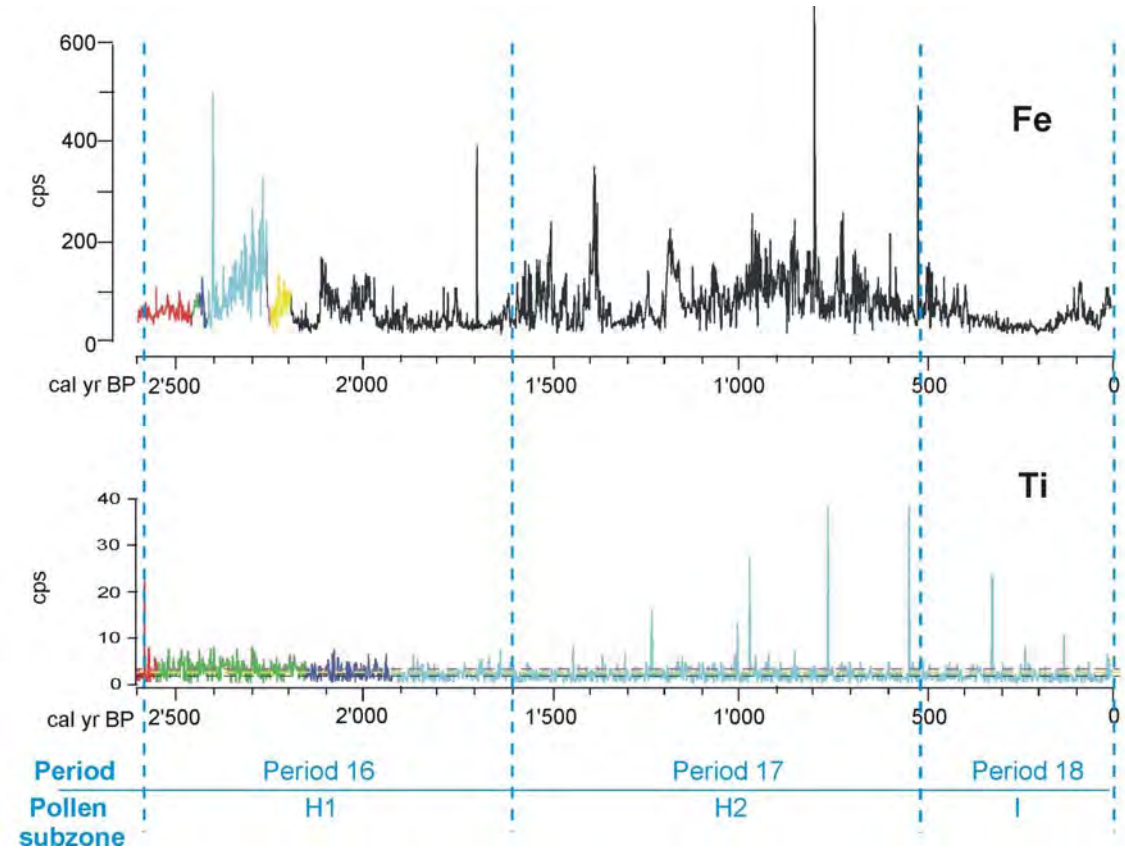

Fig. A3.5. Fe and Ti signal for interval 2'600-0 cal yr BP. Signal variations in each period are described in the text.

POLLEN ZONE H: 2,580 - 520 CAL YR BP

This pollen zone is subdivided into two subzones

Period 16: Subzone H1 (2,580 - 1,600 cal yr BP)

Corresponds to pollen subzone 3A in Velásquez (2005)

Fe signal

1. The period of stability with average value of around 60 cps extends until 2,345 cal yr BP.
2. An oscillation marked by:
   - Increase between 2,345 and 2,320 cal yr BP.
   - Decrease between 2,320 and 2,295 cal yr BP.
3. Two oscillations marked by:
   - Increase between 2,295 and 2,120 cal yr BP.
   - Decrease between 2,120 and 2,110 cal yr BP.
   - Increase between 2,110 and 2,050 cal yr BP.
   - Decrease between 2,050 and 2,025 cal yr BP.
4. Period of stability with an average value of 40 cps from 2,025 till 1,970 cal yr BP.
5. Two oscillations marked by:
   - Increase between 1,970 up to 1,955 cal yr BP.
   - Decrease between 1,955 up to 1,895 cal yr BP.
   - Increase between 1,895 up to 1,805 cal yr BP.
   - Decrease between 1,805 up to 1,785 cal yr BP.
6. Period of stability with an average value of 35 cps from 1,785 till 1,515 cal yr BP.

Ti signal

1. The signal still stable with an average value of 3 .2 cps until 2,270 cal yr BP.
2. A slight increase from 2,270 till 2,263 cal yr BP followed by a period of stability with an average value of around 4 cps from 2,263 till 1,895 cal yr BP.
3. Rapid decrease between 1,895 and 1,890 cal yr BP followed by period of stability with an average value of 3.2 cps between 1,890 and 1,685 cal yr BP.
4. Rapid decrease between 1,685 and 1,680 cal yr BP followed by a period of stability with an average value of 2.5 cps from 1,680 till 19 cal yr BP.

Period 17: Subzone H2 (1,600 - 520cal yr BP)

Correspond to pollen subzone 3B in Velásquez (2005)

Fe signal

1. The signal remains stable with an average value of 35 cps until 1,515 cal yr BP.
2. Rapid decrease between 1,515 and 1,510 cal yr BP followed by period of stability with an average value of around 26 cps between 1,510 and 1,480 cal yr BP.
3. Rapid oscillations marked by:
   - Increase between 1,480 and 1,290 cal yr BP.
   - Decrease between 1,290 and 1,280 cal yr BP.
   - Increase between 1,280 and 1,250 cal yr BP.
   - Decrease between 1,250 and 1,235 cal yr BP.
4. Slightly longer oscillations marked by:
   - Increase between 1,235 and 1,170 cal yr BP.
   - Decrease between1,170 and 1,125cal yr BP.
   - Increase between 1,125 and 1,025 cal yr BP.
   - Decrease between 1025 and 995 cal yr BP.
   - Increase between 995 and 965 cal yr BP.
   - Decrease between 965 and 890 cal yr BP.
5. Longer oscillations marked by:

- Increase between 890 and 640 cal yr BP.
- Decrease between 640 and 630 cal yr BP.
- Increase between 630 and 600 cal yr BP.
- Decrease between 600 and 575 cal yr BP.
- Increase between 575 and 540 cal yr BP.
- Decrease between 540 and 515 cal yr BP.
- Increase between 515 and 505 cal yr BP.

Ti signal
The signal remains stable with an average value of 2.5 cps during the whole period.

POLLEN ZONE I: 520 CAL YR BP - PRESENT DAY
The pollen zone is subdivided into two subzones

Period 18: Subzone I1 (520 - 130 cal yr BP)
Corresponds to pollen subzone 4A in Velásquez (2005)

Fe signal
1. The increasing trend of the previous period extends until 505 cal yr BP.
2. Decrease between 505 and 95 cal yr BP.

Ti signal
The signal remains stable with an average value of 2.5 cps during the whole period

Period 19: Subzone I2 (130 – 0 cal yr BP)
Correspond to pollen subzone 4B in Velásquez (2005)

Fe signal
1**.** Oscillations as follows:
- Decrease until 95 cal yr BP.
- Increase between 95 and 50 cal yr BP.
- Decrease between 50 and 20 cal yr BP.
- Increase between 20 and present day.

Ti signal
1. The signal remains stable with an average value of 2.5 cps until 19 cal yr BP.
2. Increasing between 19 cal yr BP and present day.